Microrespirometry with Sensor-Equipped Microtiterplates

DISSERTATION ZUR ERLANGUNG
DES DOKTORGRADES DER NATURWISSENSCHAFTEN
(DR. RER. NAT.)

DER FAKULTÄT CHEMIE UND PHARMAZIE
DER UNIVERSITÄT REGENSBURG

vorgelegt von
Sarina Arain
aus Neuss
Februar 2006

Diese Doktorarbeit entstand in der Zeit von April 2001 bis Januar 2006 am Institut für Analytische Chemie, Chemo- und Biosensorik an der Universität Regensburg.

Die Arbeit wurde angeleitet von Prof. Dr. Ingo Klimant.

Promotionsgesuch eingereicht am 31.01.2006

Kolloquiumstermin: 17.02.2006

Prüfungsausschuss:	Vorsitzender:	Prof. Dr. W. Kunz
	Erstgutachter:	Prof. Dr. O. S. Wolfbeis
	Zweitgutachter:	Prof. Dr. I. Klimant
	Drittprüfer:	Prof. Dr. A. Göpferich

Für die Erkenntnis gibt es keine endgültigen Ziele, sondern der Fortschritt der Erkenntnis ist nichts als eine Differenzierung der Fragestellungen.

Hermann Hesse

The most exciting phrase to hear in science, the one that heralds new discoveries, is not 'Eureka!' (I found it!) but 'That's funny ...'

Isaac Asimov

I've come up with a set of rules that describe our reactions to technologies:

1. Anything that is in the world when you're born is normal and ordinary and is just a natural part of the way the world works.
2. Anything that's invented between when you're fifteen and thirty-five is new and exciting and revolutionary and you can probably get a career in it.
3. Anything invented after you're thirty-five is against the natural order of things.

Douglas Adams

Danksagung

Diese Doktorarbeit entstand in der Zeit zwischen April 2001 und Januar 2006 am Institut für Analytische Chemie, Chemo- und Biosensorik der Universität Regensburg.

Mein erster Dank gilt Prof. Wolfbeis für die ausgezeichneten Arbeitsbedingungen am Lehrstuhl und die Möglichkeit, an zahlreichen nationalen und internationalen Konferenzen teilzunehmen.

Prof. Ingo Klimant gebührt besonderer Dank für die trotz beträchtlicher räumlicher Distanz hervorragende Betreuung der Arbeit und sein reges Interesse am Fortschritt derselbigen. Die zahlreichen Diskussionen, u.a. über Simulationen bzgl. Sauerstoffeintrag und Alternativen zu Tolkiens Lösung, den EINEN Ring fachgerecht zu entsorgen, haben sehr zum Gelingen der Arbeit beigetragen.

Ganz herzlich möchte ich meiner langjährigen Laborgenossin Claudia Schröder danken für die sehr schöne gemeinsame Laborzeit inklusive Faschingstreiben und diversen Pizzas auf dem Balkon.

Ein großes Dankeschön gebührt Dr. Gernot “Timetable” John für die gute Betreuung v.a. am Anfang dieser Arbeit und seine steten, wenngleich größtenteils vergeblichen Bemühungen, mir das Aufstellen (erfolgreich) und Einhalten (weniger) von Zeitplänen nahezubringen.

Bei den ehemaligen und jetzigen Mitgliedern des Lehrstuhls, vor allem Dr. Gregor Liebsch, der mir alles, was ich jemals über Excel wissen wollte, beibrachte, meinem ehemaligen und zukünftigen Kollegen Dr. Athanasios Apostolidis, Dr. Torsten Mayr, Dr. Bernhard “BMW” bzw. “Wittgem” Weidgans, Dr. Bianca Höfelschweiger (geborene Wetzl), Anna Vasilevskaya, Dr. Sergey Borisov, Gisela Hierlmeier, Petra Suchomel und Doris Burger, möchte ich mich für die sehr gute Atmosphäre am Lehrstuhl und die vielen vielen Geburtstagskuchen bedanken!

Meinem Laborkollegen Matthias Stich gebührt ein Extra-Dank für das schnelle und farbige Ausdrucken der Exemplare, dafür, dass er mich in dem großen einsamen

Labor nicht alleine gelassen hat, und für’s Kaffeekochen inklusive Lieferservice bis an den Schreibtisch.

Ein herzlicher Dank geht an die gute Seele des Lehrstuhls, Edeltraud Schmid, die mit ihrem unermüdlichen Einsatz den Lehrstuhl mit stets guter Laune und großartigem Organisationstalent am Laufen hält.

Dr. Christian Krause möchte ich für seine Firmenpresens an der Uni und die damit verbundene problemlose Beschaffung sämtlicher Sensoren und Geräte, die die PreSens besitzt, sowie für seine Allwissenheit auch bei komplizierten Themen danken.

Achim Stangelmayer danke ich für die Möglichkeit, mein Gehalt durch Zuverdienst bei PreSens aufzubessern und mich so mit Erfolg in die Firma einzuschleichen.

Ein großer Dank geht nach Saarbrücken zu meiner Projektpartnerin Svenja Weiß und Prof. Elmar Heinzle für die reibungslose Zusammenarbeit, die mehrfache Gastfreundschaft und Einblick in die simulierte Welt.

Auch bei meinen ehemaligen MitstudentInnen, v.a. meinen WG-Genossinen Dr. Frauke Henning, Dr. Mirjam Sax und Dr. Daniela Fischer, möchte ich mich für die phänomenale gemeinsame Studienzeit bedanken.

Bei der Deutschen Bundesstiftung Umwelt (DBU) bedanke ich mich für die finanzielle Unterstützung und die netten Projekttreffen.

Meinen Eltern Brigitte Arain und Abdul Qayyum Arain danke ich für ihre nicht nur finanzielle Unterstützung.

Meinem Lebensgefährten Dr. Christian Stierstorfer danke ich für seine Unterstützung und sein Verständis für schlechte Laune in stressigen Zeiten.

Abschließend möchte ich mich bei allen bedanken, die ich in dieser Danksagung vergessen habe und die ein Dankeschön verdienen.

Table of Contents

1. Introduction

1.1. Motivation

Increasing production of new chemicals and the upcoming new EU regulatory framework for chemicals (Registration, Evaluation and Authorisation of Chemicals, REACH, [1]) implicate the demand for fast and low-priced toxicological tests. Many standard tests use cuvettes or Erlenmeyer flasks as test vessels, limiting the throughput to a few samples per time. The responses are often detected by photometers, electrodes or even the eye. However, the use of these devices is not applicable for fast screening tests. A promising alternative to such low-throughput tests is the use of microtiterplates (MTPs), which enable fast screening of many samples simultaneously and offer the opportunity for automatisation.

The aim of this work was to transfer the *Pseudomonas. putida* (*P. putida*) respiration inhibition test [2] into the MTP format, using MTPs with integrated, fluorescent sensors. The *P. putida* respiration inhibition test is a German standard test which detects the oxygen decrease due to bacterial respiration and its inhibition by toxic substances with oxygen electrodes. The optical chemical sensors used in this work contain fluorescent dyes sensitive to oxygen or, for detection of a second parameter relevant for respiratory measurements, the pH value. Comparative experiments using conventional glass vessels were performed and the results compared to values given in literature to warrant the accuracy of this new method.

1.2. Toxicological Water Quality Tests

Biological water quality tests use various test organisms of different classes such as fish, daphnia, algae or bacteria. The organisms are treated with different dilutions of the test substance, and the change in the detected parameter is compared to non-inhibited samples. Various parameters can be influenced by toxic substances, e.g. mobility, turbidity (absorbance) due to growth, luminescence or oxygen consumption

due to respiratory activity. Two types of tests can be differentiated: Chronic tests require life-cycle duration and are often costly, labour-intensive and time-consuming, but give information about long-time effects towards processes regarding cell proliferation and cell structure. Acute toxicity tests take less time and indicate the toxicity towards cell metabolism, e.g. respiration, bioluminescence or motility. Evaluation of the tests varies from rather subjective observations like motility to automated, high-throughput tests. It is important to test organisms of all trophic levels for assessment of the toxicity of a sample. In the following, the most common toxicity tests are introduced. Several of these tests are standardised by international organisations like the OECD (Organisation for Economic Co-operation and Development [3]) or ISO (International Organisation for Standardisation [4]), the European Community (ECB, European Chemicals Bureau [5]) or national institutions (e.g. DIN, Deutsches Institut für Normung [6]). Only the highest-ranking institution is given as reference for reasons of clearness if more than one directive exists for a test, although the international guidelines are often adopted on European or national level.

1.2.1. Fish

Fish toxicity tests are widely used to characterise single substances or waste water samples with respect to their effect towards this class. In the *Fish Acute Toxicity Test* [7], 7 or more individuals per sample are exposed to the test substance for 96 h and the mortality after 24, 48, 72 and 96 h is recorded to give an LC_{50} value (lethal concentration, concentration of the test substance which kills 50 % of the test organisms). The fish are considered dead if there is no visible movement and if touching of the caudal peduncle produces no reaction. Various fish species can be used for this test, provided that they are available throughout the year, easy to maintain, convenient for testing and relevant with regard to economic, biological or ecological factors. Recommended fish species are Zebra-fish, Fathead Minnow, Common Carp, Ricefish, Guppy, Bluegill and Rainbow Trout. The fish are observed for 12 days under well-defined conditions with respect to light, temperature, oxygen, pH and feeding before testing. The batch is accepted if after that time less than 5 %

are dead. This test should be reduced to the inevitable minimum due to the high effort considering work, time, costs and space and the low reproducibility which results from the small number of test organisms per sample as well as for ethical reasons. Tests using microorganisms are not only less cost- and space-intensive but more suitable for automatisation and high throughput.

1.2.2. Daphnia

Several standard tests use *Daphnia magna* (s. Fig. 1.1, [8]) as test organism. Daphnia (or daphnids), broadly termed as “water fleas” due to their jerky movements through the water, are freshwater crustaceans with a size of 2 – 5 mm and a life span of ca. 50 days. They feed on algae, bacteria, fungi and decaying organic matter and are a major food source for many kind of fish. They provide for high reproduction rates, being able to replicate by pathenogenese. Their sensitivity towards traces of toxins in freshwater make them suitable for water quality testing. Two tests are standardised by the OECD, an acute and a chronic toxicity test.

The *Daphnia* shorttime-test [9] uses the decrease in mobility of daphnia as a parameter for acute toxicity. After an incubation time of 24 h, the test liquid is slightly shaken and the presence or absence of movement of the daphnia within 15 s is registered. The sensitivity of the daphnia is obtained using potassium dichromate as reference standard of known toxicity. This test is commercially available, e.g. Daphtoxkit F™ magna (Microbiotests Inc.), and can be performed in 30-well plates. In the chronic test, the *Daphnia magna* Reproduction Test [10], the number of living offsprings per individual is counted over 21 d. The daphnia are cultivated in Erlenmeyer flasks, fed with green algae and the media is changed at least 3 times a week. The offsprings are removed from the test solution daily to prevent them from consuming nutrient intended for the adult. The test solution is aerated to provide the daphnia with oxygen.

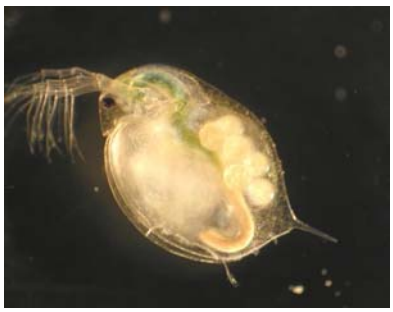

Fig. 1.1. Daphnia magna digesting its last meal of green algae.

Obviously, both tests suffers from several drawbacks: The small number of individuals (5 per sample for the acute test, at least 10 for the chronic test) leads to inaccurate results. The observation of the mobility at the acute toxicity test is rather subjective, offspring counting labour-intensive. Both methods cannot be automated. The results can only be registered after 3 weeks for the chronic test and 1 d for the "short-time" test, which – despite its name – is far away from being rapid. Furthermore, cultivation of the daphnia is rather cumbersome compared to other microorganisms like algae or bacteria, especially for the chronic test. Therefore, this test is not adequate for high-throughput screening of a large number of samples [11].

1.2.3. Algae

Several standard toxicity tests involve detection of the growth or chlorophyll fluorescence of green algae. Popular freshwater algae species used for standard tests are *Desmodesmus subspicatus* (formerly *Scenedesmus subspicatus*, [12]), which forms four-celled colonies, and *Pseudokirchneriella subcapitata* (formerly *Selenastrum capricornutum* and *Rhaphidocelis subcapitata*), a unicellular, immobile chlorophycea with a tendency for colony formation (Fig. 1.2., photos from [13] and [14]). These species are easy to cultivate and have a high reproduction rate.

The *Fresh Water Algal Growth Inhibition Test* [15] detects algal growth in Erlenmeyer flasks in intervals of at least 24 h with a total time of at least 72 h. The cell number can be detected by direct methods such as cell counting using a microscope and a counting chamber or a particle counter, or indirect methods like the detection of turbidity or the fluorescence of chlorophyll. This test provides good sensitivity and relative simplicity using an ecologically relevant, cosmopolite species. However, the duration of the test is the main

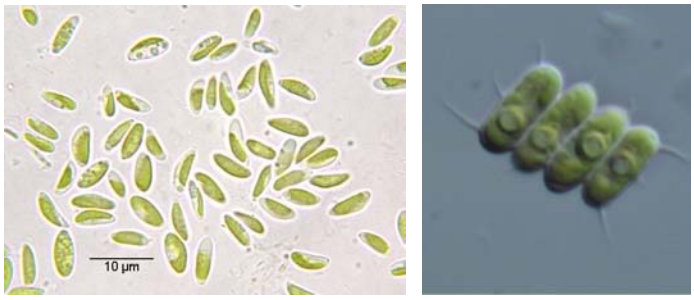

Fig. 1.2. Left: Unicellular Pseudokirchneriella subcapitata; Right: Four-celled colony of Desmodesmus subspicatus.

drawback. Early toxic effects can also be pre-screened after 5 h using the fluorescein diacetate (FDA) method [11, 16], where the fluorescein production out of FDA depends on the esterase activity of living cells, or by direct fluorescence detection after 5 h, but cannot replace the measurement after 72 h [11].

A similar growth test exists using the marine algae *Skeletonema costatum* and *Phaeodactylum tricornutum* [17]. Both Algae tests are commercially available, e.g. Algaltoxkit F™ and Marine Algaltoxkit F™ (Microbiotests Inc.).

1.2.4. Luminescent Bacteria

The use of luminescent organisms to assess toxicity has been known for 40 years [18]. About 25 years ago a toxicity bioassay using the luminescent, gram-negative, marine bacterium *Vibrio fischeri* (formerly *Photobacterium phosphoreum, see Fig. 1.3* [19, 20]) was developed [21] which determines the decrease of bacterial bioluminescence due to inhibitory substances. The mechanisms underlying the toxic effects of chemicals in these assay are both varied and complex. Toxicity may involve e.g. interactions with cell surface receptors, disruption of cell membrane functions, chemical reactions with cellular components or inhibition / competition of enzyme systems [22]. Bioluminescence is produced by the enzyme luciferase, which catalyses the oxidation of the reduced form of flavin-mononucleotid by oxygen, thereby being elevated to its excited state. The enzyme is regenerated under light emission [23]. The production of luminescence is therefore directly related to the respiratory activity of the bacteria.

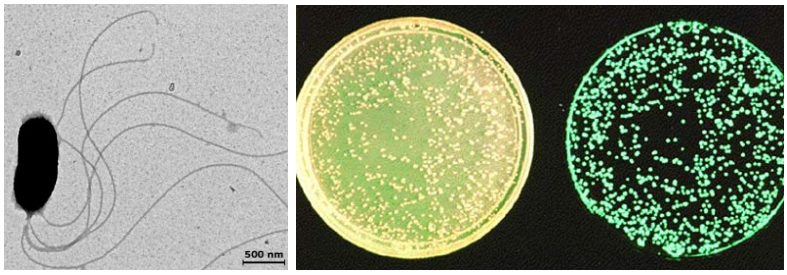

Fig. 1.3. Single cell of vibrio fischeri under an electron microscope (left) and colonies growing on an agar plate under ambient (middle) and UV light (right).

This test has been adapted for the official standards of several countries and the EU [24] and is commercially available from several companies

[25], e.g. Microtox® (AZUR environmental; e.g. [11]), ToxAlert (Merck), LUMIstox (Hach Lange) or BioTox™ (Aboatox). All tests using the same conditions yield similar results, whereas differences in procedure like the use of freeze-dried or liquid-dried bacteria lead to deviations [25]. The inhibition time varies from 22 h for chronic tests detecting the endpoint luminescence, down to 5 min for acute toxicity tests. The method provides a rather good accuracy and simple preparation of bacteria cultures. However, addition of salts to prevent contamination of the rather sensitive bacteria and referencing of each test solution by the luminescence of the respective bacteria solution without inhibitor due to inhomogeneous bacterial distribution in the inoculum prolongs the test. Furthermore, exact timing of the experiments, which are performed in cuvettes and are therefore restricted to one measurement at a time, is inevitable. Again, the use of cuvettes limits the throughput and is not applicable to a large number of screening tests. Moreover, the luciferase induction is very sensitive and depends on other factors apart from toxins, e.g. the pH. Thus, cross-sensitivities towards other parameters have to be excluded vehemently. Therefore, the points of view regarding the sensitivity of the luminescent bacteria test differ [26, 27].

A German standard test, the growth inhibition test [28], detects the turbidity of the sample after 7 h instead of the bioluminescence. Increase of the salt concentration is even more important than with the luminescence test because other bacteria interfere enormously. In other respects it requires less laborious procedures because it can easily be performed in MTPs to record many samples simultaneously. Unfortunately, the accuracy of turbidity measurements is lower than that of luminescence detection.

1.2.5. Activated Sludge

The purpose of the *Test for the Inhibition of Oxygen Consumption by Activated Sludge* [29] is to identify substances which may adversely affect aerobic microbial treatment plants and to indicate suitable non-inhibitory concentrations of test substances to be used in biodegradability tests.

The respiratory activity of activated sludge from sewage treatment plants is detected via bacterial oxygen consumption with an oxygen electrode. In contrast to other tests,

a mixed population of bacteria serves as microbial inoculum instead of a defined species. This is more representative for the bacterial composition of the natural environment than single-species assays, but also more susceptible to interferences [30]. Two methods of measurement are possible differing in sludge concentration, aeration, experimental procedure and total time of the test. Both methods suffer from inaccuracy and time consumption. The composition of the sludge and therefore its response towards the test substance varies depending on its source. This is only partly compensated by the use of a reference standard (3,5-dichlorophenol). Furthermore, the results depend on the chosen method. Laborious handling can lead to sample loss and ingress of oxygen. The total time of the test depends on the number of available oxygen electrodes and is more than 3 h or 30 min for one sample, depending on the method, which is too time-consuming for a high throughput.

1.2.6. Pseudomonas Putida

Pseudomonads are gram-negative, rod-shaped bacteria with a single polar flagellum for motility. They live ubiquitarily in soil and freshwater and even in salt water, if salinity does not exceed 3.5 %. The strictly aerobic bacteria are incapable of anaerobic fermentation. They grow at temperatures between the freezing point and 41 °C, temperatures above 60 °C are lethal. Some species produce hydrophilic pigments like pyocyanin, pyoverdin (= fluorescein), pyorubin and pyomelanin. Important members of this genus include the subspecies *Pseudomonas aeruginosa*, a pathogenic germ which causes wound infection, and the non-pathogenic *Pseudomonas fluorescens*, a luminescent species, and *Pseudomonas putida* (*P. putida*) (s. Fig. 1.4, [31]), which plays an important role in decomposition of biological compounds in soil, biodegradation of toxic substances, and the carbon and nitrogen cycle. Being saprophytes like *P. fluorescens*, they derive their nourishment from dead or decaying organic material. *P. putida* are characterised by great metabolic diversity and are able to utilise a wide range of carbon sources, including molecules which few other organisms can break down [32]. Naturally, a sensitive strain which is not tolerant versus phenols or other investigated inhibitors was chosen

Fig. 1.4. Left: Single cell of P. putida under an electron microscope; Right: Culture plate of P. putida producing fluorescein, excited with UV light. The bacteria store the fluorescent dye within their cells as well as releasing it to the ambient agar.

for the toxicity test described in this work. *P. putida* produce the fluorescent pigment pyoverdin, also known as fluorescein (s. Fig. 1.4, right). Their natural occurrence in water and soil make *P. putida* particularly suitable for tests regarding the toxicity of substances towards natural environment, representing heterotrophic microorganisms in fresh water. Due to their easy cultivation and to the fact that they are non-pathogenic, they may be used without special precautions like a sterile bank.

In the *Pseudomonas Putida Growth Inhibition Test* [33], the growth of *P. putida* and its inhibition by toxic samples are detected via turbidity measurements. After adjusting the starting concentration of a preculture of *P. putida* via the detection of its optical density (OD), the preculture is treated with dilutions of the samples and cultivated for 16 h. After that period, the turbidity of the samples is measured again. This two-point method presumes that bacterial growth is reproducible for each experiment, for no continuous monitoring is performed to detect potential irregularities during cultivation. However, the progression can be interfered by unwanted effects which are not detected with this method. Furthermore, possible contamination may lead to too low calculated inhibitions due to additional growth of other bacteria. According to the coefficients of variations of the EC_{50} values for the toxic standard 3,5-dichlorophenol given in the standard test description, this two-point test is not very accurate.

The problem of long assay times and inaccuracy of the method can be overcome by monitoring cellular metabolic activity of a constant amount of bacteria over a short period of time instead of the growth and its inhibition by test substances. This is done in the *Pseudomonas Putida Respiration Inhibition Test* [2]. A preculture is cultivated for 16 h, washed with phosphate buffer, and a distinct bacteria

concentration is adjusted via OD detection. The inoculum is treated with dilutions of the sample, incubated for 30 min, and the respiration is measured with an oxygen electrode as the decrease in oxygen per time (oxygen uptake rate, OUR). Substances which cause an inhibition of more than 20 % are defined as toxic and have to undergo further treatment before releasing them into the environment.

This test is shorter and more accurate than the *P. putida* growth inhibition test and less susceptible for effects of contamination. However, the OUR is so far detected with oxygen electrodes, which suffer from certain limitations. Besides oxygen consumption by the electrode, dependence on the approach velocity of the sample and possible contamination due to the invasiveness of this method, the greatest drawback is the limitation to one electrode per sample, which reduces the throughput and makes this set-up rather extensive considering space, costs and labour. Thus, a low-cost, contactless, easy-to-handle alternative to the oxygen electrode with the facility for high throughput screening is necessary.

1.2.7. Cell Culture Tests

Cell proliferation and viability assays enable investigation of effects of external conditions on single cell types instead of entire organisms. This enables researchers to optimise cell culture conditions, but also to facilitate the discovery of new therapeutic agents such as antibiotics and anti-cancer agents, as well as to assess the toxicity of environmental pollutants and new chemicals. There are several strategies to assess the viability of cells [34].

A common method for detection of cell proliferation is the incorporation of radiolabled nucleotides such as titrated [^{3}H]thymidine in nacently synthesised DNA [35] or the release of ^{51}Cr by dead cells. Both methods involve problems concerning the use of radioactive substances. Other molecules which are released by dead cells are the fluorescent Europium Titriplex, and lactate dehydrogenase (LDH), which can be detected by a photometric enzyme assay.

Staining is another common method for detection of living cells. The dyes are either included or excluded by viable cells and detected using a light microscope (e.g. Trypan Blue, Neutral Red, Crystal Violet) of by fluorescence (e.g. propidium

iodide, Hoechst 33342). Dyes are also used for the reduction of metabolic intermediates (NADP, FAD, FMN, NAD) yielding coloured or fluorescent compounds: The widely used MTT [36, 37] and the Biolog [38] assays both use the reduction of tetrazolium dyes within the mitochondria of metabolically active cells, thereby forming a dark blue and violet formazan dye precipitate, respectively. Other derivatives like MTS are applicable, too. The reduction of Alamar Blue (resazurin) leads to a fluorescent product [39]. Although these methods are used for HTS [40], they are of limited application due to their susceptibility to interference from drugs by reacting with reducing groups, drugs absorbing light in the visible region, or scatter or absorbance from precipitation. They are non-reversible, rely on the reaction with mitochondrial succinate dehydrogenase and may therefore themselves perturb the cell.

A widely used method utilising ATP is the luciferase bioluminescence assay [41, 42]. Luciferin reacts with oxygen and ATP to give oxyluciferin, AMP, phosphate and CO_2, thereby emitting light at 562 nm. This assay is rather sensitive and linear over a wide range.

All these methods suffer from several drawbacks: Besides the fact that radioactivity is involved in some procedures, all methods require the addition of reagents and are therefore invasive and sample-destructive. Periodical sampling as well as additional incubation times of some tests (MTT, LDH) lead to unacceptable time consumption and make these tests not suitable for continuous monitoring.

A fast, non-invasive test without the need of sampling, which can be performed in MTPs is the use of cell lines expressing GFP (green fluorescent protein) [43, 44]. However, this method is limited to distinct cell lines.

An elegant method for assessing the viability of a cell is the determination of respiratory parameters. The use of MTPs enables high throughput. Beside pH [44], oxygen is the most important parameter related to cell respiration. Dissolved, oxygen-sensitive dyes [45, 46] as well as dyes embedded in polymers [47 - 51] have been used for viability tests with mammalian cells. All these tests are non-invasive and have no need for labour-intensive sampling but can be performed on-line. This is time-saving and enables automatisation inevitable for a high throughput.

1.2.8. Other Toxicity Tests

The methods introduced above are far from describing the multitude of toxicological tests completely, but a greater elaborateness would go beyond the scope of this work. Noteworthy are bacteria tests with lux-marked *E. coli*, which are genetically modified to emit luminescence [52, 53], and commercially available biosensors (e.g. CellSense [54]) incorporating various organisms in membranes and detecting the respiration rate via amperometric devices [55].

1.3. Optical Chemical Sensors

The standard tools for pH and oxygen determination are electrochemical sensors. Electrodes are easy to calibrate, have fast response times and feature linear characteristics over a range of several orders of magnitude. However, they suffer from several drawbacks: Like all electrochemical sensors, they are susceptible towards electrical interferences and therefore not applicable for measurements involving electromagnetic fields or an explosive atmosphere. Moreover, invasive methods are always potential sources of contamination, sterilisation is rather labour-intensive, and the sample throughput is limited by the number of available electrodes and time-consuming handling. Further disadvantages are cross-sensitivity towards hydrogen sulphide, carbon dioxide, accumulation of proteins and various organic components as well as reductives. High pressure, which can lead to membrane deformation or even demolition, is also source of error.

Optical chemical sensors based on luminescence are an elegant method for determination of common parameters like oxygen partial pressure (pO_2), CO_2, NH_3 or pH and offer a number of advantages over electrodes [56]. They consist of an analyte-sensitive indicator dye embedded in an analyte-permeable polymer. Besides easy handling and fast response times [57], luminescent sensors can transport many information simultaneously, like intensity, lifetime, spatial resolution or polarisation. Sensor arrays detect various parameters at the same time by bundling different sensors for various analytes. In contrast to electrodes, optical sensors do not need an external reference due to the possibility of internal referencing. They are not

susceptible towards electromagnetic fields, robust and easy to miniaturise and sterilise. Highly flexible system formats and integration in existent systems like shaking flasks or MTPs, which are compatible to commercially available detection systems, enable their use in many fields of application.

A great advantage is the possibility of non-invasive, remote measurement, which avoids contamination and laborious sample-handling, enables in-vivo measurement and simplifies online measurement. Last but not least, low production costs make them suitable as disposables for high throughput screening. Difficulties like leaching of the dye from the polymer, photobleaching, inhomogeneous distribution of the immobilised dye in the matrix and interference of ambient light have to be accounted for by careful choice of appropriate materials and set-up. Drawbacks are possible interference of some organic solvents and proteins as well as non-linear response characteristics.

1.3.1. Formats of Optical Chemical Sensors

Luminescent or absorbance-based pH and oxygen sensors can be applied in various forms. Dissolved indicators [44, 45] are the easiest way of preparation, but suffer from certain drawbacks: Without protection, they may be susceptible towards photobleaching and interferences of sample ingredients. Exposition of fluorescent pH sensors to oxygen can lead to unwanted quenching effects. Dissolved indicators are likely to interact with the sample and may show low biocompatibility. They provide an average value over the whole sample, which can be critical in inhomogeneous samples (see chapter 3). Furthermore, internal referencing of the luminescence intensity using a second, analyte-inert dye is not possible with dissolved indicators due to too low accuracy.

Incorporating the indicator dyes in particles [58, 59] solves some of these problems: The polymer, which ideally is only permeable for the analyte, protects the dye from direct contact with the sample, thereby preventing unwanted interactions with other molecules. Furthermore, it enables dual-wavelength measurements with constant ratios of indicator and reference dye. Nevertheless, adding of the particles is possible source of contamination and involves an additional procedure step, which

can be of importance for high throughputs. Like dissolved indicators, they provide an average value over the whole sample. Both dissolved indicators and particles are limited to the use of vessels and can e.g. be applied to MTPs for a high throughput.

Embedding analyte-sensitive dyes in a polymer film is the most common format of optical sensors. Immobilisation of the dyes in a polymer leads to better stability of the sensor. Sensor films are very flexible and not as limited regarding their format as dissolved indicators or particles. The main format are absorbance- or fluorescence-based fibre-optic sensors. They consist of a sensor film which is located at the end of a glass or polymer fibre for guiding the excitation light and collecting the fluorescence emission. Remote sensing with robust minisensors over large distances is possible as is almost non-invasive measurement of high spatial resolution using needle-type microsensors. For the more robust minisensors, direct contact between fibre and sensor film is not necessary, thus enabling non-invasive measurements through transparent flasks or bags. Internal referencing of the fluorescence signal by incorporation of a reference dye with a constant ratio of the two dyes enhances the reproducibility of the signal, as does or lifetime detection. Due to the short lifetime of most pH-sensitive dye, incorporation of a reference dye is here of importance as well (see dual lifetime referencing (DLR), chapter 1.3.5)

Another application of sensor films is their use in imaging [60, 61] and fluorescence microscopy [62] to gain insight in spatial distribution of e.g. the oxygen distribution in tumour cells or tissues [63, 64], pH and oxygen values in marine sediments [65] or pressure-sensitive paints [66-68].

For high-throughput screening, the use of MTPs combined with the advantages of sensor films is a promising method. Sensor films containing indicator dyes for various analytes can be glued as sensor spots into MTPs and read out using the imaging system [61] or an MTP reader to obtain several parameters in one measurement. A more subtle method is the direct application of a so-called sensor cocktail, containing the sensor film ingredients in an appropriate solvent, to the wells of an MTP. After evaporation of the solvent, a thin film remains at the bottom of each well [48, 49, 69-71]. Similar constructions like sensor spots in home-made microbioreactors are possible as well [46, 72].

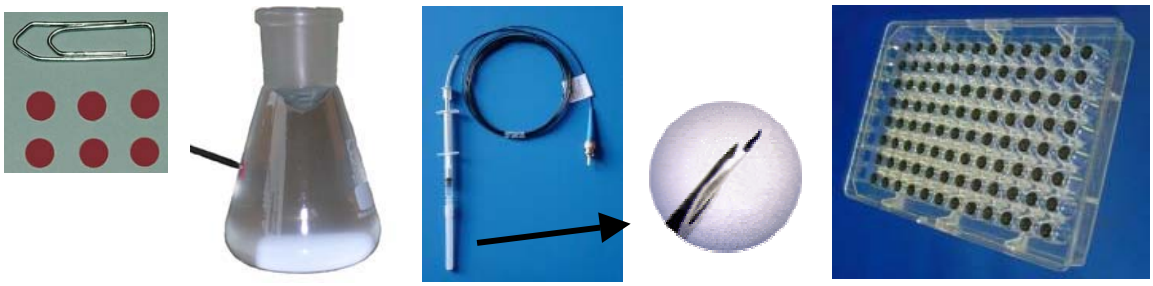

Fig. 1.5. Examples of optical sensor formats: Left: Planar sensor spots for non-invasive, fibre-optic detection through a transparent flask; Middle: Needle-type microsensor for high spatial resolution and real-time measurements; Right: Sensor-coated MTPs for high-throughput screening [73].

1.3.2. Non-invasive Methods for Cell Viability Detection

A prerequisite for high-throughput screening are non-invasive detection methods. Invasive methods not only imply the possibility of contamination of the sample by insertion of a probe, but also require one probe per sample for simultaneous detection of the respective parameter in many samples, which is time-consuming, difficult to automatise and multiplies the costs per tests. In contrast, non-invasive methods enable fast screening without the need of insertion of a probe.

The first non-invasive measurement system for detection of bacterial respiration was performed in 1977 [74, 75]: The BACTEC 460 TB radiometric system (Becton Dickinson Diagnostic Instruments) was used for AST (antimicrobial susceptibility testing). This method determines the ability of bacteria to catabolise [^{14}C] palmitic acid by detection of the produced $^{14}CO_2$ [76]. Using special liquid growth media and antibiotics for other bacteria, identification of bacteria such as *Mycobacterium tuberculosis* could be accelerated considerably. This method of using radiolabelled substrates (e.g. acetate) was used for respiratory detection without growth, as well [77]. Due to the drawbacks of the BACTEC system, such as the use of radioactive substances and needles, it was substituted in 1995 by an optical method (MGIT, Mycobacteria Growth Indicator Tube, Becton Dickinson) using test tubes with a silicone rubber impregnated with a fluorescence-quenching oxygen sensor [78]. The growth curves of bacteria, yeasts or fungi and their susceptibility

towards antimicrobials are detected via fluorescence measurement from the bottom, enabling the simultaneous recording of up to 960 tubes.

The first non-invasive microbial detection system based on optical measurement is the BacT/Alert system (bioMérieux, Nürtingen, Germany). It measures the permanent colour change of the sample to yellow due to respiratory CO_2 production of microorganisms by colourimetric reflectance. Main applications are the determination of high-acid producing organisms (e.g. *Lactobacillus*, yeasts, molds) in food and beverage products and clinical application [79].

Since then, optical methods for non-invasive measurements have been established in many varieties. Detection of the change in turbidity (optical density, OD) due to growth of organisms is a common method for toxicological tests (e.g. [33, 80, 81]). Dissolved fluorescent indicators [45, 46] as well as dyes embedded in polymers have been used for microorganism and cell viability tests [47, 82]. Here, especially sensors in the MTP format [48, 83] are worth mentioning due to the possibility of a high throughput necessary for these applications. They are used for the cultivation [71, 84], characterisation and classification of bacteria [85] as well as for the detection of biological degradation of pollutants and toxicological tests [69, 86].

1.3.3. Oxygen Sensing with Optical Sensors Based on Fluorescence

1.3.3.1. State of the Art

Oxygen is an important parameter in various fields of application [87]. In the industrial sector, oxygen monitoring serves as quality control for anaerobic processes or processes utilising metabolising organisms, such as yeast. In the medical field, respiratory and blood gas analysis as well as subcutaneous oxygen detection are key physiological parameters which are ideally monitored continuously [88, 89]. Biotechnology uses oxygen determination for controlling the cultivation conditions of bacteria or cells [90 - 92] or monitoring oxygen-consuming enzyme reactions for process control of fermenters [93-95]. In environmental analysis, continuous

monitoring of oxygen levels in the atmosphere and in water are a routine practise for guidance of the overall condition of the ecology [96]. Furthermore, oxygen is the most important parameter for the detection of respiratory activities in toxicological tests [2, 54].

The first widely-used oxygen sensors were based on polarographic methods. In 1942, a platinum electrode was used for the first time for oxygen determination in tissues [97]. Today, the standard method for oxygen determination is the Clark electrode invented in 1953 [98]. However, besides the disadvantages mentioned above, the use of oxygen electrodes suffers from several drawbacks: Due to the reduction of oxygen to the hydroxide ion at the cathode, the system consumes oxygen, which is especially critical with small sample volumes and causes oxygen diffusion from sample regions with higher oxygen content. Consequently, any factors that influence the oxygen diffusion through the membrane, like fouling or change of flow conditions in the testing fluid, can generate misleading data. Miniaturisation requires great effort and expenses [99, 100], although needle-type and Clark-type microelectrodes with dimensions up to a few µm and outstanding features such as very small response time and very small sensitivity towards stirring exist [101-103]. However, their expensive and tedious fabrication and fragility limit a more frequent application of oxygen microelectrodes and make them inapplicable for fast and low-cost screening tests.

Another tool which is frequently used for the determination of the BOD (biochemical oxygen demand) are pressure sensors for (micro-) manometric detection of oxygen in the sample headspace [104-106]. However, this method is not very sensitive, time-consuming due to the high oxygen capacity of the test vials and not suited for small sample volumes [47].

As discussed above, optical chemical sensors offer a number of advantages over electrodes. Optical microsensors are an inexpensive alternative to microelectrodes [107, 108], do not suffer from oxygen consumption, display high sensitivity, smaller size and better biocompability [109, 110]. Although absorption-based sensors for oxygen determination exist [96, 111, 112], luminescent sensors [113 - 117] are the method of choice for optical oxygen determination due to the higher sensitivity of the method [118]. The phenomenon of fluorescence quenching by oxygen is known since the late 1930s [119] and was since then used for

quantitative oxygen determination (e.g. Bergman [120]). Quenching of luminescent dyes by molecular oxygen can be evaluated via detection of intensity [89, 121 - 123] or, since 1985 [124], via lifetime [125 - 127]. The latter method is advantageous vs. intensity measurements [61], because inhomogeneous fields of the light source and inhomogeneities of the sensor layer do not matter, which is especially important for imaging and MTP applications. Lifetime measurements can be performed either in the frequency domain or the time domain [128 - 131]. The high lifetime of oxygen indicators enables – in contrast to pH sensors - a less sophisticated detection system

Crucial factors for oxygen sensors are the choice of dye and matrix material and the film preparation method [87]. The polymer has to be highly permeable to oxygen to warrant quick interaction with the dye and thus efficient quenching. Furthermore, it should provide compatible solubility for the dyes to avoid leaching [58]. Widely used polymers that fulfil these demands include polysiloxane derivatives, which are highly gas-permeable but lack the mechanical strength in thin films, organic glassy polymers (PS, PMMA, PVC), which are less oxygen-permeable but mechanically more stable, and cellulose derivatives [132]. Fluoropolymers are highly stable against photo-oxidation, whereas sol-gels enable non-leachable entrapment of water-soluble indicators without previous modification with lipophilic or reactive groups and excellent adhesion to glass and other silica substrates. However, low reproducibility and sensor ageing are drawbacks that can be avoided by the use of ormosil (organically modified silicate) glasses [133,134].

One demand for oxygen indicators is a long life-time of the emitting state, which leads to a greater extent of quenching and therefore to high sensitivity. Suitable oxygen indicators are organic probes and organometallic compounds. Polycyclic aromatic hydrocarbons (PAHs, e.g. [94, 116, 117, 120, 135, 136]) are efficiently quenched by oxygen and comprise long fluorescence lifetimes of ca. 0.2 µs. Among the organometallic complexes, ruthenium tris(diphenyl phenanthrolin) ($Ru(dpp)_3^{2+}$) plays the most important role (e.g. [93, 125, 137 - 139]). It has a long lifetime of 4.0 µs (deoxygenated) and 2.0 µs (air -saturated), respectively, compared to other ruthenium complexes, high quantum yield and sensitivity. Today, the most widely used optical oxygen probes are ruthenium diimines embedded in a

polysiloxane matrix [114, 140, 141]. Other transition metal complexes use osmium [142] and iridium [143, 144] as metal component.

The second important class of organometallic complexes are the phosphorescent platinum and palladium porphyrins [145]. Octaethylporphyrins (OEPs) comprise high quantum yields and lifetimes (Pt: ca. 100 µs, Pd: ca. 770 µs) [124, 146]. Tetrakis(pentafluorophenyl)porphyrin (TFPP) is more stable against photo-oxidation and photo-reduction [147] than OEP. OEPK, the keto form of OEP, [47, 58, 146, 148, 149], is even ca. 10 times more photostable than OEP and has longer emission and excitation wavelengths, although the oxygen-sensitivity is lower due to lower lifetime. Compared to the ruthenium dyes, metalloporphyrines have a higher lifetime and therefore a higher sensitivity. The Stokes' shift is larger, and they can be excited and emit at longer wavelengths. The latter leads to less cross-sensitivity towards light scattering and autoluminescence of biological cells, which enhances the sensitivity of the sensor. Furthermore, longer wavelengths penetrate further into cell tissues and are more bio-friendly to live cells [58].

1.3.3.2. Principle

Optical oxygen sensing is based on dynamic luminescence quenching by molecular oxygen. Collision of the luminophore in its excited state and oxygen in its ground state leads to an energy transfer between these two molecules and thereby to radiationless deactivation of the luminophore (collisional or dynamic quenching). Oxygen is transformed from its ground state (triplet, $^3O_2$) to its excited state (singlet, $^1O_2$). Dynamic quenching results in a decrease of the luminescence intensity as well as the lifetime of the excited state of the luminophore. The relation between oxygen concentration and the

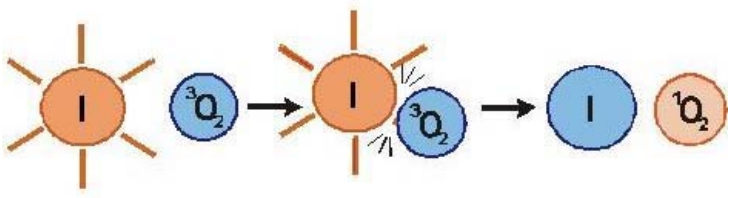

Fig. 1.6 Dynamic luminescence quenching of the excited state of the oxygen indicator I by molecular oxygen.

luminescence intensity as well as the lifetime of the excited state of the luminophore is ideally described by the Stern-Volmer equation:

$$\frac{I_0}{I} = \frac{\tau_0}{\tau} = 1 + K_{SV} \cdot [O_2] \qquad \text{eqn. 1.1}$$

I and I_0 are the luminescence intensities in presence and absence of oxygen, τ and τ_0 the luminescence decay times in presence and absence of oxygen, K_{SV} the overall quenching constant (Stern-Volmer constant), and $[O_2]$ the oxygen content. The Stern-Volmer constant quantifies the quenching efficiency and therefore the sensitivity of the sensor.

However, eqn. 1.1 is only valid if the luminophore is located in a homogeneous environment, and displays a linear correlation between I_0/I or τ_0/τ and the oxygen concentration $[O_2]$. Luminophores embedded in a polymer matrix show a non-linear response behaviour (s. Fig. 1.7), which can be described with a modified Stern-Volmer equation eqn. 1.2:

$$\frac{\tau_0}{\tau} = \left(\frac{f_1}{1 + K_{SV_1} \cdot [O_2]} + \frac{1 - f_1}{1 + K_{SV_2} \cdot [O_2]} \right)^{-1} \qquad \text{eqn. 1.2.}$$

This model is based on the assumption that the indicator is distributed in the polymer matrix at two different sites (two-site model), and each fraction (f_1, 1-f_1) shows a different quenching constant (K_{SV1}, K_{SV2}). The parameters f_1, K_{SV1} and K_{SV2} are obtained empirically for each oxygen sensor using a calibration plot. In this work, modified Stern-

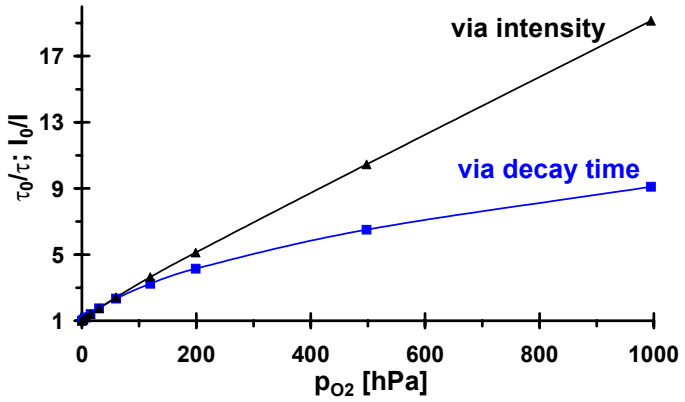

Fig. 1.7. Linear (via intensity) and non-linear (via decay time) Stern-Volmer plots of an oxygen indicator (PSt3, see chapter 2.4.2.1, page 65).

Volmer equations with the respective parameters were used for lifetime measurements, whereas the simple Stern-Volmer equations was sufficient for intensity measurements performed with the sensor-coated MTPs because of the linear behaviour of the plot regarding intensities for this sensor.

1.3.4. pH Sensing with Optical Sensors Based on Fluorescence

1.3.4.1. State of the Art

As with oxygen determination, the most widely used instrument for pH detection is the electrode. Here, highly miniaturised ISFETs (ion-sensitive field-effect transistors) [150] are worth mentioning. However, the use of a conventional reference electrode which is difficult to miniaturise limits seriously the application of ISFETs with respect to the small size. Optical methods offer a promising alternative. One of the first observations was the colour change of indicators depending on the pH value. The first “optical sensor” was a semi-qualitative, rapid test using lackmus paper [151]. Later, the dye was immobilised on cellulose or polymers to avoid leaching. The same principle was developed further to the present optical sensors.

The first fibre-optic pH sensor was an absorption-based sensor developed by Peterson in 1980 [152] using phenol red (phenol sulphone phthalein) as the indicator dye. Other typical absorption-based pH indicators are bromothymol blue [153, 154], methyl orange, bromocresol green and alizarin [155].

Saari and Seitz developed the first pH sensor based on fluorescence using fluorescein amine as the indicator [156]. In the same year, a fluorescent sensor using the pyrene derivative 1-hydroxypyrene-3,6,8-trisulphonate (HPTS) was introduced [157], which is today one of the most widely used pH indicators for optical pH sensors due to its advantageous properties. Derivatives of fluorescein are the second most widely used pH indicators [156, 158, 159]. Especially the lipophilic, ratio (dual wavelength) probes seminaphtho-rhodafluors (SNARF [160]) and seminaphtho-fluoresceins (SNAFL [161]) are advantageous due to their excellent spectral properties and stability. Other fluorescence indicators are derived from acridine [162],

naphthole [163, 164], and hydroxycoumarin [56]. They are evaluated via the detection of fluorescence intensity [165- 167], intensity ratios [168 - 173], lifetime [154, 174, 175] or polarisation [176]. Criteria for the evaluation of pH indicators are spectral properties like quantum yield, Stokes' shift, absorption and emission wavelength, photostability, pK_a-value, water solubility and the presence of functional groups for immobilisation on polymers.

1.3.4.2. Principle

Optical pH indicators are weak acids or bases that are easily protonated or deprotonated. The principle of optical pH sensing is based upon the fact that the indicator dye changes its spectral properties (absorbance and / or luminescence) with protonation / deprotonation (Fig. 1.9). Depending on the pK_a value of the dye, more dye molecules are deprotonated with increasing pH, leading to changes in absorbance or luminescence intensity or lifetime.

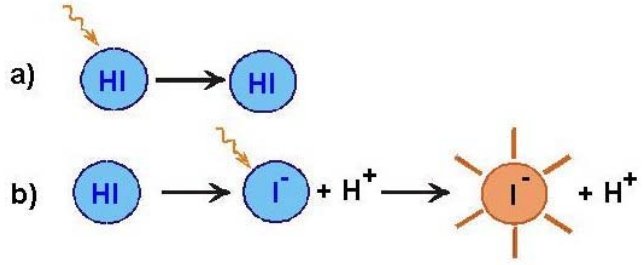

Fig. 1.8. pH sensor based on fluorescence: One form (here: protonated form, a) does not display fluorescence when excited, the other form (here: deprotonated form I^-, b) fluoresces.

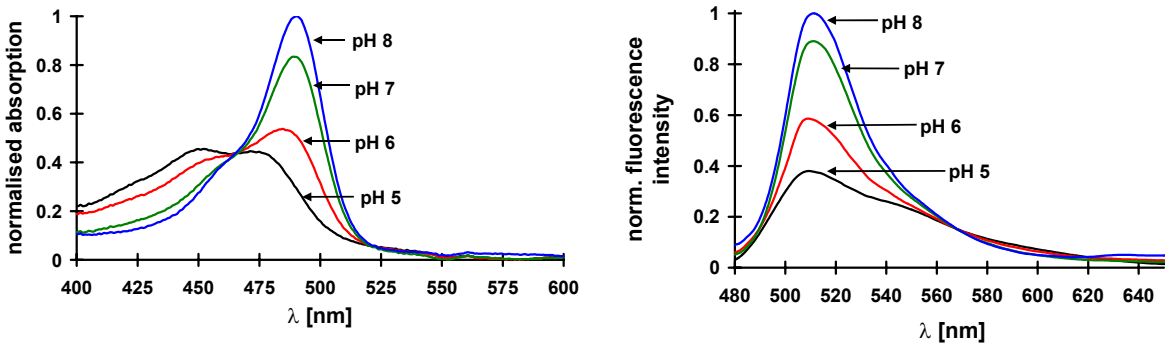

Fig. 1.9. Effect of the pH value on the absorption (left) and emission (right) spectra of the pH indicator fluorescein (c = 10^{-5} M, dissolved in 20 mM phosphate buffer).

Optical pH determinations are evaluated using sigmoidal calibration curves. pH value and dye concentration are connected via the Henderson-Hasselbalch equation for buffer systems:

$$pH = pK_a + \log\frac{a_{A^-}}{a_{HA}} = pK_a + \log\frac{c_{A^-} \cdot f_{A^-}}{c_{HA} \cdot f_{HA}} \qquad \text{eqn. 1.3}$$

where pK_a is the negative logarithm of the dissociation constant K_a, a_{A^-} and a_{HA} the activities, c_{A^-} and c_{HA} the concentrations and f_{A^-} and f_{HA} the activity coefficients of the basic and acidic form, respectively. However, using indicators embedded in a polymer, this equation describes the real response behaviour of the sensor only insufficient due to non-ideal environment. Thus, the empirical Boltzmann equation (eqn. 1.4) for sigmoidal curves is a far better approximation. By solving the equation with respect to the pH value (=x), eqn. 1.4b is obtained, where pH_0 is the point of inflexion and therefore matches the pK_a value, I is the measured intensity, I_{min} and I_{max} are the minimal and maximal values of the sigmoidal curve, and ΔpH is the slope at the point of inflexion:

$$y = \frac{A_1 - A_2}{1 + \exp(\frac{x - x_0}{dx})} + A_2 \qquad \text{eqn. 1.4.a}$$

$$pH = pH_0 + \ln\left(-\frac{I - I_{min}}{I - I_{max}}\right) \cdot \Delta pH \qquad \text{eqn. 1.4b}$$

It is notable that optical methods only detect the concentrations of the dye, whereas the pH value is defined using the activities. This affects the pH determination if the activity coefficients of the dye are changed by sample ingredients (see chapter 2.3.7).

1.3.5. Referencing Methods

To convert the detected signal into the respective analyte concentration, calibration of the sensor is necessary. For oxygen detection, this can easily be done using a two-point calibration with air-saturated water and water deoxygenated with sodium sulphite. Regarding pH measurements, the recording of calibration curves is more labour-intensive due to time-consuming preparation of calibration solutions with a distinct pH and ionic strength. For high throughput screening of a multitude of samples using MTPs, calibration-free sensors are inevitable to save time and effort. Here, calibration of only a few sensor spots per lot instead of calibration of each single sensor can be considered calibration-free. Using optical sensors based on fluorescence, different approaches are possible.

Intensity-based sensing is susceptible to fluctuations in the intensity of the light source as well as the sensitivity of the detector. Furthermore, the thickness of the sensor film varies from well to well, which leads to differing intensities for each well at the same analyte concentration. With single-intensity sensing (e.g. Oxygen BioSensor, OBS, Becton Dickinson [48]), kinetics can be referenced by dividing the actual value by the initial one to reduce the effect of irregular sensor thickness. However, it is not possible to convert this normalised intensities to the analyte concentration without calibration of each single sensor. In contrast, both irregularities in the optical path as well as in the sensor thickness can be eliminated via dual-wavelength measurements using a second, analyte-inert reference dye which is incorporated together with the indicator dye with a constant ratio (e.g. PEBBLES [58, 59], Oxo- and Hydroplate, PreSens [70, 83]). With pH sensors, a second ratiometric referencing method is possible: If the acidic and basic forms both display different fluorescence intensities, the ratio of these two intensities recorded at the respective wavelength can be used for generating a calibration-free sensor (e.g. SNARF, SNAFL; Molecular Probes). Both methods require dyes of suitable spectral characteristics to separate either the excitation or the emission intensities (or both) satisfactorily by the use of adequate filters.

In contrast to intensity measurements, lifetime-based measurements need less effort of sensor composition because these methods are internally referenced. The signal is not dependent on the total intensity and therefore less susceptible to

inhomogeneous indicator distribution, varying thickness of the sensor film, photobleaching, turbidity or coloration of the sample, reflections or variations in the opto-electronic system. Here too, two methods are possible, time-gated and frequency-domain measurement.

For time-gated measurements, several schemata exist. The one used in this work for an optically isolated oxygen sensor (see chapter 2.4.1, page 62), is called RLD (rapid lifetime determination [177]). The emission intensity of the indicator dye is recorded in two windows of a distinct interval (Fig. 1.10).

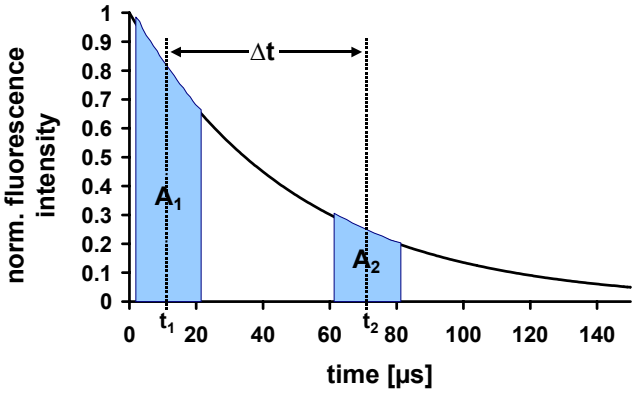

Fig. 1.10. RLD scheme for the optically isolated oxygen sensor used for MTP experiments (see chapter 2.4.1). The emission intensity of the indicator is detected in two separate time gates and can be converted into lifetimes.

The intensities A_1 and A_2 are converted into pseudo-lifetimes τ using eqn. 1.5:

$$\tau = \frac{\Delta t}{\ln(\frac{A_1}{A_2})} \qquad \text{eqn. 1.5.}$$

τ is the lifetime of the excited state of the fluorescent indicator, Δt the time interval between the averages of the integration times t_1 and t_2, and A_1 and A_2 the integrated intensities over this interval. Eqn. 1.4 yields only pseudo-lifetimes for this sensor, because it is only valid for monoexponential decay, which is mostly not given regarding fluorophores in a sensor matrix. Besides, A_1 and A_2 are originally not intensity intervals but intensities measured at distinct times t_1 and t_2. Therefore, this calculation does not yield the true lifetime of the sensor, but is sufficient for a two-point calibration of an oxygen sensor. On closer examination, this method can be defined as referenced as well, because it uses the ratio of two intensities for conversion into a lifetime.

The frequency-domain lifetime detection, which was used for fibre-optic oxygen sensing (see chapter 2.4.2, page 64), records the phase shift $\Delta\theta$ between the sinusoidally modulated excitation light and the emission of the indicator (s. *Fig. 1.11*). The quantity of the phase shift depends on the luminescence lifetime and therefore on the analyte concentration (here: oxygen partial pressure) (s. eqn. 1.6).

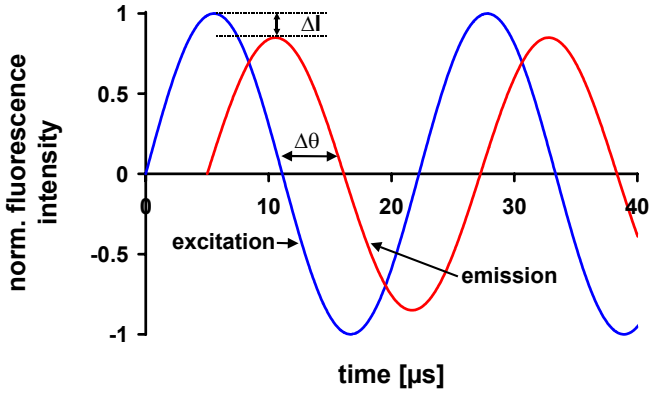

Fig. 1.11. Phase modulation of the excitation light causes a phase shift $\Delta\theta$ between excitation and emission depending on the lifetime of the excited state of the indicator dye. The amplitude of the intensity is decreased by ΔI.

$$\tau = \frac{\tan\theta}{2 \cdot \pi \cdot f_{mod}} \qquad \text{eqn. 1.6}$$

Both methods require preferably long indicator lifetimes in the µs range to lower the requirements for the optical set-up. Unfortunately, only the luminescent oxygen indicators fulfil this demand. However, pH sensors with shorter lifetime can be measured with these methods as well using an inert reference dye with a long lifetime. Thus, the resulting lifetime is a mixture between the short lifetime of the pH indicator and the long one of the reference dye. Changes in lifetime of the short-lived dye can be recorded as changes in the mixed lifetime without need for more sophisticated instrumentation. This method is called dual lifetime referencing (DLR) [178].

1.4. References

1 http://europa.eu.int/comm/environment/chemicals/reach.htm (29.11.2005).

2 *Pseudomonas putida* respiration inhibition test, DIN 38412, part L27: 1992. Deutsche Einheitsverfahren zur Wasser-, Abwasser- und Schlamm-Untersuchung, part VI. Wiley-VCH, Weinheim (2001).

3 OECD Guidelines for the Testing of Chemicals, Section 2: Effects on Biotic Systems, PDF Edition (ISSN 1607-310X). Organisation for Economic Co-operation and Development, Paris.

4 Standards and/or guides of TC 147/SC 5 (Biological methods); http://www.iso.ch/iso/en/stdsdevelopment/tc/tclist/TechnicalCommitteeStandardsListPage.TechnicalCommitteeStandardsList?COMMID=3729 (29.11.2005).

5 European Chemicals Bureau, Part C: Methods for environmental effects, ecotoxicity and environmental fate; http://ecb.jrc.it/testing-methods (29.11.2005).

6 Deutsche Einheitsverfahren zur Wasser-, Abwasser- und Schlamm-Untersuchung, part VI. Wiley-VCH, Weinheim (2001).

7 OECD Guidelines for the Testing of Chemicals, Test No. 203: *Fish Acute Toxicity Test*. (1992).

8 http://www.univ-ubs.fr/ecologie/ecotoxicologie.html (22.12.2005).

9 OECD Guidelines for the Testing of Chemicals, Test No. 202: *Daphnia sp. Acute Immobilisation Test.*

10 OECD Guidelines for the Testing of Chemicals, Test No. 211: *Daphnia magna Reproduction Test.*

11 Radix P, Leonard M, Papantoniou C, Roman G, Saouter E, Gallotti-Schmitt S, Thiebaud H, and Vasseur P. *Comparison of Four Chronic Toxicity Tests Using Algae, Bacteria, and Invertebrates Assessed with Sixteen Chemicals*. (2000). Ecotoxicology and Environmental Safety **47**(2), 186-194.

12 Hegewald E. *New Combinations in the genus Desmodesmus (Chlorophyceae, Scenedesmaceae).* Algological Studies **96**, 1-18 (2000).

13 http://www.sccap.bot.ku.dk/PHOTOS/H_0564.HTM (22.12.2005).

14 http://www.lifesciences.napier.ac.uk/JK/algalweb/selenast-a.jpg (22.12.2005).

15 OECD Guidelines for the Testing of Chemicals, Test No. 201: *Alga Growth Inhibition Test.*

16 Gilbert F, Galgani F, and Cadiou Y. *Rapid assessment of metabolic activity in marine microalgae: Application in ecotoxicological tests and evaluation of water quality.* (1992). Marine Biology **112**, 199-205.

17 *Marine algal growth inhibition test with Skeletonema costatum and Phaeodactylum tricornutum* (ISO 10253:1998). Deutsche Einheitsverfahren zur Wasser-, Abwasser- und Schlamm-Untersuchung, part VI. Wiley-VCH, Weinheim (2001).

18 Serat WF, Budinger FEJr, and Mueller PK. *Evaluation of biological effects of air pollutants by use of luminescent bacteria*. (1965). Journal of Bacteriology **90**(3), 832-833.

19 http://ergo.integratedgenomics.com/Genomes/VFI/vibrio_fischeri.html (22.12.2005)

20 http://microbiology.unh.edu/faculty/Whistler (22.12.2005).

21 Bulich AA. *Use of Luminescent Bacteria for Determining Toxicity in Aquatic Environments,* in: Marking LL and Kimerle RA (eds.): Aquatic Toxicology (1979), American Society for Testing and Materials, Philadelphia, PA, USA 98-106.

22 Cronin MTD and Schultz TW. *Structure-toxicity relationships for three mechanisms of action of toxicity to Vibrio fischeri*. (1998). Ecotoxicology and Environmental Safety **39** (1), 65-69.

23 Fent, K. *Ökotoxikologie* (1998), Thieme, Stuttgart.

24 *Determination of the inhibitory effect of water samples on the light emission of Vibrio fischeri (Luminescent bacteria test)*. ISO 11348-1 to -3: 1998. Deutsche Einheitsverfahren zur Wasser-, Abwasser- und Schlamm-Untersuchung, part VI. Wiley-VCH, Weinheim (2001).

25 Jennings VL, Rayner-Brandes MH, and Bird DJ. *Assessing chemical toxicity with the bioluminescent photobacterium (Vibrio fischeri): a comparison of three commercial systems*. (2001). Water research **35**(14), 3448-3456.

26 Munkittrick KR, Power EA, and Sergy GA. *The relative sensitivity of Microtox, daphnid, rainbow trout, and fathead minnow acute lethality tests*. (1991). Environmental Toxicology and Water Quality **6**(1), 35-62.

27 Calleja MC, Persoone G, and Geladi P. *Comparative acute toxicity of the first 50 multicenter evaluation of in vitro cytotoxicity chemicals to aquatic non-vertebrates*. (1994). Archives of Environmental Contamination and Toxicology **26**(1), 69-78.

28 *Determination of the inhibitory effect of water on the growth of bacteria (photobacterium phosphorum cell multiplication test)*. DIN 38412-37: 1999-04. Deutsche Einheitsverfahren zur Wasser-, Abwasser- und Schlamm-Untersuchung, part VI. Wiley-VCH, Weinheim (2001).

29 OECD Guidelines for the Testing of Chemicals, Test No. 209: *Test for the inhibition of oxygen consumption by activated sludge*. (1984).

30 Freitas dos Santos L, Defrenne L, and Krebs-Brown A. *Comparison of three microbial assay procedures for measuring toxicity of chemical compounds: ToxAlert CellSense and Biolog MT2 microplates*. (2002). Analytica Chimica Acta **456**(1), 41-54.

31 http://www.takenaka.co.jp/takenaka_e/techno/n22_tce/n22_tce.htm (22.12.2005).

32 Barth JAC, Kalin RM, Larkin MJ, Hall JA, and Fitzgerald U. *Isotopic composition of inorganic carbon as an indicator of benzoate degradation by Pseudomonas putida: temperature, growth rate and pH effects*. (2000). Rapid Communications in Mass Spectrometry **14**(15), 1316-1320.

33 International Standard 10712. 1995. Water quality - *Pseudomonas putida* growth inhibition test *(Pseudomonas putida* multiplication inhibition test). in: Deutsche Einheitsverfahren zur Wasser-, Abwasser- und Schlamm-Untersuchung, part VI. Wiley-VCH, Weinheim (2001).

34 http://www.biosource.com/content/literatureContent/PDFs/alamarbluebooklet.pdf

35 Marshall ES, Holdaway KM, Shaw JH, Finlay GJ, Matthews JH, and Baguley BC. *Anticancer drug sensitivity profiles of new and established melanoma cell lines*. (1993). Oncology research **5**(8), 301-309.

36 Mosmann T. *Rapid colorimetric assay for cellular growth and survival: application to proliferation and cytotoxicity assays*. (1983). Journal of immunological methods **65**(1-2), 55-63.

37 Carmichael J, DeGraff WG, Gazdar AF, Minna JD, and Mitchell JB. *Evaluation of a tetrazolium-based semiautomated colorimetric assay: assessment of radiosensitivity*. (1987). Cancer research **47**(4), 943-946.

38 Holmes B, Costas M, Ganner M, On SL, and Stevens M. *Evaluation of Biolog system for identification of some gram-negative bacteria of clinical importance*. (1994). Journal of clinical microbiology **32**(8), 1970-1975.

39 Ahmed SA, Gogal RM, Jr., and Walsh JE. *A new rapid and simple non-radioactive assay to monitor and determine the proliferation of lymphocytes: an alternative to [3H]thymidine incorporation assay*. (1994). Journal of immunological methods **170**(2), 211-224.

40 Collins LA and Franzblau SG. *Microplate Alamar blue assay versus BACTEC 460 system for high-throughput screening of compounds against Mycobacterium tuberculosis and Mycobacterium avium*. (1997). Antimicrobial Agents and Chemotherapy **41**(5), 1004-1009.

41 Kangas L, Gronroos M, and Nieminen AL. *Bioluminescence of cellular ATP: a new method for evaluating cytotoxic agents in vitro*. (1984). Medical biology **62**(6), 338-343.

42 Cree IA. *Luminescence-based cell viability testing*. (1998). Methods in Molecular Biology **102**, 169-177.

43 Hunt L, Jordan M, De Jesus M, and Wurm FM. *GFP-expressing mammalian cells for fast, sensitive, noninvasive cell growth assessment in a kinetic mode*. (1999). Biotechnology and Bioengineering **65**(2), 201-205.

44 Girard P, Jordan M, Tsao M, and Wurm FM. *Small-scale bioreactor system for process development and optimization*. (2001). Biochemical Engineering Journal **7**(2), 117-119.

45 Alderman J, Hynes J, Floyd SM, Kruger J, O'Connor R, and Papkovsky DB. *A low-volume platform for cell-respirometric screening based on quenched-luminescence oxygen sensing*. (2004). Biosensors & Bioelectronics **19**(11), 1529-1535.

46 O'Mahony FC, O'Donovan C, Hynes J, Moore T, Davenport J, and Papkovsky DB. *Optical oxygen microrespirometry as a platform for environmental toxicology and animal model studies*. (2005). Environmental science & technology **39**(13), 5010-5014.

47 O'Riordan TC, Buckley D, Ogurtsov V, O'Connor R, and Papkovsky DB. *A Cell Viability Assay Based on Monitoring Respiration by Optical Oxygen Sensing*. (2000). Analytical Biochemistry **278**(2), 221-227.

48 Wodnicka M, Guarino RD, Hemperly JJ, Timmins MR, Stitt D, and Pitner JB. *Novel fluorescent technology platform for high throughput cytotoxicity and proliferation assays*. (2000). J Biomol Screen **5**(3), 141-152.

49 Guarino RD, Dike LE, Haq TA, Rowley JA, Pitner JB, and Timmins MR. *Method for determining oxygen consumption rates of static cultures from microplate measurements of pericellular dissolved oxygen concentration*. (2004). Biotechnology and Bioengineering **86**(7), 775-787.

50 Deshpande RR, Koch-Kirsch Y, Maas R, John GT, Krause C, and Heinzle E. *Microplates with integrated oxygen sensors for kinetic cell respiration measurement and cytotoxicity testing in primary and secondary cell lines*. (2005). Assay and Drug Development Technologies **3**(3), 299-307.

51 Deshpande RR and Heinzle E. *On-line oxygen uptake rate and culture viability measurement of animal cell culture using microplates with integrated oxygen sensors*. (2004). Biotechnology Letters **26**(9), 763-767.

52 Ritchie JM, Cresser M, and Cotter-Howells J. *Toxicological response of a bioluminescent microbial assay to Zn, Pb and Cu in an artificial soil solution: relationship with total metal concentrations and free ion activities*. (2001). Environmental Pollution (Oxford, United Kingdom) **114**(1), 129-136.

53 Campbell CD, Hird M, Lumsdon DG, and Meeussen JCL. *The effect of EDTA and fulvic acid on Cd, Zn, and Cu toxicity to a bioluminescent construct (pUCD607) of Escherichia coli*. (1999). Chemosphere **40**(3), 319-325.

54 Farre M, Pasini O, Carmen Alonso M, Castillo M, and Barcelo D. *Toxicity assessment of organic pollution in wastewaters using a bacterial biosensor*. (2001). Analytica Chimica Acta **426**(2), 155-165.

55 Farre M and Barcelo D. *Characterization of wastewater toxicity by means of a whole-cell bacterial biosensor, using Pseudomonas putida, in conjunction with chemical analysis*. (2001). Fresenius' Journal of Analytical Chemistry **371**(4), 467-473.

56 Wolfbeis OS*, Fiber Optical Sensors in Analytical and Clinical Chemistry*, In: Schulman, SG (ed.), *Molecular Luminescence Spectroscopy*, 2 (1988) Wiley, NY, USA.

57 Munkholm C, Walt DR, Milanovich FP, and Klainer SM. *Polymer modification of fiber optic chemical sensors as a method of enhancing fluorescence signal for pH measurement*. (1986). Analytical Chemistry **58**(7), 1427-1430.

58 Cao Y, Koo YEL, and Kopelman R. *Poly(decyl methacrylate)-based fluorescent PEBBLE swarm nanosensors for measuring dissolved oxygen in biosamples*. (2004). Analyst (Cambridge, United Kingdom) **129**(8), 745-750.

59 Koo YEL, Cao Y, Kopelman R, Koo SM, Brasuel M, and Philbert MA. *Real-time measurements of dissolved oxygen inside live cells by organically modified silicate fluorescent nanosensors*. (2004). Analytical Chemistry **76**(9), 2498-2505.

60 Hartmann P and Ziegler W. *Lifetime Imaging of Luminescent Oxygen Sensors Based on All-Solid-State Technology*. (1996). Analytical Chemistry **68**(24), 4512-4514.

61 Liebsch G, Klimant I, Frank B, Holst G, and Wolfbeis OS. *Luminescence lifetime imaging of oxygen, pH, and carbon dioxide distribution using optical sensors*. (2000). Applied Spectroscopy **54**(4), 548-559.

62 Bedlek-Anslow JM, Hubner JP, Carroll BF, and Schanze KS. *Micro-heterogeneous Oxygen Response in Luminescence Sensor Films*. (2000). Langmuir **16**(24), 9137-9141.

63 Kellner K, Liebsch G, Klimant I, Wolfbeis OS, Blunk T, Schulz MB, and Gopferich A. *Determination of oxygen gradients in engineered tissue using a fluorescent sensor*. (2002). Biotechnology and Bioengineering **80**(1), 73-83.

64 Babilas P, Liebsch G, Schacht V, Klimant I, Wolfbeis O, Szeimies RM, and Abels C. *In vivo phosphorescence imaging of pO2 using planar oxygen*

sensors. (2005). Microcirculation (Philadelphia, PA, United States) **12**(6), 477-487.

65 Koenig B, Kohls O, Holst G, Glud RN, and Kuehl M. *Fabrication and test of sol-gel based planar oxygen optodes for use in aquatic sediments*. (2005). Marine Chemistry **97**(3-4), 262-276.

66 Watkins AN, Jordan JD, Leighty BD, Ingram JL, Oglesby DM, Development of Next Generation Lifetime PSP Imaging Systems. (2003). Technical report of the NASA Langley Research Center and Swales Aerospace. http://techreports.larc.nasa.gov/ltrs/PDF/2003/mtg/NASA-2003-20iciasf-anw.pdf.

67 Hradil J, Davis C, Mongey K, McDonagh C, and MacCraith BD. *Temperature-corrected pressure-sensitive paint measurements using a single camera and a dual-lifetime approach*. (2002). Measurement Science and Technology **13**(10), 1552-1557.

68 Gouterman M, Callis J, Dalton L, Khalil G, Mebarki Y, Cooper KR, and Grenier M. *Dual luminophor pressure-sensitive paint: III. Application to automotive model testing*. (2004). Measurement Science and Technology **15**(10), 1986-1994.

69 John GT and Heinzle E. *Quantitative screening method for hydrolases in microplates using pH indicators: determination of Kinetic parameters by dynamic pH monitoring*. (2001). Biotechnology and Bioengineering **72**(6), 620-627.

70 John GT, Klimant I, Wittmann C, and Heinzle E. *Integrated optical sensing of dissolved oxygen in microtiter plates: A novel tool for microbial cultivation*. (2003). Biotechnology and Bioengineering **81**(7), 829-836.

71 Hutter B and John GT. *Evaluation of Oxoplate for real-time assessment of antibacterial activities*. (2004). Current Microbiology **48**(1), 57-61.

72 Zanzotto A, Szita N, Boccazzi P, Lessard P, Sinskey AJ, and Jensen KF. *Membrane-aerated microbioreactor for high-throughput bioprocessing*. (2004). Biotechnology and Bioengineering **87**(2), 243-254.

73 http://www.presens.de

74 Middlebrook G, Reggiardo Z, and Tigertt WD. *Automatable radiometric detection of growth of Mycobacterium tuberculosis in selective media*. (1977). American review of respiratory disease **115**(6), 1066-1069.

75 Siddiqi SH, Libonati JP, and Middlebrook G. *Evaluation of a rapid radiometric method for drug susceptibility testing of Mycobacterium tuberculosis*. (1981). Journal of clinical microbiology **13**(5), 908-912.

76 Rastogi N, Goh KS, Berchel M, and Bryskier A. *Activity of rifapentine and its metabolite 25-O-desacetylrifapentine compared with rifampicin and rifabutin against Mycobacterium tuberculosis, Mycobacterium africanum, Mycobacterium bovis and M. bovis BCG*. (2000). Journal of antimicrobial chemotherapy **46**(4), 565-570.

77 Van Beelen P and Fleuren-Kemila AK. *A comparison between toxicity tests using single species and a microbial process*. (1999). Chemosphere **38**(14), 3277-3290.

78 Ardito F, Posteraro B, Sanguinetti M, Zanetti S, and Fadda G. *Evaluation of BACTEC mycobacteria growth indicator tube (MGIT 960) automated system for drug susceptibility testing of mycobacterium tuberculosis*. (2001). Journal of clinical microbiology **39**(12), 4440-4444.

79 Thorpe TC, Wilson ML, Turner JE, DiGuiseppi JL, Willert M, Mirrett S, and Reller LB. *BacT/Alert: an automated colorimetric microbial detection system*. (1990). Journal of clinical microbiology **28**(7), 1608-1612.

80 Bringmann G and Kuehn R. *Comparative results of the damaging effects of water pollutants against bacteria (Pseudomonas putida) and blue algae (Microcystis aeruginosa)*. (1976). GWF, Wasser/Abwasser **117**(9), 410-413.

81 Schmitz RPH, Eisentrager A, and Dott W. *Miniaturized kinetic growth inhibition assays with Vibrio fischeri and Pseudomonas putida (application, validation and comparison)*. (1998). Journal of Microbiological Methods **31**(3), 159-166.

82 Ge X, Kostov Y, and Rao G. *Low-cost noninvasive optical CO2 sensing system for fermentation and cell culture*. (2004). Biotechnology and Bioengineering **89**(3), 329-334.

83 Arain S, John GT, Krause C, Gerlach J, Wolfbeis OS and Klimant I. *Characterization of microtiterplates with integrated optical sensors for oxygen*

and pH, and their applications to enzyme activity screening, respirometry, and toxicological assays. (2005). Sensors and Actuators B., in press.

84 Duncan PA, Gallagher S, McKerral L, and Tsai PK. *Assessing the viability of a clumpy mnn9 strain of Saccharomyces cerevisiae used in the manufacture of recombinant pharmaceutical proteins*. (2004). Journal of Industrial Microbiology & Biotechnology **31**(11), 500-506.

85 Garland JL, Roberts MS, Levine LH, and Mills AL. *Community-level physiological profiling performed with an oxygen-sensitive fluorophore in a microtiter plate*. (2003). Applied and Environmental Microbiology **69**(5), 2994-2998.

86 Arain S, Klimant I. *Toxicological Screening Test in Microplates equipped with optical sensors for pH and pO2.* (2005), in preperation.

87 Amao Y, Ishikawa Y, and Okura I. *Green luminescent iridium(III) complex immobilized in fluoropolymer film as optical oxygen-sensing material*. (2001). Analytica Chimica Acta **445**(2), 177-182.

88 Huch R, Lübbers DW, Huch A, *Quantitative Continuous Measurement of Partial Oxygen Pressure on the Skin of Adults and New Born Babies* (1972), Pflügers Arch. 337, 185.

89 Peterson JI, Fitzgerald RV, and Buckhold DK. *Fiber-optic probe for in vivo measurement of oxygen partial pressure*. (1984). Analytical Chemistry **56**(1), 62-67.

90 Gupta A and Rao G. *A study of oxygen transfer in shake flasks using a non-invasive oxygen sensor*. (2003). Biotechnology and Bioengineering **84**(3), 351-358.

91 Wittmann C, Kim HM, John G, and Heinzle E. *Characterization and application of an optical sensor for quantification of dissolved O2 in shake-flasks*. (2003). Biotechnology Letters **25**(5), 377-380.

92 Tolosa L, Kostov Y, Harms P, and Rao G. *Noninvasive measurement of dissolved oxygen in shake flasks*. (2002). Biotechnology and Bioengineering **80**(5), 594-597.

93 Koneke R, Comte A, Jurgens H, Kohls O, Lam H, and Scheper T. *Fiber optic oxygen sensors for use in biotechnology, environmental, and food industries [Reprint]*. (1999). Chemical Engineering & Technology **22**(8), 666-671.

94 Kroneis HW and Marsoner HJ. *A fluorescence-based sterilizable oxygen probe for use in bioreactors*. (1983). Sensors and Actuators **4**(4), 587-592.

95 Twork JV, Yacnych AM, *Sensors in Bioprocess Control*. (1990). Marcel Dekker, NY, USA.

96 Del Bianco A, Baldini F, Bacci M, Klimant I, and Wolfbeis OS. *A new kind of oxygen-sensitive transducer based on an immobilized metallo-organic compound*. (1993). Sensors and Actuators, B: Chemical **B11**(1-3), 347-350.

97 Davies PW and Brink F, Jr. *Microelectrodes for measuring the local oxygen tension in animal tissues*. (1942). Review of Scientific Instruments **13**, 524-533.

98 Clark LC, Jr. *Polarographic cell*. (1956) US Pat., 2 913 386.

99 Trettnak W, Gruber W, Reininger F, and Klimant I. *Recent progress in optical oxygen sensor instrumentation*. (1995). Sensors and Actuators, B: Chemical **B29**(1-3), 219-225.

100 O'Keeffe G, MacCraith BD, McEvoy AK, McDonagh CM, and McGilp JF. *Development of a LED-based phase fluorimetric oxygen sensor using evanescent wave excitation of a sol-gel immobilized dye*. (1995). Sensors and Actuators, B: Chemical **B29**(1-3), 226-230.

101 Whalen WJ, Riley J, and Nair P. *A microelectrode for measuring intracellular PO2*. (1967). Journal of applied physiology **23**(5), 798-801.

102 Revsbech NP. *An oxygen microsensor with a guard cathode*. (1989). Limnology and Oceanography **34**(2), 474-478.

103 Silver IA. *Some observations on the cerebral cortex with an ultramicro, membrane-covered, oxygen electrode*. (1965). Medical electronics & biological engineering **3**(4), 377-387.

104 Halpern HJ, Yu C, Peric M, Barth ED, Karczmar GS, River JN, Grdina DJ, and Teicher BA. *Measurement of differences in pO2 in response to perfluorocarbon/carbogen in FSa and NFSa murine fibrosarcomas with low-frequency electron paramagnetic resonance oximetry*. (1996). Radiation Research **145**(5), 610-618.

105 Tzoris A, Fernandez-Perez V, and Hall EAH. *Direct toxicity assessment with a mini portable respirometer*. (2005). Sensors and Actuators, B: Chemical **B105**(1), 39-49.

106 Tzoris A, Cane D, Maynard P, and Hall EAH. *Tuning the parameters for fast respirometry*. (2002). Analytica Chimica Acta **460**(2), 257-270.

107 Klimant I, Meyer V, and Kuhl M. *Fiber-optic oxygen microsensors, a new tool in aquatic biology*. (1995). Limnology and Oceanography **40**(6), 1159-1165.

108 Klimant I, Kuehl M, Glud RN, and Holst G. *Optical measurement of oxygen and temperature in microscale: strategies and biological applications*. (1997). Sensors and Actuators, B: Chemical **B38**(1-3), 29-37.

109 Xu H, Aylott JW, Kopelman R, Miller TJ, and Philbert MA. *A real-time ratiometric method for the determination of molecular oxygen inside living cells using sol-gel-based spherical optical nanosensors with applications to rat C6 glioma*. (2001). Analytical Chemistry **73**(17), 4124-4133.

110 McDonagh C, MacCraith BD, and McEvoy AK. *Tailoring of Sol-Gel Films for Optical Sensing of Oxygen in Gas and Aqueous Phase*. (1998). Analytical Chemistry **70**(1), 45-50.

111 Baldini F, Bacci M, Cosi F, and Del Bianco A. *Absorption-based optical-fiber oxygen sensor*. (1992). Sensors and Actuators, B: Chemical **B7**(1-3), 752-757.

112 Zhujun Z and Seitz WR. *Optical sensor for oxygen based on immobilized hemoglobin*. (1986). Analytical Chemistry **58**(1), 220-222.

113 Freeman TM and Seitz WR. *Oxygen probe based on tetrakis(alkylamino)ethylene chemiluminescence*. (1981). Analytical Chemistry **53**(1), 98-102.

114 Bacon JR and Demas JN. *Determination of oxygen concentrations by luminescence quenching of a polymer-immobilized transition-metal complex*. (1987). Analytical Chemistry **59**(23), 2780-2785.

115 Wolfbeis OS and Carlini FM. *Long-wavelength fluorescent indicators for the determination of oxygen partial pressures*. (1984). Analytica Chimica Acta **160**, 301-304.

116 Luebbers DW and Opitz N. *Optical fluorescence sensors for continuous measurement of chemical concentrations in biological systems*. (1983). Sensors and Actuators **4**(4), 641-654.

117 Wolfbeis OS, Posch HE, and Kroneis HW. *Fiber optical fluorosensor for determination of halothane and or oxygen*. (1985). Analytical Chemistry **57**(13), 2556-2561.

118 Wolfbeis OS, Fuerlinger E, Kroneis H, and Marsoner H. *Fluorimetric analysis. 1. A study on fluorescent indicators for measuring near neutral (\"physiological\") pH values*. (1983). Fresenius' Zeitschrift fuer Analytische Chemie **314**(2), 119-124.

119 Kautsky H. *Quenching of luminescence by oxygen*. (1939). Transactions of the Faraday Society **35** , 216-219.

120 Bergman I. *Rapid-response atmospheric oxygen monitor based on fluorescence quenching*. (1968). Nature **218**, 396.

121 Gehrich JL, Lübbers DW, Opitz N, Hansmann DR, Miller WW, Tusa JK, and Yafuso M. *Optical fluorescence and its application to an intravascular blood gas monitoring system*. (1986). IEEE transactions on bio-medical engineering **33**(2), 117-132.

122 Mohr GJ and Wolfbeis OS. *Optical sensing of anions via polarity-sensitive dyes: a bulk sensor membrane for nitrate*. (1995). Analytica Chimica Acta **316**(2), 239-246.

123 Vaughan AA, Baron MG, and Narayanaswamy R. *Optical ammonia sensing films based on an immobilized metalloporphyrin*. (1996). Analytical Communications **33**(11), 393-396.

124 Vanderkooi JM, Wilson DF. *A New Method for measuring oxygen concentration of Biological Systems.* (1986). In: Longmuir IS, *Advances in Experimental Medicine and Biology: Oxygen transport to tissue VIII*, **200**, Plenum Press, NY, USA, 189-193.

125 Lippitsch ME, Pusterhofer J, Leiner MJP, and Wolfbeis OS. *Fiber-optic oxygen sensor with the fluorescence decay time as the information carrier*. (1988). Analytica Chimica Acta **205**(1-2), 1-6.

126 McMurray HN, Douglas P, Busa C, and Garley MS. *Oxygen quenching of tris(2,2'-bipyridine)ruthenium(II) complexes in thin organic films*. (1994). Journal of Photochemistry and Photobiology, A: Chemistry **80**(1-3), 283-288.

127 Bambot SB, Holavanahali R, Lakowicz JR, Carter GM, and Rao G. *Phase fluorometric sterilizable optical oxygen sensor*. (1994). Biotechnology and Bioengineering **43**(11), 1139-1145.

128 Wang XF, Periasamy A, Wodnicki P, Gordon GW, and Herman B. *Time-resolved fluorescence lifetime imaging microscopy: Instrumentation and biomedical applications*. (1996). Chemical Analysis (New York) **137**(Fluorescence Imaging Spectroscopy and Microscopy), 313-350.

129 Konig K, Boehme S, Leclerc N, and Ahuja R. *Time-gated autofluorescence microscopy of motile green microalga in an optical trap*. (1998). Cellular and Molecular Biology (Paris) **44**(5), 763-770.

130 Gadella TWJ, Jr., Van Hoek A, and Visser AJWG. *Construction and characterization of a frequency-domain fluorescence lifetime imaging microscopy system*. (1997). Journal of Fluorescence **7**(1), 35-43.

131 Morgan CG, Mitchell AC, Murray JG, and Wall EJ. *New approaches to lifetime-resolved luminescence imaging*. (1997). Journal of Fluorescence **7**(1), 65-73.

132 Mills A and Lepre A. *Controlling the response characteristics of luminescent porphyrin plastic film sensors for oxygen*. (1997). Analytical Chemistry **69**(22), 4653-4659.

133 McEvoy AK, McDonagh CM, and MacCraith BD. *Dissolved oxygen sensor based on fluorescence quenching of oxygen-sensitive ruthenium complexes immobilized in sol-gel-derived porous silica coatings*. (1996). Analyst (Cambridge, United Kingdom) **121**(6), 785-788.

134 Klimant I, Ruckruh F, Liebsch G, Stangelmayer A, and Wolfbeis OS. *Fast response oxygen micro-optodes based on novel soluble ormosil glasses*. (1999). Mikrochimica Acta **131**(1-2), 35-46.

135 Cox ME and Dunn B. *Detection of oxygen by fluorescence quenching*. (1985). Applied Optics **24**(14), 2114-2120.

136 Wolfbeis OS, Offenbacher H, Kroneis H, and Marsoner H. *A fast responding fluorescence sensor for oxygen. (Fluorometric analysis). IX)*. (1984). Mikrochimica Acta **1**(1-2), 153-158.

137 Hartmann P, Leiner MJP, and Lippitsch ME. *Luminescence Quenching Behavior of an Oxygen Sensor Based on a Ru(II) Complex Dissolved in Polystyrene*. (1995). Analytical Chemistry **67**(1), 88-93.

138 Holst G, Kuehl M, and Klimant I. *A novel measuring system for oxygen microoptodes based on a phase modulation technique* . (1995). Proceedings of SPIE-The International Society for Optical Engineering **2508**(Chemical, Biochemical, and Environmental Fiber Sensors VII), 387-398.

139 Gruber W, Klimant I, and Wolfbeis OS. *Instrumentation for optical measurement of dissolved oxygen based on solid state technology*. (1993). Proceedings of SPIE-The International Society for Optical Engineering **1885**(Proceedings of Advances in Fluorescence Sensing Technology, 1993), 448-457.

140 Wolfbeis OS, Leiner MJP, and Posch HE. *A new sensing material for optical oxygen measurement, with the indicator embedded in an aqueous phase*. (1987). Mikrochimica Acta **3**(5-6), 359-366.

141 Klimant I, Belser P, and Wolfbeis OS. *Novel metal-organic ruthenium(II) diimine complexes for use as long-wave excitable luminescent oxygen probes*. (1994). Talanta **41**(6), 985-991.

142 Xu W, Kneas KA, Demas JN, and DeGraff BA. *Oxygen Sensors Based on Luminescence Quenching of Metal Complexes: Osmium Complexes Suitable for Laser Diode Excitation*. (1996). Analytical Chemistry **68**(15), 2605-2609.

143 Amao Y. *Probes and Polymers for Optical Sensing of Oxygen*. (2003). Microchimica Acta **143**(1), 1-12.

144 Di Marco G, Lanza M, Mamo A, Stefio I, Di Pietro C, Romeo G, and Campagna S. *Luminescent Mononuclear and Dinuclear Iridium(III) Cyclometalated Complexes Immobilized in a Polymeric Matrix as Solid-State Oxygen Sensors*. (1998). Analytical Chemistry **70**(23), 5019-5023.

145 Papkovsky DB, et al. *Phosphorescent Polymer Films for Optical Oxygen Sensors*. (1992). Biosensors & Bioilectronics **7**, 199-206.

146 Papkovsky DB. *New oxygen sensors and their application to biosensing*. (1995). Sensors and Actuators, B: Chemical **B29**(1-3), 213-218.

147 Lee SK and Okura I. *Photostable optical oxygen sensing material: platinum tetrakis(pentafluorophenyl)porphyrin immobilized in polystyrene*. (1997). Analytical Communications **34** (6), 185-188.

148 Hartmann P and Trettnak W. *Effects of Polymer Matrixes on Calibration Functions of Luminescent Oxygen Sensors Based on Porphyrin Ketone Complexes*. (1996). Analytical Chemistry **68**(15), 2615-2620.

149 Papkovsky DB, Ponomarev GV, Trettnak W, and O'Leary P. *Phosphorescent Complexes of Porphyrin Ketones: Optical Properties and Application to Oxygen Sensing*. (1995). Analytical Chemistry **67**(22), 4112-4117.

150 Lehmann M, Wolf B. *Simultaneous measurement fo cellular respiration and acidification with a single CMOS ISFET.* (2001) Biosensors and Bioelectronics **16**, 195-203.

151 Wolfbeis OS, *Fiber Optical Sensors in Analytical and Clinical Chemistry*, In: Schulman SG (ed.) *Molecular Luminescence Spectroscopy*, 2, Wiley, NY, USA (1988).

152 Peterson JI, Goldstein SR, Fitzgerald RV, and Buckhold DK. *Fiber optic pH probe for physiological use*. (1980). Analytical Chemistry **52**(6), 864-869.

153 Kirkbright GF, Narayanaswamy R, and Welti NA. *Fiber-optic pH probe based on the use of an immobilized colorimetric indicator*. (1984). Analyst (Cambridge, United Kingdom) **109**(8), 1025-1028.

154 Kosch U, Klimant I, Werner T, and Wolfbeis OS. *Strategies To Design pH Optodes with Luminescence Decay Times in the Microsecond Time Regime*. (1998). Analytical Chemistry **70**(18), 3892-3897.

155 Galster H. *pH-Messung*. VCH, Weinheim (1990).

156 Saari LA and Seitz WR. *pH sensor based on immobilized fluoresceinamine*. (1982). Analytical Chemistry **54**(4), 821-823.

157 Fürlinger EA, *Spectroscopic Study on Fluorescent pH Indicators and their Immobilization on Polymeric Supports*. Dissertation, KF-University of Graz (1982).

158 Wolfbeis OS (ed.), *Fiber Optic Chemical Sensors & Biosensors*, 1& 2, CRC Press, Boca Raton, Florida (1991).

159 Posch HE, Leiner MJP, and Wolfbeis OS. *Towards a gastric pH-sensor: an optrode for the pH 0-7 range*. (1989). Fresenius' Zeitschrift fuer Analytische Chemie **334**(2), 162-165.

160 Bassnett S, Reinisch L, and Beebe DC. *Intracellular pH measurement using single excitation-dual emission fluorescence ratios*. (1990). American journal of physiology **258**(1 Pt 1), C171-C178.

161 Whitaker JE, Haugland RP, and Prendergast FG. *Spectral and photophysical studies of benzo[c]xanthene dyes: dual emission pH sensors*. (1991). Analytical Biochemistry **194**(2), 330-344.

162 Gafni A and Brand L. *Excited state proton transfer reactions of acridine studied by nanosecond fluorometry*. (1978). Chemical Physics Letters **58**(3), 346-350.

163 Laws WR and Brand L. *Analysis of two-state excited-state reactions. The fluorescence decay of 2-naphthol*. (1979). Journal of Physical Chemistry **83**(7), 795-802.

164 Lakowicz JR and Balter A. *Detection of the reversibility of an excited-state reaction by phase-modulation fluorometry*. (1982). Chemical Physics Letters **92**(2), 117-121.

165 Cajlakovic M, Lobnik A, and Werner T. *Stability of new optical pH sensing material based on cross-linked poly(vinyl alcohol) copolymer*. (2002). Analytica Chimica Acta **455**(2), 207-213.

166 Lobnik A, Oehme I, Murkovic I, and Wolfbeis OS. *pH optical sensors based on sol-gels. Chemical doping versus covalent immobilization*. (1998). Analytica Chimica Acta **367**(1-3), 159-165.

167 Boutin P, Mugnier J, and Valeur B. *A fast-responding optical pH sensor based on the fluorescence of eosin trapped in a TiO2 Sol-Gel thin film*. (1997). Journal of Fluorescence **7**(1, Suppl.), 215S-218S.

168 Kermis HR, Kostov Y, and Rao G. *Rapid method for the preparation of a robust optical pH sensor*. (2003). Analyst (Cambridge, United Kingdom) **128**(9), 1181-1186.

169 Nivens DA, Schiza MV, and Angel SM. *Multilayer sol-gel membranes for optical sensing applications: single layer pH and dual layer CO2 and NH3 sensors*. (2002). Talanta **58**(3), 543-550.

170 Brasselet S and Moerner WE. *Fluorescence behavior of single-molecule pH-sensors*. (2000). Single Molecules **1**(1), 17-23.

171 Michael KL, Taylor LC, and Walt DR. *A Far-Field-Viewing Sensor for Making Analytical Measurements in Remote Locations*. (1999). Analytical Chemistry **71**(14), 2766-2773.

172 Ji J and Rosenzweig Z. *Fiber optic pH/Ca2+ fluorescence microsensor based on spectral processing of sensing signals*. (1999). Analytica Chimica Acta **397**(1-3), 93-102.

173 Ferguson JA, Healey BG, Bronk KS, Barnard SM, and Walt DR. *Simultaneous monitoring of pH, CO2 and O2 using an optical imaging fiber*. (1997). Analytica Chimica Acta **340**(1-3), 123-131.

174 Grant SA and Glass RS. *A sol-gel based fiber optic sensor for local blood pH measurements*. (1997). Sensors and Actuators, B: Chemical **B45**(1), 35-42.

175 Thompson RB and Lakowicz JR. *Fiber optic pH sensor based on phase fluorescence lifetimes*. (1993). Analytical Chemistry **65**(7), 853-856.

176 Lakowicz JR, Gryczynski I, Gryczynski Z, and Dattelbaum JD. *Anisotropy-Based Sensing with Reference Fluorophores*. (1999). Analytical Biochemistry **267**(2), 397-405.

177 Ballew RM and Demas JN. *An error analysis of the rapid lifetime determination method for the evaluation of single exponential decays*. (1989). Analytical Chemistry **61**(1), 30-33.

178 Klimant I, Huber C, Liebsch G, Neurauter G, Stangelmayer A, and Wolfbeis OS. *Dual Lifetime Referencing (DLR) - a new scheme for converting fluorescence intensity into a frequency-domain or time-domain information*. (2001). Springer Series on Fluorescence **1** (New Trends in Fluorescence Spectroscopy), 257-274.

2. Sensors

2.1. Introduction

Microtiterplates (MTPs) are simple and efficient tools in clinical routine diagnostic and high-throughput screening applications. Introducing optical sensor technology into the MTP format paves the way for new applications in the field of enzyme activity screening or detection of the respiratory activity of different types of cells [1 - 10]. Two different schemes to combine optical sensors and MTP assays are possible. In the first, the indicator is dissolved or suspended in the sample [1-4], while in the second it is embedded in a polymer matrix, thus forming a thin film at the bottom of the MTP well [5 - 10].

Both approaches have specific advantages and suffer from certain limitations. By using dissolved indicators (or dispersed nanospheres with integrated sensors), the detected parameter represents an average over the whole sample volume. Thus, heterogeneities of the analyte concentration, which are often inevitable in MTP assays due to incomplete mixing [11] or gas exchange with the environment, are not taken into account. This can be critical in cases of sensing oxygen because of oxygen diffusion into the sample. As a result, the surface regions of solutions consuming oxygen at a fast rate will be more oxygenated than the sample located on the bottom. Furthermore, a dissolved indicator often involves other disadvantages like cumbersome handling, inaccurate dispensing, or inhibition if not toxicity towards sample components. On the other hand, dissolved indicators warrant fast response and flexibility in the MTP format.

When using an indicator dye immobilised in a polymer, several demands have to be fulfilled: Thin sensor layers are preferable to realise short response times which permit on-line detection of the analyte. An additional polymer foil (acting as sensor support [5]) should be avoided in order to prevent long response times and complication of the process of fabrication. Small amounts of sensor materials and simple fabrication keep the costs low, which is important for high-throughput applications. Internal referencing of the sensor signal can compensate for varying

thicknesses of the sensor spot, resulting in good reproducibility of the signal. Optimally, calibration-free sensors can be used.

In this chapter, MTPs equipped with optical chemical sensors for pH and oxygen are described which fulfil the above demands. The sensors comprise a fluorescent indicator dye embedded in a polymer together with a reference dye. A solution of the sensor materials in a solvent is placed in the wells of a 96-well MTP using a pipetting robot, generating a thin polymer layer after evaporation of the solvent. The sensor-coated MTPs are fully characterised.

Furthermore, oxygen-sensitive, fibre-optic micro- and minisensors and a sensor dish reader for read-out of oxygen-sensitive spots are described. These sensors were used for comparative experiments of the *P. putida* respiration inhibition test in glass vessels (see chapter 4).

2.2. Oxygen Sensor Embedded in Microtiterplates (OxoPlate OP96U)

2.2.1. Experimental Part

The oxygen-sensitive MTPs (OxoPlate OP96U) were obtained from PreSens Precision Sensing GmbH. For characterisation of the sensors, doubly distilled water was used for the calibration value of 100 % air saturation (a.s.) and a solution of 1 % sodium sulphite (Merck) for 0 % a.s. Experiments were performed at 30 °C unless noted otherwise.

The spectral properties of the sensors were recorded with an Aminco luminescence spectrometer AB2 (from Thermo Electron; www.thermo.com) under aerated and deaerated conditions. The MTP assays were performed with a MTP reader Fluoroskan Ascent (Thermo Electron) except for the investigation of the effects of different solvents which were determined with the Fluostar Optima (BMG Labtech). The response time of the sensor was detected by adding 180 µL of a sodium sulphite solution to 20 µL of air-saturated water with a dispenser. The same test was performed using a commercial oxygen-sensitive MTP, the BD™ Oxygen Biosensor System (OBS; Becton Dickinson). Data on resolution, accuracy and drift per hour were obtained with air-saturated, distilled water.

Cross-sensitivities of the sensor signal towards temperature and different organic solvents were investigated using air-saturated water and sulphite solution. The stability of the sensor towards different organic solvents was tested by applying various concentrations of dimethylsulfoxide (DMSO), dimethylformamide (DMF), acetone, tetrahydrofurane (THF; Carl Roth), ethanol (EtOH; Sigma-Aldrich) and methanol (MeOH; Sigma-Aldrich) in water to the oxygen-sensitive MTP for 48 h. For the measurement of the cross-sensitivity towards ingredients of bacterial culture media, water solutions containing the respective amount of ingredient were prepared (s. Table 2.1). All ingredients were purchased from Sigma-Aldrich. 0 % air saturation were achieved by saturating the solutions with nitrogen and applying them to the MTP under a nitrogen atmosphere, using an oxygen-impermeable poly-ethylene terephthalate (PET) foil (Greiner) as plate sealing.

Table 2.1 Concentrations of substances used for the investigation of the cross-sensitivity of the sensor-coated MTPs towards widely used ingredients of bacterial media.

Ingredient	concentration [g/L]
glucose	20
beef extract	10
yeast extract	5
amino acids	0.5
bile	1.5
bactotrypton	10
EC broth	34.2
AC broth	37
riboflavin	0.0004

2.2.2. Sensor Composition

The oxygen sensor is based on the use of the luminescent probe Pt(II)-pentafluorophenylporphyrine. It is incorporated in hydrophobic, oxygen-permeable particles. The particles also contain sulforhodamine B as a reference fluorophore. Incorporating both luminophores in the same particle guarantees for constant ratios and allows for internal referencing of the fluorescence intensities of the two dyes.

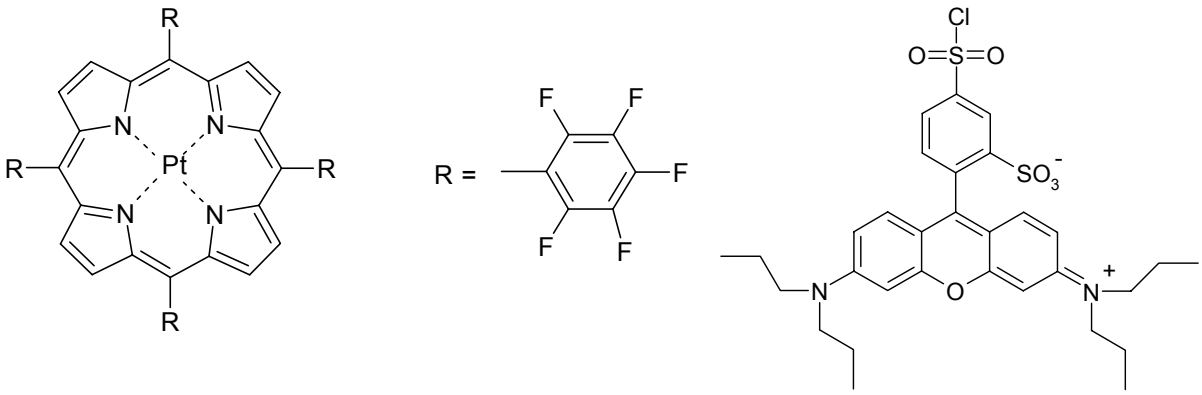

Fig. 2.1. Structure formula of the oxygen indicator Pt(II)meso-tetra(pentafluorophenyl) porphine and the reference dye sulphorhodamine B (chloride) used in the oxygen sensor OxoPlate.

The oxygen-sensitive microspheres are dispersed in a hydrogel matrix. The sensor layer has a thickness of about 10 µm and is fixed at the bottom of each well of a round bottom 96-well plate.

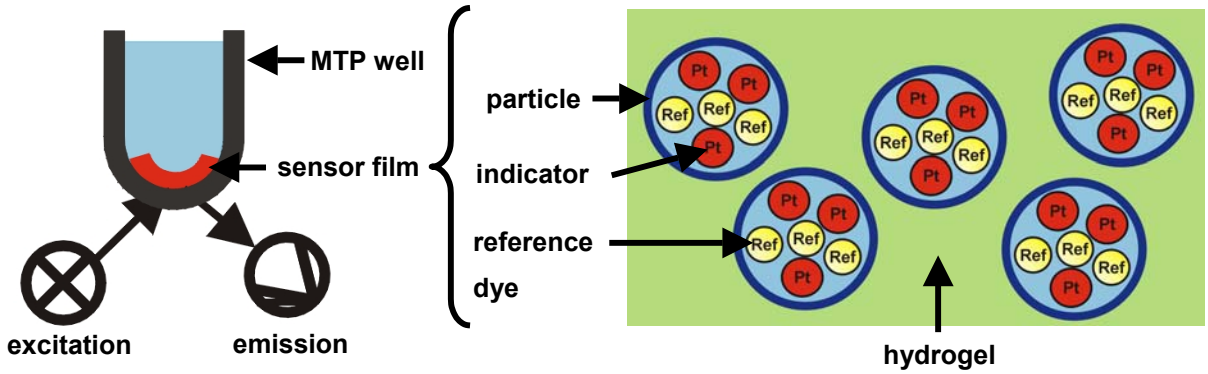

Fig. 2.2. Left: Scheme of a sensor-coated MTP: The sensor film is embedded at the bottom of a round-bottom MTP well. Excitation and detection of the emission of the fluorescent dye are performed from the bottom; Right: Both indicator and reference dye are incorporated in oxygen-permeable microsphere embedded in a hydrogel matrix.

The Stern-Volmer plot via intensities displays an almost linear behaviour. Therefore, the non-modified Stern-Volmer equation (see eqn. 1.1) has been used for calculating the oxygen content pO_2 from the referenced fluorescence intensities.

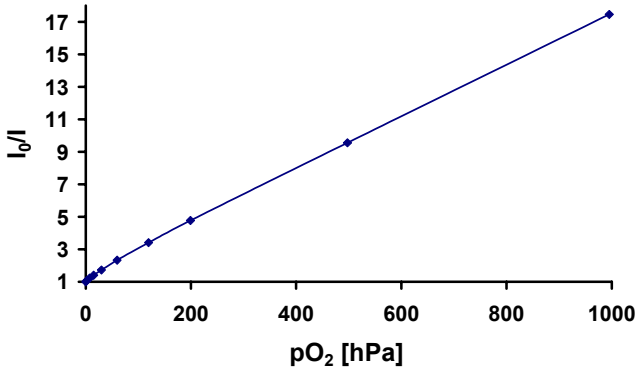

Fig. 2.3. Stern-Volmer plot of the oxygen sensor OxoPlate. The intensity plot is linear over a wide range.

2.2.3. Spectral Properties

The indicator shows two absorbance maxima at 508 nm and 540 nm, respectively, the reference dye one at 565 nm. Both the indicator and the reference dye can be excited at the same wavelength (544 nm). The indicator emits around 650 nm, whereas the reference dye has an emission maximum at 575 nm. Standard emission filters of 650 nm (indicator) and 590 nm (reference dye) were used for the MTP measurements. Fig. 2.4 shows the spectral properties of the oxygen sensor.

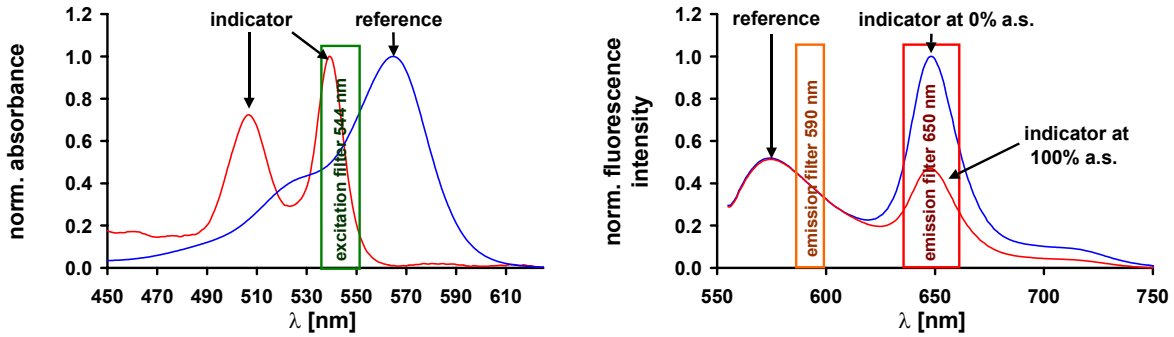

Fig. 2.4. Left: Absorption spectra of the indicator (PtTFPP in hydrogel) and reference dye (sulphorhodamine B in water). Right: Emission spectrum of the sensor (exc. at 544 nm). Included are the respective filters used for excitation and emission.

2.2.4. Response Time

The response times of the oxygen sensor OxoPlate and, for comparison, of the commercially available oxygen-sensitive MTP BD™ Oxygen Biosensor System (OBS) [9] were investigated. The response time (t_{90}) of the OxoPlate is found to be less than 10 s, whereas the t_{90} of the OBS exceeds 12 min (s. Fig. 2.5). The much smaller response time of the OxoPlate results from the small thickness of the sensor polymer film: While the OxoPlate has a thickness of only 10 µm, the estimated thickness of the OBS is more than 200 µm. Furthermore, the OBS uses polysiloxane as the polymer matrix, which serves as an oxygen reservoir due to its high solubility for oxygen [12]. The fast response time of the OxoPlate allows for the detection of true kinetic parameters such as enzyme or respiratory activities, whereas the slow response of the OBS limits the application to slow kinetics.

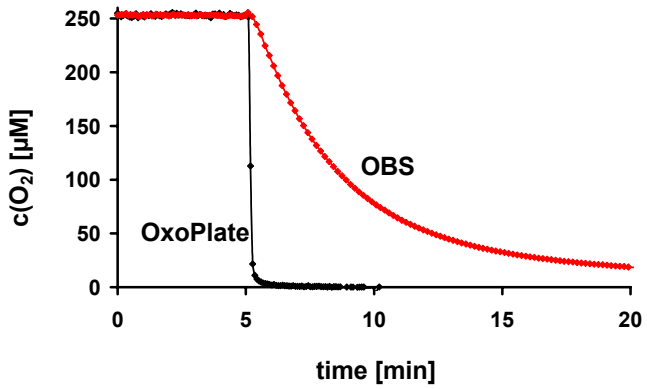

Fig. 2.5. Response times (t_{90}) of the oxygen-sensitive OxoPlate and the OBS. The hydrogel-based OxoPlate sensor responses in only a few seconds, whereas the response time of the silicone-based OBS system is several minutes.

2.2.5. Figures of Merit

Both the resolution and the accuracy depend on the oxygen content and are acceptable for most screening applications. The resolution is defined as the average over the standard deviations of 8 wells considering the last 5 data points of a 18 min kinetics. The accuracy is defined as the maximum deviation between the extremes and the average value of the 8 wells (considering only the last data points of the kinetic). The accuracy of the OxoPlate is better than 3 % air saturation (a.s.), the

resolution and drift per hour even better than 1 % a.s. (s. Table 2.2). Doubly distilled water (100 % a.s.) was chosen as the sample because these figures of merit depend on pO_2. At lower oxygen concentration, even better resolution and accuracy are achieved. Because of the high reproducibility of the signals, it is sufficient to calibrate only a few wells per MTP instead of calibrating each sensor spot. This feature makes the sensor applicable for high-throughput screening. A 2-point calibration at 0 % a.s and 100 % a.s. is sufficient to calculate the oxygen content from the measured intensities using the Stern-Volmer equation.

Table 2.2. Figures of merit of the oxygen sensor.

	[% a.s.]*	[µM]
Analytical range	0-150	0-380
Resolution (at 37°C)	up to 1	up to 2.5
Accuracy (at 37°C)	up to 3	up to 7.6
drift per hour	< 1	< 2.5

* % air saturation

2.2.6. Effect of Temperature

The signal of optical oxygen sensors is significantly influenced by temperature. Temperature not only affects the properties of the sensor (overall quenching constant and luminescence decay time of the indicator), but also the solubility of oxygen in the sample. Fig. 2.6 shows the temperature behaviour of the oxygen sensor. The fluorescence intensities are converted into oxygen concentrations $c(O_2)$ using the standard calibration values at 30 °C. Table 2.3 shows the deviations $\Delta c(O_2)$ between the oxygen concentrations calculated with the calibration points recorded at the respective temperature and at the reference temperature of 30 °C. In contrast to the low deviations at 0 % a.s., the deviations at 100 % a.s. are quite significant. This is caused by the fact that all temperature effects influence the signal in the same direction. Increasing temperature drops the luminescence decay time, increases the overall quenching constant and lowers the solubility of oxygen in water. Because thermal quenching of the indicator and the reference dye is likely to be different in per cent of their total intensities, the tendency of the ratio regarding temperature depends on which of both is quenched more efficiently. In this sensor, the indicator dye is quenched to a greater extent than the reference dye. In sum an apparent increase in

oxygen saturation is monitored at higher temperatures as shown in Fig. 2.6. The average temperature coefficient is 3.8 µM/K for 100 % a.s.. This clearly indicates that appropriate thermostatisation of the fluorescence reader is mandatory. The usual temperature stability of our MTP readers is better than ± 1 °C. As a precaution, the calibration points were measured for every experiment in addition to the samples, and calculation of the oxygen content at a distinct time was performed using the calibration values at the respective time.

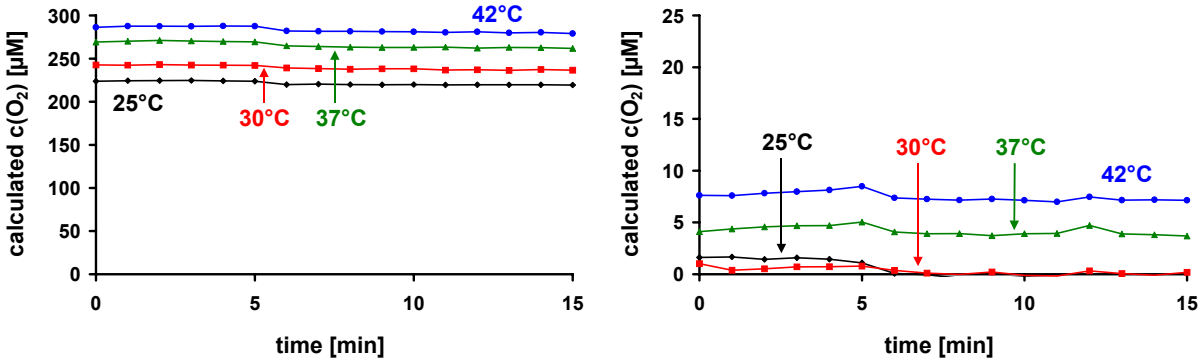

Fig. 2.6. Effect of temperature on the calibration points (left: 100 % a.s., right: 0 % a.s.) of the oxygen sensor (detected as kinetics of 15 min). The wells contained air-saturated water and 100 µL of a 1 % sodium sulphite solution, respectively. The y-axis shows the oxygen concentration calculated with the calibration points at 30 °C.

Table 2.3. Deviations in oxygen concentration ($\Delta c(O_2)$) calculated with the calibration points at the respective temperature and at 30 °C for 0 % and 100 % a.s..

T [°C]	$\Delta c(O_2)$ [µM]	Temp. coeff. [µM/K]	$\Delta c(O_2)$ [µM]	Temp. coeff. [µM/K]
	at 100 % a.s.		at 0 % a.s.	
25	-17.6	-3.5	-0.6	-0.1
37	25.5	3.6	3.9	0.6
42	43.3	3.6	7.1	0.6

2.2.7. Effect of Bacterial Culture Media and Single Ingredients

Cross-sensitivities of the oxygen sensor towards the widely used ingredients of culture media (Table 2.1) were investigated by adding the respective substances to doubly distilled, air-saturated and deaerated water, respectively. The calibration point at 0 % a.s. was taken using nitrogen instead of sulphite for deoxygenation because some ingredients of the medium react with sulphite. Comparison with samples without addition of media substances showed no deviations. Although the oxygen sensor is not optically isolated to shield the optical system from the fluorescence of substances in the sample, it is applicable for measurements of samples containing fluorescent media ingredients like yeast extract, peptone or beef extract. Fig. 2.7 displays the spectral properties of the complex culture medium AC Broth (all culture broth) compared to those of the oxygen-sensitive MTP. Although the emission spectra especially of the reference dye and the medium overlap (see Fig. 2.7, right), the fluorescent ingredients are not excited at the excitation wavelength of 544 nm used for the MTP experiments with the oxygen sensor plate (see Fig. 2.7, left).

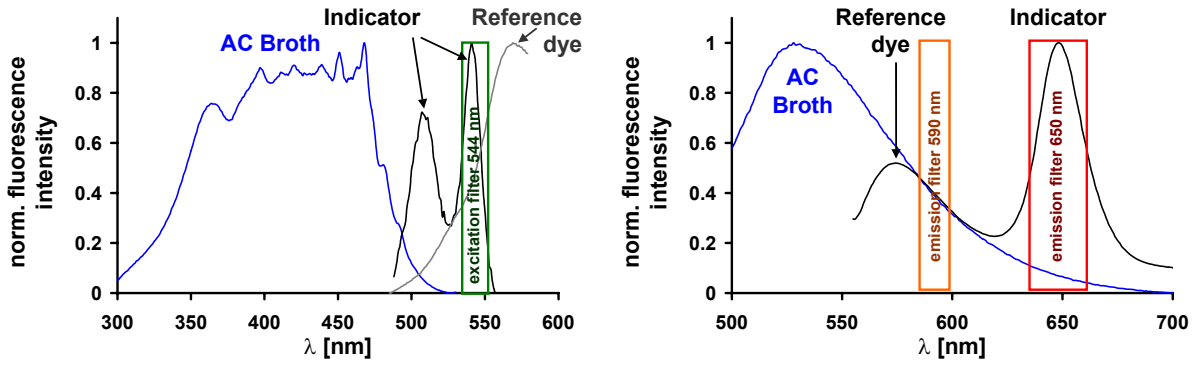

Fig. 2.7. Spectral properties of a complex culture medium (AC Broth) for bacteria and the OxoPlate. Left: Excitation spectra; Right: Emission spectra. Although the emission spectra of the fluorescent dyes and the medium overlap, the medium does not interfere the measurement because it is not excited at the wavelength used for excitation of the sensor.

2.2.8. Effects of Different Solvents

Enzyme screening is often performed in mixtures of water and organic solvents if the enzyme or the substrate are not water-soluble (e.g. oxidases for biopolymers or lipids). Therefore we tested solvents typical for this application with respect to sensor decomposition and the dynamic of the sensor signal. DMSO, DMF, EtOH, MeOH, acetone, THF and dioxane in different concentrations were applied to the oxygen sensor-coated MTP over 48 h. Concerning the mechanical stability of the sensor system, DMSO and DMF were found to be applicable up to a concentration of 80 % (v/v), methanol and ethanol in all concentrations except 80 % (v/v), acetone up to 50 % (v/v), and THF and dioxane up to 20 % (v/v). Higher fractions of solvent lead to decomposition or delamination of the sensor spots. However, the oxygen sensor-coated MTPs are only useful at concentrations up to 50 % of ethanol and methanol and 20 % of DMSO, DMF, acetone, THF or dioxane in the solution. At higher fractions of solvents the quenching efficiency was too high. The calibration points depend on the respective solvent/water mixture. Therefore, it is inevitable to record a calibration curve for each solvent/water mixture.

2.3. pH Sensor Embedded in Microtiterplates (HydroPlate HP96U)

2.3.1. Experimental Part

The pH-sensitive MTPs HydroPlate HP96U were obtained from PreSens. For characterisation of the sensor, either standard buffer solutions (Merck) or self-prepared phosphate buffered saline (PBS) solutions of a defined buffer concentration (sodium dihydrogen phosphate and disodium hydrogen phosphate from Merck), ionic strength (IS) and pH were used. The IS was adjusted with sodium chloride (Merck). The pH values of the PBS solutions were adapted with a digital pH meter (pH538 multical®, WTW). Experiments were performed at 30 °C unless noted otherwise.

The spectral properties of the sensors were recorded with an Aminco luminescence spectrometer AB2 (from Thermo Electron) using standard buffer

solutions of pH 3 to 10. The MTP assays were performed with an MTP reader Fluoroskan Ascent (Thermo Electron) except for the investigation of the effects of different solvents which were determined with the Fluostar Optima (BMG Labtech). The response time of the sensor was determined by adding 180 µL of PBS of pH 9 to 20 µL of PBS of pH 5 via a dispenser. Data on the resolution, accuracy and drift of the signals were acquired using standard buffer solutions of pH 5 to 8.

Cross-sensitivities of the sensor signal towards temperature, IS and bacterial media ingredients were investigated using PBS solutions of pH 4 to 10 and comparing the resulting calibration curves to one curve taken as the standard. Temperature effects were determined within a range of 25 to 42 ° using 50 mM PBS, IS 150 mM. The cross-sensitivity towards IS within a range of 15 to 300 mM was studied by adding the appropriate amount of NaCl to 5 mM phosphate buffer. The study on the effect of widely used ingredients of bacterial culture media (s. Table 2.1) was performed by adding the respective amount of ingredient to 50 mM PBS, IS 150 mM. Additionally to the substances listed in Table 2.1, 0.015 g/L of phenol red (Sigma-Aldrich) were tested. The effect of different solvents was investigated as described in the section on the oxygen sensor (see chapter 2.2.1, page 44).

2.3.2. Sensor Composition

The HydroPlate HP96U makes use of carboxyfluorescein as a pH indicator. It is covalently attached to oxygen-impermeable nanospheres of polyacrylonitrile containing the luminescent ruthenium(II)-tris-4,7-diphenyl-1,10-phenanthroline complex as a reference dye. This sensing material was dispersed together with carbon black (which acts as optical isolation) in a polyurethane hydrogel matrix. The sensor layer has a final thickness of about 10 µm and is fixed at the bottom of each well of a round bottom 96-well plate.

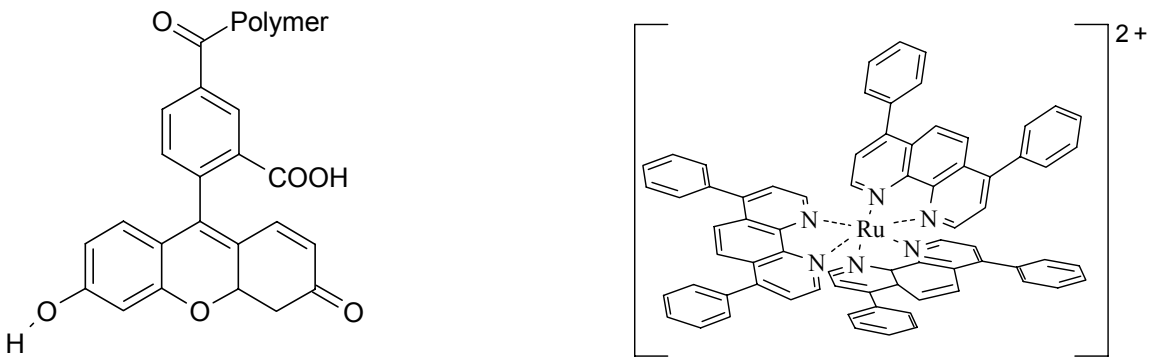

Fig. 2.8. Left: Carboxyfluorescein covalently bound to the polymer used as pH indicator for the pH-sensitive HydroPlate. Right: $Ru(dpp)_3$ is incorporated in the particles as reference dye.

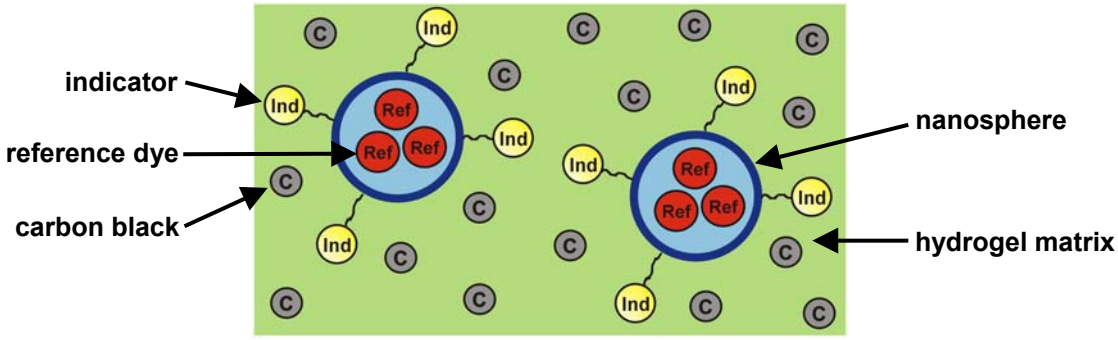

Fig. 2.9. Composition of the pH sensor HydroPlate. The indicator is covalently bound to oxygen-impermeable nanospheres containing the reference dye. The beads are dispersed together with carbon black as optical isolation in a hydrogel matrix.

2.3.3. Spectral Properties

Carboxyfluorescein has an absorbance maximum at 500 nm, the reference dye displays a broad absorbance between 430 and 465 nm. Both dyes can be excited at the same wavelength (485 nm). The pH indicator has an emission maximum at 530 nm, the reference dye one at 600 nm. Thus, the ratio of emission intensities can be used for quantitative pH measurements. While the acidic form of the indicator shows no fluorescence due to lactonisation, the basic form displays strong green fluorescence. Fig. 2.10 shows the spectral properties of the pH-sensitive material at pHs from 3 to 10.

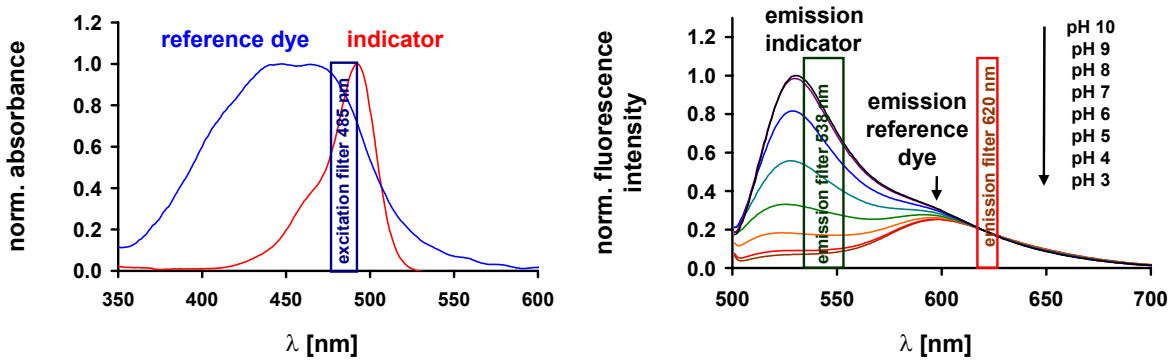

Fig. 2.10. Left: Absorption spectra of the indicator (carboxyfluorescein, in water) and reference dye ($Ru(dpp)_3$, in ethyl cellulose). Right: Emission spectrum of the sensor (exc. at 485 nm). Included are the respective filters used for excitation and emission.

2.3.4. Response time

The wetted sensor shows a response time (t_{90}) of 45 s using 50 mM PBS, IS= 150 mM (NaCl) (Fig. 2.11, left). Such a relatively fast response enables the detection of true kinetic parameters such as enzyme or respiratory activities.

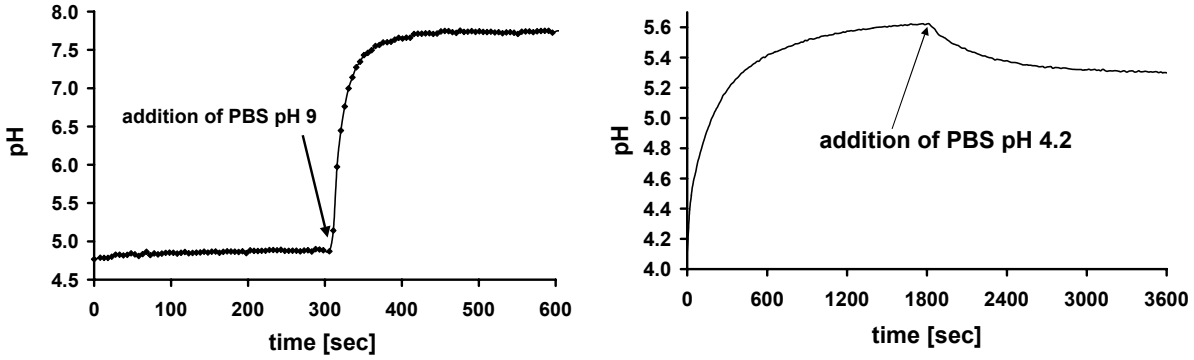

Fig. 2.11. Response of the pH sensor using 50 mM PBS, IS = 150 mM (left) and 1 mM PBS, IS = 100 mM. In contrast to the t_{90} of less than 1 min using a high buffer concentration, the response time is much slower with low buffer concentration.

However, the response time of the sensor strongly depends on the buffer concentration: Due to negative charges of the polymer, the sensor acts as a buffer itself. At low buffer concentrations, it takes some time until the buffer capacity of the

sensor is saturated. Therefore, the response time increases to 15 min using a 1 mM PBS (Fig. 2.11, right). This has to be accounted for, if low buffer concentrations cannot be avoided for the experiment (see chapter 4.5.2.1).

2.3.5. Figures of Merit

Both the resolution and the accuracy depend on the respective pH and are acceptable for most screening applications (Table 2.4). The pH drift was estimated by monitoring one well at pH 7 over 1 h. It lies within the accuracy of the sensor. Because of the good reproducibility of the signals, it is sufficient to calibrate only a few wells per MTP lot instead of calibrating each sensor spot, which makes the sensor array applicable for high-throughput screening.

Table 2.4. Figures of merit of the pH sensor.

Analytical range	pH 5.0 – 8.0
Resolution (at 37°C)	0.01 to 0.02 pH
Accuracy (at 37°C)	0.1 to 0.05 pH
pH drift per hour	< 0.02 pH / h

The fluorescence signals can be converted into pH values using calibration curves. The ratio R of the two fluorescence intensities is plotted versus the pH. The resulting sigmoidal curve is fitted using the Boltzmann equation (eqn. 1.2). For calculation of the pH value, it is necessary to know any cross-sensitivities of the pH sensor towards common parameters such as temperature or ionic strength.

2.3.6. Effect of Temperature

Temperature affects both the pH value and the fluorescence of the sensor. The pH value depends on the activity of the protons, which is different for different temperatures and buffer salts. For phosphate buffer, the temperature coefficient is -0.0028 K^{-1} [12]. Aside from the temperature dependence of the pH value, the sensor signal itself also varies with the temperature. Higher mobility of the particles carrying the fluorescent dye molecules at higher temperatures lead to more collisions and as a result to lower fluorescence signals (thermal deactivation). Furthermore, the activity coefficients of the indicator dye change with the temperature. For the described

sensor, this effect is contrary to the effect of thermal quenching and dominates over this effect until a pH of 9. For pH 9, thermal quenching dominates, leading to intensities decreasing with temperature (data not shown). The signal of the reference dye (in %) is more strongly quenched by temperature than the indicator dye. Consequently, the referenced fluorescence intensities are shifted towards higher values with increasing temperature (s. Fig. 2.12).

Table 2.5 shows the apparent pK_a values pK_a' obtained from these calibration curves. The pK_a' decreases with higher temperatures until 37 °C. Measuring at higher temperatures, the temperature dependence becomes smaller. The deviations between 37 °C and 42 °C lie within the measurement accuracy and can therefore be neglected. ΔpH (pK_a') is a parameter for the deviation found between the pH at the respective apparent pK_a' calculated with the calibration curve recorded at the respective temperature and with a calibration curve recorded at a reference temperature of 30 °C. The deviations are small but not within the sensor accuracy. Therefore, it is necessary to consider the temperature especially at low temperatures for calculation of correct pH values if temperature fluctuations of more than 3 °C are expected.

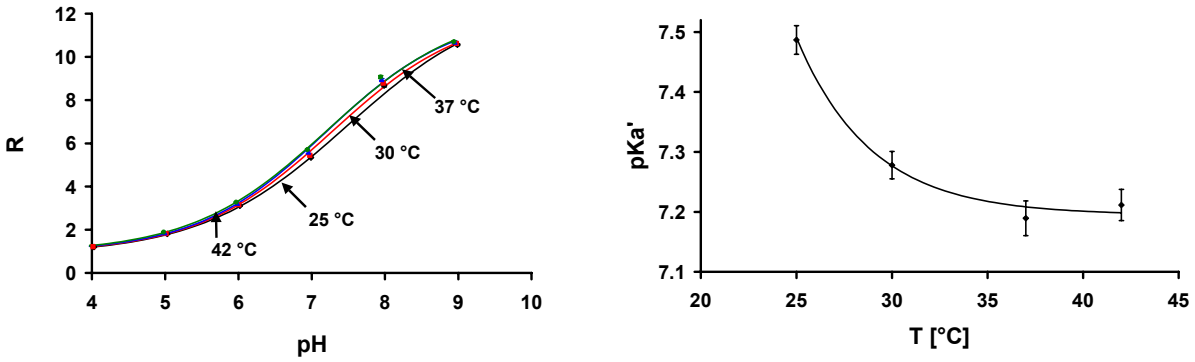

Fig. 2.12. Left: Effect of temperature on the calibration curves of the pH sensor. Right: Dependence of pK_a' on the temperature T.

Table 2.5. Apparent pK_a values (pK_a') of the pH sensor as derived from calibration curves at different temperatures. ΔpH is the deviation between the pH at the respective pK_a' value calculated using the calibration curve for a specific temperature and calculated using the calibration curve recorded at 30 °C.

T [°C]	pK_a'	ΔpH (pK_a')	temperature coefficient [K^{-1}]
25	7.49	-0.12	-0.024
30	7.28	-	-
37	7.18	0.08	0.011
42	7.21	0.09	0.008

2.3.7. Effect of Ionic Strength

Optical pH measurements are known to be strongly influenced by the ionic strength (IS) of the sample [13, 14]. The sensor signal is converted into pH via a calibration curve which plots the (referenced) concentration of the deprotonated form of the indicator versus the pH detected with a pH electrode. The Henderson-Hasselbalch equation eqn. 2.1 a relates the pH to the activities of the protonated and deprotonated forms of the indicator dye. pK_a is the negative common logarithm of the dissociation constant K_a, a_{A^-} and a_{HA} the activities of the deprotonated and protonated forms of the indicator dye, c_{A^-} and c_{HA} their concentrations and f_{A^-} and f_{HA} the respective activity coefficients.

$$pH = pK_a + \log\frac{a_{A^-}}{a_{HA}} = pK_a + \log\frac{c_{A^-} \cdot f_{A^-}}{c_{HA} \cdot f_{HA}} \qquad \text{eqn. 2.1 a}$$

$$pH = pK_a + \log\frac{f_{A^-}}{f_{HA}} + \log\frac{c_{A^-}}{c_{HA}} = pK_a' + \log\frac{c_{A^-}}{c_{HA}} \qquad \text{eqn. 2.1 b}$$

The IS influences both activities of the protons (and, thus, the pH) and of the indicator dye. Higher IS lowers the activity of the protons, which results in an increase in pH. The potential of the pH electrode depends linearly on the proton *activity*. In contrast, the optical pH sensor detects the *concentration* of the deprotonated form of the

fluorophore (c_{A^-}) and neglects the activity coefficients (see eqn. 2.1 b), resulting in differing calibration curves at different IS (s. Fig. 2.13). According to eqn. 2.5 b, the resulting point of inflexion (pK_a') is related to the true pK_a via eqn. 2.1 c:

$$pK_a' = pK_a + \log \frac{f_{A^-}}{f_{HA}} \qquad \text{eqn. 2.1c}$$

For negatively charged indicators like carboxyfluorescein, neglecting the activity coefficients leads to a pK_a' shift towards lower values at higher IS (Table 2.6). For the pH sensor HydroPlate, higher IS additionally results in a higher fluorescence of the deprotonated form at the same pH value because the higher charged anionic form is stabilised. The deviations decrease with increasing IS. Therefore it is necessary to consider the effects of IS especially at low values for calculation of correct pH values, or to provide a sufficient background IS to minimise the effects.

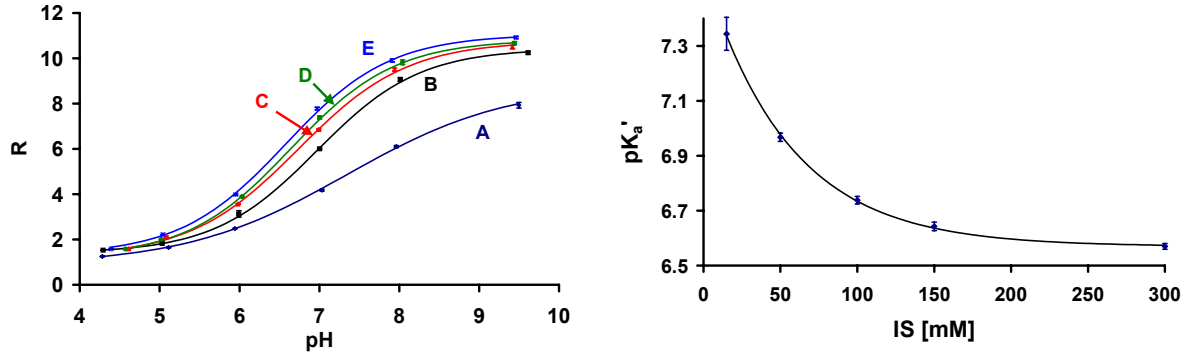

Fig. 2.13. Left: Effect of ionic strength (IS) on the calibration curves of the pH sensor. The wells contained 150 µL of a 5 mM PBS solution and respective amounts of NaCl. (A): 15 mM, (B): 50 mM, (C): 100 mM, (D): 150 mM, (E): 300 mM NaCl; Right: Dependence of pK_a' on the ionic strength IS.

Table 2.6. Apparent pK_a' values of the pH sensor derived from calibration curves obtained at different ionic strength (IS). ΔpH (pK_a') is the deviation between the pH at the respective pK_a' value calculated using the calibration curve recorded at the respective IS and calculated using the calibration curve recorded at an IS of 150 mM.

IS [mM]	pK_a'	ΔpH (pK_a')
15	7.36	-1.02
50	6.95	-0.35
100	6.69	-0.10
150	6.62	-
300	6.57	0.12

2.3.8. Effect of Bacterial Culture Media and Single Ingredients

The influence of the 20 proteinogenic amino acids, other typical media ingredients, and of two complete bacterial media (Table 2.1) on the sensor signal was investigated. The signals obtained with the optically isolated HydroPlate was compared to those detected with an MTP coated with a transparent pH sensor comprising the same pH indicator (Fig. 2.15). Beef extract, yeast extract and AC broth lead to higher signals compared to the PBS calibration curve using the transparent pH sensor because they show intrinsic fluorescence with spectral properties similar to those of the indicator dye (Fig. 2.14). In contrast, the black optical isolation of the pH sensor HydroPlate shields the fluorescence of the sample efficiently from being detected by the MTP reader.

The same result was obtained with the substances bactotrypton, EC broth, riboflavin and phenol red, whereas the amino acids, bile and dextrose did not lead to higher fluorescence of the sample. The optically isolated pH sensor can thus be used for fluorescent or turbid samples without need of additional calibration curves. This also clearly shows the advantage of sensors embedded in a polymer matrix compared to dissolved indicator dyes: With the latter, no optical isolation is possible, and the pH of such samples can only be derived using special calibration curves.

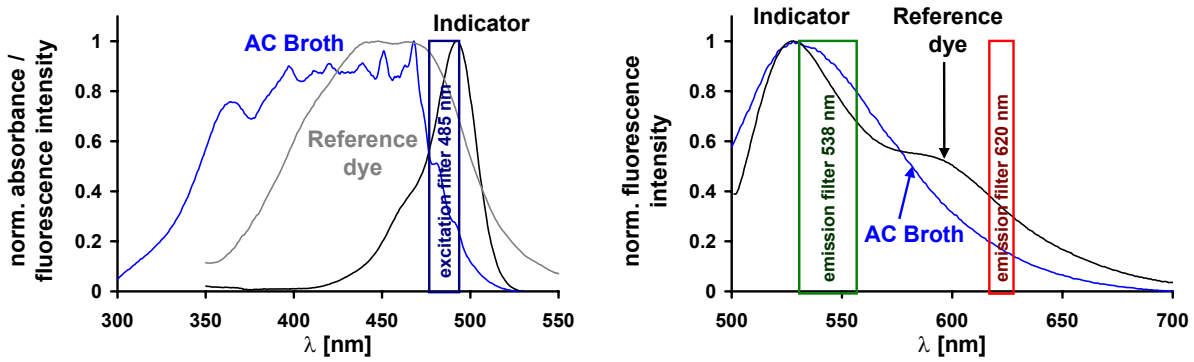

Fig. 2.14. Spectral properties of a complex culture medium for bacteria and the pH sensor HydroPlate. Left: Absorbance spectra; Right: Emission spectra. With the filter combination used for excitation and emission of the fluorescent dyes, the fluorescence of the medium is excited and detected as well. Therefore an optical isolation of the sensor is indispensable.

When recording kinetics involving changes in the fluorescence or turbidity of the sample during the experiment, e.g. in growing bacterial suspensions, a correct pH calculation is even impossible with dissolved indicators.

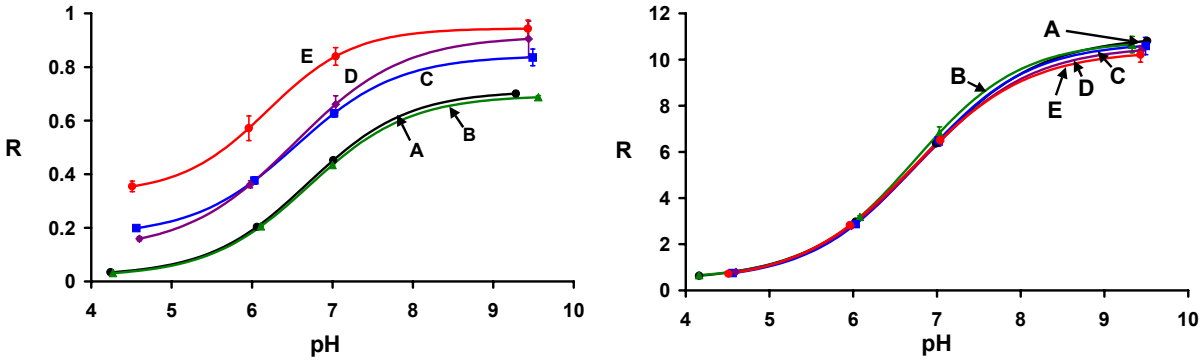

Fig. 2.15. Calibration curves of the transparent pH sensor HP96T (left) and the optically isolated pH sensor HP96U (right) with 50 mM PBS (ionic strength 150 mM) containing different ingredients of culture media: (A) PBS, (B) dextrose, (C) beef extract, (D) yeast extract, (E) AC broth.

2.3.9. Effects of Different Solvents

The effect of different solvents on the sensor material and signal were investigated as described in the section on the oxygen sensor (chapter 2.2.8, page 52). Its mechanical stability was found to be similar to that of the oxygen sensor plates. The calibration curves depend on the respective water-solvent mixture. Therefore, it is inevitable to record a calibration curve for each solvent at each concentration.

2.4. Oxygen Sensors for Comparative Experiments

2.4.1. Optically Isolated MTP Sensor (PSt3)

For samples with high turbidity, e.g. due to high concentrations of bacteria, the above described oxygen sensor is not adequate because light scattering increases the fluorescence intensity depending on the wavelength and is therefore not compensated by ratioing. For such measurements, an optically isolated sensor, which blocks turbid or fluorescent samples from being detected by the instrument, is necessary. An optically isolated sensor foil (SP-PSt3, PreSens), which was originally designed for the fibre-optic minisensor (s. chapter 2.4.2.1, page 64), was used involving high bacteria concentrations. Small sensor spots were punched from a sensor foil and glued with silicone rubber (Prod. No. 692-542, RS Components GmbH) into a PS, flat-bottom, 96-well MTP (Greiner). The sensor contains a Pt porphyrine as oxygen indicator. Carbon dispersed in the sensor polymer matrix serves as optical isolation. Instead of using an inert reference dye, time-gated intensity measurements were performed for obtaining reproducible results (Rapid Lifetime Determination, RLD; s. Fig. 1.10, page 1). The intensity of the indicator was detected directly after excitation and after a lag time of 60 µs, respectively. The resulting 2 intensities, A_1 and A_2, are the integral over the lowest possible integration time of 20 µs.

Fig. 2.16 shows the pseudo-decay curves of the optically isolated sensor for the two calibration points at 100 % a.s. and 0 % a.s.. The normalised fluorescence

intensities are plotted versus the average lag time between excitation and measurement. The minimal integration time of 20 µs causes a time delay of 20/2 = 10 µs. The dynamics of the sensor, which is defined as the difference of the intensities at 0 % a.s. and 100 % a.s. relating to the intensity at 0 % a.s. (see eqn. 2.2), is better at higher lag times. As the intensity of the air-saturated sample is high enough to guarantee for sufficient reproducibility of the signals, a lag time of 60 µs (t_2 = 70 µs) was chosen for further experiments. At this lag time, the dynamics of the sensor is 93 % (Table 2.7).

$$\text{dynamics [\%]} = 100 \cdot \frac{\text{Int}_0 - \text{Int}_{100}}{\text{Int}_0} \qquad \text{eqn. 2.2}$$

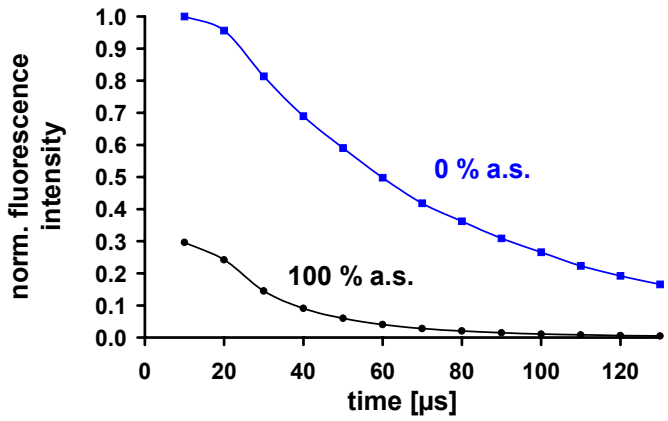

t_2 [µs]	dynamics [%]
10	70
20	75
30	82
40	87
50	90
60	92
70	93
80	94
90	95
100	96
110	96
120	97
130	97

Fig. 2.16. (left) Pseudo-decay curve of the optically isolated oxygen sensor PSt3 at the two calibration points at 100 % a.s. and 0 % a.s.; Table 2.7. (right): Dynamics of the sensor at different lag times.

All measurements were performed with the luminescence reader Tecan Genios (Tecan) using an internal gain factor of 51. The sensor was excited with one flash at 405 nm and the emission detected at 635 nm. The reader temperature was 25 °C.

2.4.2. Fibre-optic Sensors

Comparative experiments were performed with fibre-optic oxygen sensors using oxygen-impermeable glass vessels instead of the permeable PS MTP. Two types of sensors were tested, a fibre-optic minisensor (Fibox 2, PreSens), and a microsensor (Microx TX3, PreSens). The evaluation of both sensors are lifetime-based (frequency domain, see chapter 1.3.5, page 23). A two-point calibration with air-saturated, doubly distilled water and a solution of 1% sodium sulphite (Merck) in water is sufficient. The phase shifts are converted into oxygen units via an internal instrument software which uses a modified Stern-Volmer equation (eqn. 1.2).

2.4.2.1. Minisensor

An optically isolated oxygen sensor spot on a glass support (diameter: 5 mm; SP-PSt3-YOP-G-SUP-D5, PreSens) was glued with silicone rubber (Prod. Nr. 692-542, RS Components GmbH) onto the bottom of a 100 µL Erlenmeyer flask. The vessel was autoclaved before the first measurement. The sensor spot was read out non-invasively from outside through the transparent bottom of the flask using a coaster (CFG, PreSens). The coaster contains a polymer optical fibre and redirects the light, thus enabling excitation of the sensor and detection of the signal from the bottom of the flask (see Fig. 2.17). The optical fibre is connected to an oxygen meter Fibox 2 (PreSens). Table 2.8 gives some figures of merit of the oxygen minisensor PSt3 with optical isolation.

Table 2.8. Range, resolution, accuracy and response time of the oxygen minisensor PSt3 (with optical isolation; from [15]).

	[% a.s.]*	**[µM]**
range	0-500	0-1420
resolution (at 20 °C)	1 ± 0.05 100 ± 0.5	2.8 ± 0.1 283.8 ± 1.4
accuracy	± 1 at 100 % a.s. ± 0.1 at 1 % a.s.	± 2.8 at 100 % a.s. ± 0.3 at 1 % a.s.
response time (t_{90}) [s]	< 30 (stirred) < 60 (non-stirred)	

* % air saturation

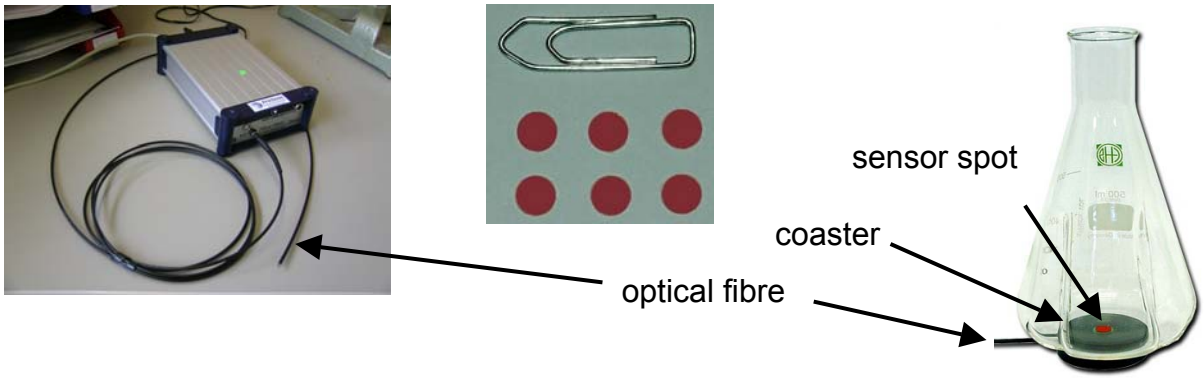

Fig. 2.17. Left: Fibox oxygen meter with fibre-optic minisensor; middle: oxygen sensor spots; right: sensor spot glued to the bottle of an Erlenmeyer flask, read out by a coaster from below [15].

2.4.2.2. Microsensor

Fig. 2.18. Left: Oxygen meter with fibre-optic microsensor; Right: Microsensor in Erlenmeyer flask. The tiny sensor tip is extended from the needle and positioned in the centre of the flask.

A second method of fibre-optic oxygen detection is a needle-type microsensor (NTH-PST1-L2.5-TS-NS 40/0.8-NOP, PreSens) instead of a minisensor. The oxygen-sensitive polymer is placed on top of a thin optical fibre (s. *Fig. 2.18*, right), which is protected from breaking by a plastic syringe housing. From this housing the sensor tip can be extracted for measurement and retracted for protection when not needed. The fibre is connected to an oxygen meter (Microx TX3, PreSens).

In contrast to the minisensor, this method is invasive because the sensor has to be placed into the sample for measurement. Besides, the sensor is not autoclavable because of its plastic components. Its great advantage, however, lies in the rapid response time, which is smaller than 1 s for DO detection with tapered sensors without optical isolation. Thus, even fast kinetics can be detected in real-time. Some figures of merit of the oxygen microsensor are summarised in Table 2.9.

Table 2.9. Range, resolution, accuracy and response time of the oxygen microsensor (tapered, with optical isolation; from [15]).

	[% a.s.]*	**[µM]**
range	0-500	0-1420
resolution(at 20 °C)	1 ± 0.05 100 ± 0.5	2.8 ± 0.1 283.8 ± 1.4
accuracy (at 20 °C)	± 1 at 100 % a.s. ± 0.1 at 1 % a.s.	± 2.8 at 100 % a.s. ± 0.3 at 1 % a.s.
response time (t_{90}) [s]	< 5 (stirred)	

* % air saturation

2.4.3. Lifetime-based Glass Vessel Sensor (SDR2)

Comparative experiments demanding a higher throughput than conveniently possible with the single measurement of a fibre-optic sensor were performed with a so-called sensor dish reader (SDR2, PreSens). The sensor dish (Fig. 2.19, A) consists of 24 separate channels for excitation and detection of the emission, which are addressed subsequently. The sensor dish reader was originally designed for 24-well MTPs containing luminescent sensor spots for the detection of oxygen and pH. For the comparative experiments for the toxicity tests, non-permeable, 5 mL glass vessels (Klaus Trott) were used, containing an oxygen-sensitive sensor spot glued to the bottom of each vessel with silicone rubber (Prod. Nr. 692-542, RS Components; see Fig. 2.19, B). 24 of these glass vessels were placed into a 24 well MTP (Nunc) which fits the dimensions of the sensor dish. Table 2.10 gives some of the figures of merit of the rather new and therefore not yet fully characterised sensor.

Table 2.10. Range, resolution, accuracy and response time of the Sensor Dish Reader SDR2 (from [15]).

	[% a.s.]*	**[µM]**
range	0-100	0-283.8
resolution(at 20 °C)	± 2	± 5.7
accuracy (at 20 °C)	± 5	± 14.2

* % air saturation

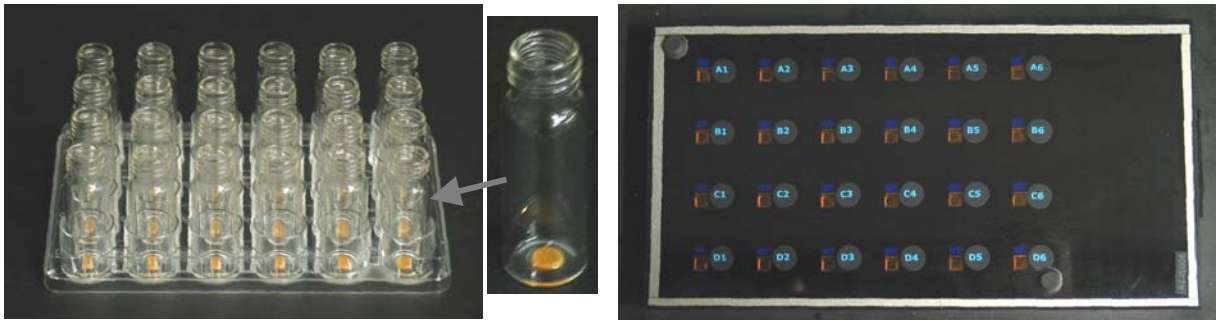

Fig. 2.19. Left: Array of 24 glass flasks with oxygen sensor spots glued to their bottoms (middle); Right: Sensor dish reader (SDR2) with 24 separate channels for excitation (blue) and emission read-out (red) of the sensor array.

2.5. References

1 Hynes J, Floyd S, Soini AE, O'Connor R, and Papkovsky DB. *Fluorescence-based cell viability screening assays using water-soluble oxygen probes*. (2003). Journal of Biomolecular Screening **8**(3), 264-272.

2 Alderman J, Hynes J, Floyd SM, Kruger J, O'Connor R, and Papkovsky DB. *A low-volume platform for cell-respirometric screening based on quenched-luminescence oxygen sensing*. (2004). Biosensors & Bioelectronics **19**(11), 1529-1535.

3 Cao Y, Koo YEL, and Kopelman R. *Poly(decyl methacrylate)-based fluorescent PEBBLE swarm nanosensors for measuring dissolved oxygen in biosamples*. (2004). Analyst (Cambridge, United Kingdom) **129**(8), 745-750.

4 Moris-Varas F, Shah A, Aikens J, Nadkarni NP, Rozzell JD, and Demirjian DC. *Visualization of enzyme-catalyzed reactions using pH indicators: rapid screening of hydrolase libraries and estimation of the enantioselectivity*. (1999). Bioorganic & Medicinal Chemistry **7**(10), 2183-2188.

5 O'Riordan TC, Buckley D, Ogurtsov V, O'Connor R, and Papkovsky DB. *A Cell Viability Assay Based on Monitoring Respiration by Optical Oxygen Sensing*. (2000). Analytical Biochemistry **278**(2), 221-227.

6 John GT and Heinzle E. *Quantitative screening method for hydrolases in microplates using pH indicators: determination of Kinetic parameters by dynamic pH monitoring*. (2001). Biotechnology and Bioengineering **72**(6), 620-627.

7 John GT, Klimant I, Wittmann C, and Heinzle E. *Integrated optical sensing of dissolved oxygen in microtiter plates: a novel tool for microbial cultivation*. (2003). Biotechnology and Bioengineering **81**(7), 829-836.

8 Deshpande RR and Heinzle E. *On-line oxygen uptake rate and culture viability measurement of animal cell culture using microplates with integrated oxygen sensors*. (2004). Biotechnology Letters **26**(9), 763-767.

9 Wodnicka M, Guarino RD, Hemperly JJ, Timmins MR, Stitt D, and Pitner JB. *Novel fluorescent technology platform for high throughput cytotoxicity and proliferation assays*. (2000). Journal of Biomolecular Screening **5**(3), 141-152.

10 Guarino RD, Dike LE, Haq TA, Rowley JA, Pitner JB, and Timmins MR. *Method for determining oxygen consumption rates of static cultures from microplate*

measurements of pericellular dissolved oxygen concentration. (2004). Biotechnology and Bioengineering **86**(7), 775-787.

11 Weiss S, John GT, Klimant I, and Heinzle E. *Modeling of mixing in 96-well microplates observed with fluorescence indicators*. (2002). Biotechnology Progress **18**(4), 821-830.

12 Stannett V, in: Crank J, Park GS (eds.). *Diffusion in Polymers*. Academic Press, London (1968), pp.41-73.

13 Janata J. *Do optical sensors really measure pH?* (1987). Analytical Chemistry **59**(9), 1351-1356.

14 Weidgans BM, Krause C, Klimant I, and Wolfbeis OS. *Fluorescent pH sensors with negligible sensitivity to ionic strength*. (2004). Analyst **129**(7), 645-650.

15 http://www.presens.de (05.01.2006).

3. Oxygen Ingress into Microtiterplates and its Effect on Kinetic Parameters

3.1. Introduction

Microtiterplates (MTPs) are indispensable for fast and low-priced screening tests in medical and pharmaceutical research. They are mainly used for PCR and ELISA tests [1, 2], but other applications like the detection of enzymatic and respiratory activities are also possible [3, 4, 5, 6]. For this purpose, optical sensors are convenient tools for indirect measurement of metabolism and enzymatic activities via essential parameters like NH_3, CO_2, pH and pO_2. There are three strategies to measure these parameters: Dissolved indicator dyes or particles with embedded indicators provide an average value over the whole well. However, a dissolved dye usually involves disadvantages like inaccurate dispensing, inhibition or toxicity towards sample components or acts as source of contamination. Using a small electrode or a fibre-optic sensor, the sensor is reasonably placed in the centre of the well because here the influence of oxygen diffusion into the sample from the ambient air is smallest. With MTPs, this technique is not adequate, though. Sensor films containing an indicator dye embedded in a polymer combine the advantages of optical sensing and the screening technique without the disadvantages of a dissolved indicator. In the experiments described here, the oxygen-sensitive MTP OxoPlate (see chapter 2.2) and a fibre-optic microsensor (see chapter 2.4.2.2) were used.

Respiratory studies are often performed in glass vessels (e.g. [7]). Transferring the task to the MTP format, it has to be considered that oxygen diffuses constantly into the sample due to oxygen-permeable sealings and MTP materials [[8]]. The effect is all the greater as the surface-to-volume ratio of the MTP well is much higher than that of a large volume vessel. Oxygen-impermeable glass MTPs are also available but inapplicable due to their high costs. This diffusion leads to oxygen heterogeneities within the sample. Therefore, it is important to consider the sensor position within the well: pO_2 measured at the bottom of the well does not necessarily represent the pO_2 in other parts of the well or an average value. Knowing the oxygen

distribution within the well is essential for obtaining correct kinetic parameters, e.g. of enzyme kinetics or respiratory rates of bacteria or higher cells. This is especially important with high oxygen gradients between sample and ambient air and with insufficient mixing. It has earlier been shown that mixing can be incomplete in MTPs [9]. If mixing is insufficient, the location of a sensor is critical. Furthermore, the contribution of the oxygen flux into the well to the total signal should be preferably small to achieve the best possible accuracy and to allow the detection of small pO_2 changes and metabolic rates within the sample.

In this chapter, the effect of oxygen diffusion into the sample from ambient air on kinetics detected in open or variously sealed MTP wells is compared to those obtained in a hermetically sealed system. The kinetics were measured with sensor-coated MTPs. A model is introduced to describe oxygen diffusion into a sample in an MTP well and to calculate correct kinetic parameters of enzyme reactions. Furthermore, the oxygen distribution within the well was measured with a fibre-optic sensor and simulated for various MTP sealings and materials to investigate the influence of different oxygen permeability on the kinetics.

3.2. Oxygen Ingress Using Various Plate Sealings

The oxygen ingress into nitrogen-saturated water in the well of an MTP was investigated applying various plate sealings to the oxygen sensor OxoPlate and a glass MTP. The sample consisted of nitrogen-saturated water containing 0.5 % (w/w) of sodium azid to prevent bacteria from consuming oxygen and thereby effecting the detection of oxygen ingress from ambient air. Additionally, the influence of different plate materials and sealings was studied using mathematical models.

3.2.1. Models for Oxygen Ingress and Enzyme Kinetics in Microtiterplates

3.2.1.1. Model without Convection

The ingress of oxygen into deaerated samples in MTPs was simulated for different MTP materials and plate sealings using the simulation program BERKELEY-MADONNA [10]. Mass balances served as basic principle of the models, resulting in equations according to [11]:

$$\begin{pmatrix}\text{rate of}\\ \text{oxygen}\\ \text{accumulation}\end{pmatrix} = \begin{pmatrix}\text{oxygen}\\ \text{diffusion into}\\ \text{the system}\end{pmatrix} - \begin{pmatrix}\text{oxygen}\\ \text{diffusion out}\\ \text{of the system}\end{pmatrix} - \begin{pmatrix}\text{rate of}\\ \text{oxygen}\\ \text{consumption}\\ \text{by a reaction}\end{pmatrix} \qquad \text{eqn. 3.1}$$

Oxygen diffusion into and out of the sample are due to the permeability of the MTP material and – if employed - the cover. The rate of oxygen accumulation corresponds to the kinetics measured with the fibre-optic sensor and the sensor plates, respectively. Using deaerated water for detection of increasing pO_2, the initial pO_2 and the rate of oxygen consumption are both 0 and the measured kinetic is an oxygen accumulation as stated in eqn. 3.1. In some experiments, the MTP material and the paraffin oil were not completely deaerated. This was accounted for by a factor named “saturation”, which was fitted to the respective kinetics detected with the oxygen sensor.

The general equation describing the oxygen transfer rate (OTR, in mol/s) into a well-mixed volume element is given as

$$\mathrm{OTR} = \frac{dcO_2}{dt} = k_L a \cdot (cO_2^{\,*} - cO_2) = k_L a \cdot S_{O2} \cdot (pO_2^{\,*} - pO_2) \qquad \text{eqn. 3.2}$$

where k_La is the volumetric mass transfer coefficient, cO_2* the oxygen saturation concentration, cO_2 the oxygen concentration of the sample, S_{O2} the oxygen solubility, pO_2* the oxygen saturation partial pressure and pO_2 the oxygen partial pressure of

the sample. Unfortunately, eqn. 3.2 describes the applied system only insufficiently. Especially with low OTR, the simulated kinetics did not agree with the measured ones because the system was not well-mixed. Therefore the model was modified by taking into account incomplete mixing in the liquid. This was done by setting up a one-dimensional diffusion model dividing the system into sample, MTP material and, for paraffin oil cover, the plate sealing with horizontal layers (Fig. 3.1). Horizontal oxygen diffusion through the MTP walls was neglected to simplify the model. This was justifiable because the sensor covering the entire bottom of the MTP provides an average signal in horizontal direction. Therefore, the oxygen diffusion through the wall does not change the oxygen distribution in the centre of the bottom of the sensor plates, where the sensor is located and illuminated, although it contributes to the overall mass transfer.

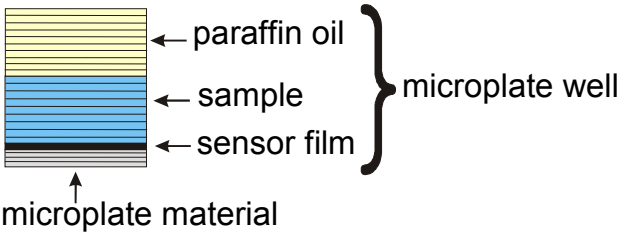

Fig. 3.1. Set-up for the simulation of oxygen diffusion through the MTP material and sealing. Sample, MTP material and oil sealing were divided into horizontal layers with interchanging oxygen flows. Oxygen diffusion from the walls of the well was neglected.

For each layer, a differential equation was set up (eqn. 3.3), which is only valid for models without convection, i.e. with rigid plate sealings like wax or foils or completely unshaken measurements.

$$\frac{dcO_2[i]}{dt} = \frac{D_{O2}}{d[i]} \cdot \frac{A[i]}{V[i]} \cdot (cO_2[i-1] + cO_2[i+1] - 2 \cdot cO_2[i]) \quad \text{eqn. 3.3}$$

The index i indicates the number of the layer. D is the diffusion constant, d the layer thickness, A is the diffusion area and V the volume of the considered element i. For vertical, 1-dimensional diffusion in the cylindrical sample, V = A·d, and therefore $\frac{A[i]}{V[i]} = \frac{1}{d[i]}$. Regarding adjacent layers of different materials a and b, different oxygen solubilities, diffusion constants and layer thicknesses have to be accounted for, which

results in different flows $J_{a\rightarrow b}$. An average flow J is calculated to describe the equilibrium of flows between these two layers.

$$J_{(a\rightarrow b)}(a) = \frac{D_{O2}(a)}{d(a)^2} \cdot (cO_2(a)[m] - cO_2(b)[1] \cdot \frac{S_{O2}(a)}{S_{O2}(b)}) \qquad \text{eqn. 3.4a}$$

$$J_{(a\rightarrow b)}(b) = \frac{D_{O2}(b)}{d(b)^2} \cdot (cO_2(a)[m] \cdot \frac{S_{O2}(b)}{S_{O2}(a)} - cO_2(b)[1]) \qquad \text{eqn. 3.4b}$$

$$J = \frac{J_{(a\rightarrow b)}(a) + J_{(a\rightarrow b)}(b)}{2} \qquad \text{eqn. 3.4c}$$

$cO_2(a)[m]$ is the oxygen concentration in the last layer of material a which is adjacent to the first layer of material b with the oxygen concentration $cO_2(b)[1]$. The average flow J is subtracted from the differential equation of the last layer m of material a and added to the first layer of material b. D and S values were taken from literature (Table 3.1) except the solubility of polystyrene for the exact value for the MTPs used in these experiments is not known. Therefore it is reasonable to slightly adjust it to fit the experimental data by comparing the simulated kinetics to measurements using a deaerated polystyrene (PS) MTP sealed with aluminium foil. The number of layers in the MTP material and the sample was each chosen 30 to provide sufficient accuracy of the model.

Table 3.1. Diffusion (D) and solubility coefficients (S) for oxygen in different materials.

material	D [$cm^2 \cdot s^{-1}$]	S [$cm^3(STP) \cdot cm^{-3} \cdot Pa^{-1}$]	references
water	$2.1 \cdot 10^{-5}$	$2.67 \cdot 10^{-7}$	
paraffin oil	$2.61 \cdot 10^{-5}$	$1.44 \cdot 10^{-6}$	[21], [22]
polystyrene (PS)	$1.1 \cdot 10^{-7}$	$4.29 \cdot 10^{-7}$ (cf. $1.79 \cdot 10^{-6}$)	fitted to measurement, ([23])
polypropylene (PP)	$9 \cdot 10^{-8}$	$1.92 \cdot 10^{-6}$	[23] , [24]
polyethylene terephthalate (PET)	$3.5 \cdot 10^{-9}$	$7.4 \cdot 10^{-7}$	[23]
silicone	$1.7 \cdot 10^{-5}$	$2.67 \cdot 10^{-6}$	[23], [26]

3.2.1.2. Model with Convection

Regarding measurements using paraffin oil or no plate sealing, inevitable movement of the MTP in a reader causes convection which is not accounted for in the above model. Unfortunately, convection is very difficult to describe mathematically. The problem was simplified by using the model without convection and multiplying the diffusion constants for water and, in case of oil sealing, paraffin oil by different factors $\mathbf{F_w}$ and $\mathbf{F_{oil}}$, respectively, with $F_{oil} < F_w$ due to the higher viscosity of paraffin oil.

For kinetics without plate sealing, the water volume was divided into a homogeneous upper layer of variable thickness ("**watertop**") with contact to ambient air, thereby increasing its surface, and the remaining layers which were treated in the way described above. The greater surface of the upper layer was accounted for using an extra factor $\mathbf{F_{conv}} > F_w$ for this layer. The model is described in the Appendix (11.1.2.1).

Considering kinetics with paraffin oil sealing, two different modes were distinguished: Without "**additional**" shaking (i.e. no shaking except due to the movement of the MTP for measurement) or with slight shaking (180 rpm / 10 mm), the oil layer was divided into a homogenous upper layer (thickness: "**oiltop**") and remaining layers like the water volume in the model without sealing. Again, a factor F_{conv} accounted for the greater surface of this layer, whereas convection was regarded by the factor F_{oil}. This model is shown in the Appendix (11.1.2.2).

For fast plate shaking (1200 rpm / 1 mm) using paraffin oil sealing, the model was modified (see Appendix 11.1.2.3) by assuming one homogeneous oil layer with increased surface (F_{conv}, F_{oil}) and a water sample that is divided into a homogeneous upper layer and remaining water layers, in analogy to the model without cover described above.

For all 3 models, additional shaking (i.e. shaking during the kinetic intervals between the measurement points) was accounted for by multiplying all factors F by a constant shaking factor named "**shake**". Thus, the convection factors were increased likewise with faster shaking. For no additional shaking, the shake factor was set to 1, for shaken measurements it was > 1.

To minimise the number of variables for the model with oil sealing, the factor regarding the enhanced surface of the upper layer with contact to ambient air (F_{conv}) and its part of the total volume (oiltop) were constituted to be constant (F_{conv} = 10,

oiltop = 25 µL), which leaves the number of variables to 2 (F_w and F_{oil}) for kinetics with oil cover and no additional shaking. These variables were fitted and found to be in good accordance for measurements using different volumes of oil sealing. They were applied for the model with fast plate shaking, thereby reducing the number of fit variables in this model to only 2 (shake and watertop), which were fitted and found to be in good accordance regarding measurements with different oil volumes and without cover. The variables for all model fits with convection are summarised in Table 3.2.

Clearly, these models are far away from delivering accurate physical constants. Even fitting only 2 variables can lead to good fits with more than one set of suitable, but completely different variables. Moreover, it is rather laborious to find factors that make sense, i.e. similar convection factors for experiments using the same shaking mode and different amounts of paraffin oil as sealing. Although describing the real kinetics rather well, these models do not deliver one overall value for oxygen ingress for comparison of the effectivity of the sealing with respect to its inhibition of oxygen ingress. Therefore, the kinetics obtained from experiments were additionally fitted with the simple k_La model (see eqn. 3.2), although most of these fits match the real kinetics rather unsatisfyingly. However, the more complex simulations are essential if experimental data are not available (e.g. with different MTP materials) and for obtaining correct kinetic parameters of oxygen-consuming reactions.

Table 3.2. Varied parameters for models involving convection: The parameters were fitted to the experimental data for measurements with different shaking modes (no additional (no add.), slow (180/10) and fast (1200/1) shaking) and sealings (no sealing, 50, 100 and 150 µL of paraffin oil).

sealing	shaking		F_w	F_{oil}	F_{conv}	shake	oiltop [µL]	watertop [cm]	rest
no	no add.		2.9	-	10	1	-	0.0925	1.047
	180/10					2	-	0.13	1.04
	1200/1					2.4	-	0.18	1.025
50 µL	no add.		2.9	1.5	10	1	25 µL	-	-
oil	180/10					1.65	25 µL	-	-
	1200/1					2.4	-	0.11	1.087

100 µL oil	no add. 180/10 1200/1		2.9	1.5	10	1 1.65 2.4	25 µL 25 µL -	- - 0.09	 1.095
150 µL oil	no add. 180/10 1200/1		2.9	1.5	10	1 1.65 2.3	25 µL 25 µL -	- - 0.09	 1.087

3.2.2. Experimental

The MTP experiments were performed with the oxygen-sensitive OxoPlate (see chapter 2.2) and a quartz glass MTP (Hellma) coated with an oxygen sensor film (PreSens). Water containing 0.5 % sodium azide (Sigma-Aldrich) was saturated with nitrogen. The MTPs were filled under nitrogen atmosphere with different volumes of water depending on the cover and the maximum filling volume. They were covered under nitrogen atmosphere with 50 µL, 100 µL or 150 µL of deaerated paraffin oil (bioMérieux), 100 µL of deaerated, liquid paraffin wax (MP 46 - 48°C; Merck), and 100 µL of deaerated paraffin wax dissolved in petroleum ether (0.6 g/mL; Merck), with a punctured 96-well cap mat made of EVA (poly(ethylene-co-vinyl) acetate; Prod. Nr. 850277, HJ-Bioanalytik) and with stripes of foils consisting of cellulose acetate (CA; Sarstedt), polyester (poly(ethylene terephthalate) = PET; Greiner) and aluminium (Costar®, Corning). The MTPs were read out from the bottom with an MTP fluorescence reader Fluoroskan Ascent (ThermoLabsystems). The reader temperature was 30°C except for the measurements with paraffin wax in organic solvent where it was 25°C. No additional shaking was performed, if not indicated otherwise.

Differing from this general procedure, some experiments were performed with completely deaerated MTPs which were stored under nitrogen atmosphere for 3 days. In one experiment the MTP was shaken with 1200 rpm and a diameter of 1 mm (1200/1) and with 180 rpm and 10 mm diameter (180/10) in the background mode (i.e. all the time except during the measurement).

3.2.3. Results and discussion

3.2.3.1. MTP materials

Comparative experiments with PS MTPs and a glass MTP were performed to study the influence of oxygen diffusion through the material of the PS MTP. The wells were filled with deaerated water containing 0.5 % sodium azide to prevent bacterial growth from interfering with the results by consuming oxygen. The MTPs were covered with aluminium foils under nitrogen atmosphere to inhibit oxygen diffusion through the sealing. Maximum filling volumes of 300 µL (PS MTPs) and 400 µL (glass MTP) were chosen to minimise the remaining gas phase. Unfortunately, it was impossible to avoid a small gas bubble which remained between foil and sample.

For filling and sealing, the MTPs were stored under nitrogen atmosphere for about 1 h, which is not sufficient for complete deaeration of the PS and results in kinetics starting at about 70 µM and immediate increase of pO_2 (Fig. 3.2). The stronger increase of pO_2 at the beginning of the kinetic with incomplete deaeration is due to temperature effects. Fig. 3.2 also shows the kinetic of a completely deaerated MTP which was stored under nitrogen atmosphere for 3 days to extract all oxygen from the plastic. In contrast to the kinetic using the incompletely deaerated MTP, it started at 0 µM and pO_2 increased with a delay time of 40 min in which the oxygen diffusing through the initially deaerated MTP material reaches the sensor. Comparison of this kinetic with the incompletely deaerated PS MTP indicates that the MTP material serves as a significant oxygen reservoir. The comparative experiment with the glass MTP (left) demonstrates that the increase of oxygen in the PS MTPs was totally due to the diffusion through the MTP material and not to leaks between plate sealing and MTP.

The measurements were confirmed by simulations. Fig. 3.2, left, shows the simulated kinetic of a completely deaerated MTP. The simulation fits the measurement perfectly well. The simulation of the incompletely deaerated PS MTP was performed assuming that the PS is air-saturated to a content of 72.6 % due to its rather short storage under nitrogen atmosphere in the glovebox. Oxygen ingress was also simulated for MTPs made of polypropylene (PP), which is quite equally permeable to oxygen as PS, and polyethylene terephthalate (PET), with very low

permeability towards oxygen. With PET, oxygen ingress would only take place significantly (> 1.4 µM = 0.5 % air saturation = a.s.) after 12 h (data not shown). Thus, oxygen ingress can be decreased enormously by using a less permeable material as PET (P_{PET} = $2.6 \cdot 10^{-15}$ $cm^3 \cdot cm \cdot cm^{-2} \cdot s^{-1} \cdot Pa^{-1}$). Unfortunately, the most widely used, commercially available MTPs are made either of PS or PP. Another possibility to decrease oxygen ingress is coating of the commercially available PS or PP MTPs (P_{PS} = $2 \cdot 10^{-13}$ $cm^3 \cdot cm \cdot cm^{-2} \cdot s^{-1} \cdot Pa^{-1}$, P_{PP} = $1.7 \cdot 10^{-13}$ $cm^3 \cdot cm \cdot cm^{-2} \cdot s^{-1} \cdot Pa^{-1}$) with a thin film of an even less oxygen-permeable material like PAN (P = $1.5 \cdot 10^{-17}$ $cm^3 \cdot cm \cdot cm^{-2} \cdot s^{-1} \cdot Pa^{-1}$ [23]). Coating of plastics to decrease oxygen ingress is today performed e.g. in food and beverage industry for protection of beverage ingredients from oxidation by oxygen from ambient air.

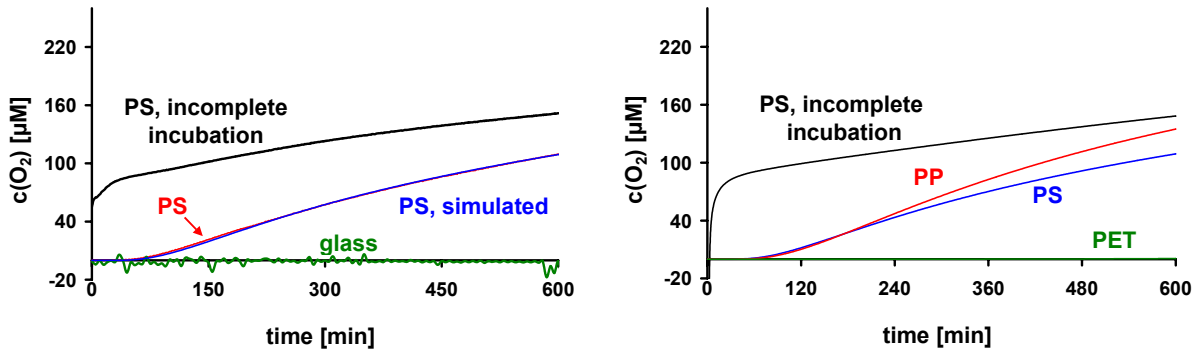

Fig. 3.2. Left: ***Measured*** *oxygen content in deaerated water in an incompletely deaerated MTP, a totally deaerated PS MTP and a glass MTP detected over 10 h. All MTPs were sealed with aluminium foil. The simulated kinetic for the deaerated PS MTP fits the measurement perfectly well. Right:* ***Simulated*** *oxygen increase in deaerated water in an incompletely deaerated PS MTP, and completely deaerated MTPs made of PS, PP and PET.*

Comparing kinetics detected with a PS MTP sealed with aluminium, PET and CA foils and wax (page 84, Fig. 3.5, right) with the ones detected with a glass MTP (left), it is obvious that the oxygen increase in the former is only partly caused by diffusion through the cover. Here, using the impermeable aluminium foil, oxygen ingress is completely due to diffusion through the PS. This diffusion is rather slow compared to oxygen ingress into oil-covered samples and considering the total measurement time of 10 h, but faster than the diffusion through all tested rigid sealings (see chapter

3.2.3.3, Table 3.4). Consequently, oxygen diffusion through the MTP material cannot be neglected using covers of low oxygen permeability.

3.2.3.2. Plate sealings

The sample/air interface is the second source of oxygen exchange between sample and environment. Especially in shaken wells using liquid plate sealings the effect can be enormous. Therefore various MTP sealings with different permeability towards oxygen were tested to reduce this exchange. The PS MTP wells were filled with deaerated water containing 0.5 % sodium azide. With foil covers, the filling volume was 300 µL, with paraffin oil and wax sealings and without cover it was 100 µL. No additional shaking of the MTP was performed if not indicated otherwise. However, shaking of the MTP could not be prevented completely because of the automatic plate movement during the measurement and to the resting position during the waiting interval.

- **Paraffin oil cover**

Paraffin oil is a common sealing for MTP wells to avoid evaporation of the sample. In addition, it can reduce the gas exchange with the environment. However, with non-stagnant measurement conditions as in an MTP reader, paraffin oil proved to be a rather poor protection from oxygen ingress into the sample, because the exchange is not only driven by diffusion but forced by convection. The resulting kinetics are depicted in Fig. 3.3.: Even with an oil volume of 150 µL, the initially oxygen-free samples became almost air-saturated after 2 h (t_{90}). With 50 µL and 100 µL of paraffin oil, t_{90} was 1.5 h, without any cover it was only 20 min. For these experiments, the oil was deaerated with nitrogen to avoid unknown oxygen content due to incomplete deaeration during the filling time in the glove box. Using non-deaerated oil, oxygen ingress takes place even faster because paraffin oil acts as an oxygen reservoir which rapidly releases oxygen into the sample (data not shown). In contrast, impermeable aluminium sealing prevents oxygen ingress from ambient air for almost 1 h. After that time, oxygen diffuses slowly into the sample through the

MTP material. Consequently, foil sealings are more advisable for protecting the sample from oxygen ingress, if a maximum filling volume is applicable for the experimental set-up.

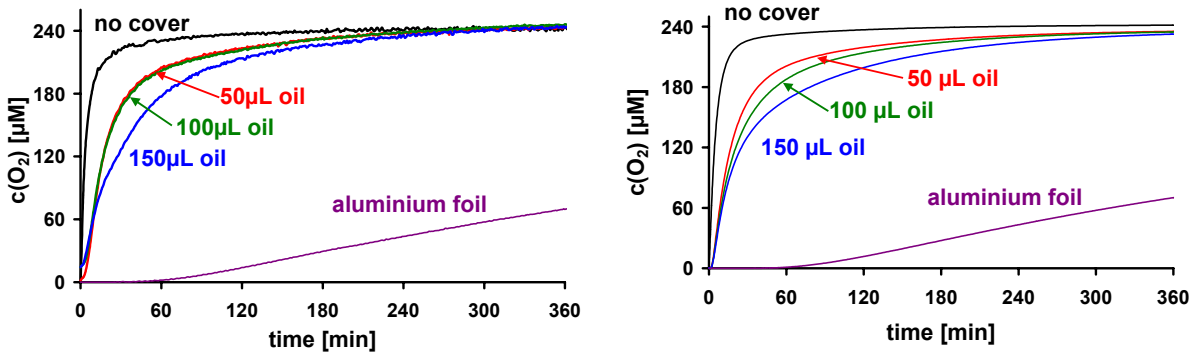

Fig. 3.3. ***Measured*** *(left) and* ***simulated*** *(right) oxygen ingress into 100 µL of nitrogen-saturated water without cover and covered with different amounts of paraffin oil (50, 100 and 150 µL) and using an impermeable aluminium sealing for comparison.*

- **Plate shaking**

Many experimental set-ups require shaking to guarantee homogeneity of the sample or to prevent solid ingredients like bacteria from precipitating. Using non-rigid plate sealings, plate shaking causes convection. Its influence was investigated using 100 µL of paraffin oil as sealing and 2 different modes of shaking: Slow shaking with 180 rpm and a shaking diameter of 10 mm (180/10), and a more rapid mode with 1200 rpm combined with a 1 mm diameter (1200/1). Comparison with MTP reader experiments without additional shaking, and a completely unshaken measurement using a microsensor with its tip placed in the centre of the sample showed that the oxygen ingress through the paraffin oil strongly depends on the shaking speed. Increased disturbances in the oil layer lead to a larger contact surface to ambient air and cause a faster oxygen ingress into the sample [9, 12]. With rapid shaking (Fig. 3.4. 1200/1), the sample was air-saturated after less than 10 min (t_{90}) even with oil sealing, whereas lower plate shaking (180/10) resulted in air saturation after ca. 30 min. Oxygen ingress into the sample without additional shaking of the MTP was slower due to fewer disturbances in the oil layer, but the effect was still obvious

comparing it to a completely unshaken kinetic obtained with the fibre-optic sensor because of the unavoidable movement of the MTP in the reader. The convection can be reduced by choosing a preferably slow plate acceleration, if possible. Paraffin oil is thus not advisable as plate sealing for shaken measurements, e.g. in an MTP reader, especially if the plate acceleration cannot be regulated. Furthermore, it is difficult to establish a satisfactory mathematical model for the oxygen transfer in a sample if convection is involved. Premising a reproducible oxygen ingress and a detectable oxygen increase which is not completely compensated by the oxygen ingress, such a model would allow for correct calculation of real oxygen uptake rates (OURs) of samples involving oxygen-consuming reactions despite the oxygen ingress.

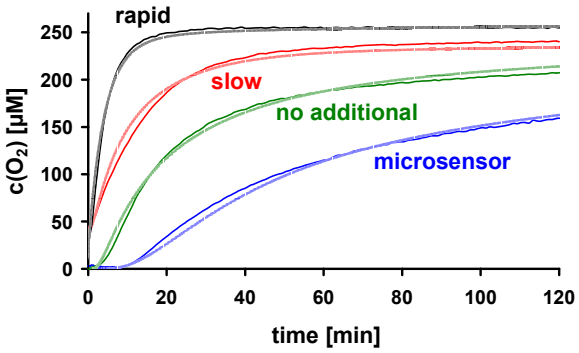

Fig. 3.4. ***Measured*** *(strong line) and* ***simulated*** *(weak line) oxygen ingress into deaerated water covered with 100 µL of paraffin oil. Rapid (1200/1), slow (180/10) and no additional plate shaking in the reader and no shaking, measured with the fibre-optic microsensor.*

- **Foil and wax sealings**

Solid sealings were investigated to avoid any convection in the sample. With paraffin wax sealings, the volume of the sample was 100 µL. With foil sealings, maximum filling volumes (PS MTP: 300 µL, glass MTP: 400 µL) were chosen for reasons mentioned before. Aluminium, PET and cellulose acetate (CA) foils, 100 µL of paraffin wax and 100 µL of paraffin wax dissolved in petroleum ether were tested.

Using the deaerated PS MTP (s. Fig. 3.5., left), pO_2 at the bottom of the well started to increase after 40 minutes with the aluminium and PET foils, which was the

diffusion time for oxygen through the deaerated MTP material. Filling the MTP under ambient air instead of nitrogen atmosphere, foils are not suitable, though, because of an inevitable air phase which remains between sample and foil cover which stores much more oxygen than e.g. paraffin oil. With the more oxygen-permeable CA foil, the signal increased almost immediately because the gas phase, which was nitrogen at the start of the measurement, became oxygenated and the oxygen was transported to the sensor layer by convection due to the gas phase.

In contrast, deaerated paraffin wax proved to be a sufficient protection from oxygen diffusion into the sample for more than 2 h. The process of becoming solid did not involve production of a gas phase in the sample, therefore no convection took place. After that time, however, pO_2 in the sample increased more rapidly than through CA foil due to its higher permeability. A disadvantage of liquid wax even with a low melting point is that it has to be heated to more than 50 °C to transfer it conveniently into the well. The resulting temperature gradient within the sample after adding the wax has no effect on the shown kinetics because they start at 0 µM and contain no reaction which influences pO_2. However, with an initial pO_2 different from 0 µM, a temperature effect caused by the smaller oxygen solubility in a warmer solution and by effects due to the sensor properties is inevitable. Furthermore, temperature inhomogeneities in the sample lead to different enzyme activities and influence bacterial activity as well.

An alternative is deaerated paraffin wax dissolved in small amounts of petroleum ether. The wax is dissolved in the organic solvent at a temperature only a few degrees above the temperature of the reader and becomes almost rigid shortly after covering the sample with it. The oxygen permeability of the almost rigid wax is slightly higher than that of pure paraffin wax, but still the oxygen increase is much lower than with paraffin oil sealings (s. Fig. 3.3.). On a first look, paraffin wax dissolved in organic solvents seems to be an appropriate, easy-to-handle alternative to the more permeable paraffin oil and the more laborious foil sealings. However, like with pure wax, an inevitable temperature effect is observable even at small temperature differences. Furthermore, the solvent seems to have an activating or stressing effect on bacteria, causing faster respiration. The greatest drawback, however, is the constant evaporation of solvent, which leads to changing composition of the dissolved wax and therefore to varying oxygen permeability. Due to this

disadvantages and the fact that handling gets cumbersome with time due to wax deposits inside the pipette, this plate sealing was abandoned.

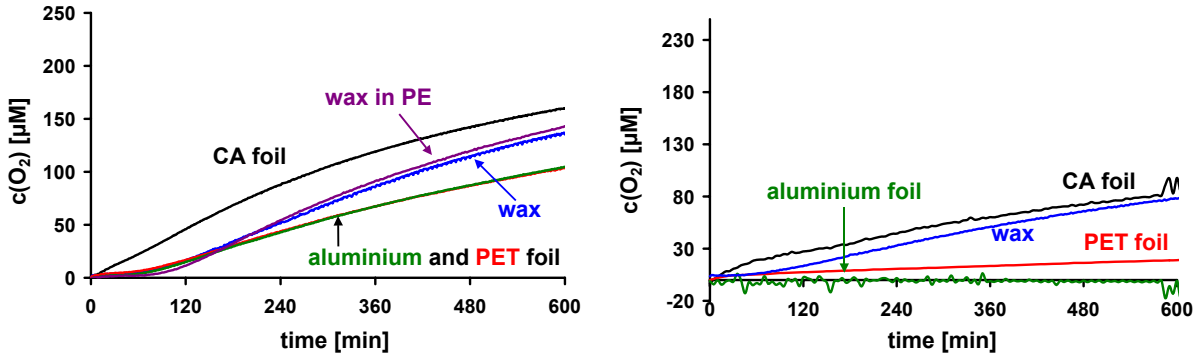

Fig. 3.5. Oxygen ingress into deaerated water using an oxygen-free PS MTP (left) and a quartzglass MTP (right) covered with cellulose acetate (CA), PET and aluminium foil, paraffin wax sealing and 100 µL of paraffin wax dissolved in petroleum ether (PE).

Besides foils, other rigid plate sealings are commercially available. Capmats made of polymers with a low oxygen permeability (e.g. EVA) are easy-to-handle and prevent convection. However, as with foils, a small air phase is likely to remain between cover and sample, providing it with abundant oxygen. Therefore each well of the capmat was punctured with a hot wire. Applying the punctured capmat directly from above and pressing it vertically on the MTP provides for elusion of excess air. Despite the small hole, oxygen ingress is reduced enormously compared to paraffin oil sealing due to lack of convection. Unfortunately, exact closing of the MTP without a remaining air phase proved to be quite difficult and resulted in outliers, which leads to time-consuming evaluation and is unacceptable for high throughput screening.

The simplest and easiest applicable plate sealing is paraffin oil. As the experiments with paraffin wax proved, convection rather than the oxygen permeability or the oil causes problems. To reduce convection, the lowest plate acceleration (v=1) of our reader was chosen. Although the oxygen ingress was significantly higher than with the capmat or foil sealings, this plate sealing was nevertheless sufficient for our purposes (see chapter 4.4.3) because the calculated inhibition of the bacterial respiration was the same as with comparative experiments without oxygen ingress. Besides easy application, a great advantage of this plate sealing is the high well-to-

well reproducibility which spares labour-intensive outsourcing of outliers and allows for easy and fast evaluation and automatisation which is indispensable for a high throughput. Unfortunately, low plate accelerations are not available for every MTP reader. The Fluoroskan Ascent (Thermo Labsystems) offers 10 different speeds for plate acceleration.

3.2.3.3. Overview over oxygen ingress via k_La values

As mentioned in chapter 3.2.1.2, the simulations performed with complex models describe the experimental kinetics excellently, but do not deliver overall kinetic constants that allow for a rough comparison of the effectiveness of the applied sealings with respect to their protection of the sample from oxygen ingress. Therefore, the experiments were simulated using the simple k_La model (eqn. 3.1), often resulting in rather inaccurate fits (see Fig. 3.6) but delivering comparable k_La values.

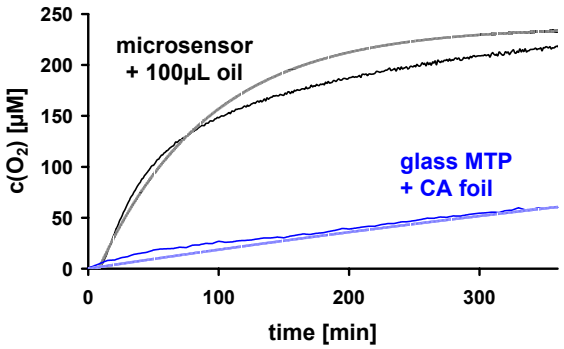

Fig. 3.6. The k_La fits (light lines) match the experimental kinetics (strong lines) rather poorly.

Table 3.3 compares the oxygen ingress into a PS MTP sealed with **various covers**. To increase the quality of the fits, the starting times of kinetics with a time delay between start of the measurement and beginning oxygen increase (i.e. with foil or wax sealing) within the sample was delayed as well and therefore neglected for the k_La fit, whereas the initial oxygen content for kinetics with incomplete deaeration of the MTP material was fitted as well. Liquid sealings like paraffin oil decrease the oxygen ingress only by a factor of 4 (50 and 100 µL oil) to 7 (150 µL oil), whereas wax sealings and CA foil decrease it by a factor of more than 100, aluminium and PET foil even of near 200. It is notable that the latter as well as wax sealings prevent oxygen ingress within the sample for ca. 1 h, which is not accounted for at the

comparison of k_La, whereas the kinetic using the CA foil sealing start to rise immediately. This behaviour is reproducible and assumed to be due to the much higher permeability of this material towards oxygen.

Table 3.3. k_La values for oxygen ingress into a PS MTP using various plate sealings.

cover	k_La [min^{-1}]	x times less O_2 ingress than without cover
aluminium foil	0.0011*	172**
PET foil	0.0010*	188**
CA foil	0.0019	101
wax in PE	0.0018*	110**
wax	0.0017*	115**
150 µL oil	0.0273	7
100 µL oil	0.0455	4.2
50 µL oil	0.0474	4.1
no cover	0.1923	1

* start of fit after 60 min delay time

** not regarding the delay time

As has been shown on page 84, **oxygen ingress through the MTP material** cannot be neglected using plate sealings of low oxygen permeability. The k_La values obtained with foil and wax sealings using a PS MTP were compared to those obtained with a glass MTP. The kinetics using the glass MTP and wax (and, curiously, the CA foil) sealing do not start at 0 µM as the experiment using the PS MTP due to incomplete deaeration of the wax. This was corrected by fitting the initial $c(O_2)$ as well. The permeability of the MTP material was a) obtained as the oxygen ingress into the PS well sealed with the completely impermeable aluminium foil, and b) calculated by subtraction of the k_La obtained with the glass MTP of the one obtained with the PS MTPs using the same plate sealing. a) resulted in a k_La of $1.1 \cdot 10^{-3}$ $min^{-1}$for oxygen ingress through the PS MTP material, which was confirmed by the deviations of PS and glass MTP experiments using PET foil ($1.0 \cdot 10^{-3}$ min^{-1}) and wax ($9.7 \cdot 10^{-4}$ min^{-1}). For wax in PE, the oxygen ingress into the sample using the glass MTP was greater than the one using the PS MTP, which indicates the poor reproducibility of this plate sealing.

Table 3.4. k_La values for oxygen ingress into glass and PS MTPs using different rigid sealings.

MTP	cover	k_La [min^{-1}]	$k_La - k_La_{alu}$ [min^{-1}]	$k_La_{PS} - k_La_{glass}$ [min^{-1}]	init $c(O_2)$ [µM]	fit range [min]
PS	alu	$1.1 \cdot 10^{-3}$*	0	-	0	70-360
PS	PET	$1.0 \cdot 10^{-3}$*	$-9.4 \cdot 10^{-5}$	$1.0 \cdot 10^{-3}$	0	90-1000
PS	CA	$1.9 \cdot 10^{-3}$	$7.9 \cdot 10^{-4}$	$-2.1 \cdot 10^{-4}$	0	0-360
PS	wax/PE	$1.8 \cdot 10^{-3}$*	$6.4 \cdot 10^{-4}$	$-1.7 \cdot 10^{-3}$	0	90-360
PS	wax	$1.7 \cdot 10^{-3}$*	$5.6 \cdot 10^{-4}$	$9.7 \cdot 10^{-4}$	0	90-360
glass	alu.	0	-		5	0-1800
glass	PET	$9.9 \cdot 10^{-4}$	-		0	60-360
glass	CA	$2.1 \cdot 10^{-3}$	-		19.9	0-20
glass	wax/PE	$3.4 \cdot 10^{-3}$	-		36.8	35-900
glass	wax	$7.0 \cdot 10^{-4}$	-		15.0	120-900

* start of fit after 60 min delay time

To investigate the influence of **different shaking speeds**, experiments using a PS MTP and liquid or no plate sealings and an unshaken kinetic using a microsensor were compared. Like before, incomplete deaeration of the paraffin oil for the shaken measurements was accounted for by fitting the initial oxygen concentration. The fitting range was 0 – 120 min. The resulting k_La were compared to the k_La of the respective unshaken measurement using the same plate sealing. Slow plate shaking (180/10) increases the oxygen ingress only by a factor of 1.2 to 1.8, whereas rapid plate shaking (1200/1) is more effective and leads to an oxygen ingress increased by the factor 4.8 (no cover) to 8.1 (50 µL oil). Compared to the completely unshaken measurement using the microsensor and 100 µL paraffin oil as plate sealing, the oxygen ingress of the "unshaken" plate in the reader is 4 times higher. Thus, low plate acceleration, long measurement intervals or even no movement at all of the plate have a positive effect on inhibition of oxygen ingress. Slow plate shaking (180/10) leads to a 6 times, rapid shaking (1200/1) even to a 23 times faster oxygen ingress.

Table 3.5. k_La values for oxygen ingress into a PS MTPs using different non-rigid sealings or no sealing, with different shaking speeds.

device	cover	shake	k_La [min^{-1}]	x times more O_2 ingress than without shaking*	init c(O_2) [µM]
microsensor	100 µL oil	-	0.0118		
MTP (PS)	150 µL oil	-	0.0273	-	0
MTP (PS)	100 µL oil	-	0.0455	-	0
MTP (PS)	50 µL oil	-	0.0474	-	0
MTP (PS)	no cover	-	0.1923	-	0
MTP (PS)	150 µL oil	180 / 10	0.0336	1.2	18.1
MTP (PS)	100 µL oil	180 / 10	0.0682	1.5	36.7
MTP (PS)	50 µL oil	180 / 10	0.0856	1.8	12.2
MTP (PS)	no cover	180 / 10	0.3223	1.7	74.6
MTP (PS)	150 µL oil	1200 / 1	0.1773	6.5	1.8
MTP (PS)	100 µL oil	1200 / 1	0.2735	6.0	6.9
MTP (PS)	50 µL oil	1200 / 1	0.3831	8.1	3.5
MTP (PS)	no cover	1200 / 1	0.9304	4.8	17.9

* comparing measurements with the same cover

3.3. Effect of Oxygen Ingress Considering Enzyme Kinetics as Example

In quantification of oxygen-involving reactions, oxygen diffusion into the sample and the resulting gradients can lead to deviations in essential parameters like enzyme activity or oxygen uptake rate (OUR), because it partially compensates the oxygen consumption by the employed reaction. This is the case especially at low rates, e.g. in the cultivation of mammalian cells. Most bacterial cultures grow much faster and require therefore much higher oxygen transfer rates obtained by shaking [13]. In such cases oxygen transfer through the liquid surface is dominating. Very low cell concentrations or very slowly growing cells would also require consideration of diffusional effects described in this chapter. With enzymatic reactions, the reaction rate can be adjusted easily by adjusting the enzyme concentration. Low rates as e.g. in the experiments described in chapter 3.3.5.1. would require the consideration of

diffusional effects through the walls. Here it is desirable to quantify and minimise the oxygen exchange between sample, ambient air and plate material.

3.3.1. Glucose Oxidase

Glucose oxidase (GOx, EC Nr. 1.1.3.4, beta-D-glucose:oxygen 1-oxidoreductase) catalyses the oxidation of β-D-glucose to give D-glucono-δ-lactone and hydrogen peroxide:

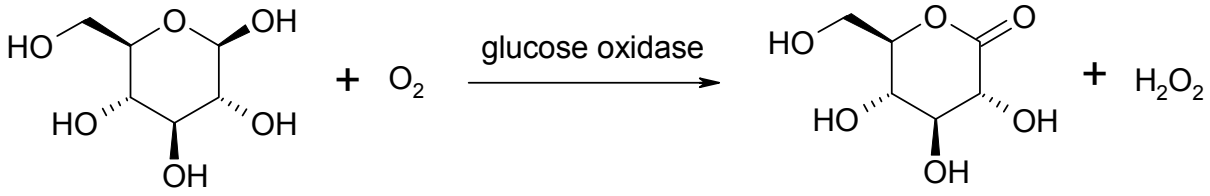

The cofactor involved in this process is FAD (flavin-adenine dinucleotide), which reacts with glucose to yield $FADH_2$ and is then recovered by oxygen. The mechanism is rather complex and consists of several partial reactions.

For hydrogen peroxide destroys GOx, it is advisable to add excess of the enzyme catalase (EC Nr. 1.11.1.6, hydrogen peroxide oxidoreductase) to the sample to remove the peroxide as fast as possible. Catalase disproportionates hydrogen peroxide into water and oxygen, thereby producing half of the amount of oxygen that is consumed by the glucose oxidation:

$$H_2O_2 \xrightarrow{\text{catalase}} H_2O + \frac{1}{2} O_2$$

The gluconolactone reacts with water to give D-gluconic acid. The overall reaction using both enzymes can be written as:

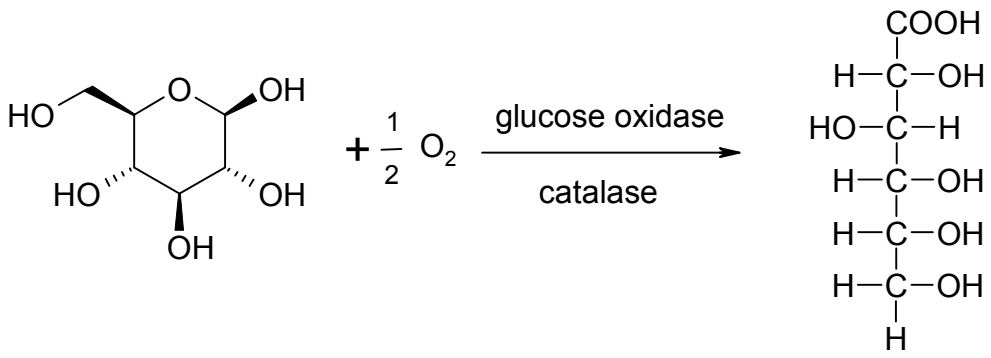

The free enzymes involved in this reaction are rather unstable and are slowly destroyed by their substrates: Catalase as well as the reduced form of GOx are inactivated by hydrogen peroxide [14]. Furthermore, GOx is also destroyed by oxygen [15]. For the experiments performed in this work, the stability is of less importance because the aim was not to obtain correct kinetic parameters but to investigate the influence of oxygen ingress into the sample on an oxygen-consuming reaction.

3.3.2. Detection of Effective Enzyme Activity

The maximum activity of GOx given on the package (245 900 U/mg solid) is only valid for ideal conditions (pH = 5.1, T = 35 °C). However, conditions differing from these ideal ones were used in the experiments. The temperature was 30 °C to decrease the difference between reader and sample stored under ambient air (T = 20-28 °C) to minimise unwanted temperature effects of the sensor (see chapter 2.2.6). Although the pH optimum of GOx is 5-6 [16], the enzymes and glucose were solved in buffer solution pH 7.0 (Merck) because the mutorotation of α– to β– glucose is optimal at this pH [17]. This is of importance because the racemic form of glucose was used as substrate, whereas GOx only catalyses the β-form. The effective GOx activity under measurement conditions was obtained via a parameter not influenced by the investigated oxygen ingress. The formation of hydrogen peroxide, which is produced during the GOx-catalysed glucose oxidation (in absence of catalase) was detected via oxidation of ABTS (2,2'-azino-bis(3-ethylbenzthiazoline-6-sulphonic acid, diammonium salt), thereby forming a green, positively charged

radical which is stable at temperatures up to 35 °C [18]. The reaction is catalysed by the enzyme peroxidase (POx, EC-Nr. 1.11.1.7, hydrogen-peroxide oxidoreductase). One molecule of hydrogen peroxide oxidises 2 molecules of ABTS:

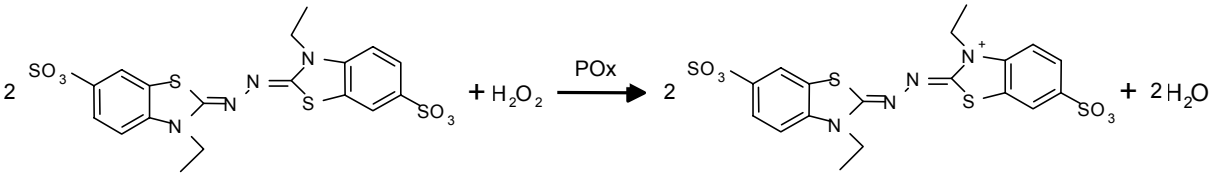

A calibration curve using different amounts of hydrogen peroxide was recorded. A 30 % (w/w) solution of hydrogen peroxide (Merck) was diluted appropriately. 10 µL of the peroxide solution were added to 120 µL of a 30 mM glucose solution and 5 mM ABTS solution in 50 mM phosphate buffer pH 7, and the absorbance spectra were scanned with an MTP absorbance scanner Ascent iEMS Reader MF (Thermo Labsystems). The calibration curve was recorded at an absorbance of 450 nm within a H_2O_2 range of 0 – 0.044 µmol/well.

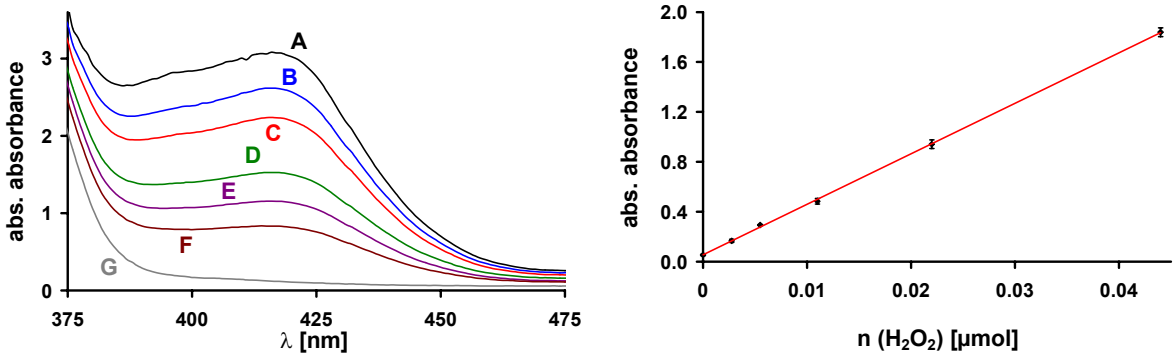

Fig. 3.7. Left: Absorbance spectra using different amounts of H_2O_2: (A): 0.017, (B): 0.015, (C): 0.013, (D): 0.009, (E): 0.006, (F): 0.004, and (G): 0 µmol (reduced form of ABTS); Right: Calibration plot at 450 nm.

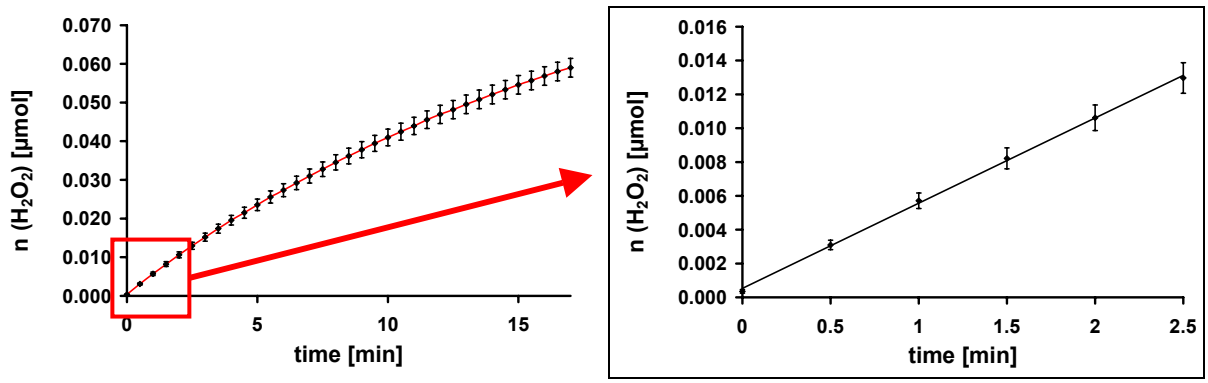

Fig. 3.8. Determination of GOx activity using ABTS as H_2O_2 indicator. The activity is calculated from the slope of the linear range at the beginning of the enzyme kinetic.

The effective activity of GOx was determined by mixing 10 µL of a 10 µg/mL GOx solution to 60 µL of a 5 mM ABTS solution and 10 µL of a 117.5 U/mL peroxidase solution. The reaction was started by adding 60 µL of a 30 mM glucose solution and the kinetic recorded over 30 min. All solutions were dissolved in phosphate buffer, pH 7. The effective GOx activity was calculated from the slope of the linear fit over 2.5 min. Differing from the maximum activity specified on the package, an activity of only $^1/_5$ (ca. 50000 U/g) was obtained.

3.3.3. Model Simulation

Vertical gradients within a sample containing an oxygen-consuming enzyme reaction were simulated for different MTP materials and covers. For this purpose, the model for oxygen ingress (chapter 3.2.1.1) was extended by an oxygen uptake rate (OUR) in the water layers described by enzyme kinetic equations [19] (see Appendix 11.2). Michaelis constants were taken from literature [20] as well as the diffusion constant and solubility of oxygen in paraffin oil [21, 22]. The OUR depends on cO_2 and is therefore different for each layer.

$$\frac{dcO_2[i]}{dt} = \frac{D_{O2}}{d[i]^2} \cdot (cO_2[i-1] + cO_2[i+1] - 2 \cdot cO_2[i]) - OUR[i] \qquad \text{(equation 5)}$$

Employing an oxygen-consuming enzyme kinetic, the initial pO_2 corresponds to air saturation. If the rate of oxygen consumption by the enzyme kinetic is higher than the oxygen ingress into the sample from ambient air, oxygen decrease in the sample takes place instead of accumulation stated in eqn. 3.1.

3.3.4. Experimental

For the fibre-optic sensor experiments, 120 µL of a 100 mM glucose solution (Merck) and 10 µL of a 88 U/mL catalase solution (from bovine liver, 2200 U/mg solid; Sigma) were pipetted into the well of a 96-well polystyrene (PS) MTP (U bottom; Greiner, Catalogue No. 650101). The sensor-coated tip of a fibre-optic microsensor (NTH-L2.5-TF-NS 0.40x40mm-PA0-YOP, PreSens) was positioned in the middle of the well (s. Fig. 3.9). The reaction was started by addition of 0.005 U and 0.02 U GOx (from Aspergillus niger, maximum activity 245000 U/g; Sigma), respectively. The solution was mixed by rinsing the pipette tip with the sample two times immediately after addition of GOx. Then 100 µL of paraffin oil were added. pO_2 was measured continuously with an oxygen meter (Microx TX2; PreSens).

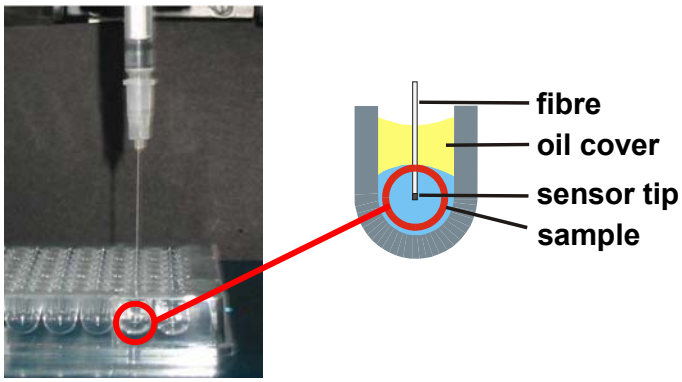

Fig. 3.9. Set-up for the fibre-optic sensor experiments. The sensor tip (circle) was positioned in the centre of the well and then gradually moved vertically and horizontally, respectively, by means of a micromanipulator to obtain the pO_2 distribution within the paraffin oil-covered sample.

The detection of enzyme kinetics in a sensor-coated PS MTP was performed with 120 µL of a 30 mM glucose solution and 10 µL of a 88 U/mL catalase solution. In the experiment with 100 µL of paraffin oil as plate sealing, the reaction was started by addition of various GOx activities ranging from 0.004 U/well to 0.1 U/well. After 120 min, the measurement interval was changed from 30 s to 2 min. The experiment was repeated with a measurement interval of 30 s and 60 µL of glucose and GOx activities ranging from 0.002 U/well to 0.05 U/well and compared with absorption measurements using 5 mM ABTS and 10 µl of 117 U/mL of peroxidase instead of catalase (see chapter 3.3.2). Finally, the effect of various plate sealings with differing permeability towards oxygen were tested. In this experiment, 120 µL of a 100 mM glucose solution was mixed with 10 µL of a 88 U/mL catalase solution. The reaction was started by addition of 0.02 U GOx solution (20 µL). The enzymes and glucose were solved in buffer solution pH 7 (Merck). The solution was mixed by rinsing the pipette tip with the sample two times immediately after addition of GOx. Then the wells were covered with the respective sealing. Using foil sealings, two-fold volumes of glucose and enzyme solutions were applied. Using paraffin wax as plate sealing, this enzyme kinetic was also detected with another commercially available oxygen-sensitive MTP, the Oxygen BioSensor (OBS, Becton Dickinson).

3.3.5. Results and Discussion

3.3.5.1. Heterogeneous Distribution of pO_2 within the Microtiterplate Well

Oxygen diffusion through the MTP sealing and material leads to a gradient within the sample. These oxygen gradients in MTP wells were either measured with a fibre-optic sensor or simulated using a mathematical model. Considering the vertical gradient within the sample, pO_2 values were taken from the end point of the enzyme kinetics when a dynamic equilibrium between oxygen flux into the sample and oxygen consumption by the enzyme kinetic was reached. pO_2 of this steady-state depends on the enzyme activity. Fig. 3.10. shows the vertical pO_2 distribution in the sample simulated for a paraffin oil-covered PS MTP and different enzyme activities. pO_2 is highest near the oil cover and decreases with increasing distance as

expected. However, after reaching a minimum, pO_2 increases again measurably towards the bottom of the well. With low enzyme activities, pO_2 does not decrease to zero even in the middle of the well where the influence of oxygen diffusion from the ambient air is lowest. This shows that the oxygen exchange with the MTP bottom and walls has to be taken into consideration.

The oxygen gradient within the sample is the greater, the less convection takes place. Best possible homogeneity can be reached by rapid plate shaking [9], which, however, leads to a high oxygen ingress using no or paraffin oil covers, as shown above, and has no great effect using wax or foil sealings. Without additional plate shaking, pO_2 detected with a sensor film located at the bottom of the MTP well is measurably influenced by oxygen diffusion through the MTP material because of the immediate contact of sensor and MTP.

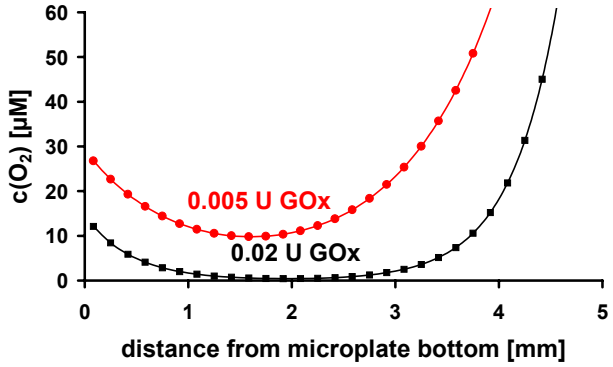

Fig. 3.10. Simulated vertical oxygen gradients in a paraffin oil-covered sample with low oxygen content containing different GOx activities. After a minimum, oxygen increases again towards the bottom of the well.

The simulations were confirmed by measurements of pO_2 heterogeneities within an oil-covered sample in a PS MTP well using a fibre-optic oxygen microsensor. The small size of the microsensor guarantees only minimal effect on the layering of the sample and enables a pO_2 resolution of less then 50 µm. Glucose oxidation by two different GOx activities was employed as an oxygen-consuming enzyme reaction to obtain a low constant pO_2 within the sample. Excess catalase was added to prevent the thereby formed hydrogen peroxide from destroying the GOx. The sample was covered with 100 µL of paraffin oil. For technical reasons it was impossible to use foil or wax covers for these experiments. The sensor tip was first placed in the middle of the well near the oil cover and then gradually moved downwards by means of a micromanipulator to obtain the heterogeneities in vertical direction. The heterogeneities in horizontal direction were measured by positioning

the sensor tip at a height of 2.5 mm from the bottom of the well and moving it towards the edge of the well until it touched the wall. The results are depicted in Fig. 3.11.

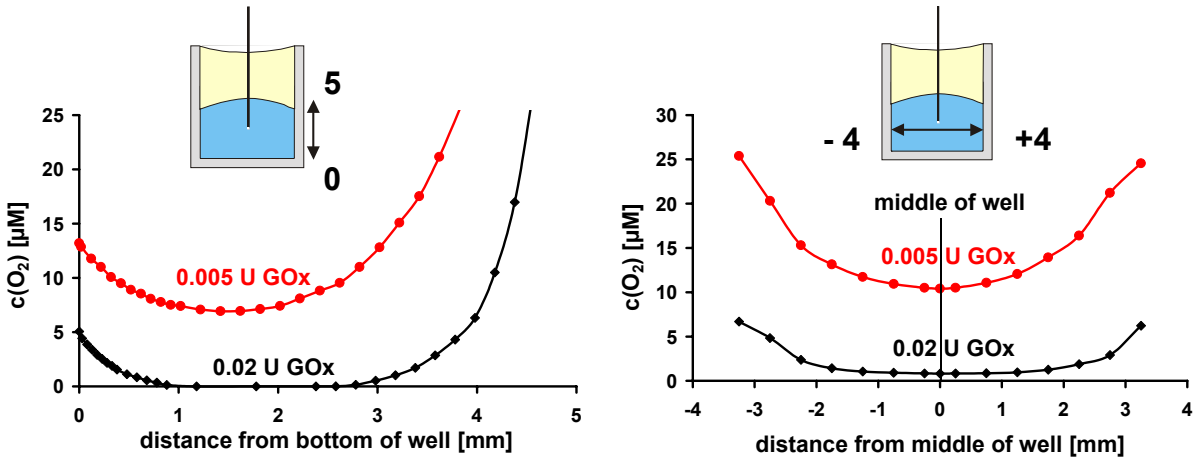

Fig. 3.11. Vertical (left) and horizontal (right) oxygen gradient within the paraffin oil-covered sample obtained with the fibre-optic sensor.

The vertical pO_2 distribution showed an increase towards the cover and the bottom of the well as simulated (Fig. 3.11, left). The same effect could be seen with the horizontal oxygen gradient (Fig. 3.11, right): It was observed that pO_2 increased near the edge of the well, although the oil layer is thinnest in the middle of the well due to different wetting properties and the resultant menisci and a pO_2 maximum should therefore be expected in the middle of the well. This is another evidence that oxygen significantly diffuses into the sample not only through the oil cover, but also through or from the PS MTP.

$c(O_2)$ increase at the bottom of the well can be minimised using less oxygen-permeable MTP materials. Fig. 3.12. (left) shows the effect of different materials on the oxygen diffusion into an unshaken, paraffin oil-covered sample. The model was simulated for completely deaerated PS, polypropylene (PP) and PET MTPs. Polypropylene MTPs, which represent the second commonly used MTP type, are similarly permeable towards oxygen as PS MTPs due to similar oxygen solubility and permeability coefficients [23, 24]. With PET MTPs the gradient at the bottom of the well is much smaller than with PS or PP MTPs due to lower solubility and diffusion coefficients of PET, resulting in slower oxygen diffusion through the MTP material into the sample. Thus, PET barriers or coatings of likewise low permeability are an efficient protection against oxygen diffusion into the sample through the MTP.

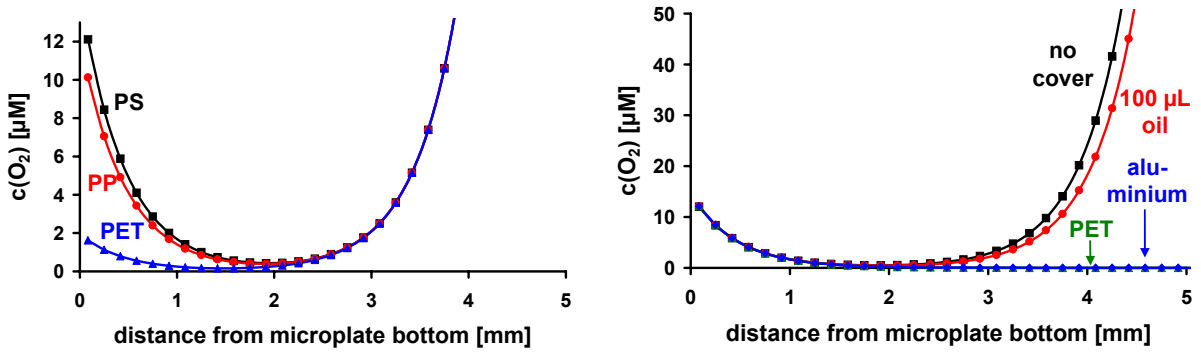

Fig. 3.12. Left: Simulated vertical oxygen gradient in a paraffin oil-covered sample containing 0.02 U GOx with different MTP materials (PS, PP, PET). Right: Simulated vertical oxygen gradient in a sample with no cover and sealed with 100 µL of paraffin oil, PET and aluminium foil, respectively.

Simulations employing different MTP sealings (Fig. 3.12. right) showed that the use of paraffin oil results in heterogeneities similar to those without cover, which is due to its large oxygen solubility. The oil acts as an oxygen reservoir which rapidly releases the oxygen into the sample. In contrast, PET foil with its low oxygen permeability reduced the gradient almost to zero, which makes it as applicable as aluminium foil.

3.3.5.2. Effects of Oxygen Ingress on Enzyme Kinetic Detection

Concerning kinetic parameters of enzyme kinetics or respirometry measurements, oxygen ingress into the sample can lead to incorrect results. In an oxygen-consuming enzyme reaction like the oxidation of glucose by GOx, oxygen entering the sample partially compensates the oxygen consumption and leads to lower apparent enzyme activities. The same is true for oxygen consumption by respiratory activity of bacteria. The consequences of oxygen ingress into the sample using oxygen sensors is shown considering the oxidation of glucose by various activities of GOx as example.

Using 100 µL paraffin oil as plate sealing, oxygen ingress into the sample is rather high because it is not only driven by diffusion but forced by convection. This high oxygen ingress partly compensates the oxygen consumption of the enzyme reaction depending on its oxygen uptake rate (OUR). Whereas the kinetics using high GOx activities converge to zero (Fig. 3.13 E, F), lower enzyme activities are more

influenced by oxygen ingress: After initial oxygen decrease, a steady-state between oxygen ingress into the sample and oxygen consumption by the enzyme kinetic is formed, its level depending on both the enzyme activity and the amount of oxygen ingress. After 120 min, the measurement interval was changed from 30 s to 2 min, which leads to a lower oxygen ingress and lowers the level of the steady state. After some time, however, pO_2 starts to increase, which indicates deactivation of the GOx either directly due to destruction by oxygen [15], or indirectly by H_2O_2 due to deactivation of catalase [14]. The point in time of this increase depends on the applied total enzyme activity: Whereas the kinetic using the lowest activity (Fig. 3.13 A) starts to increase even within 2 h, higher activities lead to a later increase (B, C), or the enzyme destruction is even negligible compared to the total enzyme activity (D - F).

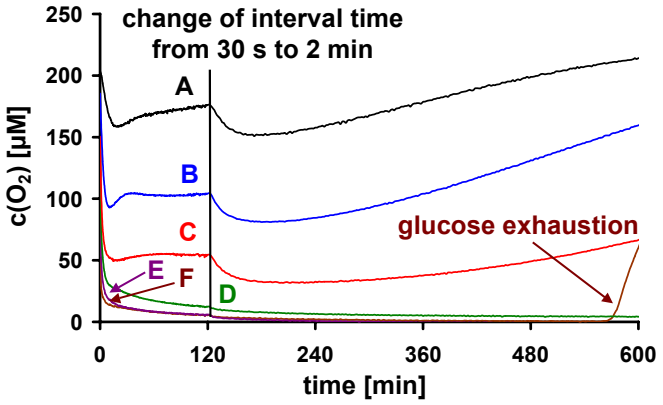

Fig. 3.13. Oxygen decrease due to the oxidation of 30 mM glucose by different amounts of GOx: (A) 0.004, (B) 0.01, (C) 0.02, (D) 0.04, (E) 0.05, (F) 0.1 U/well. The MTP was sealed with 100 µL of paraffin oil.

The enormous influence of the oxygen ingress using permeable sealings was further illustrated by a comparative experiment using the determination of the product H_2O_2 by ABTS instead of the detection of the educt oxygen. The same enzyme activities, glucose concentration and plate sealing (100 µL paraffin oil) were used for both experiments. The increase of absorbance of ABTS by production of H_2O_2 by GOx was converted into µmol H_2O_2 using a calibration curve (see Fig. 3.7, right). The formation of H_2O_2 equals the consumption of the same amount of oxygen (see page 89). More than the 6-fold amount of oxygen diffuses into the sample within 2 h and is consumed by the enzyme reaction (Fig. 3.14, left). After that time, the indicator dye ABTS is completely consumed and the kinetic converges towards an end value. The kinetics involving the two highest enzyme activities (0.1 U and 0.25 U) show a slightly different behaviour: After a rapid oxygen decrease, the curve grows more shallow, and the end value of the other kinetics is not reached. It is assumed that either ABTS is destroyed during

the reaction, or that the H_2O_2 production is faster than its reaction with ABTS, which decreases during the reaction, leading to a destruction of GOx by excess H_2O_2. Substrate limitation was ruled out as possible reason due to comparison with the oxygen determination with the oxygen sensor (Fig. 3.14, right). Glucose exhaustion would lead to rapid oxygen increase because the oxygen ingress dominates over the consumption (see Fig. 3.13, F). The determination of the enzyme activity via a parameter independent of oxygen shows the great influence of oxygen ingress on the results obtained with oxygen sensors. Thus, using the initial slope as parameter for the kinetic determination of enzyme activities, oxygen sensors in permeable PS MTPs are not suitable. However, the formation of a steady-state between oxygen consumption and ingress can be used for an end-point determination of the GOx activity. At known and reproducible oxygen ingress, even fast activities, which would be difficult to detect kinetically, can be obtained.

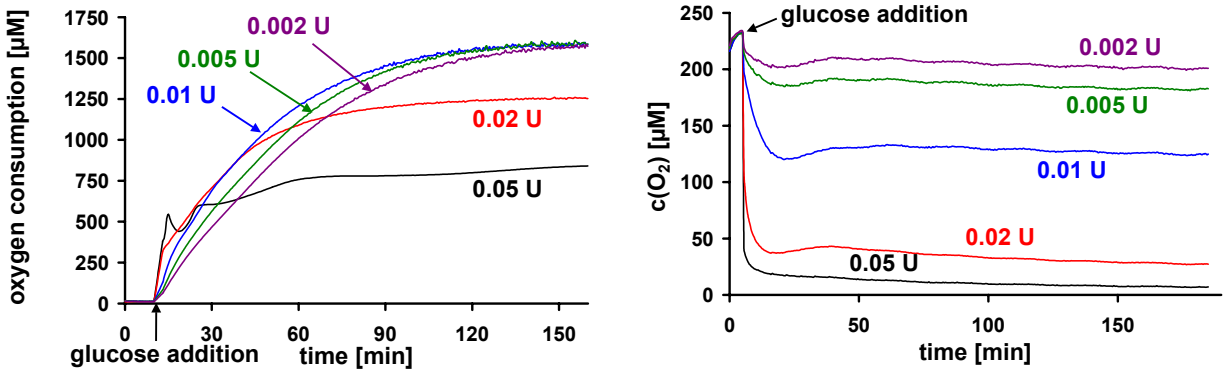

Fig. 3.14. Oxygen consumption due to the oxidation of 30 mM glucose by different amounts of GOx: 0.002, 0.005, 0.01, 0.02, 0.025, 0.05 U/well. The MTPs were sealed with 100 µL of paraffin oil. Left: Calculated oxygen consumption detected by absorbance measurement using ABTS. Right: Detection using the oxygen-sensitive MTP OxoPlate.

The influence of the plate sealing was investigated by glucose oxidation using 0.5 U GOx/mL in differently covered samples in a PS MTP. The value after 240 min was compared to the same enzyme kinetic measured in a hermetically sealed glass MTP covered with PET foil. Fig. 3.15, right, shows the deviations in $c(O_2)$ measured with the PS MTP at the time point (240 min) when the oxygen content is almost zero in the glass MTP well. Without any cover, the deviation of 82 µM from the correct value

is almost one third of air saturation, with 50 µL of paraffin oil cover it is still 21 µM, whereas all 3 tested foil covers and paraffin wax with and without solvent minimise the deviation. The remaining deviation of 5 µM is therefore due to the oxygen diffusion through the PS MTP material, which has direct contact to the oxygen sensor located at the bottom of the plate.

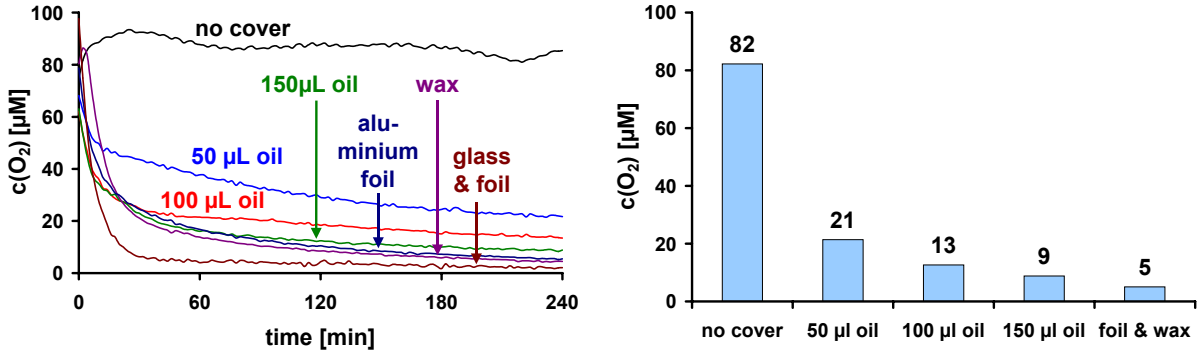

Fig. 3.15. Oxygen concentration at the enzymatic oxidation of glucose using 0.5 U/mL GOx in differently sealed PS plates. Left: Kinetics over 4 h; Right: Oxygen content after 240 min. At this time, $c(O_2)$ in the hermetically sealed reference glass plate is less than 0.6 µM.

3.3.5.3. Influence of the Sensor Location and Composition on Detection of Kinetics

Enzyme kinetics measured with the fibre-optic sensor were compared to those obtained with the sensor-coated MTP. Using the fibre-optic sensor, the sample was covered with 100 µL paraffin oil, whereas the sensor plate experiments were performed using 100 µL of paraffin wax to exclude influences due to convection. The results are depicted in Fig. 3.16: Despite similar permeabilities of paraffin oil and wax towards oxygen, the enzyme kinetic measured with the fibre-optic sensor positioned in the centre of the well seems to be faster and results in a lower steady state pO_2 than the one measured with the sensor film at the bottom of the well. This shows the importance of considering the **location of the sensor**: Oxygen ingress is greater at the bottom of the well due to the permeability of the MTP material than in the middle despite the closer distance to the permeable cover.

Another parameter which strongly influences the oxygen signal is the **composition of the sensor**. Fig. 3.16 shows the measured (left) and simulated (right) enzyme kinetics detected with a commercially available polysiloxane-based sensor (OBS) with an estimated thickness of 200 µm [25]. The kinetics using the polysiloxane-based sensor are much slower than the ones obtained with the hydrogel-based sensor (sensor film thickness 10 µm) due to greater sensor film thickness and the higher oxygen solubility of polysiloxane compared to hydrogel [23, 26]. The sensor film serves as an oxygen reservoir which is deoxygenated by the enzyme kinetic. Thus, the resulting response time of the sensor strongly influences the correctness of the obtained kinetic.

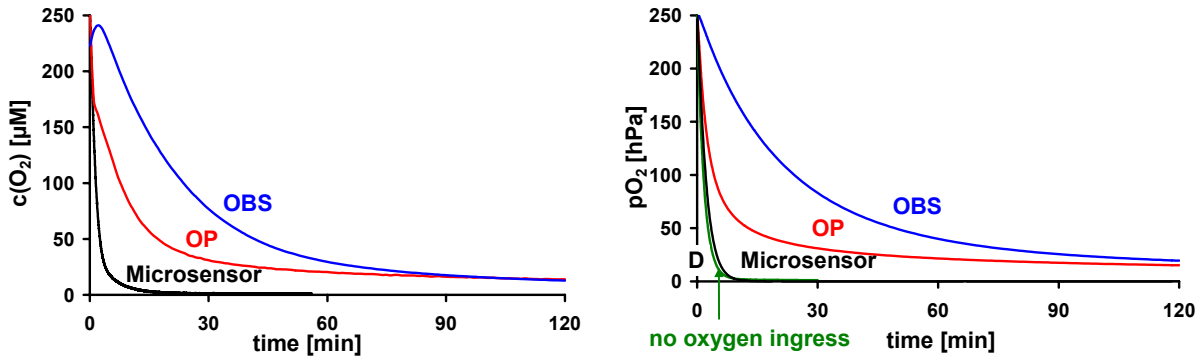

Fig. 3.16. ***Measured*** *(left) and* ***simulated*** *(right) oxygen decrease in an enzyme kinetic detected with the fibre-optic sensor using 100 µL paraffin oil sealing and the reader using 100 µL paraffin wax sealing with 0.02 U GOx per well. Two types of commercially available oxygen-sensitive MTPs were tested, the OxoPlate (OP) and the Oxygen BioSensor (OBS). For comparison, the simulated enzyme kinetic without oxygen diffusion from ambient air is shown..*

3.4. Conclusion

Detecting low enzymatic or metabolic rates based on oxygen measurements in MTP wells, oxygen diffusion through the cover and the MTP material play an important role and have therefore to be taken into account to obtain correct results. The cover should be preferably impermeable towards oxygen to detect even low oxygen uptake rates. For application in high-throughput screening, another parameter of high importance is the well-to-well reproducibility without any outliers which is the pre-requisition for automated evaluation.

Using MTPs, paraffin oil proved to be a poor protection from oxygen diffusion into the sample even with large amounts of paraffin oil, due to convection caused by inevitable movement of the MTP during the measurement. Shaking during lag times, which is sometimes necessary for homogeneity in the sample and prevention from precipitation of solid particles, increases the convection depending on the shaking mode. To avoid convection, rigid sealings have to be used. Foils of low or no permeability towards oxygen, e.g. based on PET or aluminium, would be the optimal protection from oxygen transfer through the cover if bubble-free sealing was possible. However, an inevitable gas phase, which contributes largely to the oxygen reservoir in the sample if filling takes place under ambient air, the requirement of a maximum filling volume to minimise this gas phase, and cumbersome handling make these sealings less attractive. Paraffin wax dissolved in volatile solvents, which can be pipetted on the sample and gets almost rigid very quickly, avoids convection and a remaining gas phase and results in good well-to-well reproducibility but proved to be inapplicable due to inevitable temperature effects, cumbersome handling and, most important, low reproducibility of the resulting oxygen ingress because evaporation of the solvent during storage causes varying solvent content. With cap mats punctured for elusion of excess air, the same problem as with foil sealings occurred: Inevitable gas phases remained in some wells. These sorting out of outliers makes evaluation unacceptably labour-intensive for high throughput screening. The method of choice was the use of 100 µL paraffin oil using the lowest possible plate acceleration of the reader. Despite higher oxygen ingress than with rigid sealing, this method showed excellent well-to-well reproducibility and was applicable for calculation of correct inhibitions in toxicological test (see chapter 4).

Although suitable for the task of this work, our sealing of choice is not ideal for detection of lower oxygen consumptions due to the unavoidable convection of liquid plate sealings in MTP reader measurements, which can even lead to a total compensation of low OURs by oxygen ingress. For the application of rigid sealings is difficult to automatise, which is a major prerequisite for a high throughput, convection has to be decreased by other means. Choosing an MTP format with wells of a lower diameter, e.g. a 384-well or PCR plate, convection of the sample, especially covered with a liquid of high density, could solve this problem [27]. A contrary approach is the plate format designed by Papkovsky et al. [28]: The wells display a rather large surface-to-volume ratio. The MTP is covered with a thin glass lid as impermeable sealing, and excess sample is driven out into overspill areas. The interaction of the large aqueous surface and the glass lid provides for its adhesion on the sample. The samples themselves are kept in the wells by surface tension. However, besides the danger of cross-contamination due to overspilling, this format uses capillary effects and is designed for very small sample volumes (< 1 µL) and a dissolved oxygen indicator and is not applicable for coated MTPs.

Last but not least, convection can be eliminated by using a set-up where the MTP is stagnant and either the optical system moves for measurement, or the each well is addressed separately (c.f. SDR2, chapter 2.4.3). Both methods, however, complicate the instrument set-up considerably.

Aside from the oxygen diffusion through the cover, diffusion through the MTP material was observed. Furthermore, the PS MTP proved to act as an air reservoir which rapidly releases oxygen into samples with low pO_2. This diffusion is negligible compared to the oxygen flux involving convection, but greater than the oxygen ingress from the cover using rigid sealings of lower permeability such as aluminium and PET foils or paraffin wax. Model simulations showed that this oxygen diffusion through the MTP material could be dramatically reduced using less permeable materials like PET. Another approach is the coating of the MTP with even less permeable polymer films made of PAN. Here, the latter method could be applied without the need of fabrication of completely new MTPs.

3.5. References

1 Ruitenberg EJ, Brosi BJ, and Steerenberg PA. *Direct measurement of microplates and its application to enzyme-linked immunosorbent assay*. (1976). Journal of Clinical Microbiology **3**(5), 541-542.

2 Mulder J, McKinney N, Christopherson C, Sninsky J, Greenfield L, and Kwok S. *Rapid and simple PCR assay for quantitation of human immunodeficiency virus type 1 RNA in plasma: application to acute retroviral infection*. (1994). Journal of Clinical Microbiology **32**(2), 292-300.

3 John GT and Heinzle E. *Quantitative screening method for hydrolases in microplates using pH indicators: determination of Kinetic parameters by dynamic pH monitoring*. (2001). Biotechnology and Bioengineering **72**(6), 620-627.

4 Moris-Varas F, Shah A, Aikens J, Nadkarni NP, Rozzell JD, and Demirjian DC. *Visualization of enzyme-catalyzed reactions using pH indicators: rapid screening of hydrolase libraries and estimation of the enantioselectivity*. (1999). Bioorganic & Medicinal Chemistry **7**(10), 2183-2188.

5 Eisentraeger A, Dott W, Klein J, and Hahn S. *Comparative studies on algal toxicity testing using fluorometric microplate and Erlenmeyer flask growth-inhibition assays*. (2003). Ecotoxicology and Environmental Safety **54**(3), 346-354.

6 Hynes J, Floyd S, Soini AE, O'Connor R, and Papkovsky DB. *Fluorescence-based cell viability screening assays using water-soluble oxygen probes*. (2003). J Biomol Screen **8**(3), 264-272.

7 Wittmann C, Yang T, Kochems I, and Heinzle E. *Dynamic respiratory measurements of Corynebacterium glutamicum using membrane mass spectrometry*. (2001). Journal of Microbiology and Biotechnology **11**(1), 40-49.

8 König B. *Enzymatic Determination of Glucose by a Combination of Optode and Microplate Techniques.* (1997). Diploma thesis, University of Regensburg, Germany.

9 Weiss S, John GT, Klimant I, and Heinzle E. *Modeling of mixing in 96-well microplates observed with fluorescence indicators*. (2002). Biotechnology Progress **18**(4), 821-830.

10 Ingham J, Dunn IJ, Heinzle E, and Prenosil JE. *Chemical Engineering Dynamics: Modelling with PC Simulation*. 2nd edition, Wiley-VCH, Weinheim (2000).

11 Dunn IJ, Heinzle E, Ingham J, and Prenosil JE. *Biological Reaction Engineering*. *Dynamic Modelling Fundamentals with Simulation Exercises.* Wiley-VCH, Weinheim (1992).

12 Maier U and Buchs J. *Characterisation of the gas-liquid mass transfer in shaking bioreactors*. (2001). Biochemical Engineering Journal **7**(2), 99-106.

13 John GT, Klimant I, Wittmann C, and Heinzle E. *Integrated optical sensing of dissolved oxygen in microtiter plates: a novel tool for microbial cultivation*. (2003). Biotechnology and Bioengineering **81**(7), 829-836.

14 Greenfield PF, Kittrell JR, and Laurence RL. *Inactivation of immobilized glucose oxidase by hydrogen peroxide*. (1975). Analytical Biochemistry **65**(1), 109-124.

15 Venugopal R and Saville BA. *The effect of oxygen upon the kinetics of glucose oxidase inactivation*. (1993). Canadian Journal of Chemical Engineering **71**(6), 917-924.

16 Schomburg D. *Enzyme Handbook*, Volume 7: Class 1.5 - 1.12: Oxidoreductases. Springer, Berlin (1994).

17 Bergmeyer HU. *Methods of Enzymatic Analysis*, Vol II. Verlag Chemie, Weinheim, (1983) 200-203

18 Danneel HJ, Roessner E, Zeeck A, and Giffhorn F. *Purification and characterization of a pyranose oxidase from the basidiomycete Peniophora gigantea and chemical analyses of its reaction products*. (1993). European Journal of Biochemistry **214**(3), 795-802.

19 Gibson QH, Swoboda BE, Massey V. *Kinetics and mechanism of action of glucose oxidase.* (1964). Journal of Biologivcal Chemistry **239**, 3927-3934.

20 Nakamura S, Hayashi S, and Koga K. *Effect of periodate oxidation on the structure and properties of glucose oxidase*. (1976). Biochimica et Biophysica Acta **445**(2), 294-308.

21 Novak K. *Estimation of oxygen dissolved in liquids*. (1962). Chemicky Prumysl **12**, 658-660.

22 Kekedy L and Teuca I. *Study of oxygen permeability of thin protective organic liquid layers using a Clark-type oxygen sensor*. (1994). Magyar Kemiai Folyoirat **100**(6), 248-250.

23 Yasuda H, Stannett V. *Permeability Coefficients.* In: Bandrup J (ed.). *Polymer Handbook*. (1999). **4th ed.** New York: Wiley. p. III-229-II-239.

24 Eken M, Turhan S, Kaptan Y, and Gueven O. *Diffusion of oxygen into irradiated polypropylene films*. (1995). Radiation Physics and Chemistry **46**(4-6, Proceedings of the 9th International Meeting on Radiation Processing, 1994, Pt. 1), 809-812.

25 Wodnicka M, Guarino RD, Hemperly JJ, Timmins MR, Stitt D, Pitner JB. 2000. Novel fluorescent technology platform for high throughput cytotoxicity and proliferation assays. Journal of Biomolecular Screening 5:141-152.

26 Stannett V. *Simple Gases*. In: Crank J and Park GS. *Diffusion in Polymers*. Academic Press, London (1968) p.41-73.

27 O'Mahony FC, O'Donovan C, Hynes J, Moore T, Davenport J, and Papkovsky DB. *Optical oxygen microrespirometry as a platform for environmental toxicology and animal model studies*. (2005). Environmental Science & Technology **39**(13), 5010-5014.

28 Alderman J, Hynes J, Floyd SM, Kruger J, O'Connor R, and Papkovsky DB. *A low-volume platform for cell-respirometric screening based on quenched-luminescence oxygen sensing*. (2004). Biosensors & Bioelectronics **19**(11), 1529-1535.

4. *Pseudomonas Putida* Respiration Inhibition Test Performed in Microtiterplates

4.1. Introduction

Increasing production of new chemicals demands fast and low-cost toxicity tests. The effect of substances on the respiratory activity of test organisms is a sensitive way to assess its toxicity. The most significant parameter considering respiratory activity is oxygen, which is widely detected with oxygen electrodes [1, 2]. Besides drawbacks as oxygen-consumption, dependence on the flow velocity interference by sample ingredients and the non-invasiveness of the method, which is possible source of contamination, oxygen electrodes are costly, difficult to miniaturise and not suitable for high throughput screening. A more adequate method is the combination of microtiterplate (MTP) assays with non-invasive optical sensor technology [3]. In this chapter, a German toxicological standard test, the *Pseudomonas putida* respiration inhibition test [4], which is usually performed with oxygen electrodes, is transferred to the MTP format using 96-well MTPs containing an oxygen-sensitive fluorescent sensor film at the bottom of their wells. The results are investigated with respect to their repeatability and well-to-well reproducibility, accuracy with respect to a comparative experiment and the influence of different plate sealings and bacteria concentrations. Detection of a second parameter important for respiratory determination, the pH value, was performed as promising alternative to oxygen detection and both results compared to those obtained with a set-up using glass vessels. Various toxic substances were screened with both pH and oxygen sensors.

4.2. Monitoring of Bacterial Growth

Before investigating the respiratory activity of a constant amount of bacteria, the growth of *Escherichia coli* (*E. coli*), strain K12, and *Pseudomonas putida* (*P. putida*) MIGULA, strain Berlin (DSMZ, German Collection of Microorganisms and Cell Cultures) was detected using the optically isolated pH sensor and the oxygen-sensitive MTP. *E. coli* were cultivated for 24 h on a Mueller-Hinton agar plate (Oxoid) at 37 °C. 100 mL of *E. coli* broth (Sigma-Aldrich) were inoculated with the grown bacteria and shaken for 16 h with an orbital flask shaker (Sartorius BBI Systems) at 230 rpm. *P. putida* were treated accordingly, but grown on standard agar S1 (Sigma-Aldrich) at 25 °C, and the preculture cultivated in standard medium S1 (Sigma-Aldrich) at 25 °C. Starting from the preculture, four dilutions with the respective medium were made, each in a ten-fold lower concentration. The bacteria concentration was determined by the plate count method (see chapter 4.3.2.2). 150 µL/well of the dilutions were covered with a PET foil sealing (No. 676001, from Greiner) and measured for 15 h at 37 °C (*E. coli*) and 25 °C (*P. putida*), respectively, in the MTP reader at a shaking mode of 600 rpm.

Respiration of the bacteria leads to a pH decrease due to CO_2 production. At the same time, oxygen is consumed. The inoculum in the culture media was diluted 4 times, each dilution with a 10-fold lower concentration, starting from 4.6×10^3 cfu/mL (*E. coli*, pH experiment), 6.5×10^5 cfu/mL (*E. coli*, oxygen detection) and 8×10^6 cfu/mL (*P. putida*), respectively. The bacteria concentration was detected using the plate count method. The kinetics are shown in Fig. 4.1. Using the oxygen-sensitive MTP OxoPlate, oxygen decrease was registered over a period of ca. 75 min (*E. coli*, top & left) and between 82 and 116 min (*P. putida*, top & right), respectively, between the respective concentrations (values taken at 125 µM). The growth curve of *E. coli* detected with the pH-sensitive MTP HydroPlate (top & right) shows a pH decrease from pH 6.8 to 6.0 which could be detected over a period of approx. 1 h between the respective concentrations (values taken at pH 6.0). The growth curve of *P. putida* (bottom & right) shows a different behavior. The pH seems to increase from 5.5 to more than 8.0. The reason for this behavior is the production of fluorescein (pyoverdine) of *P. putida* during growth (see chapter 1.2.6), which diffuses into the sensor polymer matrix and leads to higher fluorescence. Therefore the use of this

sensor is not advised for pH monitoring in case of fluorescein-producing organisms like *P. putida.*

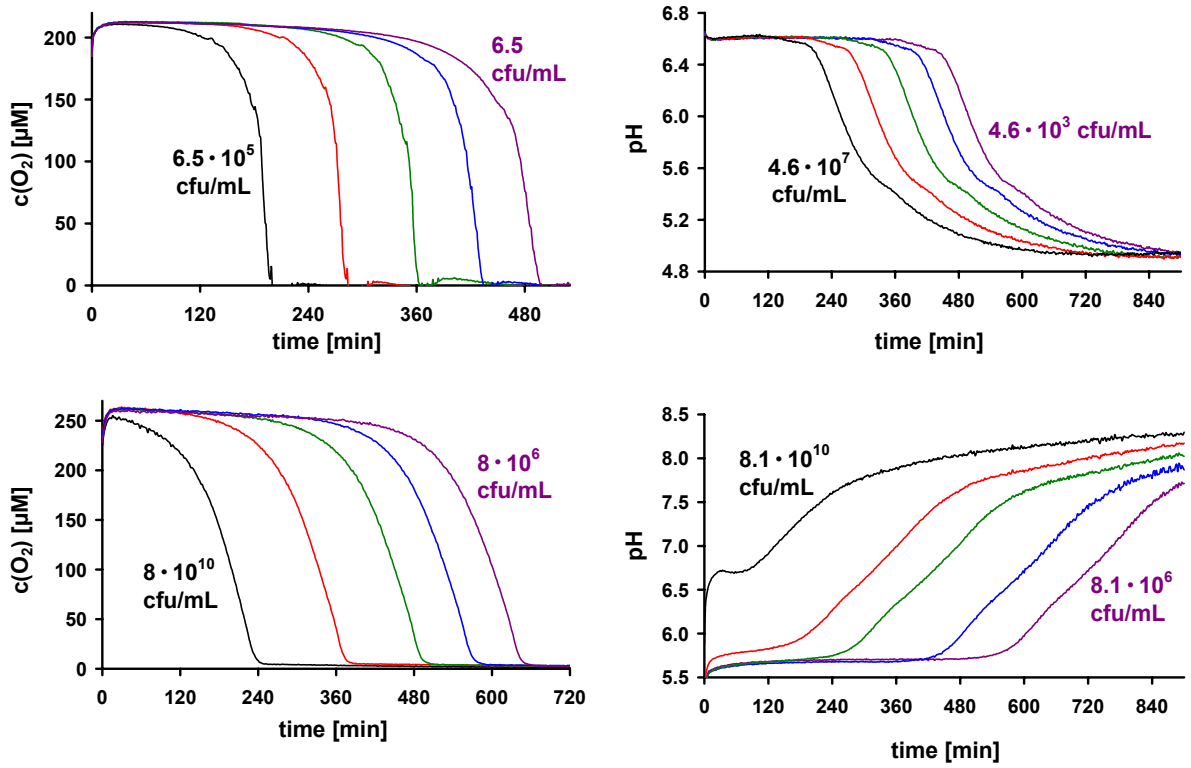

Fig. 4.1. Top: Growth kinetics of E. coli monitored with the OxoPlate (left) and the HydroPlate (right). Bottom: Growth kinetics of P. putida detected with the OxoPlate (left) and the HydroPlate (right). The inoculum was diluted 4 times with a ten-fold lower concentration, respectively.

4.3. Experimental Part

4.3.1. Preparation and Storage of the Inoculum

The bacteria were treated according to the German standard test [4]. *Pseudomonas putida* MIGULA, strain Berlin (DSMZ) were cultivated on an agar plate for at least 24 h at 25 °C. The agar for cultivation contained 7.5 g/L peptone from casein, 7.5 g/L peptone from meat, 3 g/L yeast extract, 6 g/L NaCl, 1 g/L glucose and 12 g/L agar. A preparatory culture with 50 mL of culture medium, which contained the same ingredients as the culture agar except the agar, in the same concentrations, was inoculated with the bacteria and shaken for (16 ± 1) h at 21 °C in a 250 mL Erlenmeyer flask with baffles sealed with an air-permeable cap. Several flask shakers and one MTP shaker (s. Table 4.1) were tested to provide sufficient oxygen supply during cultivation. Oxygen was monitored using with an oxygen sensor spot (PSt3, PreSens) glued to the bottom of the flask and read out with an oxygen meter (Fibox2, PreSens). No shaker could provide the overnight culture with sufficient oxygen for more than 12 h (Fig. 4.2). The oxygen increase using shaker (B) is due to excessive formation of foam. Shaker (E) had no proper equipment for mounting Erlenmeyer flasks. Therefore shaker (D) was used for all further experiments. The oxygen consumption of the preculture was tested after cultivation to guarantee a sufficient amount and activity of the bacteria. 5 mL of preculture were filled in a 5 mL glass vessel with a PSt3 sensor spot glued to the bottom of the vessel. Precultures with an OUR of less than 25 µM/ min were discarded.

Table 4.1. Shakers tested for oxygen supply during the cultivation of the bacteria.

	shaking mode	**shaking speed**	**type / company**
A	orbital	250 rpm	Stuart S150, Bibby Sterilin
B	linear	340 strokes /min	Gerhardt
C	orbital	not known (fast)	Yellow Line OS2 basic, IKA-Werke
D	orbital	250 rpm	HT TR1, B. Braun
E	linear	not known	Heidolph Instruments

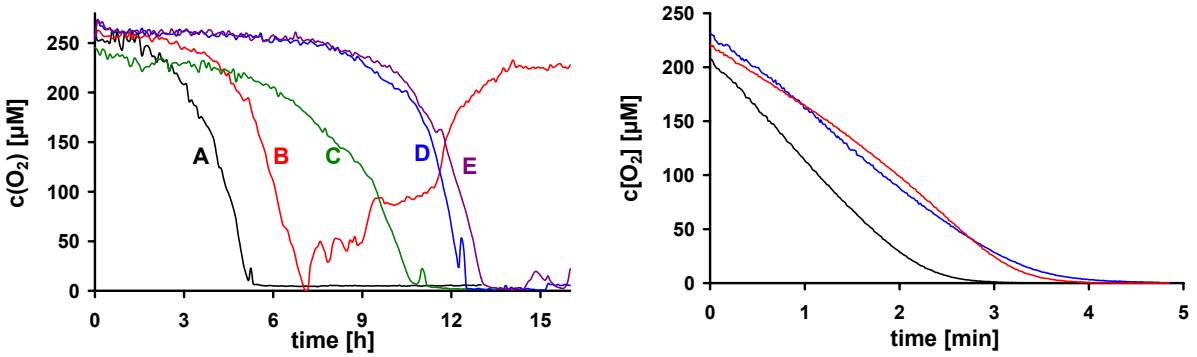

Fig. 4.2. Left: Oxygen consumption of the preculture during cultivation, measured with the fibre-optic minisensor using different shakers; Right: OUR of three precultures, ranging from 66 to 95 µM/ min.

The bacteria solution was centrifuged at 4000 g for 10 min (Biofuge primo, Heraeus Instruments, Hanau, Germany) and washed two times with 50 mM phosphate buffer solution, pH 7.2 (6.8 g/L KH_2PO_4 + 1.4 g/L NaOH). The bacteria were resuspended in phosphate buffer. All substances were purchased from Sigma-Aldrich or Merck.

4.3.2. Adjustment of Bacterial Concentration

For reproducible toxicity tests, it is essential to use similar bacteria concentrations for each test. Otherwise, the results will vary, for a higher amount of bacteria leads to less inhibition and therefore to higher EC_{50} values. EC_{50} is the Effective Concentration of a toxic substance which causes an inhibition of 50 %. A convenient and, for this purpose, sufficiently accurate method for obtaining the concentration is the adjustment of the optical density (OD) of a diluted sample of the inoculum at a distinct wavelength. The OD of low concentrations is usually detected as scattered light, whereas at higher bacterial concentrations, measurement of the absorption is more appropriate. Before obtaining the OD, the UV-Vis spectrophotometer has to be calibrated with turbid standards, for the characteristics of the instrument are different for each instrument and can change with time.

4.3.2.1. Calibration of the Spectrophotometer with Formazin

According to the European Norm *Determination of Turbidity* [5], the UV-Vis spectrophotometer (Cary 50, Varian) was calibrated with formazin standards of different concentrations. Formazin is a turbid polymer which is formed from hydrazine sulphate and hexamethylenetetramine (urotropin). In a first step, urotropin reacts with sulphuric acid (from hydrazine sulphate) to give formaldehyde, which reacts in a second step with hydrazine to yield formazin (s. Fig. 4.3).

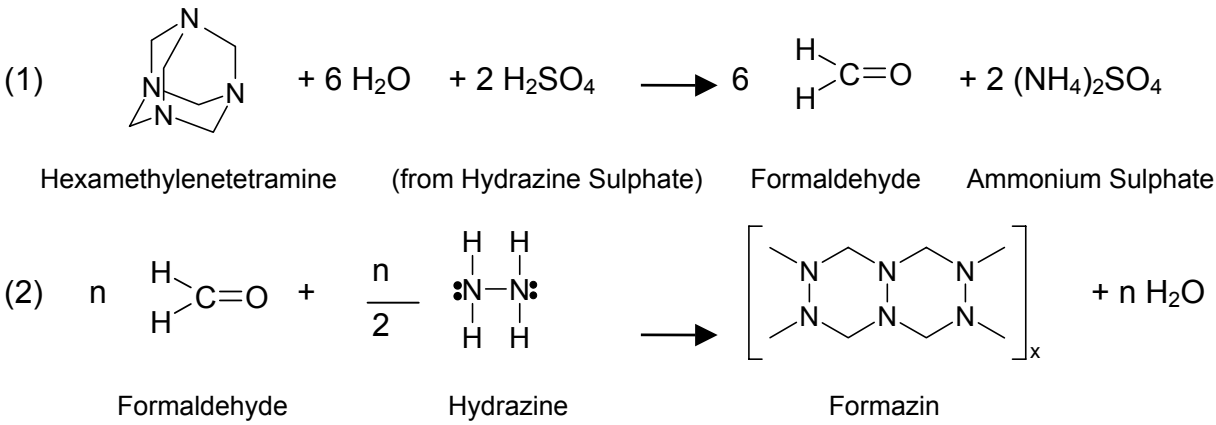

Fig. 4.3. 2-step formation of the turbid polymer formazin from hexamethylenetetramine (urotropin) and hydrazine sulphate.

2.5 g hexamethylenetetramine and 0.25 g hydrazine sulphate (both from Merck) were dissolved in 20 mL doubly distilled water, respectively. The two solutions were merged and filled up to 50 mL with doubly distilled water. The resulting suspension had a concentration of 4000 FAU (formazin attenuation units). This stock solution was stored at (25 ± 3) °C for 24 h and then diluted appropriately to obtain concentrations of 40, 80, 160, 200, 400, 750 and 1000 FAU.

For calibration, the OD of the dilutions was detected at a wavelength of 860 nm (OD_{860}). Plotting OD_{860} versus the formazin attenuation units FAU results in a linear correlation (s. Fig. 4.4). In the *P. putida* respiration inhibition test, the bacteria concentration of a $^1/_{100}$ dilution of the inoculum is prescribed to be (160 ± 60) FAU, which corresponds to an absorbance of (0.12 ± 0.05).

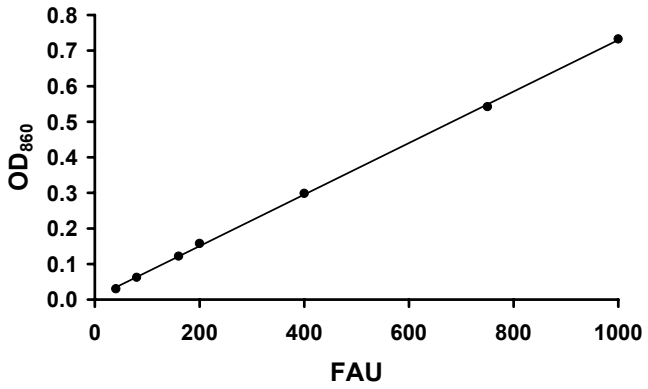

Fig. 4.4. Calibration plot of the optical density at 860 nm (OD_{860}) versus formazin attenuation units (FAU). The quality factor R^2 of the linear fit is better than 0.999.

4.3.2.2. Calculation of the Number of Bacteria

The number of bacteria corresponding to various ODs was determined via the plate count method [6]: Dilutions of the inoculum were prepared and the OD was detected at 436 nm (OD_{436}). The lowest concentration was diluted further. 20 µL of these dilutions were transferred onto agar plates, respectively, and distributed homogeneously on the agar using a Drigalski spatula. After 24 h of incubation at 25 °C, the number of grown colonies were and multiplied by the dilution factor to obtain viable count of colony-forming units (cfu) per mL in the original sample. One cfu equals one individual, assuming that one bacterium produces one colony. Only colonies per plate in the range of 10 to 200 were chosen for evaluation to provide sufficient accuracy. The plot OD_{436} versus cfu/mL (Fig. 4.5) reveals a linear correlation. The OD_{436} of (0.12 ± 0.05) corresponds to $(1.0 \pm 0.4) \cdot 10^8$ cfu/mL and equals $2.0 \cdot 10^8$ cfu/mL in the test solution.

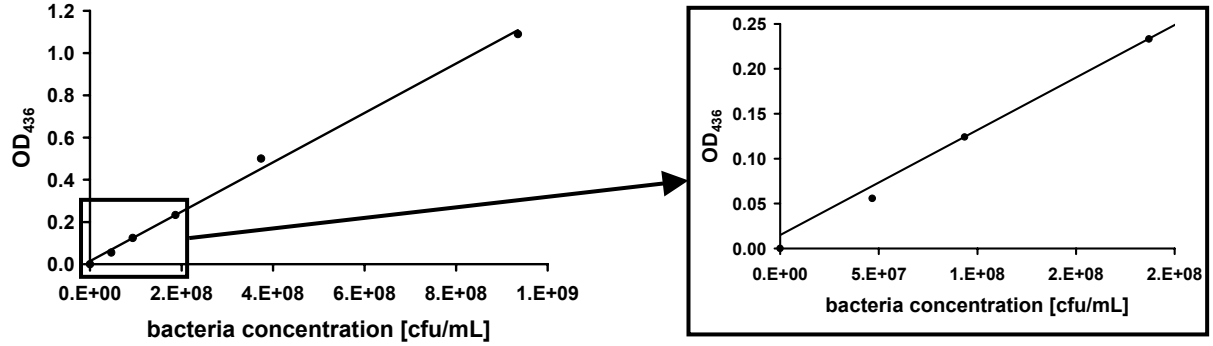

Fig. 4.5. Correlation between optical density at 436 nm (OD_{436}) and the bacteria concentration (cfu/mL) obtained with the plate count method.

4.3.2.3. Adjustment of the Concentration of P. Putida

For the *P. putida* respiration inhibition test, the inoculum was diluted 1:100 with 50 mM phosphate buffer. The optical density of this dilution was adjusted with 50 mM phosphate buffer to 0.12 ± 0.05 at 436 nm (OD_{436}), if not noted otherwise.

4.3.3. Test Solution

The test solution contained 2 mL of inoculum, 2 mL of a 2.5 M D(+) glucose solution (Merck) and 96 mL of dilution water, prepared from each 1 mL of the stock solutions S_1 to S_4, which consisted of 8.5 g/L KH_2PO_4, 21.75 g/L K_2HPO_4, 33.4 g/L $Na_2HPO_4 \cdot 2H_2O$, and 1.7 g/L NH_4Cl (S_1), 22.5 g/L $MgSO_4 \cdot 7H_2O$(S_2), 27.5 g/L $CaCl_2$ (S_3), and 0.25 g/L $FeCl_3 \cdot 6H_2O$ (S_4). Table 4.2 shows the ingredients and concentrations of the test solution. The dilution of the inoculum in the test solution is $^1/_{50}$, which corresponds to a bacterial concentration of $2 \cdot 10^8$ cfu/mL in the test solution. All ingredients were purchased from Merck. For measurements of inhibited bacterial activities, the dilution water contained additionally the respective amount of inhibitor.

Table 4.2. Ingredients and concentrations for the test solution (without inhibitor).

Ingredient	mg/L	mM
KH_2PO_4	144.5	1.062
K_2HPO_4	21.75	0.125
$Na_2HPO_4 \cdot 2H_2O$	33.4	0.188
NH_4Cl	1.7	0.032
$MgSO_4 \cdot 7H_2O$	22.5	0.091
$CaCl_2$	27.5	0.248
$FeCl_3 \cdot 6H_2O$	0.25	0.0009
NaOH	28	0.035
glucose	9.91	50
NaCl	5.8	100

4.3.4. General Measurement Procedure

The measurement procedure differs slightly depending on the respective sensor. All sensors and the oxygen meters were obtained from PreSens.

4.3.4.1. Transparent Oxygen-Sensitive Microtiterplate (OxoPlate OP96U)

In the experiments using the transparent, oxygen-sensitive MTP OxoPlate, 4.8 mL of test substance in dilution water, 100 µL of a 2.5 M glucose solution and 100 µL of inoculum were mixed in 20 mL glass vials. The test solutions were incubated for 30 min at room temperature (21 °C) on a flask shaker using an air-permeable sealing for sufficient oxygen supply. After the incubation time, in which the toxic substance reacts with the bacteria and develops its maximum inhibition, 150 µL test solution per well were transferred into the oxygen-sensitive MTP and covered with the respective plate sealing (see chapter 4.4.3, page 136). 4 wells per test solution were used to provide sufficient accuracy. The oxygen decrease was measured for 15 min with an interval of 1 min with an MTP fluorescence reader Fluoroskan Ascent (Thermo

Labsystems) at ambient temperature. Both indicator and reference dye were excited at 544 nm, the emission was recorded at 650 nm (indicator) and 590 nm (reference dye), respectively. During measurement, the plate was not shaken, if not noted otherwise. Fig. 4.6 depicts the flow chart of the general procedure of the *P. putida* respiration inhibition test using the oxygen sensor-coated MTP.

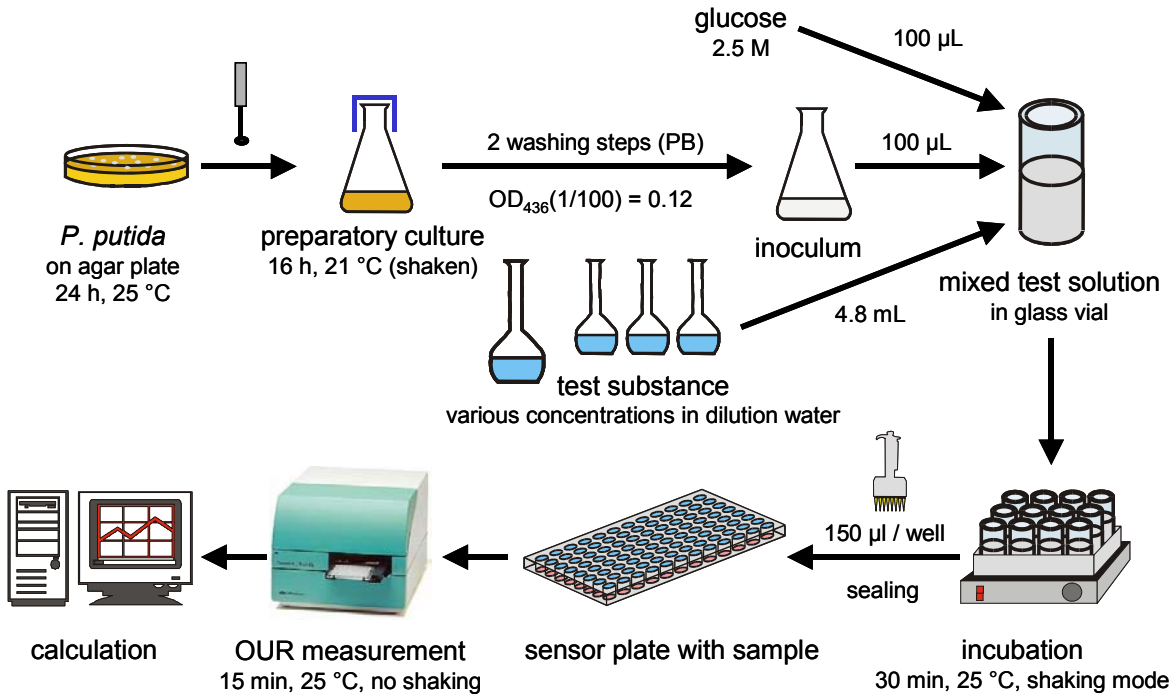

Fig. 4.6. Procedure of the P. putida respiration inhibition test performed with the oxygen sensor-coated MTP.

4.3.4.2. Optically Isolated Oxygen-Sensitive Microtiterplate (PSt3)

For experiments requiring high amounts of bacteria, the transparent oxygen sensor OxoPlate is not suitable because the turbidity of the sample causes light scattering, which leads to higher fluorescence. Remedy can be found by using an optical isolation which blocks the fluorescence of the sample completely. Thus, only the fluorescence within the sensor membrane is detected. Unfortunately, the intensity of the transparent sensor OxoPlate was too low for application of such an optical isolation, which reduces the detected fluorescence intensity. Therefore, another oxygen sensor (PSt3), which was originally designed for fibre-optic minisensors (see chapter 2.4.2.1), was incorporated into 96 well flat-bottom MTPs (Greiner) with

silicone rubber compound (product no: 692-542, RS Components) and read out using a time-gated measurement (see chapter 2.4.1, page 62). Except for the total volume of 200 µL per well, the experiment was performed according to those using the transparent oxygen sensor. Fig. 4.7 shows the oxygen decrease due to respiration of *P. putida* using the transparent, sensor-coated MTP OxoPlate (left), and the optically isolated oxygen sensor PSt3 (right). The transparent sensor simulates negative final values due to too high fluorescence. Calibration with the minimum value of the kinetic instead of a sodium sulphite solution reduces the effect, but cannot compensate it because especially at a low shaking rate the bacteria tend to precipitate upon the sensor membrane, causing higher light scattering increasing with time. Therefore, the amount of scattered fluorescence is not constant during the measurement. In contrast, the optically isolated MTP shows a correct final oxygen content of 0 µM. Unfortunately, the response time of this sensor is rather high (see chapter 2.4.2.1), which can lead to non-linear kinetics. In this case, the kinetic is not suitable for the respiration inhibition test because linear kinetics are required for obtaining a constant OUR. Therefore, this sensor was not used in further experiments, but a bacteria concentration suitable for the transparent sensor was chosen where these effects are negligible.

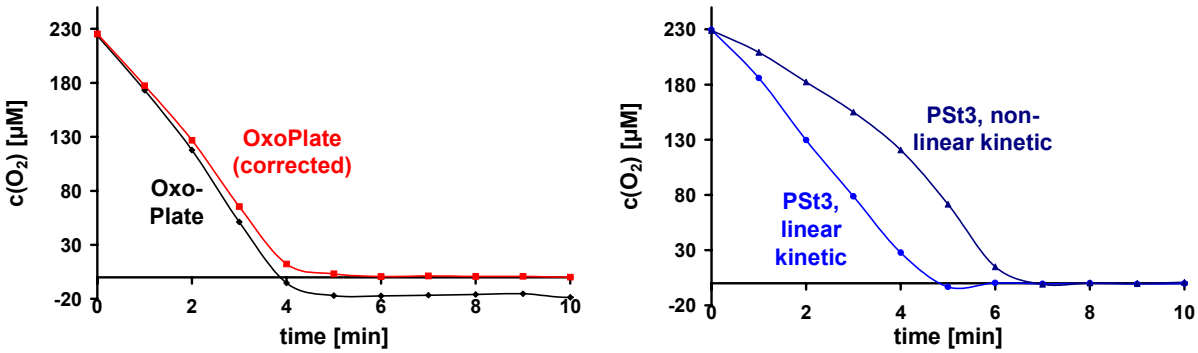

Fig. 4.7. Oxygen decrease by respiration of P. putida. Left: Transparent oxygen sensor OxoPlate, original kinetic and corrected kinetic calibrated with the minimum of the kinetic; Right: Optically isolated oxygen sensor PSt3, linear and non-linear kinetics.

4.3.4.3. Optically Isolated, pH-Sensitive MTP (HydroPlate HP96U)

4.8 mL of dilution water, 100 µL of a 2.5 M glucose solution and 100 µL of inoculum were mixed in 20 mL glass vials. 150 µL per well of the test solutions were transferred into the pH-sensitive MTP HydroPlate. 4 wells per test solution were used for sufficient accuracy. The MTP was shaken for 30 min at 600 rpm and with a diameter of 1 mm (600/1) in the MTP reader at 25 °C. It is also possible to use an MTP shaker for incubating instead of the reader to save time. This procedure differs from the oxygen measurements and was necessary because of the higher response time of the pH sensor at low buffer concentrations (s. chapter 2.3.4). After the incubation time, the respiration of the bacteria was obtained over 15 min with an interval of 1 min. The wells were not covered with plate sealings.

4.3.4.4. Fibre-Optic pO_2 Minisensor

Experiments using glass vessels and without shaking of the samples were performed to compare the results obtained with the MTP with an oxygen-impermeable system. For the experiment using the fibre-optic minisensor, 144 mL of test substance in dilution water, 3 mL of inoculum and 3 mL of a 2.5 M glucose solution were mixed in a 500 mL Erlenmeyer flask and incubated for 30 min shaken on a flask shaker using an air-permeable cap for sufficient oxygen supply. A 100 mL Erlenmeyer flask containing the sensor spot (PSt3, see chapter 2.4.2.1, page 64) was filled to the top with the test solution and closed with a glass plug, thereby displacing excess sample. It has been taken care that no air bubbles remained in the flask. The sensor spot was read out with an oxygen meter (Fibox 2) via a fibre-optic probe. The probe is inserted into a coaster for shaking and spinner flasks (CFG) which redirects the light, so that the sensor spot can be

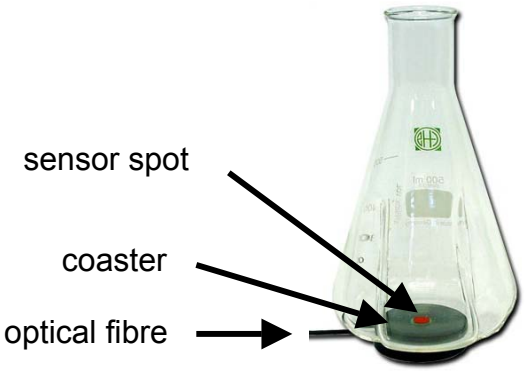

Fig. 4.8. Erlenmeyer flask with sensor spot glued to the bottom and read out with a coaster.

conveniently read out from the bottom without additional equipment. The oxygen decrease was detected over 15 min with an interval of 10 s.

4.3.4.5. Oxygen-Sensitive, Fibre-Optic Microsensor

Alternatively, the comparative experiment was performed with a fibre-optic microsensor using the same composition of test solution and inhibition conditions as with the minisensor. A microsensor (NTH-PSt1, see chapter 2.4.2.2, page 66) was inserted as low as possible into a 100 mL Erlenmeyer flask, placing the sensor tip approx. 5 cm below the upper edge of the flask (see Fig. 4.9). After incubation, the flask was filled with the test solution up to the edge and the measurement was started immediately with a total time of 15 min and intervals of 10 s. No sealing was used because the oxygen diffusion from the sample surface to the sensor tip is negligible within the measurement time. This was proved by using the same set-up with water as sample and saturating it with nitrogen via a diffuser. After turning off the nitrogen, the oxygen content was measured over a period of 15 min. Within this time, the oxygen content rose from 0 µM to 2.3 µM., which lies within the accuracy of the sensor. The results of this experiment was confirmed with the simulation program Berkeley Madonna (see Appendix 11.1.1.2).

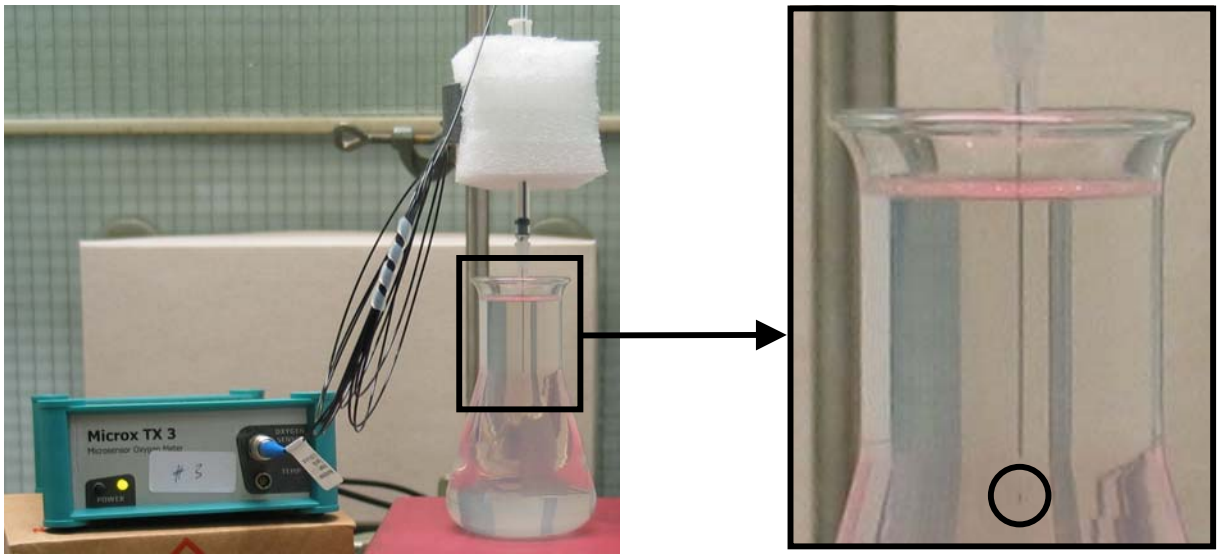

Fig. 4.9. Left: Set-up of the experiments using the fibre-optic microsensor; Right: Enlarged section showing the position of the sensor tip (circle).

4.3.4.6. Comparison of Minisensor and Microsensor

The fibre-optic minisensor enables non-invasive measurements from outside the glass vessel without the danger of contamination of the sample. The robust system can be sealed hermetically with a glass plug. The low-cost sensor-spots and the silicone for gluing them onto the bottom of the glass vessel are autoclavable. Unfortunately, the response time of the dry sensor is rather slow, resulting in non-linear kinetics (s. Fig. 4.10, top & left). Fig. 4.10, top & right, shows the OURs calculated from the slopes of the kinetic over an interval of 1 min with shifted starting positions. The OURs detected with the minisensor depend very strongly on the position where the slope is taken. Therefore, the minisensor is not suitable for fast measurements. Regarding slower kinetics (s. Fig. 4.10, bottom), the sensor can be used if the slope is taken after the response time.

In contrast to the rather slow minisensor, the needle-type microsensor with its very small sensor tip responses in real time. Fig. 4.10, left, shows the resulting linear kinetics detected with the microsensor. Even at fast kinetics, the segment where the slope is taken is not as critical for calculation of the OUR as with the minisensor (s. Fig. 4.10, top & right). Although the microsensor is not autoclavable, the contamination due to unwanted bacteria is negligible with relatively robust bacteria in high concentrations and a short measurement time of only 15 min. However, care has to be taken handling the fibre and the sensor tip, because the microsensor is not as robust as the minisensor.

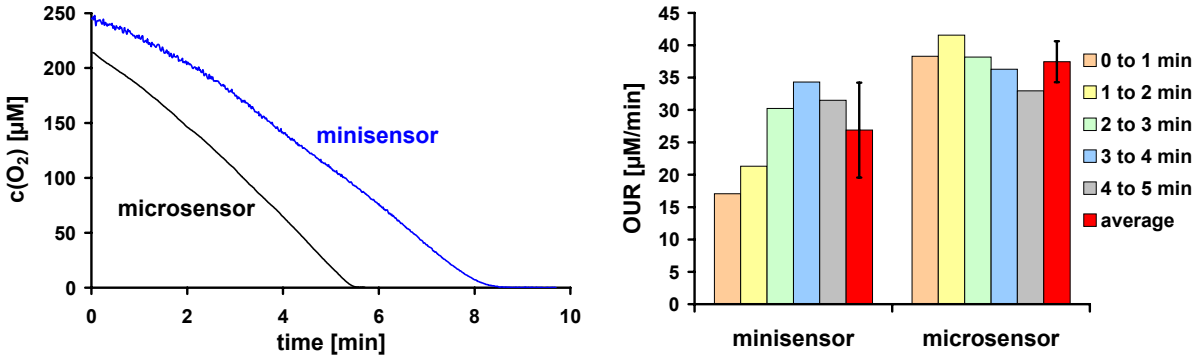

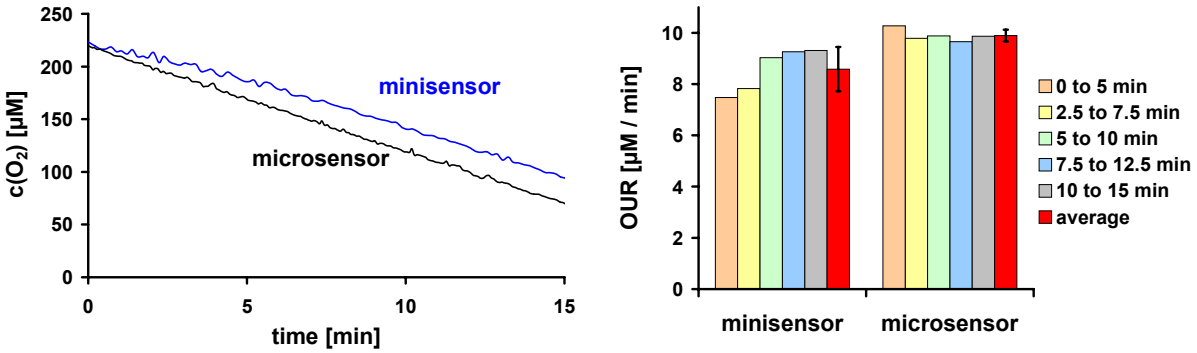

Fig. 4.10. Comparison of the fibre-optic oxygen minisensor and microsensor. Top: Fast kinetic with $6.7 \cdot 10^8$ cfu/mL; Bottom: Low kinetic using $2.0 \cdot 10^8$ cfu/mL; Left: Oxygen consumption kinetic; Right: OURs calculated from the slope at different times of the kinetics .

4.3.4.7. 24-Well Sensor Dish Reader (SDR2)

Comparative experiments demanding a higher throughput than possible with a fibre-optic sensor were performed with a sensor dish reader (SDR2, see chapter 2.4.3, page 67). 28.8 mL of test substance in dilution water, 600 µL of inoculum and 600 µL of a 2.5 M glucose solution were shaken for 30 min in a 100 mL Erlenmeyer flask on a flask shaker employing an air-permeable cap. After 30 min of incubation, 5 mL of the respective test solution were transferred into a 5 mL glass vessel containing an oxygen sensor spot. 4 vessels per test solution were used for sufficient accuracy. 24 of the glass vials were put into an empty 24 well MTP placed on the SDR2. The oxygen content of the test solutions was measured for 15 min in

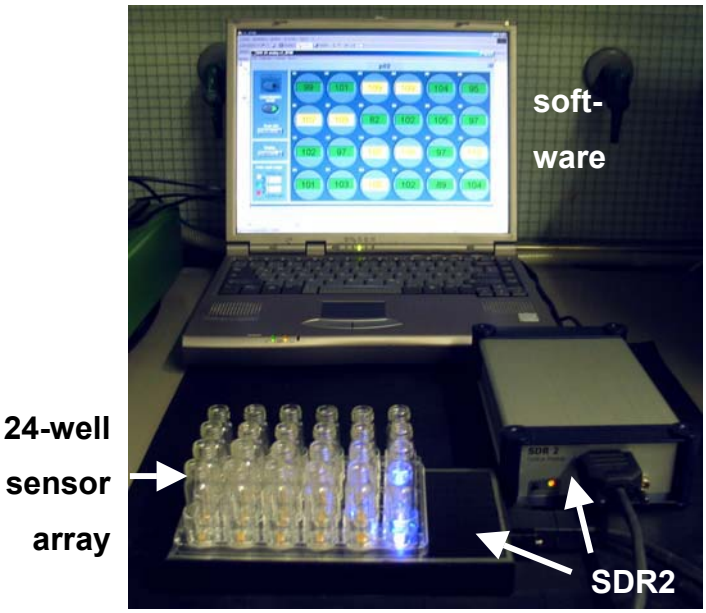

Fig. 4.11. Set-up for the oxygen measurements with the sensor dish reader SDR2.

intervals of 10 s. As with the microsensor, no sealing was used because the oxygen diffusion from the surface of the sample to the bottom of the glass vessel is negligible within the measurement time.

4.3.5. Evaluation

For determination of the inhibition of the tested substance, the sensor response of samples containing toxic substances was compared to those without inhibitor. In the MTP experiments and the comparative experiment using the sensor dish reader, 4 samples per inhibitor concentration were used for calculation of the respective standard deviation. The error in inhibition was calculated via error propagation. Using the fibre-optic sensors, only one measurement per sample was performed for reasons of time saving. Here, no error calculation was possible. Two kinetic methods were used for calculation of the inhibition, continuous monitoring and an two-point calculation.

4.3.5.1. Continuous oxygen monitoring

The kinetic measured with an oxygen sensor is ideally a linear decrease in oxygen content. Usually, the slope between 5 and 10 min was taken for calculation of the **oxygen uptake rate** (**OUR**), which is defined as the oxygen decrease per minute. Regarding fast kinetics, the slope was taken at earlier times. The inhibition I (in %) of the bacterial respiration was calculated by comparing the OURs of the inoculum inhibited by toxic substances (OUR_{Tox}) and the non-inhibited inoculum (OUR_0), referring to the non-inhibited one:

$$I = \frac{OUR_0 - OUR_{Tox}}{OUR_0} \cdot 100\,\% \qquad \text{eqn. 4.1}$$

The error in inhibition is calculated by the Gaussian error propagation according to

$$\Delta I = \sqrt{(\frac{\partial I}{\partial OUR_0})^2 \cdot \Delta OUR_0{}^2 + (\frac{\partial I}{\partial OUR_{Tox}})^2 \cdot \Delta OUR_{Tox}{}^2} \qquad \text{eqn. 4.2}$$

with

$$\frac{\partial I}{\partial OUR_0} = \frac{100 \cdot OUR_{Tox}}{OUR_0{}^2} \qquad \text{eqn. 4.3}$$

and

$$\frac{\partial I}{\partial OUR_{Tox}} = -\frac{100}{OUR_0} \qquad \text{eqn. 4.4}$$

4.3.5.2. pH Kinetics

Although the pH kinetics are rather linear, the parameter which depends on the bacterial respiration is the proton concentration. However, the phosphate buffer of the inoculum and the phosphates in the dilution water (see Table 4.2, page 115) have to be taken into consideration when calculating the **proton production rate (PPR)**, which is defined as proton increase per min. This was done with the calculation program Berkeley-Madonna (see chapter 3.2.1, page 72), using the Henderson-Hasselbalch equation eqn. 2.1 a, page 58). Ideal behaviour was postulated, thus setting the activity coefficients f to 1:

$$pH = pK_a + \log\frac{c_{A^-}}{c_{HA}} \qquad \text{eqn. 4.5 a}$$

The acidic concentration can be described as

$$c_{HA} = c_{tot} - c_{A^-} \qquad \text{eqn. 4.5 b}$$

with c_{tot} being the total phosphate concentration in the test solution. Solving the concentration-based Henderson-Hasselbalch equation eqn. 4.5 a for the anionic concentration c_{A^-} and setting the initial conditions pH = pH(0), $c_{A^-} = c_{A^-}(0)$ and $c_{HA} = c_{HA}(0)$ at t = 0 (before start of the bacterial respiration) results in

$$c_{A^-}(0) = \frac{c_{tot} \cdot 10^{pH(0)-pK_a}}{1+10^{pH(0)-pK_a}} \qquad \text{eqn. 4.5 c}$$

with pK_a being the negative logarithm of the dissociation constant. Due to the bacterial respiration, the basic buffer concentration decreases with –PPR, while the acidic buffer concentration changes with +PPR. Starting with the calculated initial concentrations, the initial pH(0) and the proton production rate PPR were estimated for a first result and then fitted by the program to a measured kinetic. The model is attached to this thesis as Appendix 11.3 (page 203). The inhibition was then calculated by comparing the PPR with inhibitor (PPR_{Tox}) to the PPR without inhibitor (PPR_0) in analogy to the oxygen measurements:

$$I = \frac{PPR_0 - PPR_{Tox}}{PPR_0} \cdot 100\ \% \qquad \text{eqn. 4.6}$$

The error in inhibition, ΔI, was calculated according to eqn. 4.2, substituting OUR with PPR. ΔPPR was received by taking the standard deviation of the PPRs fitted for the 4 wells per sample.

Using this model for calculation of the inhibition instead of ΔpH provides not only slightly different values for I, but also improves reproducibility. Whereas the decrease in pH is rather small due to the phosphate buffer included in the test solution, the model calculates the real increase in protons and yields therefore higher values with smaller standard deviations.

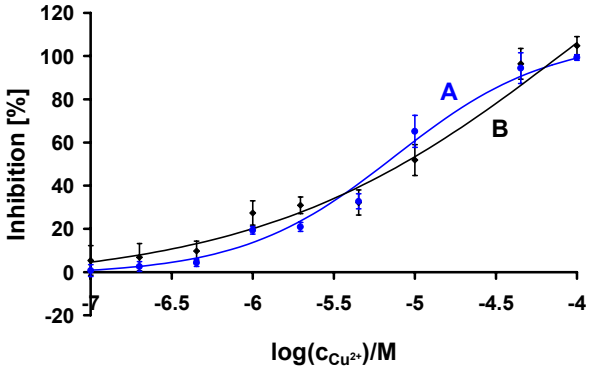

Fig. 4.12. Dose-response curve of $6.7 \cdot 10^8$ cfu/mL of P. putida detected with the pH-sensitive MTP, using Cu^{2+} as inhibitor. (A): Calculated with the Henderson-Hasselbalch model; (B): Calculated via the linear pH decrease.

4.3.5.3. Two-point Method

A time-saving alternative to continuous oxygen measurement is a two-point calculation. Here, the oxygen content of the sample is measured at only two fixed times and the OUR calculated with these two oxygen values. The inhibition and its deviation are obtained as with the continuous mode. With automatisation of the plate exchange, the throughput can be increased considerably. This is especially important for high throughput screening with high numbers of test substances.

4.3.5.4. Reproducibility and Range

To determine the reproducibility of the EC_{50} values, sigmoidal curves were fitted through the minimum and maximum well-to-well deviations of the measurement points. The EC_{50} values of these two extremal curves were defined as deviations in EC_{50}. However, it is likely that these deviations from the average value are not equal. Therefore both deviations are given in the tables. As range, the concentrations corresponding to 20 to 80 % inhibition were chosen. Within this range, the dynamic of the system is greatest and almost linear. Below 20 % and above 80 % inhibition, the sigmoidal curve flattens and even small deviations cause great errors in concentration. Fig. 4.13 illustrates the determination of the deviations in the EC_{50} value (left) and the range (right).

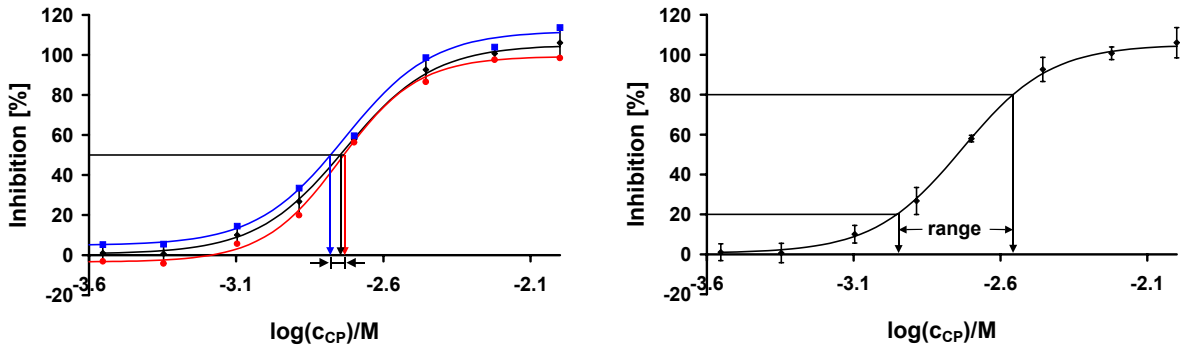

Fig. 4.13. Determination of the deviation in ΔEC_{50} (left) and the range (right).

4.4. Reproducibility

The most difficult demand to meet is sufficient reproducibility of the calculated inhibition. This depends on the reproducibility of the bacterial activity as well as – regarding oxygen measurements - on oxygen diffusion into the sample which partly compensates the oxygen uptake by the bacteria. The repeatability of the toxicity test was investigated using the oxygen-sensitive MTP. The oxygen uptake rate (OUR) of the bacteria without inhibitor and with a distinct concentration of toxic substance was measured 4-5 times in succession, and the inhibition was calculated. The influence of the oxygen diffusion into the MTP on the accuracy of the results was investigated by performing the same experiment in a hermetically sealed glass vessel read out with a fibre-optic sensor and comparing the calculated inhibition with that obtained with the sensor-coated MTP. Various plate sealings were tested to improve the performance.

4.4.1. Storage of Bacteria

The bacterial activity strongly depends on the storage medium and storage conditions of the bacteria stock solution between the measurements. Different methods have been tested.

4.4.1.1. Storage in Phosphate Buffer with Stirring

The bacteria stock solution was stored in 50 mM phosphate buffer and stirred with a magnetic stirrer according to the German standard test [4]. However, this resulted in unsteady bacteria activities. Fig. 4.14 shows the OURs without inhibitor and with $3 \cdot 10^{-7}$ M Cu^{2+} measured with the MTP (A) and the fibre-optic minisensor (B), respectively. After an increase, the OURs decrease rapidly over 5 h down to 50 % of the initial value. This indicates that the bacteria are inhibited due to lack of oxygen, food, too low pH value etc. Furthermore, in the first few hours OUR_{Tox} is greater than OUR_0, resulting in an apparent activation instead of inhibition (s. negative signs in

Table 4.3). The bacteria are stressed by the inhibitor or unfavourable conditions which leads to a higher respiration rate and therefore to an increasing OUR. Table 4.3 shows the OURs and the calculated inhibition of the MTP and fibre-optic sensor experiment. For comparison, only the OURs of the MTP experiment measured simultaneously to the fibre-optic experiment were taken, i.e. only every 2nd value. The inhibition was calculated using the subsequent OURs of the uninhibited and the inhibited sample. While the calculated inhibitions using the oxygen-sensitive MTP increase from negative values to positive ones, the ones detected with the fibre-optic sensor are rather stable after 1.5 h despite the decrease in OUR.

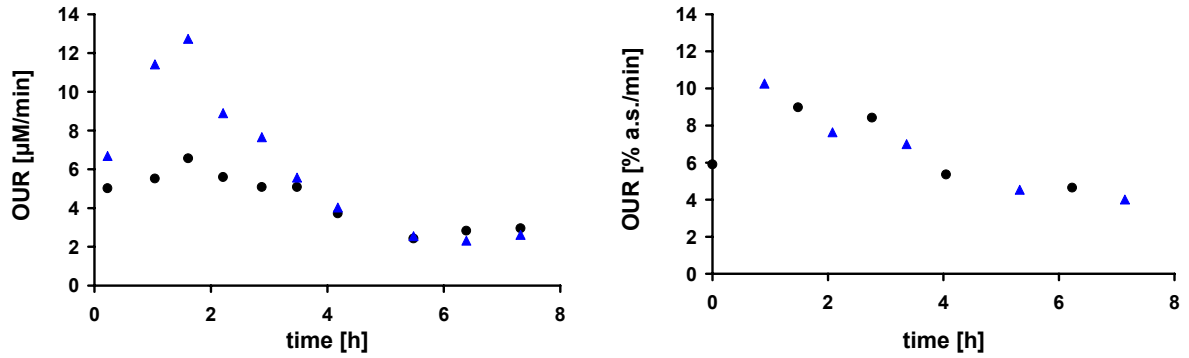

Fig. 4.14. Left: OURs detected for 10 subsequent measurements with the oxygen-sensitive MTP. Right: OURs obtained for 5 subsequent measurements with the fibre-optic sensor. The circles (●) represent the uninhibited samples, the triangles (▲) the samples containing $3 \cdot 10^{-7}$ M $CuSO_4$. In both cases the OUR decreases rapidly after a short increase. The bacteria were stored in 50 mM phosphate buffer.

Table 4.3. OURs and resulting inhibitions obtained with the OxoPlate and the fibre-optic sensor, respectively. The bacteria were stored in 50 mM phosphate buffer.

	MTP			**Fibre-optic sensor**		
dt [h]	OUR_0 [µM / min]	OUR_{Tox} [µM/ min]	Inhibition [%]	OUR_0 [µM / min]	OUR_{Tox} [µM/ min]	Inhibition [%]
0	5.0	11.4	-127	5.9	10.3	-74
1.5	6.6	8.9	-36	9.0	7.6	15
3	5.1	5.6	-10	8.4	7.0	17
4	3.7	2.5	32	5.4	4.5	15
6	2.8	2.6	8	4.6	4.0	14

4.4.1.2. Storage in Test Solution with Shaking

To avoid inactivation of the bacteria due to lack of nutriment, the bacteria were stored in the test solution, which contains glucose and salts necessary for respiration. Instead of stirring, the solution was shaken with a flask shaker. The concentration of the inhibitor $CuSO_4$ was changed from $3 \cdot 10^{-7}$ M to $5 \cdot 10^{-7}$ M to obtain a greater inhibition and to avoid activation or stress of the bacteria.

The tendencies of the OURs are the same as described above: After a short increase, the OUR decreases rapidly down to 12-15 % of the initial value (OUR_0) (s. Fig. 4.15). However, the resulting calculated inhibition is constant over 3 h (MTP) and 2 h (fibre-optic sensor), respectively. Furthermore, both devices provide identical inhibitions concerning these 2 h (s. Table 4.4). The OURs measured with the MTP are smaller than the ones measured with the fibre-optic sensor, which is due to the oxygen diffusion into the MTP. However, calculating the inhibition, this effect is quite compensated.

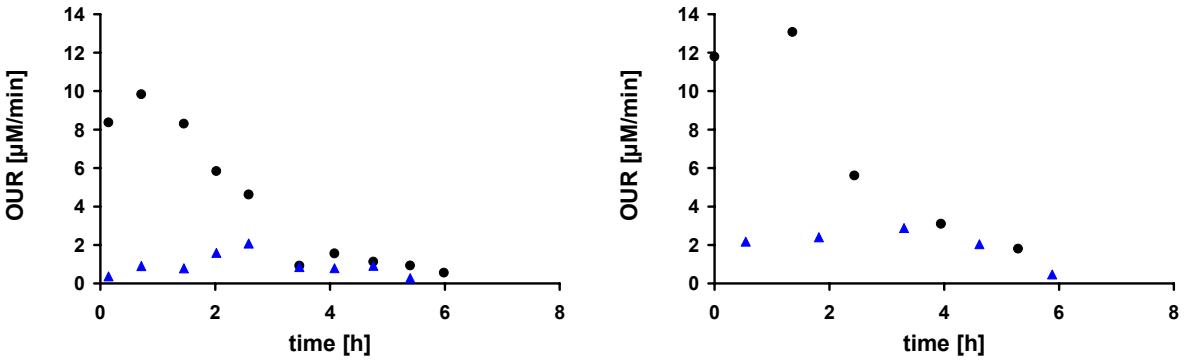

Fig. 4.15. Left: OURs detected for 10 subsequent measurements with the oxygen-sensitive MTP. Right: OURs obtained for 5 subsequent measurements with the fibre-optic sensor. The circles (●) represent the uninhibited samples, the triangles (▲) the samples containing $5 \cdot 10^{-7}$ M $CuSO_4$. In both cases the OUR decreases rapidly, in the MTP it increases first. The bacteria were stored in test solution.

Table 4.4. OURs and resulting inhibitions obtained with the sensor-coated MTP and the fibre-optic sensor, respectively. The bacteria were stored in test solution.

	MTP			**Fibre-optic sensor**		
dt [h]	OUR_0 [µM/ min]	OUR_{Tox} [µM / min]	Inhibition [%]	OUR_0 [µM / min]	OUR_{Tox} [µM / min]	Inhibition [%]
0	8.4	0.9	89	11.8	2.2	82
1.5	8.3	1.6	81	13.1	2.4	82
2.5	4.6	0.9	82	5.6	2.9	49
4	1.6	0.9	41	3.1	2.0	34
5.5	0.9	-0.8	190	1.8	0.5	74

A possible reason for the decrease of the OURs after 2 h is lack of glucose. This was investigated by detecting the OUR of a non-inhibited bacteria solution 6 times in succession with the fibre-optic minisensor and adding 2 mL of a 2.5 M glucose solution to the storage solution after 3 h. The OUR did not recover its initial value but continued to decrease (s. Fig. 4.16), which proves that the cause of the inactivation of the bacteria was not lack of glucose.

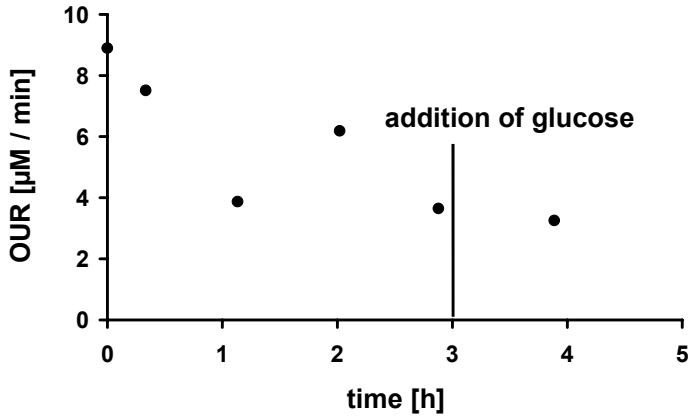

Fig. 4.16. OURs of an uninhibited bacterial solution measured with the fibre-optic sensor. After the 5th measurement (after 3 h), 2 mL of a 2.5 M glucose solution were added. The OUR continued to decrease.

Another possible reason for inactivation is the pH value. CO_2 production by respiration decreases the pH in the low-buffered test solution (1.3 mM PB). The pH change during 4 h was detected with the pH-sensitive HydroPlate (PreSens). Fig. 4.17 shows that the pH of the test solution drops from approximately 6.5 to 4.0 within 1.5 h. This indicates that the decrease of the OUR during storage of the bacteria in test solution is caused by increasing acidity of the solution [7].

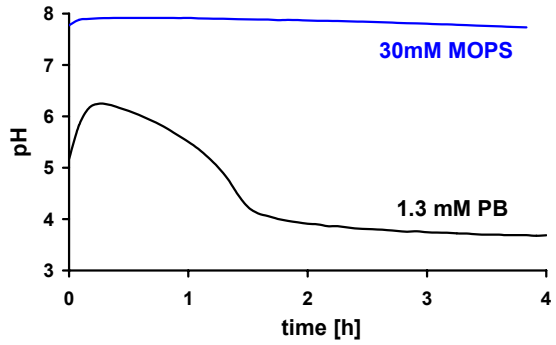

Fig. 4.17. pH of the test solution (containing 1.3 mM phosphate buffer) decreases from ca. 6.5 to 4.0 within 1.5 h. The strong increase during the first 15 min is due to the rather slow response of the sensor in low-buffered solutions. In contrast, the pH of the MOPS-buffered test solution with bacteria is constant over 4 h.

4.4.1.3. Storage in MOPS Buffer with Shaking

To avoid pH decrease during storage, the dilution water was prepared with 30 mM MOPS buffer. MOPS was used instead of phosphate buffer because the latter forms insoluble precipitates with heavy metals, which were used as inhibitors. The solution was shaken during storage. Fig. 4.17 shows that this buffer concentration is sufficient to maintain a constant pH of the bacterial solution over 4 h.

However, using a buffered system and supplying the bacteria with excess nutrition, undesirable growth of the bacteria could not be prevented. The OURs increase over the first 3 h with both sensor devices by more than 100 %. The calculated inhibitions range between 73 and 84 % (MTP) and 79 and 93 % (fibre-optic sensor), respectively, and are thus comparable to some extent. Though, measurements performed with different bacteria solutions of the same initial

concentration differ widely. A second measurement produced inhibitions between 53 and 67 % (MTP) and 59 and 70 % (fibre-optic sensor), respectively (data not shown). Although the non-inhibited OUR_0 was comparable to that of the shown experiment, OUR_{Tox} was considerably larger, resulting in a lower inhibition. This indicates different sensitivity of the bacteria which may be due to different growth phases.

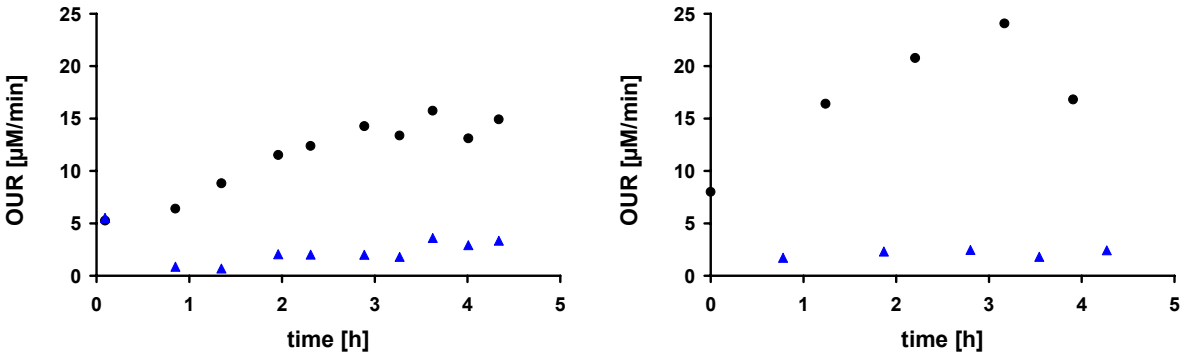

Fig. 4.18. Left: OURs detected for 10 subsequent measurements with the oxygen-sensitive MTP. Right: OURs obtained for 5 subsequent measurements with the fibre-optic minisensor. The circles (●) represent the uninhibited samples, the triangles (▲) the samples containing $5 \cdot 10^{-7}$ M $CuSO_4$. In both cases the OUR increases considerably, especially within the first 3 h. The bacteria were stored in test solution buffered with 30 mM MOPS.

Table 4.5. OURs and resulting inhibitions obtained with the sensor-coated MTP and the fibre-optic sensor, respectively. The bacteria were stored in test solution buffered with 30 mM MOPS.

	MTP			**Fibre-optic sensor**		
dt [h]	OUR_0 [µM/ min]	OUR_{Tox} [µM / min]	Inhibition [%]	OUR_0 [µM / min]	OUR_{Tox} [µM / min]	Inhibition [%]
	5.3	0.9	84	8.0	1.7	79
	8.8	2.1	77	16.4	2.3	86
	12.4	2.0	84	20.8	2.5	88
	13.4	3.6	73	24.1	1.8	93
	13.1	3.3	75	16.8	2.4	86

4.4.1.4. Storage in Phosphate Buffer with Shaking

Growing of the bacteria during storage was avoided by using 50 mM phosphate buffer as storage medium, as described in chapter 4.4.1.1. Instead of stirring with a magnetic stirrer, the solution was shaken rapidly in an orbital flask shaker. With this method, the activity of the bacteria decreased less than with method 1 or 2 and did not increase like shown in chapter 4.4.1.3 (s. Fig. 4.19). The resulting inhibitions decrease slightly to a minimum of 80 % of the initial value (s. Table 4.6). Calculating the inhibition measured with the MTP using simultaneously-measured OURs, the inhibitions are even constant (disregarding the first value; s. Table 4.7). However, repeating this experiments under the same conditions showed deviating inhibitions with both devices, but especially with the MTP (data not shown). The reason for the different results measured with the fibre-optic sensor (inhibition: 70-80 %) can be the relatively small OURs, leading to greater errors especially with only one measurement at one time. The deviations with the sensor-coated MTP can be due to differing oxygen diffusion from the plate sealing, which was paraffin wax dissolved in petroleum ether. The solvent evaporates partially during storage and has to be refilled to guarantee good pipetting properties of the wax. Therefore the composition of the dissolved wax varies, which leads to different oxygen diffusion from the wax into the sample. Both influences were investigated.

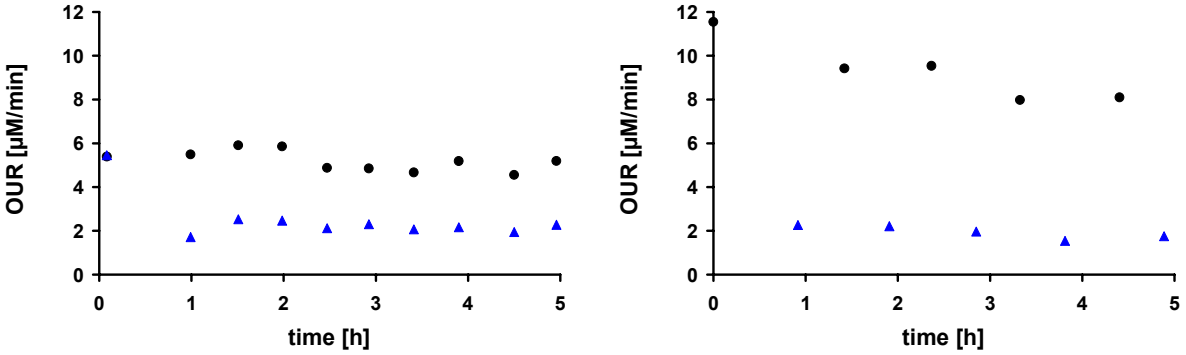

Fig. 4.19. Left: OURs detected for 10 subsequent measurements with the oxygen-sensitive MTP. Right: OURs obtained for 5 subsequent measurements with the fibre-optic minisensor. The circles (●) represent the uninhibited samples, the triangles (▲) the samples containing $5 \cdot 10^{-7}$ M $CuSO_4$. In both cases the OUR decreases slightly. The bacteria were stored in PBS and shaken rapidly.

Table 4.6. OURs and resulting inhibitions obtained with the sensor-coated MTP and the fibre-optic sensor, respectively. The bacteria were stored in PBS and shaken rapidly.

	MTP			**Fibre-optic sensor**		
dt [h]	OUR_0 [µM / min]	OUR_{Tox} [µM / min]	Inhibition [%]	OUR_0 [µM / min]	OUR_{Tox} [µM / min]	Inhibition [%]
0	5.4	1.7	62	11.5	2.3	80
1.5	5.9	2.5	56	9.4	2.2	81
2.5	4.9	2.3	51	9.5	2.0	78
3.5	4.7	2.2	49	8.0	1.5	78
4.5	4.6	2.3	50	8.1	1.8	77

Table 4.7. All OURs and resulting inhibitions obtained with the sensor-coated MTP. The inhibitions were calculated with the simultaneously measured OURs instead with the alternately measured OURs.

dt [h]	OUR_0 [µM / min]	OUR_{Tox} [µM / min]	Inhibition [%]
0.1	5.4	-	-
1	5.5	1.7	64
1.5	5.9	2.5	56
2	5.9	2.5	57
2.5	4.9	2.1	55
2.9	4.9	2.3	51
3.4	4.7	2.1	54
3.9	5.2	2.2	55
4.5	4.6	1.9	57
5	5.2	2.3	55

4.4.2. Bacteria Concentrations

The well-to-well reproducibility and the reproducibility of successive MTP experiments depend on the bacteria concentration. Relatively small OURs can lead to greater deviations in kinetics and resulting inhibitions. Four different bacteria concentrations were tested: $1.5 \cdot 10^7$ cfu/mL, $3.1 \cdot 10^7$ cfu/mL, $7.8 \cdot 10^7$ cfu/mL, and $1.8 \cdot 10^8$ cfu/mL. The samples were incubated and shaken (600/1) for 30 min in the reader. After the incubation time, one plate was sealed with 150 µL of paraffin wax dissolved in petroleum, whereas the other experiment was performed without sealing, thus representing the two extremal values concerning oxygen ingress from the sample surface. Different plate sealings are investigated in more detail in chapter 4.4.3. During the experiment, the unsealed MTP was not shaken to minimise convection and thereby oxygen ingress. $5 \cdot 10^{-4}$ M 3,5-dichlorophenol (3,5-DCP) was used as inhibitor and the deviations ΔOUR per 4 wells and the respective inhibitions ΔI were calculated. The results are shown in Table 4.8 and Fig. 4.20.

The oxygen content at the beginning of the measurement depends on the bacteria concentration. The faster the respiration, the less effect has the oxygen ingress due to shaking during the incubation time, thus resulting in lower start values. Besides, in the lag time between sealing the wells and start of the measurement, the plate is not shaken and the oxygen content decreases faster than during the incubation time. With the highest bacteria concentration and wax sealing, the initial value is too low for correct determination of OUR_0 (Fig. 1.4, top and left). On the other hand, too low bacteria concentrations and insufficient protection from oxygen ingress from ambient air lead to small OURs and high deviations (s. Table 4.8). Furthermore, higher OURs yield calculated inhibitions comparable to those obtained in previous experiments (s. Table 4.7). The inhibitions calculated with lower OURs are smaller, which seems to be odd at first sight, for less bacteria should be more inhibited by the same amount of toxic substance. The reason for this behaviour, however, lies in the oxygen ingress from ambient air and the calculation of the inhibition: OUR_{Tox} is less influenced by oxygen ingress than OUR_0 because of the smaller gradient between sample and ambient air. Considering the equation for calculation the inhibition (see eqn. 4.1, page 122), this effect influences the numerator more than the denominator and leads to smaller calculated inhibitions.

Table 4.8. OURs and inhibition for different bacteria concentrations and sealings.

sealing		without sealing				wax in PE			
cfu/mL	Inh*	OUR [µM/min]	ΔOUR [%]	I [%]	ΔI	OUR [µM/min]	ΔOUR [%]	I [%]	ΔI
$1.5 \cdot 10^8$	-	2.6	13.6			4.3	9.0		
$1.5 \cdot 10^8$	yes	2.2	14.1	16	16	2.3	1.2	47	5
$3.1 \cdot 10^8$	-	5.4	9.9			11.6	4.0		
$3.1 \cdot 10^8$	yes	3.2	8.8	40	8	4.5	1.6	61	2
$7.8 \cdot 10^8$	-	12.9	2.6			33.7	1.5		
$7.8 \cdot 10^8$	yes	6.1	4.0	53	2	11.8	3.5	65	1
$1.8 \cdot 10^9$	-	29.4	5.7			-**	-**		
$1.8 \cdot 10^9$	yes	11.6	2.6	61	2	19.6	8.8	-**	-**

* inhibitor

** not detectable

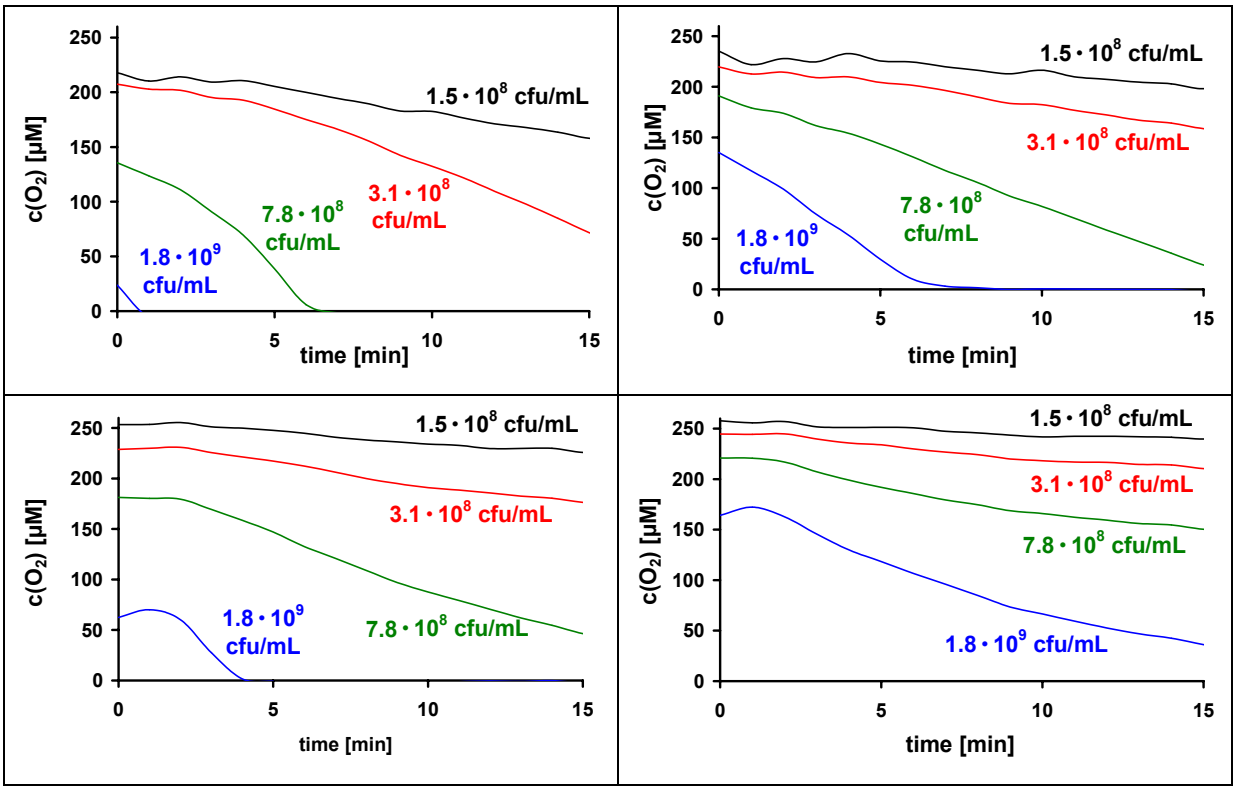

Fig. 4.20. Oxygen decrease using 4 different bacteria concentrations. Top: Wax sealing; Bottom: No plate sealing; Left: Without inhibitor; Right: With inhibitor 3,5-DCP ($5 \cdot 10^{-4}$M). The kinetic using wax sealing is too slow at the start due to temperature effects, whereas the kinetics using no plate sealing are too slow at the end due to increasing oxygen ingress.

4.4.3. Plate Sealings

Although providing reproducible results over several hours, the inhibitions obtained with the oxygen-sensitive MTP differ from those detected with the comparative experiments. This is due to oxygen ingress through the cover and MTP material (see also chapter 3). The influence of the MTP sealing on the calculated inhibition and on the reproducibility of the results was investigated using no cover, paraffin oil at two different plate accelerations, paraffin wax dissolved in petroleum ether, and PET foil.

Furthermore, a cap mat (Greiner) made of EVA (ethyl-vinylacetate) was pierced using a hot wire, yielding one small hole per well through which excess air can escape when applying the cap mat vertically and with homogeneous pressure onto the MTP.

Considering the results of chapter 4.4.2, a medium bacteria concentration of $6.7 \cdot 10^8$ cfu/mL was used for investigation of the influence of different plate sealings on the results. 4 measurements on 3 different days were performed using $5 \cdot 10^{-4}$ M 3,5-DCP as inhibitor, except the experiment without plate sealing, which was only performed on one day. The results were compared to those obtained with the fibre-optic micro- and minisensor, respectively. The experiment with 150 µL of paraffin oil as plate sealing and the lowest possible plate acceleration was performed with 10^{-5} M of $CuSO_4$ instead of 3,5-DCP, and the comparative experiment was performed with a sensor dish reader instead of a fibre-optic sensor. This experiment was performed only once on 3 different days. The procedure of this experiment is described in chapter 4.3.4.7.

Without plate sealing, the OURs are quite small due to rapid oxygen ingress. This leads to inaccuracy of the results and a higher detection limit. Comparing the obtained inhibition with the ones obtained with the comparative experiments, the deviation is very high. Although this method would be the easiest-to-handle, it is unacceptable for this application. The same is true for the widely used paraffin oil: Inevitable shaking of the samples during measurement leads to irreproducible convection and high deviations in OUR and inhibition.

With wax dissolved in petroleum ether, convection is avoided, which leads to lower oxygen ingress through the sealing. On the other hand, solvent evaporates constantly during storage, so that the composition and therefore the permeability of this sealing is not constant. Furthermore, solvent has to be refilled from time to time,

so not to let the wax get rigid before applying it to the MTP. This causes great deviations in OUR and calculated inhibition. In contrast to the experiments with oil-covered samples, the inhibition measured on 3 different days produce the same calculated inhibition, however. Remarkably, despite the oxygen ingress, OUR_{Tox} is higher than with the comparative experiments using this plate sealing, which leads to too low calculated inhibitions. This indicates that solvent diffusing into the sample stresses the bacteria and causes higher respiration, which disqualifies this sealing for tests with living systems. Besides, the dissolved wax tends to diffuse into the pipette and closes the channels, so that handling gets rather cumbersome.

With PET foil as plate sealing, the deviations are much smaller and the repeatability is acceptable as well. The calculated inhibitions differ less from that discovered with the comparative experiments than that obtained using no or oil sealing. Nevertheless, covering a whole MTP without remaining air channels is rather difficult, which results in outliers and complicates evaluation. Using the punctuated cap mat, which ideally avoids convection as with oil or no cover, and the gas phase between sample and sealing as with foil sealing, the well-to-well reproducibility and repeatability are even better. In contrast to wax sealing, it is easy to apply and features always the same consistency. The deviation between calculated and true inhibition is the same as with PET foil sealing. Unfortunately, covering all wells without an air bubble remaining in the well is quite difficult, with the same consequences as with the foil sealing.

None of the plate sealings described above proved to be adequate: Liquid sealings are easy to apply and show good well-to-well reproducibility, but let past too much oxygen due to convection, whereas rigid sealings avoid convection but were either difficult to handle, or comprise outliers, which make evaluation very time-consuming. Therefore, paraffin oil was tested again as plate sealing, but the plate acceleration during the measurement was turned from the highest to the lowest velocity, thus decreasing convection. This resulted in very good well-to-well reproducibility without any outliers and in a calculated inhibition equal to that of the comparative experiment (see Fig. 4.21, F). Therefore, 150 µL of paraffin oil were used as plate sealing for further experiments and the lowest possible plate velocity was chosen.

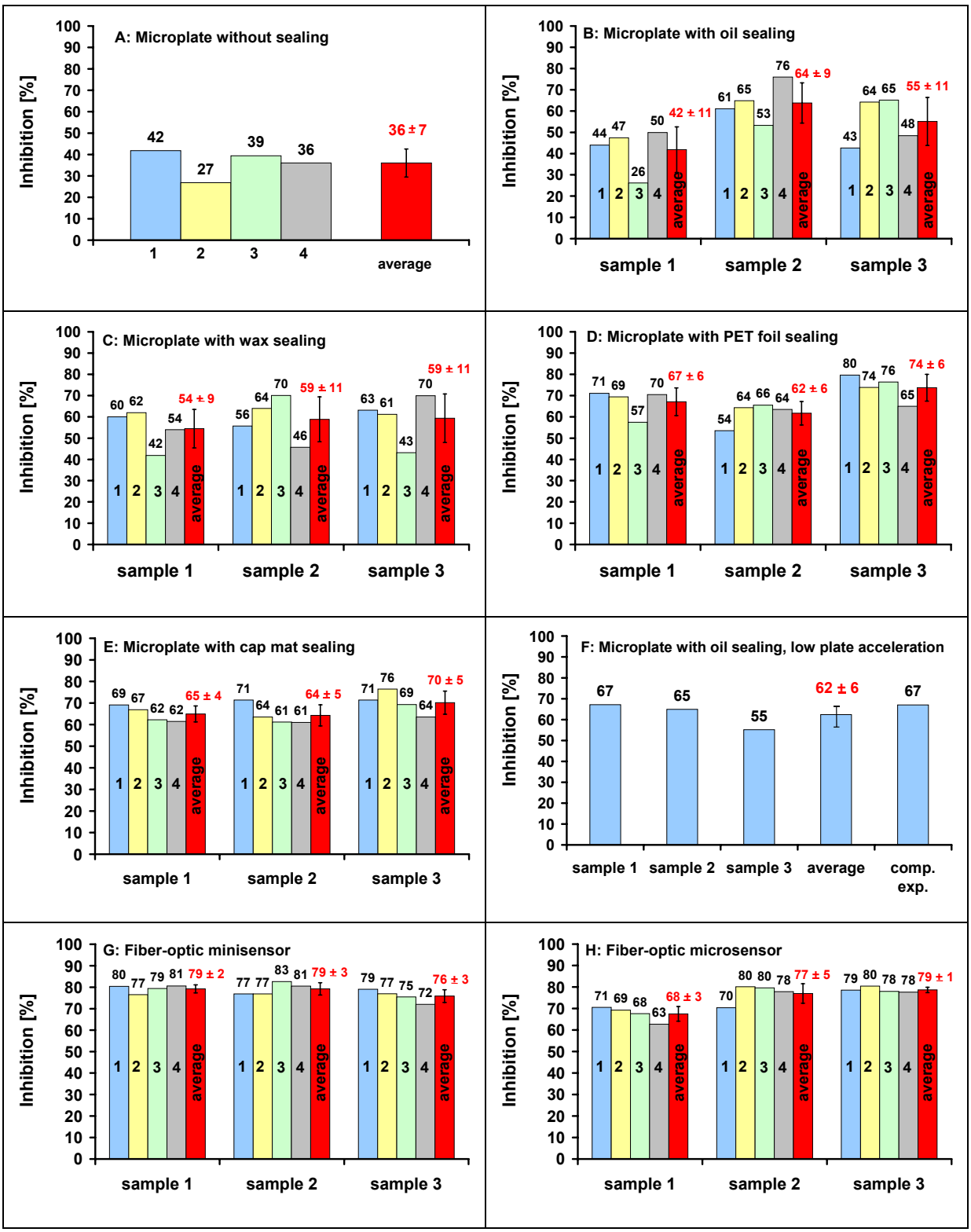

Fig. 4.21. Reproducibility of the calculated inhibition detected with the oxygen-sensitive MTP using different plate sealings: (A): no sealing, (B): paraffin oil, high plate speed, (C): 150 µL of paraffin wax dissolved in petroleum ether, (D): PET foil, (E): EVA cap mate, (F): 150 µL of paraffin oil, low plate speed, and obtained with the fibre-optic minisensor (G) and microsensor (H). (F) used 10^{-5} M Cu^{2+} as inhibitor, the others $5{\cdot}10^{-4}$ M 3,5-DCP.

4.4.4. Two-Point Calculation

A time-saving alternative to continuos measurements is a two-point calculation. Here, the oxygen content of the sample is measured at only two fixed times, which saves time especially with automatisation of the plate exchange process. However, the accuracy and precision of the results can suffer by employing only two values instead of 6 as with the MTP kinetics. Therefore, the inhibition of $2.0 \cdot 10^8$ cfu/mL of *P. putida* with $2 \cdot 10^{-6}$ M $CuSO_4$, calculated with the continuous method and the two-point method, were compared with respect to their well-to-well reproducibility, repeatability and accuracy regarding the comparative experiment (SDR2). 150 µL of paraffin oil as plate sealing and a low plate acceleration were chosen for the MTP experiments. The results are shown in Table 4.9. The calculated inhibitions differ only slightly using the two evaluation methods. Both are in good agreement with the comparative experiment. The standard deviation in inhibition is as low using the two-point method as using the continuous method. The fast response time of the sensors, which results in linear kinetics, leads to high accuracy of the calculated inhibitions even with only two points for evaluation.

Table 4.9. Comparison of the continuous and two-point method.

	OxoPlate Inhibitions [%]	**OxoPlate well-to-well StD (4 wells) [%]**	**OxoPlate Average Inhibition [%]**	**SDR2 Inhibition [%]**
Continuos method	64 – 61 - 53	5 – 3 - 3	60 ± 6	59 ± 2
Two-point method	66 – 61 - 54	5 – 3 - 3	60 ± 6	60 ± 1

4.4.5. Summary

Different methods of bacteria storage were investigated to maintain a constant bacterial activity. Bacterial growth was inhibited by choosing a storage medium without sufficient supply with nutrients. The pH was kept constant at an optimal value of 7.2 with a sufficient amount of buffer salts. Therefore, 50 mM phosphate buffer was applied as storage medium. Shaking of the bacterial solution instead of stirring has turned out to be vital. Otherwise, the activity decreases rapidly even in buffered solution due to mechanical destruction of the bacteria. Different flask shakers were tested and the one with the most effective shaking regarding the oxygen supply of the bacteria was chosen for cultivation and storage.

Bacteria concentrations between ca. $7 \cdot 10^8$ and $2 \cdot 10^8$ cfu/mL can be chosen for the dose-response curves described in the next chapter. Higher concentrations cause too fast oxygen decrease which cannot be detected, lower concentrations yield too slow kinetics of insufficient accuracy.

Concerning oxygen sensing in non-closed systems, oxygen ingress through the surface of the sample is critical. Different plate sealings have been investigated with respect to their permeability, handling and prevention of convection. The sealing of choice were 150 µL of easy-to-handle paraffin oil combined with the lowest plate acceleration of the MTP reader to minimise convection. Although oxygen ingress through the permeable oil could not be avoided completely, the well-to-well reproducibility was excellent and the calculated inhibition was consistent with the results obtained with the comparative experiment in a closed system.

For evaluation of the results, two kinetic methods are possible: Continuous monitoring where the kinetic is measured in intervals, and a two-point method where only two points of the kinetic are detected. The inhibitions calculated with these two methods differed only slightly and lie within the accuracy of the test. Although the continuous method was expected to be more accurate, the accuracy of the two-point method proved to be as good. This is because of the excellent linearity of the kinetics detected with the MTP sensors as well as with the fibre-optic microsensor and the sensor dish reader. Therefore, for automated tests were the plates are not exchanged manually, the two-point method is the method of choice because it increases the throughput considerably.

4.5. Dose-Response Curves

Having established the routine for the *P. putida* respiration inhibition test using oxygen-sensitive MTPs and after ensuring the reproducibility of the results for one inhibitor concentration, full dose-response curves were detected in a next step, following the procedure described in chapter 4.3.4. The results obtained with the oxygen-sensitive MTP were examined with respect to their repeatability by performing the same experiment 3 times. The accuracy was investigated by comparing the results with those obtained with a system without oxygen ingress. The 24-channel SensorDish Reader (SDR2, see chapter 2.4.3) was applied instead of the one-channel micro- or minisensor to save time, work and material. Besides the oxygen measurements, the experiment was performed additionally with pH-sensitive MTPs and the results compared to those obtained with the oxygen sensor.

4.5.1. Oxygen Measurements

4.5.1.1. Reproducibility

The reproducibility of a test is composed of different components: The well-to-well reproducibility of the sensor signal can be determined by measuring several replicates of an uncritical sample (e.g. water, sodium sulphite solution, buffer solutions; see chapters 2.2.5 and 2.3.5). The advantage of MTPs is that several replicates of one sample can be measured simultaneously, therefore facilitating the determination of the well-to-well reproducibility of the assay. Another factor is the precision of the sample concentration, which depends on the precision of the pipettes and the balance for weighing the inhibitor for the stock solution as well as on the solubility of the inhibitor and the homogeneity of the stock solution. However, the main source of error is the reproducibility of the biological system. The optical density (OD), weight and activity of the bacteria depend strongly on their growth conditions. Even small deviations can have great effect [8]. To obtain the overall repeatability of the assay, the following test was performed 3 times using the oxygen-sensitive MTP.

0.0125 g of $Cu(SO_4) \cdot 5H_2O$ (M = 249.69 g/mol) were dissolved in 50 mL of doubly distilled water, giving a stock solution with a concentration of 10^{-3} M (250 mg/L). 3 drops of 1 M HCl were added to avoid precipitation of $Cu(OH)_2$ ($K_{sp} = 4.8 \cdot 10^{-20}$ mol^3/L^3 [9]). The stock solution was diluted appropriately with dilution water down to 10^{-7} M (0.025 mg/L). For reasons discussed in chapter 4.5.2, the dilution water contained additionally 100 mM of NaCl. Bacteria concentrations of $2.0 \cdot 10^8$ and $6.7 \cdot 10^8$ cfu/mL were applied. The OUR and the inhibition were obtained according to chapter 4.3.5.1. Plotting the inhibition versus the logarithm results in sigmoidal dose-response curves, which were fitted using the Boltzmann-equation:

$$y = \frac{A_1 - A_2}{1 + e^{\frac{(x - x_0)}{dx}}} + A_2 \qquad \text{eqn. 4.7}$$

with A_1 being the initial value of the sigmoidal curve, A_2 its endpoint, x_0 the x value at 50 % of the y range (i.e., if A_1 is exactly 0 % and A_2 100 %, x_0 equals EC_{50}), and dx the width at this point.

The effective concentration of the toxin at an inhibition of 50 % (EC_{50}) and the ranges (EC_{20} to EC_{80}) were calculated using the Boltzmann equation. Fig. 4.22 shows the 3 dose-response curves using $6.7 \cdot 10^8$ cfu/mL (left) and $2.0 \cdot 10^8$ cfu/mL (right) of bacteria. The curves match rather satisfactorily. Whereas two are in excellent agreement, respectively, the respective third differs somehow more. However, compared to the general imprecision of the test [4, 11], even these curves can be considered sufficiently accurate. As for the EC values (Table 4.10), the reproducibility is very good. Moreover, the values for $2.0 \cdot 10^8$ cfu/mL are in good agreement with the values of $4.0 \cdot 10^{-7}$ M for EC_{20} and $9.6 \cdot 10^{-7}$ M for EC_{50} given in the DIN test.

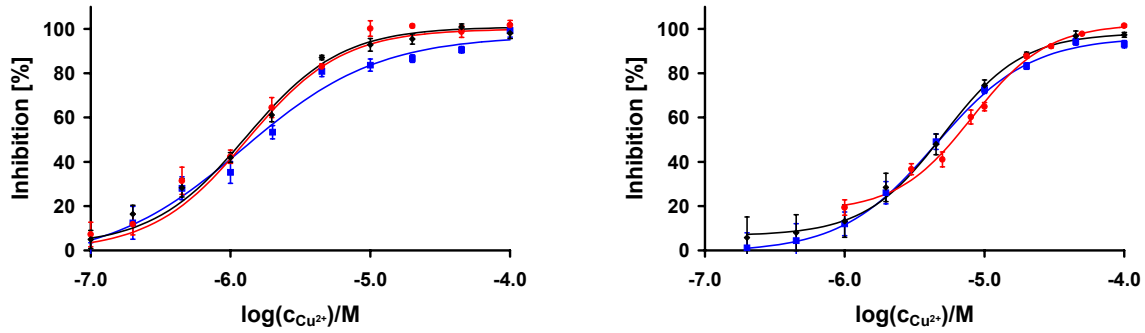

Fig. 4.22. Dose-response curves detected with the oxygen-sensitive MTP on 3 different days. Left: $2.0 \cdot 10^8$ cfu/mL; Right: $6.7 \cdot 10^8$ cfu/mL.

Table 4.10. EC_{50} values and ranges (EC_{20} – EC_{80}) of the dose-response curves of 3 measurements, respectively, performed with $2.0 \cdot 10^8$ and $6.7 \cdot 10^8$ cfu/mL of P. putida.

cfu/mL	**EC_{50} [M]**	**ΔEC_{50} (min) [M]**	**ΔEC_{50} (max) [M]**	**range [M]**
$2.0 \cdot 10^8$				
(1)	$1.5 \cdot 10^{-6}$	$-0.2 \cdot 10^{-6}$	$0.3 \cdot 10^{-6}$	$3.5 \cdot 10^{-7} – 7.3 \cdot 10^{-6}$
(2)	$1.4 \cdot 10^{-6}$	$-0.3 \cdot 10^{-6}$	$0.03 \cdot 10^{-6}$	$3.6 \cdot 10^{-7} – 4.2 \cdot 10^{-6}$
(3)	$1.3 \cdot 10^{-6}$	$-0.1 \cdot 10^{-6}$	$0.1 \cdot 10^{-6}$	$3.8 \cdot 10^{-7} – 3.6 \cdot 10^{-6}$
$6.7 \cdot 10^8$				
(1)	$4.6 \cdot 10^{-6}$	$-0.5 \cdot 10^{-6}$	$0.5 \cdot 10^{-6}$	$1.5 \cdot 10^{-6} – 1.6 \cdot 10^{-5}$
(2)	$4.5 \cdot 10^{-6}$	$-0.4 \cdot 10^{-6}$	$0.9 \cdot 10^{-6}$	$1.7 \cdot 10^{-6} – 1.3 \cdot 10^{-5}$
(3)	$6.0 \cdot 10^{-6}$	$-0.3 \cdot 10^{-6}$	$0.6 \cdot 10^{-6}$	$1.9 \cdot 10^{-6} – 1.5 \cdot 10^{-5}$

4.5.1.2. Accuracy

The *accuracy* of the results, i.e. the agreement with results obtained with other tests, has to be considered along with the reproducibility. Although the good agreement of the EC values with those given in literature indicates a sufficient accuracy of the results obtained with the oxygen-sensitive MTPs, additional comparative experiments were performed with the sensor-dish reader. Again, two different bacteria concentrations were applied. The results of these experiments are depicted in Fig.

4.23, together with the ones obtained with the oxygen-sensitive MTP. The dose-response curves as well as the EC values shown in Table 4.11 are in very good agreement with each other and - for the lower bacteria concentration - with literature. This shows that despite the oxygen ingress which take place in the permeable MTPs and through the oil sealing, the resulting calculated inhibition is not influenced. Although the oxygen ingress, which depends on the gradient between ambient air and sample, cannot be truncated in the formula for inhibition, has not to be considered. This makes the MTP assay more advantageous for this test than the widely used oxygen electrode.

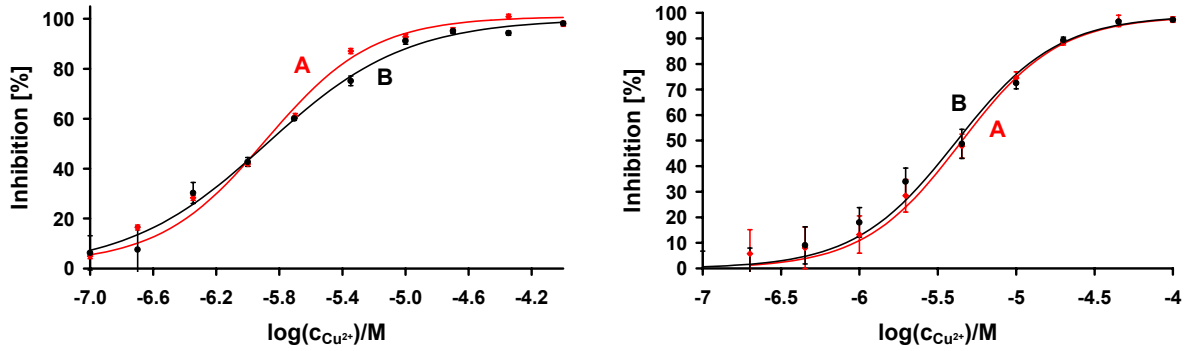

Fig. 4.23. Dose-response curves for two different bacteria concentrations detected with the oxygen-sensitive MTP (A) and the sensor dish reader (B) using copper sulphate as inhibitor. Left: $2.0 \cdot 10^8$, Right: $6.7 \cdot 10^8$ cfu/mL.

Table 4.11. EC_{50} values and ranges of the dose-response curves of measurements performed with the oxygen-sensitive OxoPlate (OP) and the sensor dish reader (SDR2), using Cu^{2+} as inhibitor and bacteria concentrations of $2.0 \cdot 10^8$ and $6.7 \cdot 10^8$ cfu/mL, respectively.

cfu/mL	**EC_{50} [M]**	**ΔEC_{50} (min) [M]**	**ΔEC_{50} (max) [M]**	**range [M]**
$2.0 \cdot 10^8$				
OP	$1.3 \cdot 10^{-6}$	$-0.1 \cdot 10^{-6}$	$0.1 \cdot 10^{-6}$	$3.8 \cdot 10^{-7} – 3.6 \cdot 10^{-6}$
SDR2	$1.3 \cdot 10^{-6}$	$-0.1 \cdot 10^{-6}$	$0.1 \cdot 10^{-6}$	$3.2 \cdot 10^{-7} – 5.4 \cdot 10^{-6}$
$6.7 \cdot 10^8$				
OP	$4.5 \cdot 10^{-6}$	$-0.4 \cdot 10^{-6}$	$0.8 \cdot 10^{-6}$	$1.7 \cdot 10^{-6} – 1.3 \cdot 10^{-5}$
SDR2	$4.5 \cdot 10^{-6}$	$-0.9 \cdot 10^{-6}$	$0.5 \cdot 10^{-6}$	$1.5 \cdot 10^{-6} – 1.2 \cdot 10^{-5}$

Using MTPs made of PS, organic test substances may adsorb on the walls of the MTP. This would shift the dose-response curves towards higher values because the adsorbed inhibitor is less available for the bacteria, which is not accounted for in evaluation. Therefore, the same experiment as described above was performed with the lower bacteria concentration using 3,5-dicholorophenol (3,5-DCP) as inhibitor. The dose-response curves detected with the OxoPlate and in the comparative experiment do not match as good as the ones with Cu^{2+}. However, the measurement range is in sufficiently good accordance, and the EC values match rather well.

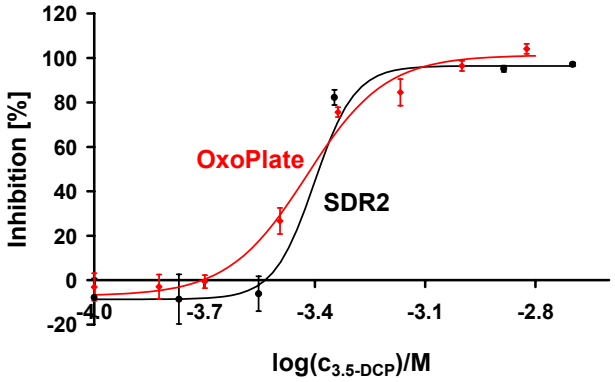

Fig. 4.24. Dose-response curves detected with the OxoPlate and the sensor dish reader (SDR2) using 3,5-DCP as inhibitor and a bacteria concentration of $2.0 \cdot 10^8$ cfu/mL.

Table 4.12. EC_{50} values and ranges of the dose-response curves of measurements performed with the oxygen-sensitive MTP OxoPlate (OP) and the sensor dish reader (SDR2), using 3,5-DCP as inhibitor and a bacteria concentration of $2.0 \cdot 10^8$ cfu/mL.

	EC_{50} [M]	**ΔEC_{50} (min) [M]**	**ΔEC_{50} (max) [M]**	**range [M]**
OxoPlate	$3.9 \cdot 10^{-4}$	$-0.1 \cdot 10^{-4}$	$0.3 \cdot 10^{-4}$	$2.9 \cdot 10^{-4} – 5.4 \cdot 10^{-4}$
SDR2	$4.1 \cdot 10^{-4}$	$-0.4 \cdot 10^{-4}$	$0.7 \cdot 10^{-4}$	$3.5 \cdot 10^{-4} – 4.9 \cdot 10^{-4}$

4.5.2. pH Measurement

Oxygen is not the only parameter related to respiration. The simultaneous production of carbon dioxide (CO_2) produces carbonic acid in aqueous solutions and therefore lowers the pH value. Measuring changes in the pH value instead of the oxygen content is advantageous for MTP experiments because the oxygen ingress has not to be accounted for and difficulties in finding an adequate plate sealing do not occur.

However, other aspects have to be taken in consideration when using the pH-sensitive MTP HydroPlate.

4.5.2.1. Ionic Strength

Most optical pH measurements depend strongly on the ionic strength (see chapter 2.3.7). Therefore, 100 mM NaCl were added to the dilution water to minimise the influence of the inhibitor concentration to the otherwise low ionic strength. This concentration is used in the culture medium and thus supposed not to have a negative influence on the activity of the bacteria. For calculation of the pH value out of the measured fluorescence signals, a calibration curve with dilution water, 1 mM phosphate buffer (from the bacteria storage medium), 100 mM NaCl and 50 mM glucose was recorded.

4.5.2.2. Response Time

Another difficulty which has to be considered is the response time of the pH sensor. The negatively charged polymer features a certain buffer capacity itself which leads to slow response times with samples of low buffer concentrations. The sample has a phosphate buffer concentration of 1.325 mM (see Table 4.2). To investigate the response time of the pH-sensitive MTP HP96U, a test solution without inoculum, containing dilution water, 1 mM phosphate buffer, 100 mM NaCl and 50 mM glucose, was prepared. 150 µL of test solution were applied to the pH-sensitive MTP and the kinetic detected for 45 min with an interval of

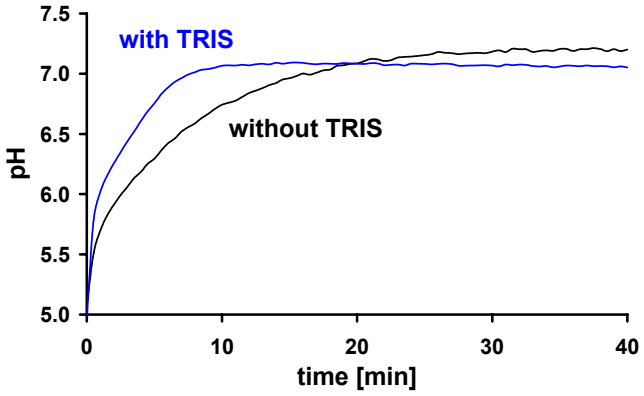

Fig. 4.25. Response time of the pH-sensitive MTP HP96U at low buffer concentration and with 5 mM TRIS.

0.5 min. The results are shown in Fig. 4.25. The response time of the dry sensor is 30 min (t_{99}). This is rather critical, because even small increases in the fluorescence signal due to the response time can strongly influence the small pH decrease due to bacteria respiration. To overcome this problem, the response time of the sensor using a test solution with additional 5 mM of TRIS buffer was investigated. TRIS buffer was chosen, because it influences the detection of respiration only little, which starts at a pH of 7 and decreasing over time, , due to its pK_a of 8.06. The response time of the sensor using this test solution was only 8.5 min. Therefore the influence of TRIS buffer in the test solution was investigated further.

4.5.2.3. Influence of the Sample Composition on Dose-Response Curves

A disadvantage of the addition of TRIS buffer is that, even while the pH value at the start of the measurement is not exactly within its dynamic range, the pH decrease due to respiration is more buffered by this system than without the TRIS buffer. Fig. 4.26 shows the respiration of $6.7 \cdot 10^8$ cfu/mL of *P. putida* detected with the pH-sensitive MTP using test solution with and without 5 mM of TRIS buffer. Without TRIS, the pH decreases more rapidly (-0.0104 / min) than with TRIS buffer (-0.0067 / min). This may lead to difficulties using lower bacteria concentrations due to bad reproducibility of the signals.

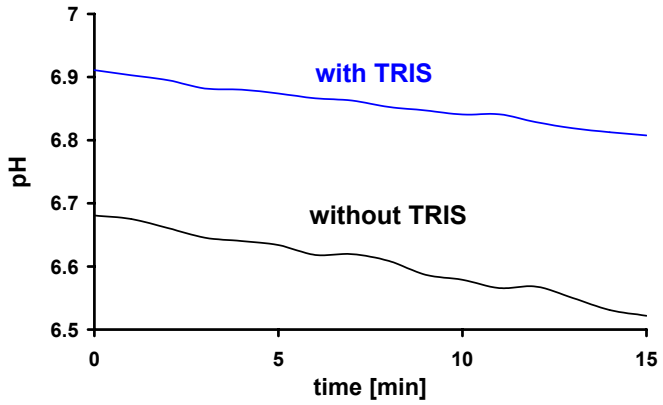

Fig. 4.26. Respiration of $6.7 \cdot 10^8$ cfu/mL of P. putida using dilution water with 5 mM TRIS and without TRIS. The change in pH per minute is -0.0067 (with TRIS) and -0.0104 (without TRIS).

Another aspect to be considered is that adding extraordinary components to the test solution may influence the sensitivity towards inhibitors. Dose-response curves with pure dilution water, dilution water with 100 mM NaCl and dilution water containing 100 mM NaCl and 5 mM TRIS buffer were recorded with the oxygen-sensitive MTP at a bacteria concentration of $2.0 \cdot 10^8$ cfu/mL, using Cu^{2+} as inhibitor. This test was not performed with the pH-sensitive MTP because the effect on the biological system should be tested, not the sensory one.

The resulting dose-response curves differ considerably. Whereas the EC_{50} value of the test using the original sample composition ($6.3 \cdot 10^{-7}$ M) agrees the most with the value given in the DIN test ($9.6 \cdot 10^{-7}$ M), addition of 100 mM NaCl (EC_{50} = $1.3 \cdot 10^{-6}$ M) and 5 mM TRIS (EC_{50} = $2.2 \cdot 10^{-6}$ M) leads to lower sensitivity of the bacteria towards the inhibitor. One reason for this tendency may be that the results of a toxicity test depends on factors like temperature, pH as well as the ionic strength [11]. Furthermore, with 100 mM of NaCl, which is the concentration used for cultivation, the bacteria are more robust and not so easily stressed by the inhibitor, leading to a lower sensitivity. Regarding TRIS buffer, which tends to complex heavy metals, lowers the actual concentration of inhibitor in solution. Therefore lower sensitivity is simulated because the concentrations given on the x-axis are the employed ones. However, the best correctness of the result is not associated with the best reproducibility: Repeating the experiment gave the largest deviations using the pure dilution water, whereas the other two compositions where highly reproducible.

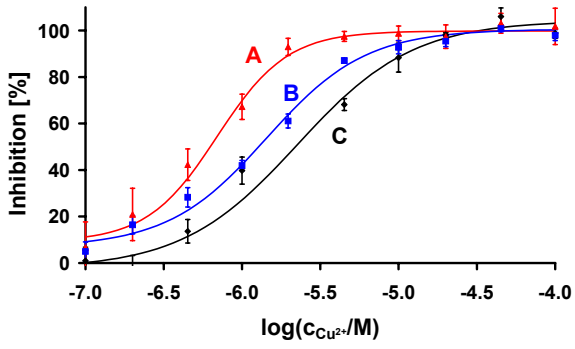

Fig. 4.27. Dose-response curves using (A) pure dilution water, (B) dilution water with 100 mM NaCl and (C) dilution water with NaCl mM and 5 mM TRIS (detected with the oxygen-sensitive MTP).

Table 4.13. EC_{50} values and ranges of the dose-response curves obtained with the oxygen-sensitive MTP using Cu^{2+} as inhibitor and a bacteria concentration of $2.0 \cdot 10^8$ cfu/mL. (A) Pure dilution water, (B) dilution water with 100 mM NaCl and (C) dilution water with NaCl mM and 5 mM TRIS.

	EC_{50} [M]	**ΔEC_{50} (min) [M]**	**ΔEC_{50} (max) [M]**	**range [M]**
A	$6.3 \cdot 10^{-7}$	$-1.4 \cdot 10^{-7}$	$0.6 \cdot 10^{-7}$	$2.5 \cdot 10^{-7} – 1.3 \cdot 10^{-6}$
B	$1.4 \cdot 10^{-6}$	$-0.1 \cdot 10^{-6}$	$0.09 \cdot 10^{-6}$	$3.8 \cdot 10^{-7} – 3.6 \cdot 10^{-6}$
C	$2.2 \cdot 10^{-6}$	$-0.6 \cdot 10^{-6}$	$0.06 \cdot 10^{-6}$	$7.4 \cdot 10^{-7} – 6.4 \cdot 10^{-6}$

The experiment was also performed with different bacteria concentrations to investigate if the influence of sample composition on the sensitivity is proportional to the total amount of bacteria. Concentrations of $4.2 \cdot 10^7$, $2.0 \cdot 10^8$, $3.3 \cdot 10^8$ cfu/mL and $6.7 \cdot 10^8$ cfu/mL were used. Only the two extremal solutions, dilution water with and without addition of 5 mM TRIS and 100 mM NaCl were investigated to save time and labour. The dose-response curves of the measurements with pure dilution water were shifted towards lower sensitivity with growing bacteria concentration, as expected. The EC_{50} of the bacteria concentration of $2.0 \cdot 10^8$ cfu/mL (10^{-6} M) was in best accordance to the literature value ($9.6 \cdot 10^{-7}$M). Surprisingly enough, the dose-response curves of the experiment with addition of TRIS and NaCl seemed not to be influenced much by the bacteria concentration. The curves with the lowest and the highest concentration (A and D) even match rather well. Whereas the EC_{50} values with pure dilution water span a decade, the range of the EC_{50} values with TRIS/NaCl are distributed rather homogeneously, lacking any tendencies. An explanation for this behaviour may be that the negatively charged bacteria attract the positively charged Cu^{2+}, thereby detoxicating the sample. This means that with higher bacteria concentration, there are less assessable dissolved Cu^{2+} ions than with a lower bacteria concentration, which is not accounted for on the x-axis (left). In contrast, TRIS complexes Cu^{2+} independent of the bacteria concentration. Therefore, the Cu^{2+} concentration given on the x-axis is too low for all bacteria concentrations.

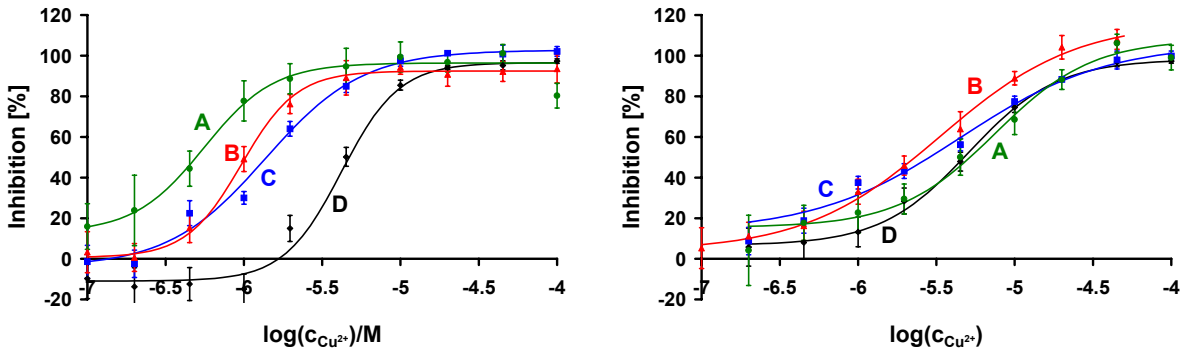

Fig. 4.28. Dose-response with different bacteria concentrations: (A) $4.2 \cdot 10^7$, (B) $2.0 \cdot 10^8$, (C) $3.4 \cdot 10^8$, and (D) $6.7 \cdot 10^8$ cfu/mL. Left: Pure dilution water; Right: Dilution water containing 5 mM TRIS and 100 mM NaCl.

Table 4.14. EC_{50} values and ranges of Cu^{2+} using 4 different bacteria activities and two different compositions of test solutions.

cfu/mL	**EC_{50} [M]**	**ΔEC_{50} (min) [M]**	**ΔEC_{50} (max) [M]**	**range [M]**
pure dilution water				
$4.2 \cdot 10^7$	$4.9 \cdot 10^{-7}$	$-0.2 \cdot 10^{-6}$	$0.2 \cdot 10^{-6}$	$1.6 \cdot 10^{-7} – 1.1 \cdot 10^{-6}$
$2.0 \cdot 10^8$	$1.0 \cdot 10^{-6}$	$-0.04 \cdot 10^{-6}$	$0.1 \cdot 10^{-6}$	$5.7 \cdot 10^{-7} – 2.0 \cdot 10^{-6}$
$3.4 \cdot 10^8$	$1.4 \cdot 10^{-6}$	$-0.2 \cdot 10^{-6}$	$0.3 \cdot 10^{-6}$	$5.7 \cdot 10^{-7} – 3.5 \cdot 10^{-6}$
$6.7 \cdot 10^8$	$4.7 \cdot 10^{-6}$	$-0.5 \cdot 10^{-6}$	$0.3 \cdot 10^{-6}$	$2.9 \cdot 10^{-6} – 8.6 \cdot 10^{-6}$
Dilution water containing 5 mM TRIS and 100 mM NaCl				
$4.2 \cdot 10^7$	$5.2 \cdot 10^{-6}$	$-1.6 \cdot 10^{-6}$	$0.7 \cdot 10^{-6}$	$9.1 \cdot 10^{-7} – 1.4 \cdot 10^{-5}$
$2.0 \cdot 10^8$	$2.3 \cdot 10^{-6}$	$-0.4 \cdot 10^{-6}$	$0.7 \cdot 10^{-6}$	$5.6 \cdot 10^{-7} – 6.9 \cdot 10^{-6}$
$3.4 \cdot 10^8$	$2.9 \cdot 10^{-6}$	$-0.6 \cdot 10^{-6}$	$0.2 \cdot 10^{-6}$	$2.9 \cdot 10^{-7} – 1.2 \cdot 10^{-5}$
$6.7 \cdot 10^8$	$4.7 \cdot 10^{-6}$	$-0.6 \cdot 10^{-6}$	$0.7 \cdot 10^{-6}$	$2.9 \cdot 10^{-6} – 8.6 \cdot 10^{-6}$

Better reproducibility and the fact that a certain ionic strength is inevitable for pH measurements with respect to the influence of the IS of the toxin, militates in favour for adding 100 mM NaCl to the dilution water. The resulting EC_{50} is still in good accordance to the literature value. TRIS buffer, which shifts the dose-response curve and therefore the EC_{50} still further, was abandoned.

4.5.2.4. Bacteria Concentrations

Due to the dependency of the bacteria concentration on the sensitivity of the test, different concentrations were investigated with respect to the reproducibility and accordance of the results to those obtained with the oxygen measurements. Bacteria concentrations of $2.0 \cdot 10^8$ cfu/mL, $3.4 \cdot 10^8$ cfu/mL, $5.0 \cdot 10^8$ cfu/mL and $6.7 \cdot 10^8$ cfu/mL were used. The results are depicted in Fig. 4.29. The dose-response curves of all 4 concentrations agree satisfactorily with those obtained with the oxygen-sensitive MTP. The EC_{50} values obtained with the pH-sensitive MTP tend to be somewhat higher than the ones obtained with the oxygen sensor, especially at high bacteria concentrations, but provide sufficient accuracy. The EC_{50} for the lowest bacteria concentration is in best accordance with the value given in literature. Unfortunately, too small changes in pH lead to enormous standard deviations. Repeatability proved to be rather poor using this low concentration. Therefore the highest bacteria concentration of $6.7 \cdot 10^8$ cfu/mL, which featured the best reproducibility, was chosen for all following experiments using the pH sensor.

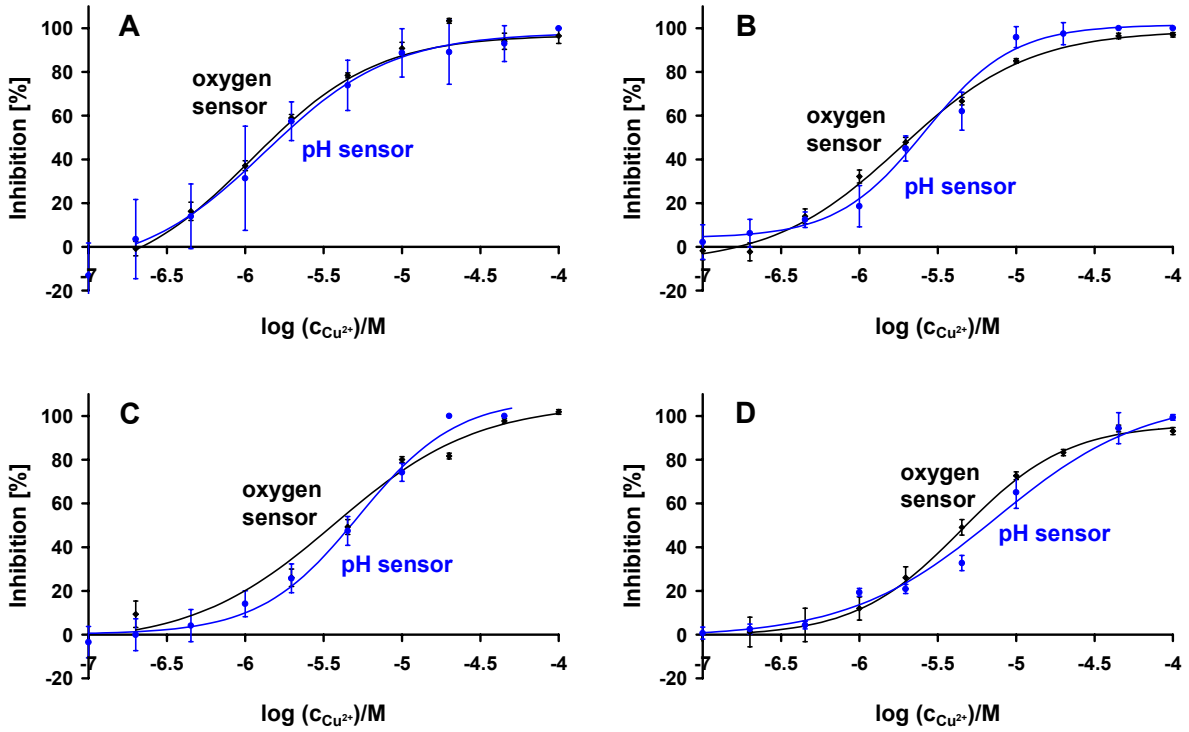

Fig. 4.29. Dose-response curves with different bacteria concentrations, obtained with the pH- and the oxygen-sensitive MTP. A: $2.0 \cdot 10^8$, B: $3.4 \cdot 10^8$, C: $5.0 \cdot 10^8$ cfu/mL, D: $6.7 \cdot 10^8$ cfu/mL.

Table 4.15. EC_{50} values and range obtained with the pH- and the oxygen-sensitive MTP using different bacteria concentrations.

cfu/mL	**EC_{50} [M]**	**ΔEC_{50} (min) [M]**	**ΔEC_{50} (max) [M]**	**range [M]**
$2.0 \cdot 10^8$				
O2	$1.5 \cdot 10^{-6}$	$-0.1 \cdot 10^{-6}$	$0.08 \cdot 10^{-6}$	$5.6 \cdot 10^{-7} – 5.5 \cdot 10^{-6}$
pH	$1.7 \cdot 10^{-6}$	$-0.7 \cdot 10^{-6}$	$1.3 \cdot 10^{-6}$	$5.7 \cdot 10^{-7} – 6.0 \cdot 10^{-6}$
$3.4 \cdot 10^8$				
O2	$2.1 \cdot 10^{-6}$	$-0.2 \cdot 10^{-6}$	$0.2 \cdot 10^{-6}$	$6.9 \cdot 10^{-7} – 7.8 \cdot 10^{-6}$
pH	$2.4 \cdot 10^{-6}$	$3.5 \cdot 10^{-6}$	$6.6 \cdot 10^{-6}$	$9.1 \cdot 10^{-7} – 5.9 \cdot 10^{-6}$
$5.0 \cdot 10^8$				
O2	$3.6 \cdot 10^{-6}$	$0.7 \cdot 10^{-6}$	$1.5 \cdot 10^{-6}$	$9.9 \cdot 10^{-7} – 1.3 \cdot 10^{-5}$
pH	$4.7 \cdot 10^{-6}$	$-0.8 \cdot 10^{-6}$	$0.8 \cdot 10^{-6}$	$1.8 \cdot 10^{-6} – 1.1 \cdot 10^{-5}$
$6.7 \cdot 10^8$				
O2	$4.6 \cdot 10^{-6}$	$-0.3 \cdot 10^{-6}$	$0.6 \cdot 10^{-6}$	$1.5 \cdot 10^{-6} – 1.6 \cdot 10^{-5}$
pH	$6.5 \cdot 10^{-6}$	$-0.6 \cdot 10^{-6}$	$2.5 \cdot 10^{-6}$	$1.6 \cdot 10^{-6} – 2.4 \cdot 10^{-5}$

4.5.2.5. Summary

The application of the *P. putida* respiration inhibition test to the pH-sensitive MTP stipulates certain modifications of the standard procedure. Due to the dependence of optical pH measurement on the ionic strength of the sample, 100 mM NaCl were added to the dilution water to minimise the influence of the IS of the test substance towards the overall IS.

Furthermore, the rather long response time of 30 min of the dry sensor towards samples of small buffer concentrations, as used for this test, has to be considered. Adding 5 mM TRIS to the dilution water to increase the buffer concentration shortens the response time to 8.5 min. However, this procedure was abandoned because it decreased the sensitivity of the test by shifting the dose-response curves towards higher concentrations. Moreover, although the buffer capacity of TRIS is only small at pH 7, the pH decrease was smaller compared to the less-buffered system, which can lead to lower reproducibility and accuracy of the test.

The long response time of the test without TRIS buffer was accounted for by incubating the samples with the toxins in the MTP instead of glass vials on a shaker. The MTP was shaken during the incubation time of 30 min in the reader with a shaking mode of 600 rpm / 1 mm. During this time, the sensor has nearly equilibrated.

The proton increase per time was calculated with a simulation program Berkeley-Madonna using the Henderson-Hasselbalch equation instead of the pH decrease per time. This provided correct results and improved the reproducibility of the test (see chapter 4.3.5.2, page 123, and Appendix B).

A bacteria concentration of $6.7 \cdot 10^8$ cfu/mL was chosen for the screening tests regarding the pH measurements, although the concentration used in the DIN test was lower ($2.0 \cdot 10^8$ cfu/mL). This was necessary because the pH decrease was too small to give reproducible results. Moreover, varying response times of the sensor of sometimes more than 30 min at low buffer concentrations adulterate the kinetic and can even lead to a signal increase instead of a decrease at slow kinetics (near 100 % inhibition). This effect is less pronounced at faster kinetics, i.e. with higher bacteria activities, because the pH decrease is less compensated by the signal increase due to the response time. The oxygen screening tests are performed with both $6.7 \cdot 10^8$ cfu/mL for to ensure the correctness of the results obtained with the pH sensor, and with $2.0 \cdot 10^8$ cfu/mL for comparison with literature values. Direct comparison of the results of the pH measurements with literature was not possible due to the higher bacteria concentration and the addition of NaCl, which are both indispensable for the pH tests.

4.5.3. Screening of Different Toxic Substances

Several substances were screened for their toxicity towards *P. putida*. Dose-response curves were taken with a bacteria concentration of $6.7 \cdot 10^8$ cfu/mL using both the pH- and the oxygen-sensitive MTPs, and additionally with a concentration of $2.0 \cdot 10^8$ cfu/mL using the oxygen-sensitive MTP. For reasons discussed in chapter 4.5.2, 100 mM NaCl were added to the dilution water for these experiments. Variability of the results was reduced by using the same solutions in each assay. The

tests were characterised with respect to their EC_{50} values and their ranges. The ranges were defined as the concentrations of toxic substance causing an inhibition between 20 and 80 %, which roughly represents the linear range of the sigmoidal curve. The EC_{20} value was further defined as limit of detection (LOD) because the usual definition (i.e. three times the standard deviation of the lowest detectable value) is not appropriate for dose-response curves due to the absence of a blank [10]. Two classes of environmentally significant toxic substances were investigated: Heavy metals and chlorophenols.

4.5.3.1. Heavy Metals

Metals with a density of more than 6 g/cm^3 are referred to as heavy metals. They include essential elements like iron, copper or zinc, which are trace elements and part of metalloproteins, as well as non-essential elements like cadmium, lead or mercury. Natural sources like soil, ores, water or plants contain only small amounts of these substances. Increased concentrations of heavy metals or rather their free ions cause growth inhibition and metabolism disruption.

In general heavy metals produce their toxicity by forming complexes with organic compounds. These modified biological molecules lose their ability to function properly, and result in malfunction or death of the affected cells. The most common groups involved in ligand formation are oxygen, sulphur, and nitrogen. When metals bind to these groups they may inactivate important enzyme systems, or affect protein structure.

The toxicity of heavy metals depends on their bioavailability as free ions. Factors like the pH value, temperature, composition of the sample (e.g. presence of organic or inorganic ligands) or ionic strength have a strong influence on the bioavailability. The Van't Hoff rule states that a temperature rise of 10 °C multiplies the toxicity of a substance by the factor 2 – 3. Although this is true for a lot of toxins, in some cases the tendency is contrary [11]. For regarding the total amount of heavy metals may result in differing dose-response curves [12], usually the amount of free ions is used instead. However, with biochemical tests, the concentrations involved

are often too small to be detected precisely by conventional instruments. Therefore, in this experiments, the total amount of heavy metal is used.

- Copper

Copper and most copper compounds are semi-synthetic in origin. Although some natural deposits of metallic copper have been found, it is generally mined either as sulphide or oxide ores and processed by grinding, washing, melting and casting [13, 14]. Copper compounds are commonly used in agriculture to treat plant diseases like mildew, for water treatment, and as preservatives for wood, leather, and fabrics. [15]

In small concentrations, copper is an essential trace element because Cu^{2+} is part of metalloproteins. The blood of crustaceans and molluscs contains cupriferous haemocyanin instead of haemoglobin. Green plants display plastocyanin in their chloroplasts which supports the production of chlorophyll. However, too high concentrations of copper salts are toxic, especially to algae. In mammals, the cytotoxicity leads to damages of the gastrointestinal tract, the liver, kidneys and the nervous system. Local effects are irritations of the skin or eye from exposure to copper salts. Chronic exposure to copper salts may lead to lung cancer [11, 16]. $Cu(SO_4) \cdot 5H_2O$, which was used for these experiments, is used as emetic [17].

Experimental: 0.0125 g of $Cu(SO_4) \cdot 5H_2O$ (M = 249.69 g/mol) were dissolved in 50 mL of doubly distilled water, giving a stock solution with a concentration of 10^{-3} M (250 mg/L). 3 drops of 1 M HCl were added to avoid precipitation of $Cu(OH)_2$ ($K_{sp} = 4.8 \cdot 10^{-20}$ mol^3/L^3 [9]). The stock solution was diluted appropriately with dilution water down to 10^{-7} M (0.025 mg/L). The characteristics of the resulting dose-response curves are summarised in Table 4.16. The dose-response curves using the higher bacteria concentration detected with the oxygen- and the pH-sensitive MTPs match perfectly well (Fig. 4.30, left). Using a lower bacteria concentration, the EC_{50} and the range are shifted to lower concentrations (Fig. 4.30, right). The EC_{50} and EC_{20} values are in good accordance with those given in literature. The range for both bacteria concentrations covers ca. 1.5 orders of magnitude.

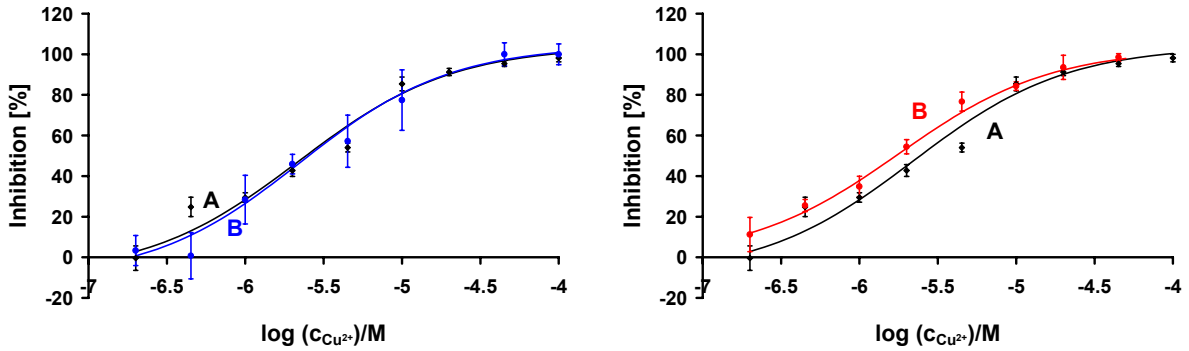

Fig. 4.30. Dose-response curves with Cu^{2+} as inhibitor. Left: $6.7 \cdot 10^8$ cfu/mL, obtained with the oxygen- (A) and pH- (B) sensitive MTPs; Right: (A): $6.7 \cdot 10^8$ cfu/mL and (B): $2.0 \cdot 10^8$ cfu/mL, obtained with the oxygen-sensitive MTP.

Table 4.16. EC_{50} values and ranges for Cu^{2+} obtained with the OxoPlate (OP) for two different bacteria concentrations, and the HydroPlate (HP) for the higher bacteria concentration.

cfu/mL	**EC_{50} [M]**	**ΔEC_{50} (min) [M]**	**ΔEC_{50} (max) [M]**	**range [M]**
OP $2.0 \cdot 10^8$	$1.7 \cdot 10^{-6}$	$-0.2 \cdot 10^{-6}$	$0.3 \cdot 10^{-6}$	$3.8 \cdot 10^{-7} – 7.3 \cdot 10^{-6}$
OP $6.7 \cdot 10^8$	$2.4 \cdot 10^{-6}$	$-0.6 \cdot 10^{-6}$	$0.6 \cdot 10^{-6}$	$6.7 \cdot 10^{-7} – 9.6 \cdot 10^{-6}$
HP $6.7 \cdot 10^8$	$2.5 \cdot 10^{-6}$	$-0.6 \cdot 10^{-6}$	$0.3 \cdot 10^{-6}$	$7.4 \cdot 10^{-7} – 9.5 \cdot 10^{-6}$
Literature data	$9.6 \cdot 10^{-7}$			EC_{20}: $4.6 \cdot 10^{-7}$

- Cobalt

Cobalt occurs in ores almost always in conjunction with nickel. Besides in alloys, it is used for pigments in glasses, enamels and ceramics, in mixed catalysators and siccatives. Cobalt is essential as central atom of vitamin B_{12}, which is responsible for the formation of erythrocytes. For humans, oral uptake is little toxic. At concentrations of 25-30 mg/d it causes skin and lung diseases, stomach trouble and damage of kidneys, liver and heart. Cobalt powder and aerosols are carcinogenic [11, 16].

Experimental: 0.1746 g of $Co(NO_3)_2 \cdot 6H_2O$ (M = 291.04 g/mol) were dissolved in 20 mL of dilution water, giving a stock solution with a concentration of $3 \cdot 10^{-2}$ M (8731 mg/L). This stock solution was diluted appropriately with dilution water down to 10^{-6} M (0.291 mg/L). The characteristics of the resulting dose-response curves are summarised in Table 4.17. The dose-response curves using the higher bacteria concentration detected with the pH and the oxygen sensor are in good accordance (Fig. 4.31, left). Using a lower bacteria concentration, EC_{50} and range are shifted towards lower inhibitor concentrations (Fig. 4.31, right). The range for both concentrations spans 1.5 orders of magnitude.

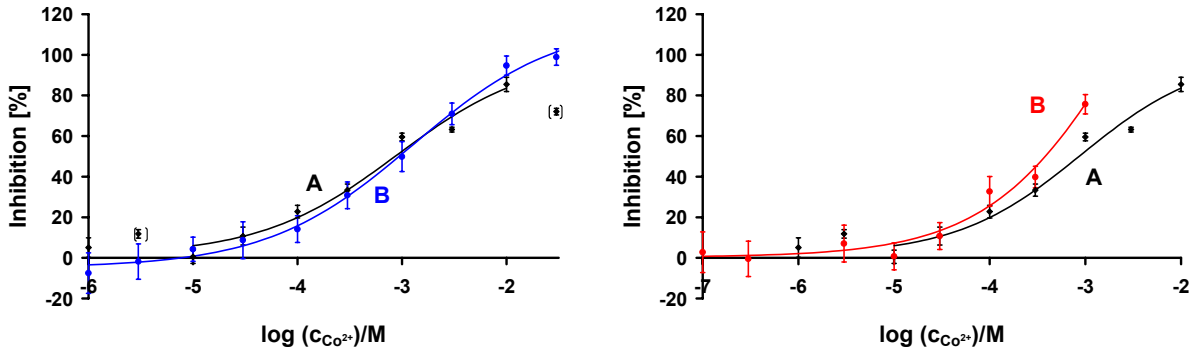

Fig. 4.31. Dose-response curves with Co^{2+} as inhibitor. Left: $6.7 \cdot 10^8$ cfu/mL, obtained with the oxygen- (A) and pH- (B) sensitive MTPs; Right: (A): $6.7 \cdot 10^8$ cfu/mL and (B): $2.0 \cdot 10^8$ cfu/mL, obtained with the oxygen-sensitive MTP.

Table 4.17. EC_{50} values and ranges for Co^{2+} obtained with the OxoPlate (OP) for two different bacteria concentrations, and the HydroPlate (HP) for the higher bacteria concentration.

cfu/mL	**EC_{50} [M]**	**ΔEC_{50} (min) [M]**	**ΔEC_{50} (max) [M]**	**range [M]**
OP $2.0 \cdot 10^8$	$3.8 \cdot 10^{-4}$	$-1.0 \cdot 10^{-4}$	$0.5 \cdot 10^{-4}$	$6.3 \cdot 10^{-5} – 1.1 \cdot 10^{-3}$
OP $6.7 \cdot 10^8$	$8.6 \cdot 10^{-4}$	$-2.3 \cdot 10^{-4}$	$0.3 \cdot 10^{-4}$	$1.0 \cdot 10^{-4} – 7.0 \cdot 10^{-3}$
HP $6.7 \cdot 10^8$	$9.4 \cdot 10^{-4}$	$-2.7 \cdot 10^{-4}$	$3.7 \cdot 10^{-4}$	$1.4 \cdot 10^{-4} – 5.0 \cdot 10^{-3}$

- Cadmium

Like zinc, cadmium forms stable complexes with organic ligands, carbonates and chorid- and sulphur-containing compounds. It accumulates strongly in sewage sludge. Cadmium is used for Ni-Cd batteries, corrosion protection, pigments, soaps, and PVC stabilisers. It is prohibited as ingredient in cosmetics and herbicides due to its toxicity.

The inhibition mechanisms of cadmium is not yet clarified completely. Acute toxic effects involve sickness, irritation of the gastrointestinal and respiratory tract, damage of the liver, convulsions and headaches. Cadmium accumulates in the liver and kidneys. Chronic absorption by mammals leads to anaemia and damages of bones (osteoporosis) and kidneys. It is assumed that cadmium inhibits competitively the absorption of iron in the intestinals and inhibits the synthesis of vitamin D3. [11, 16]

Experimental: 0.6170 g, 0.1234 g and 0.04627 g of $Cd(NO_3)_2 \cdot 4H_2O$ (M = 291.04 g/mol) were dissolved in 30 mL of dilution water, respectively, giving solutions with concentrations of 10^{-1} M (30850 mg/L), $2 \cdot 10^{-2}$ M (6170 mg/L), and $5 \cdot 10^{-3}$ M (1542 mg/L). The latter two solutions were not diluted from the first one to avoid inherited errors in concentration due to precipitation of the hardly soluble $Cd(OH)_2$. The latter solution was diluted appropriately with dilution water down to 10^{-7} M (0.030 mg/L). The characteristics of the resulting dose-response curves are summarised in Table 4.18. The dose-response curves using the higher bacteria concentration detected with the oxygen- and the pH-sensitive MTPs match rather well (Fig. 4.32, left). In contrast to dose-response curves obtained with other inhibitors, the characteristics of the curve are quite independent from the bacteria concentration (Fig. 4.32, right). The range of these dose-response curves is rather large and spans ca. 3 orders of magnitude.

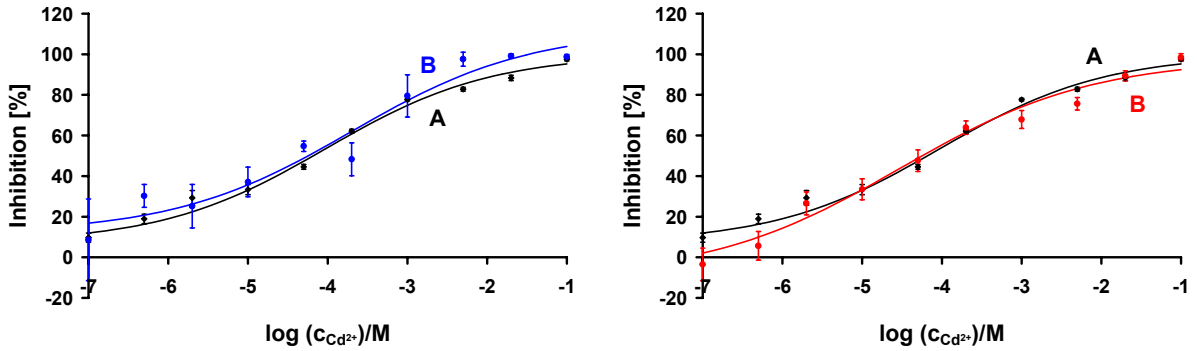

Fig. 4.32. Dose-response curves with Cd^{2+} as inhibitor. Left: $6.7 \cdot 10^8$ cfu/mL, obtained with the oxygen- (A) and pH- (B) sensitive MTPs; Right: (A): $6.7 \cdot 10^8$ cfu/mL and (B): $2.0 \cdot 10^8$ cfu/mL, obtained with the oxygen-sensitive MTP.

Table 4.18. EC_{50} values and ranges for Cd^{2+} obtained with the OxoPlate (OP) for two different bacteria concentrations, and the HydroPlate (HP) for the higher bacteria concentration.

cfu/mL	**EC_{50} [M]**	**ΔEC_{50} (min) [M]**	**ΔEC_{50} (max) [M]**	**range [M]**
OP $2.0 \cdot 10^8$	$5.7 \cdot 10^{-5}$	$-2.6 \cdot 10^{-5}$	$2.9 \cdot 10^{-5}$	$2.2 \cdot 10^{-6} – 2.7 \cdot 10^{-3}$
OP $6.7 \cdot 10^8$	$6.6 \cdot 10^{-5}$	$-2.0 \cdot 10^{-5}$	$0.4 \cdot 10^{-5}$	$1.2 \cdot 10^{-6} – 2.1 \cdot 10^{-3}$
HP $6.7 \cdot 10^8$	$5.7 \cdot 10^{-5}$	$-1.6 \cdot 10^{-5}$	$2.8 \cdot 10^{-5}$	$3.9 \cdot 10^{-7} – 1.4 \cdot 10^{-3}$

- Zinc

Being a base metal, zinc occurs only in compounds, e.g. with lead or cadmium. Zinc forms stable complexes with organic ligands, carbonates and chorid- and sulphur-containing compounds. It accumulates strongly in sewage sludge. It is used for electrogalvanisation of steel, in paints for protection against corrosion and in zinc compounds (e.g. brass). Zinc oxide is antiseptic, astringent and fungistatic and is used in skin care products and anti-dandruff-shampoos.

Zinc is an essential trace element, metallic part of more than 200 enzymes and activator for many other enzymes (e.g. vitamin A). Like copper, it forms

metallothionein complexes. Zinc deficiency causes skin diseases and growth inhibition in mammals and birds and is limiting factor for the biosynthesis of DNA and proteins in microorganisms. Too high concentrations lead to corrosion, sickness and inflammation of the digestion organs [11, 16, 18].

Experimental: 0.0883 g of $Zn(NO_3)_2 \cdot 6H_2O$ (M = 297.48 g/mol) were dissolved in 30 mL of dilution water, giving a stock solution with a concentration of 10^{-2} M (2975 mg/L). This stock solution was diluted appropriately with dilution water down to 10^{-7} M (0.030 mg/L). The characteristics of the resulting dose-response curves are summarised in Table 4.19. The dose-response curves using the higher bacteria concentration detected with the oxygen and the pH sensor match satisfactory (Fig. 4.33, left) except for the maximum inhibition obtained with the oxygen sensor, which is 80 % instead of 100 %. This behaviour was reproducibly obtained with both bacteria concentrations and indicates oxygen production at higher Zn^{2+} concentration, for which no reason could be found. Incomplete solubility of Zn^{2+} could be excluded because this would have the same influence on the dose-response curve obtained with the pH sensor. The reliably detectable inhibitor concentration ranges over 1.5 – 2 orders of magnitude.

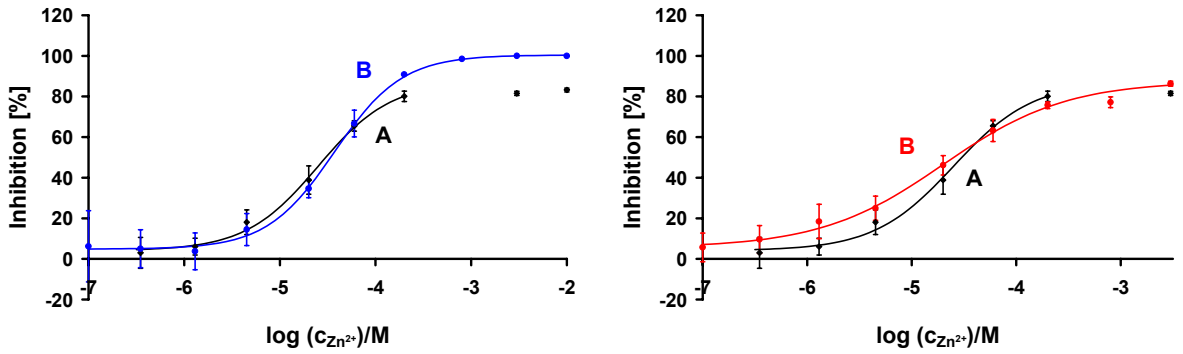

Fig. 4.33. Dose-response curves with Zn^{2+} as inhibitor. Left: $6.7 \cdot 10^8$ cfu/mL, obtained with the oxygen- (A) and pH- (B) sensitive MTPs; Right: (A): $6.7 \cdot 10^8$ cfu/mL and (B): $2.0 \cdot 10^8$ cfu/mL, obtained with the oxygen-sensitive MTP.

Table 4.19. EC_{50} values and ranges for Zn^{2+} obtained with the OxoPlate (OP) for two different bacteria concentrations, and the HydroPlate (HP) for the higher bacteria concentration.

cfu/mL	**EC_{50} [M]**	**ΔEC_{50} (min) [M]**	**ΔEC_{50} (max) [M]**	**range [M]**
OP $2.0 \cdot 10^8$	$2.5 \cdot 10^{-5}$	$-0.8 \cdot 10^{-5}$	$0.8 \cdot 10^{-5}$	$2.5 \cdot 10^{-6} – 4.4 \cdot 10^{-4}$
OP $6.7 \cdot 10^8$	$3.0 \cdot 10^{-5}$	$-0.4 \cdot 10^{-5}$	$0.3 \cdot 10^{-5}$	$7.1 \cdot 10^{-6} – 2.0 \cdot 10^{-4}$
HP $6.7 \cdot 10^8$	$3.4 \cdot 10^{-5}$	$-0.6 \cdot 10^{-5}$	$0.9 \cdot 10^{-5}$	$9.6 \cdot 10^{-6} – 1.1 \cdot 10^{-4}$

- Nickel

Nickel occurs almost always compound with other elements (e.g. S, As, Sb or silicic acid). It is used for steel refinement, in alloys, Ni-Cd batteries and as catalyst.

Little is known about the physiological role of this trace element. It is assumed that it is involved in the carbohydrate metabolism and is part of enzymes of certain microorganisms and plants (archaebacteria, sword bean).

Many nickel salts are toxic, mutagen or allergenic. They can sensitise, cause dermatitis and irritate the eyes, skin, the respiratory tract, stomach and intestinals. Nickel is also known for its carcinogenic effect: It damages the chromatin in the cell nucleus by DNA oxidation, which causes inhibition of DNA replication and repair mechanisms [11, 16].

Experimental: 0.1745 g of $Ni(NO_3)_2 \cdot 6H_2O$ (M = 290.91 g/mol) were dissolved in 20 mL of dilution water, giving a stock solution with a concentration of $3 \cdot 10^{-2}$ M (8727 mg/L). This stock solution was diluted appropriately with dilution water down to 10^{-6} M (0.291 mg/L). The characteristics of the resulting dose-response curves are summarised in Table 4.20. The dose-response curves using the higher bacteria concentration detected with the oxygen- and the pH-sensitive MTPs match rather well (Fig. 4.34, left). Using lower bacteria concentrations, the curve characteristics are shifted towards lower inhibitor concentrations (Fig. 4.34, right). The range of these dose-response curves spans ca. 1.5 orders of magnitude.

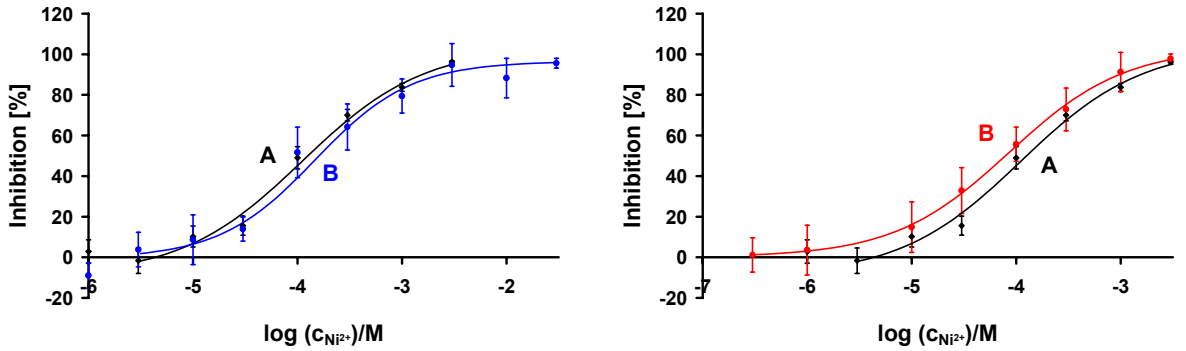

Fig. 4.34. Dose-response curves with Ni^{2+} as inhibitor. Left: $6.7 \cdot 10^8$ cfu/mL, obtained with the oxygen- (A) and pH- (B) sensitive MTPs; Right: (A): $6.7 \cdot 10^8$ cfu/mL and (B): $2.0 \cdot 10^8$ cfu/mL, obtained with the oxygen-sensitive MTP.

Table 4.20. EC_{50} values and ranges for Ni^{2+} obtained with the OxoPlate (OP) for two different bacteria concentrations, and the HydroPlate (HP) for the higher bacteria concentration.

cfu/mL	**EC_{50} [M]**	**ΔEC_{50} (min) [M]**	**ΔEC_{50} (max) [M]**	**range [M]**
OP $2.0 \cdot 10^8$	$7.9 \cdot 10^{-5}$	$-0.8 \cdot 10^{-5}$	$1.4 \cdot 10^{-5}$	$1.4 \cdot 10^{-5} – 4.1 \cdot 10^{-4}$
OP $6.7 \cdot 10^8$	$1.3 \cdot 10^{-4}$	$-0.2 \cdot 10^{-4}$	$0.2 \cdot 10^{-4}$	$2.7 \cdot 10^{-5} – 6.5 \cdot 10^{-4}$
HP $6.7 \cdot 10^8$	$1.6 \cdot 10^{-4}$	$-0.9 \cdot 10^{-4}$	$0.8 \cdot 10^{-4}$	$3.7 \cdot 10^{-5} – 7.8 \cdot 10^{-4}$

- Chromate

Like zinc and nickel, chrome occurs almost always in compounds. It is used for steel, alloys and catalyst, chromate serves as oxidant for many chemical reactions. Furthermore, the deep green Cr(III) and the bright yellow (chromate), orange (dichromate) or red Cr(VI) compounds are popular pigments, although even hardly soluble salts of the latter are supposed to be carcinogenic and therefore avoided recently.

In living organisms, the trace element chrome exists mostly as Cr(III) and is involved in the glucose metabolism. Cr(IV), however, is much more toxic and

absorbed better than Cr(III). Being strong oxidants, Cr(VI) compounds are corrosive to skin and mucous, toxic and cause abscesses, inflammation of the gastrointestinal tract and damage of liver and kidneys. It is sensitising, mutagen and carcinogenic [11, 16].

Experimental: 0.0883 g of potassium dichromate ($K_2Cr_2O_7$, M = 294.19 g/mol) were dissolved in 30 mL of dilution water, giving a stock solution with a concentration of 10^{-2} M (2942 mg/L). This stock solution was diluted appropriately with dilution water down to 10^{-7} M (0.029 mg/L). The characteristics of the resulting dose-response curves are summarised in Table 4.21. The dose-response curves using the higher bacteria concentration detected with the oxygen- and the pH-sensitive MTPs match rather well (Fig. 4.35, left). Curiously, the characteristics of the curve using lower bacteria concentration are shifted towards higher inhibitor concentration (Fig. 4.35, right). Rather large standard deviations imply impreciseness of the measurement as reason for this behaviour. The range of these dose-response curves is about 1.5 orders of magnitude.

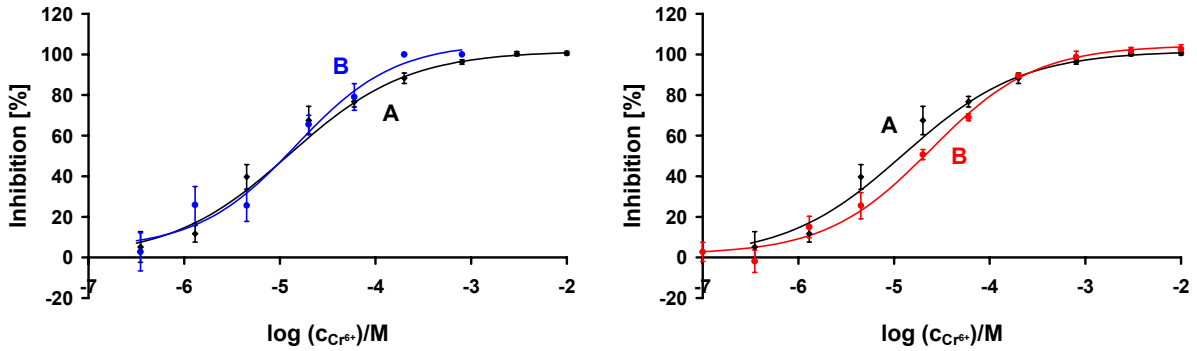

Fig. 4.35. Dose-response curves with Cr^{6+} as inhibitor. Left: $6.7 \cdot 10^8$ cfu/mL, obtained with the oxygen- (A) and pH- (B) sensitive MTPs; Right: (A): $6.7 \cdot 10^8$ cfu/mL and (B): $2.0 \cdot 10^8$ cfu/mL, obtained with the oxygen-sensitive MTP.

Table 4.21. EC_{50} values and ranges for Cr^{6+} obtained with the OxoPlate (OP) for two different bacteria concentrations, and the HydroPlate (HP) for the higher bacteria concentration.

cfu/mL	**EC_{50} [M]**	**ΔEC_{50} (min) [M]**	**ΔEC_{50} (max) [M]**	**range [M]**
OP	$2.1 \cdot 10^{-5}$	$-0.5 \cdot 10^{-5}$	$0.2 \cdot 10^{-5}$	$3.5 \cdot 10^{-6}$ – $1.0 \cdot 10^{-4}$

$2.0 \cdot 10^8$				
OP $6.7 \cdot 10^8$	$1.2 \cdot 10^{-5}$	$-0.5 \cdot 10^{-5}$	$0.06 \cdot 10^{-5}$	$1.7 \cdot 10^{-6} – 8.0 \cdot 10^{-5}$
HP $6.7 \cdot 10^8$	$1.2 \cdot 10^{-5}$	$-0.3 \cdot 10^{-5}$	$0.4 \cdot 10^{-5}$	$1.9 \cdot 10^{-6} – 5.3 \cdot 10^{-5}$

- Comparison of the Different Heavy Metals

Fig. 4.36 gives and overview over the dose-response curves the 6 investigated heavy metals obtained with the oxygen- and pH-sensitive MTP with different bacteria concentrations using the oxygen sensor. The results are in excellent accordance with each other. The toxicity of the heavy metals increases in the order of Co^{2+} < Ni^{2+} < Zn^{2+} < Cd^{2+} < Cr^{6+} < Cu^{2+}. The rather broad range using Cd^{2+}, which indicates low sensitivity of this bacteria test towards the inhibitor, is also illustrated.

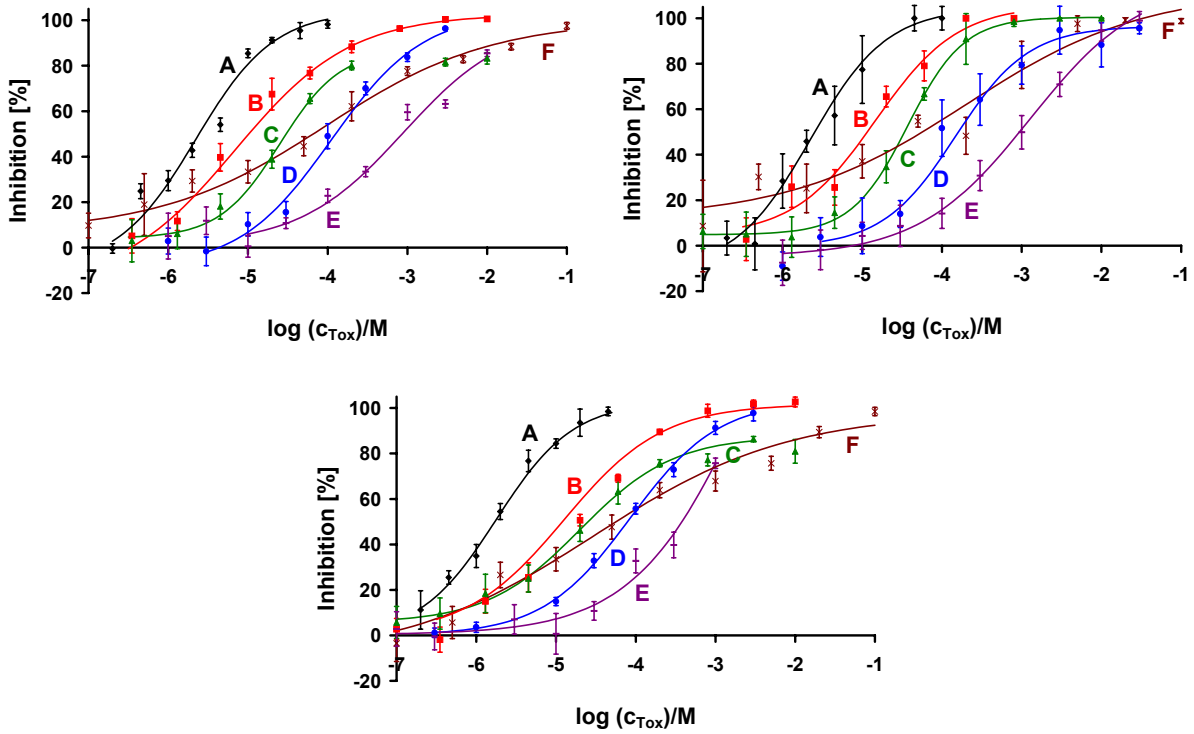

Fig. 4.36. Comparison of dose-response curves using (A) Cu^{2+}, (B) Cr^{6+}, (C) Zn^{2+}, (D) Ni^{2+}, (E) Co^{2+} and (F) Cd^{2+} as inhibitor. Top & left: $6.7 \cdot 10^8$ cfu/mL, obtained with the oxygen-sensitive MTP; Top & right: $6.7 \cdot 10^8$ cfu/mL, obtained with the pH-sensitive MTP; Bottom: $2.0 \cdot 10^8$ cfu/mL, obtained with the oxygen-sensitive MTP.

4.5.3.2. Chlorophenols

Chlorophenols are employed as intermediates in industrial syntheses, as biocides for fungi, insects or weeds, as disinfectants in hospitals, preservatives for wood, leather or glue, in medical products, dyes, plasticisers, plastics, explosives, emulsifier, detergents, antioxidants, and in paper and pulp industry. Due to their toxicity, several chlorophenols became prohibited in some countries over the last 20 years. However, many chlorophenols are persistent and can still be found in soil and water. Additionally, they are a common by-product at chlorine bleaching of paper. Important members are 2,4-dichlorophenol, which is used as mothproofing agent, antiseptic seed disinfectant and herbicide, and pentachlorophenol (PCP), a fungicide which is widely used as wood preservative and is prohibited in Germany. A 1:1 mixture of butylesters of 2,4-DCP and 2,4,5-TCP gained notoriety as “Agent Orange”, a defoliant in the Vietnam War. An impurity at the production of 2,4,5-TCP is the well-known Seveso-toxin dioxin (2,3,7,8-tetrachlorodibenzo-p-dioxin).

A natural source of chlorinated orcinoles is the Japanese lily *Lilium leichtlinii va. maximowiczii*, which synthesises trichlorophenols to kill gram-negative bacteria and moulds in case of infestation. After killing the moulds, the chlorophenols decompose easily [19].

Phenol itself is a protoplasm toxin and therefore displays a bacteriostatic and disinfecting effect. At skin contact, phenol is corrosive and easily adsorbed. Inhalation leads to respiratory paralysis, cardiac arrest, chronic toxication and kidney damage. At oral taking, 1 g is lethal. Chlorophenols are, increasing with the degree of chlorination, bactericidal up to trichlorophenol. They block the synthesis of adenosine triphosphate and oxidative phosphorylation. The phytotoxicity also increases with the degree of chlorination [20]. Similar to phenol, chlorophenols cause irritation of the eyes, the respiratory tract and organ, the skin and mucous membrane. Absorption can lead to tremors, convulsion and even coma. With increasing chlorination, the convulsory effect decreases and the inhibition of the oxidative phosphorylation increases. Especially highly substituted chlorophenols are bioaccumulated in the body. As long-term effect, chlorophenols can cause damages of organs as liver, kidney and the central nervous system. Being less carcinogenic than phenol, they can nevertheless lead to tumours, lymphoid cancer and leukaemia.

Due to their toxicity and poor biodegradability, chlorophenols are assigned to the water hazard class 3. Their toxicity towards invertebrates, crustaceans and fish increases with increasing degree of chlorination. High concentrations can affect the efficiency of degradation in wastewater treatment plants. Biological decomposition requires the presence of bacteria adapted to these conditions. Some strains of *Pseudomonas putida* are known for their ability to metabolise chlorophenols [21]. Oxidation of chlorophenols using chemical catalysators are also a possibility to degrade them [e.g. 22]. Besides, chlorophenols decompose when exposed to sunlight.

For the *P. putida* respiration inhibition test performed with sensor-coated MTPs, the toxicity of three chlorophenols were investigated: 3,5-dichlorophenol (3,5-DCP), its isomer 3,4-dichlorophenol (3,5-DCP), and the monochlorinated 4-chlorophenol (4-CP).

- 3,5-Dichlorophenol (3,5-DCP)

3,5-DCP is mainly used as intermediate for acgrochemicals and other compounds like fungicides, bactericides and algicides [23]. It strongly irritates the eyes, skin and respiratory tract and can be absorbed by the skin. It may cause diarrhoea, dizziness, headache, sickness and weakness. Exposure may result in chloroacne. The biodegradability is rather poor [24]. 3,5-DCP is often used as standard in toxicological tests (e.g. 4) to obtain the sensitivity of the test organisms.

Experimental: 0.0815 g of 3,5-DCP (M = 163.00 g/mol) were dissolved in 50 mL of dilution water, giving a stock solution with a concentration of 10^{-2} M (1630 mg/L). The solution was ultrasonicated for several minutes to dissolve the substance completely. This stock solution was diluted appropriately with dilution water down to 10^{-4} M (16.3 mg/L). The characteristics of the resulting dose-response curves are summarised in Table 4.22. The dose-response curves using the higher bacteria concentration detected with the oxygen- and the pH-sensitive MTPs match rather well (Fig. 4.37, left). The characteristics of the curve obtained with the lower bacteria concentration are slightly shifted towards lower inhibitor concentrations (Fig. 4.37, right). Comparison with values given in literature shows sufficient accordance with

the EC values obtained with this concentration. The range of these dose-response curves spans ca. 0.5 orders of magnitude.

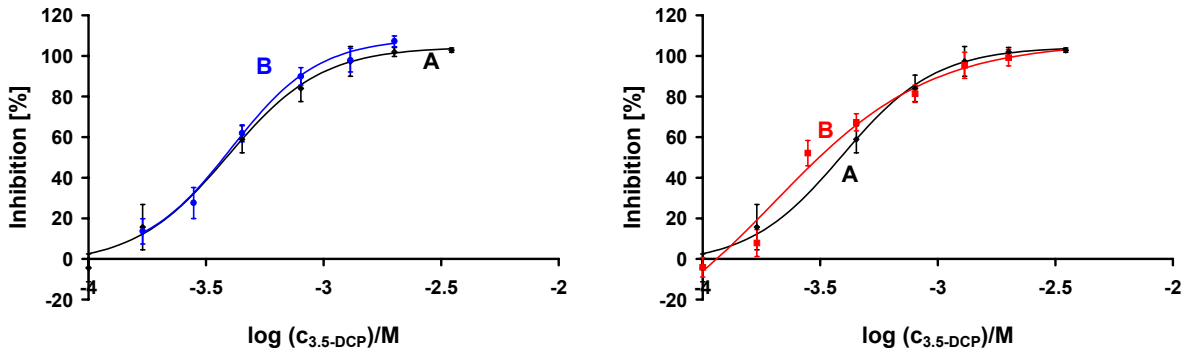

Fig. 4.37. Dose-response curves with 3,5-DCP as inhibitor. Left: 6.7·10^8 cfu/mL, obtained with the oxygen- (A) and pH- (B) sensitive MTPs; Right: (A) 6.7·10^8 cfu/mL and (B): 2.0·10^8 cfu/mL, obtained with the oxygen-sensitive MTP.

Table 4.22. EC_{50} values and ranges for 3,5-DCP obtained with the OxoPlate (OP) for two different bacteria concentrations, and the HydroPlate (HP) for the higher bacteria concentration.

cfu/mL	**EC_{50} [M]**	**ΔEC_{50} (min) [M]**	**ΔEC_{50} (max) [M]**	**range [M]**
OP 2.0·10^8	$3.1 \cdot 10^{-4}$	$-0.3 \cdot 10^{-4}$	$0.4 \cdot 10^{-4}$	$1.7 \cdot 10^{-4}$ – $6.8 \cdot 10^{-4}$
OP 6.7·10^8	$3.9 \cdot 10^{-4}$	$-0.5 \cdot 10^{-4}$	$0.2 \cdot 10^{-4}$	$2.1 \cdot 10^{-4}$ – $6.9 \cdot 10^{-4}$
HP 6.7·10^8	$3.8 \cdot 10^{-4}$	$-0.1 \cdot 10^{-4}$	$0.6 \cdot 10^{-4}$	$2.1 \cdot 10^{-4}$ – $6.3 \cdot 10^{-4}$
Literature	$2.6 \cdot 10^{-4}$			EC_{20}: $1.4 \cdot 10^{-4}$

- 3,4-Dichlorophenol (3,4-DCP)

3,4-DCP occurs as intermediate for agrochemicals and other compounds like fungicides, bactericides and algaecides [23]. Potential health effects are irritation of

the eyes and skin and of the digestive tract if swallowed. 3,4-DCP may cause burning sensations, coughing, wheezing, laryngitis, shortness of breath and headache. Inhalation leads to irritation of the respiratory tract. Exposure produces central nervous system depression and may cause liver damage. Prolonged exposure can lead to chronic damage of the eyes, severe irritation or burns. However, the toxicological properties have not been fully investigated [25].

Experimental: 0.0815 g of 3,4-DCP (M = 163.00 g/mol) were dissolved in 50 mL of dilution water, giving a stock solution with a concentration of 10^{-2} M (1630 mg/L). The solution was ultrasonicated for several minutes to dissolve the substance completely. This stock solution was diluted appropriately with dilution water down to 10^{-4} M (16.3 mg/L). The characteristics of the resulting dose-response curves are summarised in Table 4.23. The dose-response curves using the higher bacteria concentration detected with the oxygen- and the pH-sensitive MTPs match less well than using other inhibitors (Fig. 4.38, left). In contrast to most of the dose-response curves obtained with other inhibitors, the characteristics of the curve are quite independent from the bacteria concentration (Fig. 4.38, right). Similar to 3,5-DCP, the range of these dose-response curves spans ca. 0.5 orders of magnitude.

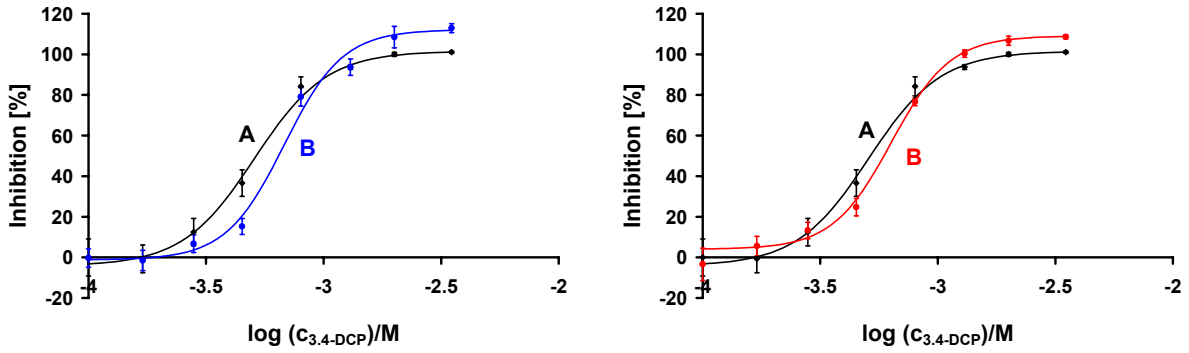

Fig. 4.38. Dose-response curves with 3,4-DCP as inhibitor. Left: $6.7 \cdot 10^8$ cfu/mL, obtained with the oxygen- (A) and pH- (B) sensitive MTPs; Right: (A): $6.7 \cdot 10^8$ cfu/mL and (B): $2.0 \cdot 10^8$ cfu/mL, obtained with the oxygen-sensitive MTP.

Table 4.23. EC_{50} values and ranges for 3,4-DCP obtained with the OxoPlate (OP) for two different bacteria concentrations, and the HydroPlate (HP) for the higher bacteria concentration.

cfu/mL	**EC_{50} [M]**	**ΔEC_{50} (min) [M]**	**ΔEC_{50} (max) [M]**	**range [M]**
OP $2.0 \cdot 10^8$	$5.9 \cdot 10^{-4}$	$0.3 \cdot 10^{-4}$	$0.6 \cdot 10^{-4}$	$3.9 \cdot 10^{-4} – 8.3 \cdot 10^{-4}$
OP $6.7 \cdot 10^8$	$5.2 \cdot 10^{-4}$	$0.1 \cdot 10^{-4}$	$0.8 \cdot 10^{-4}$	$3.3 \cdot 10^{-4} – 8.2 \cdot 10^{-4}$
HP $6.7 \cdot 10^8$	$6.4 \cdot 10^{-4}$	$-0.03 \cdot 10^{-4}$	$0.4 \cdot 10^{-4}$	$4.5 \cdot 10^{-4} – 8.9 \cdot 10^{-4}$

- 4-Chlorophenol (4-CP)

  4-CP is used as intermediate for higher chlorophenols and dyes, fungicides, drugs and antiseptics [23]. A natural source is the degradation of 2.4-DCP [26], which is produced by a soil fungus (*Penicillium sp*.) [27]. 4-CP is characterised by its acute toxicity and low biodegradability [28]. It is corrosive and extremely destructive to tissues of the mucous membranes and upper respiratory tract, eyes, and skin. High exposure can cause headache, dizziness, fatigue, restlessness, muscle weakness, tremors, seizures, coma and even death. 4-CP may damage the liver and kidneys [29, 30].

  Experimental: 0.0643 g of 4-CP (M = 128.56 g/mol) were dissolved in 50 mL of dilution water, giving a stock solution with a concentration of 10^{-2} M (1286 mg/L). The solution was ultrasonicated for several minutes to dissolve the substance completely. This stock solution was diluted appropriately with dilution water down to 10^{-4} M (12.9 mg/L). The characteristics of the resulting dose-response curves are summarised in Table 4.24. Similar to 3,4-DCP, the dose-response curves using the higher bacteria concentration detected with the oxygen- and the pH-sensitive MTPs match rather poorly (Fig. 4.39, left). The characteristics of the curve using a lower bacteria concentration are slightly shifted towards lower

inhibitor concentrations (Fig. 4.39, right). The range of these dose-response curves is rather small and spans ca. 1.5 orders of magnitude.

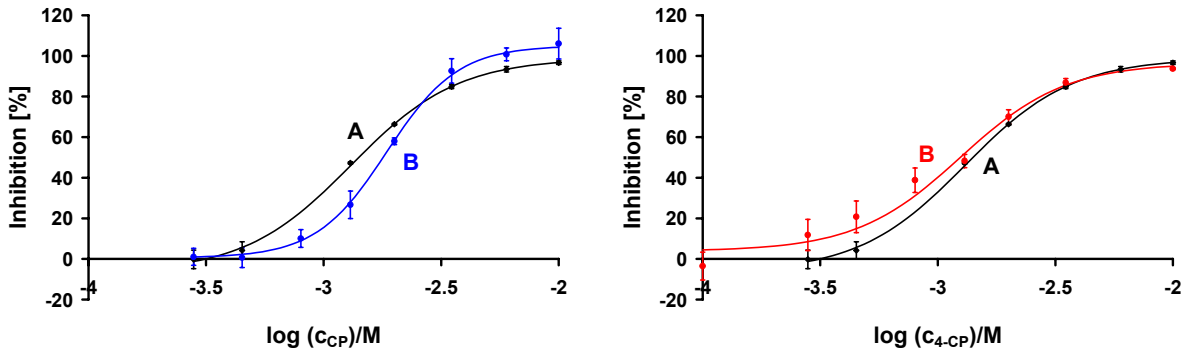

Fig. 4.39. Dose-response curves with 4-CP as inhibitor. Left: 6.7·10^8 cfu/mL, obtained with the oxygen- (A) and pH- (B) sensitive MTPs; Right: (A): 6.7·10^8 cfu/mL and (B): 2.0·10^8 cfu/mL, obtained with the oxygen-sensitive MTP.

Table 4.24. EC_{50} values and ranges for 4-CP obtained with the OxoPlate (OP) for two different bacteria concentrations, and the HydroPlate (HP) for the higher bacteria concentration.

cfu/mL	**EC_{50} [M]**	**ΔEC_{50} (min) [M]**	**ΔEC_{50} (max) [M]**	**range [M]**
OP 2.0·10^8	$1.2 \cdot 10^{-3}$	$0.2 \cdot 10^{-4}$	$0.04 \cdot 10^{-4}$	$5.6 \cdot 10^{-4} – 2.7 \cdot 10^{-3}$
OP 6.7·10^8	$1.4 \cdot 10^{-3}$	$0.2 \cdot 10^{-4}$	$0.1 \cdot 10^{-4}$	$7.4 \cdot 10^{-4} – 2.9 \cdot 10^{-3}$
HP 6.7·10^8	$1.8 \cdot 10^{-4}$	$-0.1 \cdot 10^{-4}$	$0.05 \cdot 10^{-4}$	$1.1 \cdot 10^{-3} – 2.8 \cdot 10^{-3}$

- Comparison of the Different Chlorophenols

Fig. 4.40 gives an overview over the dose-response curves of the 3 investigated chlorophenols detected with the pH- and the oxygen-sensitive MTP and, for the oxygen sensor, at two different bacteria concentrations. The tendency of all 3 sets of

experiments is congruent: 4-CP displays the lowest toxicity towards *P. putida*, whereas 3,4-DCP is slightly less toxic than 3.5-DCP.

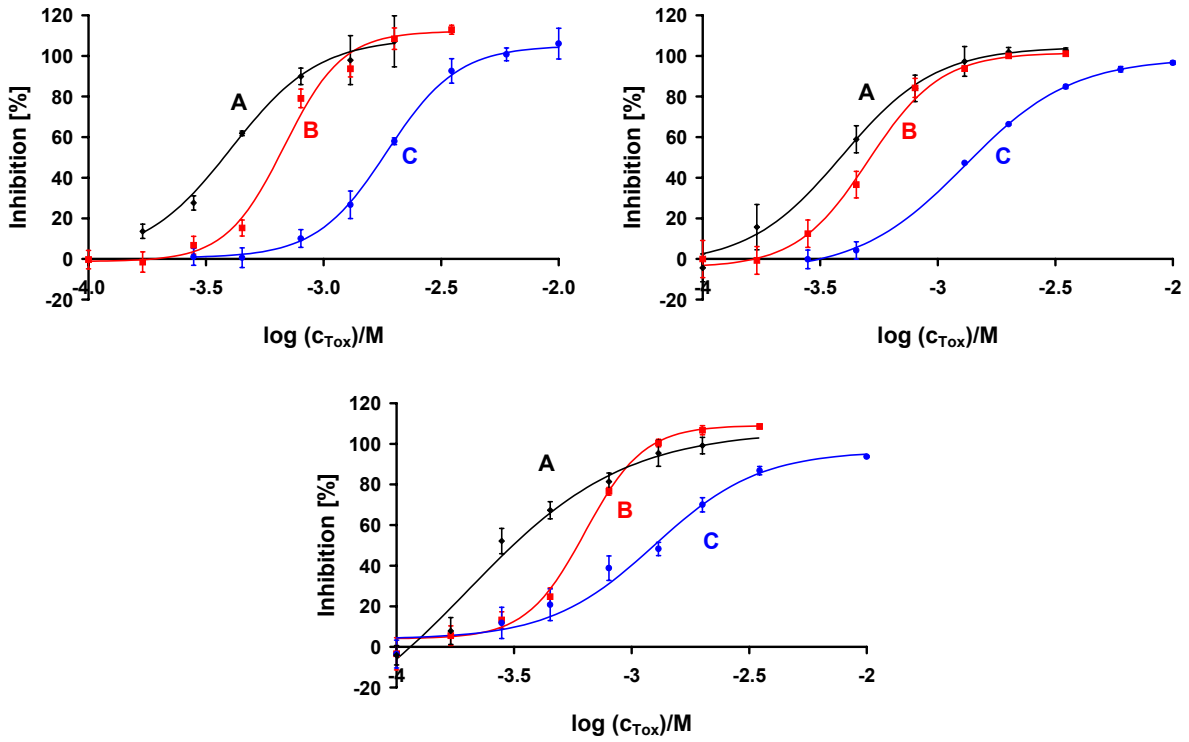

Fig. 4.40. Comparison of dose-response curves using (A) 3,5-DCP, (B) 3,4-DCP and (C) 4-CP as inhibitor. Top & left: 6.7·10^8 cfu/mL, obtained with the oxygen-sensitive MTP; Top & right: 6.7·10^8 cfu/mL, obtained with the pH-sensitive MTP; Bottom: 2.0·10^8 cfu/mL, obtained with the oxygen-sensitive MTP.

4.6. Discussion

The *P. putida* respiration inhibition test was successfully applied to the oxygen-sensitive as well as to the pH-sensitive MTP. Oxygen measurements were performed according to the German standard test. Oxygen ingress through the plate sealing proved to be critical. An appropriate cover must on the one hand protect the sample of too high oxygen ingress, predominantly by preventing convection, on the other hand it must guarantee for a good well-to-well reproducibility without any outliers for convenient evaluation, be easy-to handle and suitable for automatisation. 100 µL of paraffin oil combined with the lowest possible plate acceleration of the reader was

used as a compromise. Comparison to experiments using glass vials as completely impermeable system showed that, despite the oxygen ingress through the oil cover and the therefore lower OURs, the use of the oxygen-sensitive MTP yields correct calculated inhibitions. Furthermore, this method showed a rather good repeatability. EC_{50} and EC_{20} values for Cu^{2+} and 3,5-DCP using the lowest applied bacteria concentration, which was used in the German standard test, showed good accordance with the values given in literature.

To avoid the problem of a plate sealing and therefore to simplify the set-up, the detection of the pH decrease due to respiration was employed as second parameter, using pH-sensitive MTPs. Although here the oxygen ingress from ambient air is irrelevant, other factors have to be accounted for. Due to the cross-sensitivity of optical pH detection towards ionic strength, 100 mM of NaCl have to be added to the test solution to minimise the effect of the inhibitor on the sensor signal. This shifts the dose-response curve towards higher inhibitor concentrations. Furthermore, the sensor suffers from high response times using low-buffered systems. This and the general rather low signal change has to be accounted for by application of a higher bacteria concentration than used for the oxygen measurements. Regarding evaluation, the presence of buffer in the test solution was accounted for by fitting the proton production rate to the measured kinetics using the Henderson-Hasselbalch equation. This was done using the simulation program Berkeley-Madonna and is rather labour-intensive and time-consuming. However, applying macros in Excel, this method of evaluation can be automated as well as the evaluation of the oxygen measurements by detection of the slope.

Comparing the two methods using pH and oxygen detection for investigation of the inhibition of test substances, oxygen detection is preferable if the oxygen ingress can be minimised by choosing a low plate acceleration as possible for the MTP reader used for these experiments. Although applying a liquid cover means an additional procedure step, this is not too time- and labour-intensive using a pipetting robot in automated processes. Rather high signal changes compared to pH detection lead to a high well-to-well reproducibility and the possibility of using lower bacteria concentrations, which increases the homogeneity of the inoculum and therefore the repeatability of the test and lowers the limit of detection. Calibration is easier than with the pH sensor, and the two calibration points can be applied to every

measurement for calculation, which minimises effects like temperature changes within the reader.

For measurements where the oxygen ingress cannot be minimised (e.g. if the applied reader has no option for regulation of the plate acceleration), the pH method is preferable. Here, handling is easier, but higher bacteria concentrations have to be used to yield reproducible pH changes, which prevents comparison of the results with values given in literature and increases the limit of detection. Furthermore, changes in the set-up like addition of substances or changes in concentrations of ingredients require new calibration curves. However, both methods imply the possibility of screening of large sample numbers with good reproducibility and accuracy and are therefore preferable to the conventional oxygen electrode.

4.7. References

1 Kohra S, Tominaga N, Takao Y, Nagae M, Ishibashi Y, Ueda K, and Arizono K. *A rapid respiratory toxicity test using Caenorhabditis elegans with an oxygen electrode system*. (2002). Journal of Health Science **48**(3), 269-272.

2 Inui T, Tanaka Y, Okayasu Y, and Tanaka H. *Application of toxicity monitor using nitrifying bacteria biosensor to sewerage systems*. (2002). Water Science and Technology **45**(4/5, Instrumentation, Control and Automation 2001), 271-278.

3 Arain S, John GT, Krause C, Gerlach J, Wolfbeis OS and Klimant I. *Characterization of microtiterplates with integrated optical sensors for oxygen and pH, and their applications to enzyme activity screening, respirometry, and toxicological assays.* (2005). Sensors and Actuatuators B., in press.

4 *Pseudomonas putida* respiration inhibition test, DIN 38412, part L27: 1992. Deutsche Einheitsverfahren zur Wasser-, Abwasser- und Schlamm-Untersuchung, part VI. Wiley-VCH, Weinheim (2001).

5 *Determination of turbidity*, EN ISO 7027: 1999. Deutsche Einheitsverfahren zur Wasser-, Abwasser- und Schlamm-Untersuchung, part VI, Wiley-VCH, Weinheim (2001).

6 Hobson NS, Tothill I, and Turner AP. *Microbial detection*. (1996). Biosensors & bioelectronics **11**(5), 455-477.

7 Anderson TH and Joergensen RG. *Relationship between SIR and FE estimates of microbial biomass C in deciduous forest soils at different pH*. (1997). Soil Biology & Biochemistry **29**(7), 1033-1042.

8 Van Beelen P and Fleuren-Kemila AK. *A comparison between toxicity tests using single species and a microbial process*. (1999). Chemosphere **38**(14), 3277-3290.

9 http://www.ktf-split.hr/periodni/en/abc/kpt.html (22.11.2005).

10 Behnisch PA, Allen R. *Harmonised Quality Criteria for Chemical and Bioassays Analyses of PCDDs/PCDFs in Feed and Food, Part 2: General Considerations, Bioassay Methods. (2001).* http://www.biodetectionsystems.com/news0209_bio.html# (06.01.2006)

11 Fent, K. *Ökotoxikologie*. Thieme, Stuttgart (1998).

12 Sunda WG, Engel DW, and Thuotte RM. *Effect of chemical speciation on toxicity of cadmium to grass shrimp, Palaemonetes pugio: importance of free cadmium ion*. (1978). Environmental Science and Technology **12**(4), 409-413.

13 Schienberg HI. *Copper, alloys and compounds.* In: Parmeggiani L (ed.). *Encyclopaedia of occupational health and safety.* International Labour Organization Publications, Geneva, 546-548 (1983).

14 Stokinger HE. *The metals.* In: Clayton, GD and Clayton, FE (eds*.) Patty's Industrial Hygiene and Toxicology, volume 2A Toxicology*. NY, USA, 1620-1630 (1981).

15 Minnesota pollution control agency, http://www.pca.state.mn.us/ (17.11.2005)

16 Falbe J, Regitz M (eds.). *Roempp Chemie-Lexikon on CD-ROM*, 9th ed., version 1.0 (1995).

17 Reisman DJ. (1987) *Summary Review of the health effects associated with copper*, *EPA report* - EPA/600/8-87/001.

18 Williams RJP. *Zinc: what is its role in biology?* (1984). Endeavour **8**(2), 65-70.

19 Monde K, Satoh H, Nakamura M, Tamura M, and Takasugi M. *Organochlorine Compounds from a Terrestrial Higher Plant: Structures and Origin of Chlorinated Orcinol Derivatives from Diseased Bulbs of Lilium maximowiczii*. (1998). Journal of Natural Products **61**(7), 913-921.

20 Syhre M, Hanschmann G, and Heber R. *Chlorophenols - derivatization and determination by using modern reagents*. (1994). GIT Fachzeitschrift fuer das Laboratorium **38**(11), 1232, 1235-1232, 1236.

21 Si-Jing Wang, Kai-Chee Loh, Shao Siong Chua. *Prediction of critical cell growth behavior of Pseudomonas putida to maximize the cometabolism of 4-chlorophenol with phenol and sodium glutamate as carbon sources.* (2003) Enzyme and Microbial Technology **32**, 422–430.

22 Gupta SS et al. *Rapid total destruction of chlorophenols by activated hydrogen peroxide*. (2002). Science **296**(5566), 326-328.

23 http://www.chemicalland21.com/arokorhi/industrialchem/organic/oCHLORO PHENOL.htm (21.11.2005).

24 International Chemical Safety Cards, 3,5-dichlorophenol, http://www.ilo.org/ public/english/protection/safework/cis/products/icsc/dtasht/_icsc04/icsc0440.htm (21.11.2005).

25 Material Safety Data Sheet, Acros Organics N.V., Fair Lawn, NJ, USA; http://www.coleparmer.com/catalog/Msds/39601.htm (17.11.2005).

26 Baker MD, Mayfield CI, and Inniss WE. *Degradation of chlorophenols in soil, sediment and water at low temperature*. (1980). Water Research **14**(12), 1765-1771.

27 Gribble GW. *The natural production of chlorinated compounds*. (1994). Environmental Science and Technology **28**(7), 310A-319A.

28 Calvo L, Mohedano AF, Casas JA, Gilarranz MA, and Rodriguez JJ. *Treatment of chlorophenols-bearing wastewaters through hydrodechlorination using Pd/activated carbon catalysts*. (2004). Carbon **42**(7), 1377-1381.

29 Hazardous substance fact sheet, New Jersey Department of Health and Senior Services, NJ, USA; http://www.state.nj.us/health/eoh/rtkweb/0401.pdf.

30 http://www.camd.lsu.edu/msds/c/4-chlorophenol.htm#Toxicity, 16.11.2005

5. Conclusion

In this work, the *P. putida* respiration inhibition test was successfully transferred into the microplate format. Microplates with embedded fluorescent sensors warrant a high throughput and high sensitivity. Although intensity-based, the fluorescence signals showed excellent accuracy and reproducibility due to internal referencing using an analyte-inert reference dye. This makes the assay independent of well-to-well variations in film thickness or fluctuations in the excitation light intensity or the sensitivity of the detector and enables a calibration-free application of the set-up. Cross-sensitivities towards turbidity or fluorescent sample ingredients were excluded by optical isolation (pH sensor) and choice of a rather long-wave oxygen indicator.

Concerning oxygen detection, the well-known complications resulting from oxygen ingress into the sample was investigated using various plate sealings and shaking speeds. The experiments were confirmed by mathematical simulations and the oxygen ingress roughly compared via k_La fits. Whereas the use of paraffin oil sealings cause fast oxygen ingress due to convection, rigid sealings were found to be quite effective considering the prevention of oxygen ingress. However, homogenous application of these sealings is rather complicated and cannot be automated. Small gas phases remaining between cover and sample lead to outliers which have to be sorted out manually, making evaluation rather time-consuming. Therefore, 150 µL of paraffin oil in combination with a low plate acceleration of the MTP in the reader were chosen for the screening tests due to much better well-to-well reproducibility and repeatability.

Effects of the oxygen ingress on oxygen-consuming reactions were illustrated using an enzyme kinetic. For low enzyme concentrations and rather permeable plate sealings like paraffin oil, the oxygen content does not converge towards zero, but a steady-state is formed between oxygen ingress and consumption. The level of this steady-state depends on the enzyme activity. Here, enzyme activities cannot be obtained as the initial slope of the kinetic because oxygen ingress partially compensates the consumption, leading to incorrect kinetic parameters. However, formation of a steady-state can be used for endpoint evaluations. The properties of the sensor proved to be vital for the obtained results: Using relatively thick sensor

layers of high oxygen solubility, the response time of the sensor is increased considerably because the sensor serves as an oxygen reservoir which releases oxygen into the sample. This results in too slow kinetics and corrupted kinetic parameters.

Toxicological tests using the oxygen-sensitive MTP were investigated with respect to the reproducibility and accordance to a comparative experiment using a closed system. The assay was optimised with respect to the storage conditions of the bacteria solution, the MTP sealing and bacteria concentration. The resulting calculated inhibitions using 100 µL of paraffin oil as plate sealing combined with a low plate acceleration were constant over several hours and in good accordance with the comparative experiment and with values given in literature. The toxicological test was further performed with pH-sensitive MTPs and optimised considering the test solution ingredients and bacteria concentrations. Here, addition of 100 mM of NaCl and a higher bacteria concentration than used for the oxygen experiments was found to be vital, although shifting the dose-response curves towards higher inhibitor concentrations and therefore making the test less sensitive. The dose-response curves agreed very well with the ones detected with the oxygen measurements recorded with the same composition of test solution and bacteria concentration.

Dose-response curves for different inhibitors were recorded with the oxygen- and the pH-sensitive MTPs. The resulting dose-response curves match rather well. This makes both the pH- and the oxygen-sensitive MTP an appropriate alternative to the oxygen electrode which enables high throughput screening of a large number of samples.

6. Abbreviations & Acronyms

(v/v)	volume per cent
(w/w)	weight per cent
a.s.	air saturation
ABTS	2,2'-azino-bis(3-ethylbenzthiazoline-6-sulphonic acid, diammonium salt
AMP	adenosine monophosphate
AST	antimicrobial susceptibility testing
ATP	adenosine triphosphate
BOD	biochemical oxygen demand
CA	cellulose acetate
cfu	colony-forming units
CP	chlorophenol
D	diffusion coefficient
DCP	dichlorophenol
DLR	dual lifetime referencing
DMF	dimethyl formamide
DMSO	dimethyl sulphoxide
DNA	desoxyribonuclein acid
DO	dissolved oxygen
E. coli	*Escherichia coli*
e.g.	for example
EC	effective concentration
EC Broth	Escherichia coli broth
ELISA	enzyme-linked immunosorbent assay
EtOH	ethanol
EVA	poly(ethylene-co-vinyl) acetate
FAU	formazin attenuation units
FDA	fluorescein diacetate
GFP	green fluorescent protein
GOx	glucose oxidase
h	hour

HP	HydroPlate
HTS	high-throughput screening
I	intensity
IS	ionic strength
K_La	volumetric mass transfer coefficient
K_{SP}	solubility product constant
K_{SV}	Stern-Volmer constant
LC	lethal concentration
LDH	lactate dehydrogenase
LOD	limit of detection
MeOH	methanol
min	minute
MOPS	3-(N-morpholino) propanesulfonic acid
MTP	microtiterplate
MTS	3-(4,5-dimethylthiazol-2-yl)-5-(3-carboxymethoxyphenyl)-2-(4-sulfophenyl)-2H-tetrazolium inner salt
MTT	3-(4,5-dimethylthiazol-2-yl)-2,5-diphenyl-tetrazolium bromide
OBS	Oxygen BioSensor
OD	optical density
OEP	octaethylporphyrine
OEPK	octaethylporphyrine ketone
OP	OxoPlate
OTR	oxygen transfer rate
OUR	oxygen uptake rate
P. putida	*Pseudomonas putida*
PAH	polycyclic aromatic hydrocarbons
PAN	polyacrylonitrile
PBS	phosphate buffer saline
PCP	pentachlorophenol
PCP	pentachlorophenol
PCR	polymerase chain reaction
PET	polyethylenetherephthalat
PMMA	poly(methoxymethacrylat)

pO_2	oxygen partial pressure
POx	peroxidase
PP	polypropylene
PPR	proton production rate
PS	polystyrene
PVC	polyvinyl chloride
RLD	rapid lifetime determination
rpm	rotations per minute
$Ru(dpp)_3$	ruthenium diphenyl phenanthroline
S	solubility
s	second
SDR2	SensorDish Reader
SNAFL	seminaphtho-fluorescein
SNARF	seminaphtho-rhodafluor
StD	standard deviation
T	temperature
t_{90}	response time (time for the sensor to reach 90 % of the final value)
TFPP	tetrakis(pentafluorophenyl)porphyrin
THF	tetrahydrofurane
TRIS	Tris(hydroxymethyl)aminoethane
U	unit
v	velocity
V. fischeri	*Vibrio fischeri*
τ	lifetime

7. Locations and Homepages of Companies for the Experimental Sections

Company	Location	Homepage
Aboatox	Turku, Finland	www.aboatox.com
AZUR environmental	Newark, Delaware, USA	www.azurenv.com
Becton Dickinson	Sparks, Md, USA	www.bd.com
Bibby Sterilin	Stone, UK	www.bibby-sterilin.com
bioMérieux	Nürtingen, Germany	www.biomerieux.com
BMG Labtech	Offenburg, Germany	www.bmglabtech.com
Carl Roth	Karlsruhe, Germany	www.carl-roth.de
Corning	Bucks, UK	www.corning.com
DSMZ	Braunschweig, Germany	www.dsmz.de
Gerhardt	Königswinter, Germany	www.gerhardt.de
Greiner	Frickenhausen, Germany	www.greinerbioone.de
Hach Lange	Düsseldorf, Germany	www.hach-lange.de
Heidolph Instruments	Schwabach, Germany	www.heidolph.com
Hellma	Mühlheim, Germany	www.hellma-worldwide.de
HJ-Bioanalytik	Mönchengladbach, Germany	www.hj-bioanalytik.de
IKA-Werke	Staufen, Germany	www.ika.de
Klaus Trott	Kriftel, Germany	www.czt.de/
Merck	Darmstadt, Germany	www.merck.de
Microbiotests Inc.	Nazareth, Belgium	www.microbiotests.be
Molecular Probes	Karlsruhe, Germany	www.probes.invitrogen.com
Nunc	Wiesbaden, Germany	www.nunc.de
Oxoid		www.oxoid.com
PreSens Precision Sensing	Regensburg, Germany	www.presens.de
RS Compounds	Mörfelden-Walldorf, Germany	www.rsonline.de
Sarstedt	Nümbrecht, Germany	http://www.sarstedt.com
Sartorius BBI Systems	Melsungen, Germany	www.bbraunbiotech.com

Sigma-Aldrich	Taufkirchen, Germany	www.sigmaaldrich.com
Tecan	Crailsheim, Germany	www.tecan.com
Thermo Electron	Dreieich, Germany	www.thermo.com
Varian	Darmstadt, Germany	www.varianinc.com
WTW	Weilheim, Germany	www.wtw.com

8. Curriculum vitae

Name:	Arain	
Vorname:	Sarina	
Geburtsdatum:	07.08.1975	
Geburtsort:	Neuss (Nordrhein-Westfalen)	
Nationalität:	deutsch	
Familienstand:	ledig	
Schulbildung:	1982 - 1985	Grundschule Holzbüttgen (Nordrhein-Westfalen)
	1985 – 1986	Volksschule Kellberg (Bayern)
	1986 – 1995	Gymnasium Untergriesbach (Bayern)
	6/1995	Abschluss: Abitur
Studium:	11/1995 – 2/2000	Studium der Chemie an der Universität Regensburg
	2/2000	Diplomprüfung
	5/2000 – 2/2001	Diplomarbeit am Institut für Analytische Chemie, Chemo- und Biosensorik der Universität Regensburg. Titel: *"Mikrotiterplatten mit integrierten optischen Sensoren für pH und Sauerstoff"*
	2/2001	Abschluss: Diplom
	seit 4/2001	Promotion am Institut für Analytische Chemie, Chemo- und Biosensorik der Universität Regensburg. Titel: *"Microrespirometry with Sensor-Equipped Microtiterplates"*

9. List of Publications

Papers

1) Weiss S, John GT, Heinzle E, Schultheiss E, Jose J, Arain S, Krause S, Klimant I, Waltenberger H, Maier J, Raebiger T. *Screening von Biokatalysatoren mit Sauerstoff- und pH-Mikrotiterplatten.* (2001) BioSpectrum, Sonderband Biokatalyse, 54-60.

2) Heinzle E, Weiss S, Wolfbeis O, Arain S, Klimant I, John GT, Raebiger T, Mueller G, Waltenberger H, Schultheiss E, Jose J. *Mikrotiterplatten-Reaktoren mit integrierten pH-Sensoren und Autodisplay in E. coli zur evolutiven Enzymentwicklung.* (2003) Transkript **9**, 59-62.

3) Arain S, Weiss S, Heinzle E, John GT, Krause C and Klimant I. *Gas sensing in MTPs with optodes – a study on the influence of oxygen exchange between sample, air and plate material.* (2003) Biotechnol. Bioeng. **81**(7), 829-836.

4) Arain S, John GT, Krause C, Gerlach J, Wolfbeis OS and Klimant I. *Characterization of microtiterplates with integrated optical sensors for oxygen and pH, and their applications to enzyme activity screening, respirometry, and toxicological assays* (2005) Sensors Actuat., B., in press.

5) Borisov SM , Krause C , Arain S and Wolfbeis OS. *Composite Material for Simultaneous and Contactless Luminescent Sensing and Imaging of Oxygen and Carbon Dioxide.* (2006) Advanced Materials (submitted).

6) Arain S, Klimant I. *Toxicological Screening Test in Microplates equipped with Optical Sensors for pH and pO_2* (2006), in preparation.

Poster Presentations

1) *MTPs with integrated optical sensors for pH and oxygen.* Arain S, Krause C, Klimant I, Waltenberger H, Maier J, Mueller G. (2002), **International Congress on Biocatalysis (Biocat)**, Hamburg-Harburg, Germany

2) *Oxygen uptake characteristics in MTPs.* Arain S, Weiss S, John GT, Krause C, Heinzle E and Klimant I (2002), **21. DECHEMA-Jahrestagung der Biotechnologen**, Garching b. München, Germany

3) *Novel fluorescein derivatives for pH measurements in the neutral and basic pH range.* Schroeder C, Arain S, Weidgans B and Klimant I (2003), **8th Conference on Methods and Applications of Fluorescence Spectroscopy, Imaging and Probes (MAF)**, Prague, Czech Republic.

4) *Respiration-based toxicological tests with MTPs equipped with optical oxygen optodes.* Arain S, John GT, Krause C and Klimant I (2004), **Europt(r)ode VII**, Madrid, Spain.

5) The Pseudomonas putida respiration inhibition test using optical oxygen sensors and pH sensors in MTPs. Arain S, Klimant I. (2005), **4. Deutsches BioSensor Symposium (DBS)**, Regensburg, Germany

6) *P. putida Respiration Inhibition Test – Toxicological Screening Tests with Optical Sensors in MTPs.* Arain S, Krause, C, Klimant I. (2006), **Europt(r)ode VIII,** Tuebingen, Germany (accepted).

10. Zusammenfassung (deutsch)

In der vorliegenden Dissertation wurde der *P. putida* Atmungshemmtests erfolgreich auf das Mikrotiterplattenformat übertragen. Mikrotiterplatten mit integrierten Fluoreszenzsensoren gewähren einen hohen Durchsatz und eine hohe Empfindlichkeit dieser Methode. Durch interne Referenzierung mit einem zweiten, analytunabhängigen Fluoreszenzfarbstoff weisen die Fluoreszenzsignale trotz Verwendung der Intensität als Messparameter eine ausgezeichnete Genauigkeit und Reproduzierbarkeit auf. Dadurch ist das Signal unabhängig von der Schichtdicke der Sensorspots, Schwankungen in der Intensität der Anregungslichtquelle oder der Detektorempfindlichkeit, was kalibrierfreie Messungen ermöglicht. Quer-empfindlichkeiten gegenüber trüben oder fluoreszierenden Probenbestandteilen wurden durch optische Isolierung des pH-Sensors bzw. Wahl eines langwelligen Sauerstoffindikators ausgeschlossen.

Bei den Sauerstoffmessungen wurde das wohlbekannte Problem des Sauerstoffeintrags in die Probe unter Verwendung verschiedener Abdeckungen und Schütttelgeschwindigkeiten untersucht. Die Experimente wurden durch mathematische Simulationen bestätigt und der ungefähre Sauerstoffeintrag mittels k_La-Fits verglichen. Feste Abdeckungen stellten sich als relativ effektiv bezüglich der Verhinderung des Sauerstoffeintrags heraus, wogegen die Verwendung von Paraffinöl als Abdeckung schnellen Sauerstoffeintrag durch Konvektion zur Folge hat. Gleichmäßiges Aufbringen der festen Abdeckungen auf die Probe ist jedoch relativ schwierig und nicht automatisierbar. Kleine Gasblasen zwischen Abdeckung und Probe führen zu Ausreißern, die per Hand aussortiert werden müssen, wodurch sich die Auswertung sehr zeitaufwändig gestaltet. Deshalb wurden 150 µL Paraffinöl kombiniert mit einer langsamen Plattengeschwindigkeit der MTP im Reader für die Screening-Tests verwendet, welche eine um einiges bessere well-zu-well- und zeitliche Reproduzierbarkeit zur Folge hat.

Die Auswirkung des Sauerstoffeintrags auf sauerstoffverbrauchende Reaktionen wurde anhand einer Enzymkinetik veranschaulicht. Bei geringen Enzymaktivitäten und relativ durchlässigen Abdeckungen wie Paraffinöl sinkt der Sauerstoffgehalt nicht auf 0. Statt dessen stellt sich ein dynamisches Gleichgewicht

zwischen Sauerstoffverbrauch und Sauerstoffeintrag ein, dessen Lage von der Enzymaktivität abhängt. Hierbei können Enzymaktivitäten nicht als Anfangssteigung der Kinetik bestimmt werden, da der Sauerstoffeintrag den Sauerstoffverbrauch teilweise kompensiert und zu falschen kinetischen Konstanten führt. Die Ausbildung eines dynamischen Gleichgewichts kann jedoch für Endpunkt-Bestimmungen verwendet werden. Auch die Eigenschaften des Sensors selbst beeinflussen das Ergebnis: Bei relativ dicken Sensorschichten und hoher Sauerstofflöslichkeit des verwendeten Polymers erhöht sich die Ansprechzeit des Sensors erheblich, da der Sensor als Sauerstoffreservoir fungiert, der Sauerstoff an die Probe abgibt. Dadurch werden kinetische Messungen erheblich verfälscht.

Toxikologische Tests mit der sauerstoffempfindlichen MTP wurden bezüglich ihrer Reproduzierbarkeit und Übereinstimmung mit Ergebnissen aus Vergleichsexperimenten mit geschlossenen Systemen untersucht. Der Test wurde in Hinblick auf die Bedingungen bei der Aufbewahrung der Bakterienlösung, die Art der Abdeckung und die Bakterienkonzentration optimiert. Die berechnete Hemmung bei geschüttelter Aufbewahrung der Bakterien in 50 mM Phosphatpuffer war über einige Stunden hinweg konstant. Die Verwendung von 100 µL Paraffinöl als Abdeckung kombiniert mit einer möglichst langsamen Plattengeschwindigkeit ergab eine gute Übereinstimmung der Hemmung mit der des Vergleichsexperiments und mit Literaturwerten. Der toxikologische Test wurde außerdem in MTPs mit fluoreszierenden pH-Sensorspots durchgeführt und in Hinblick auf die Bestandteile der Testlösung und die Bakterienkonzentration optimiert. Hierbei waren die Zugabe von 100 mM NaCl und eine höhere als bei den Sauerstoffmessungen verwendete Bakterienkonzentration erforderlich, wobei dies die Dosis-Wirkungskurven in Richtung höhere Hemmstoffkonzentrationen verschiebt. Die Dosis-Wirkungskurven stimmten sehr gut mit denen der Sauerstoffmessungen überein, die unter Verwendung derselben Probenzusammensetzung und Bakterienkonzentration durchgeführt wurden.

Dosis-Wirkungs-Kurven wurden für verschiedene Hemmstoffe sowohl mit der sauerstoff- als auch mit der pH-empfindlichen MTP aufgenommen. Diese stimmen in den meisten Fällen sehr gut überein. Daher sind sowohl die MTP mit Sauerstoffsensoren als auch die mit pH-Sensoren eine geeignete Alternative zur Sauerstoffelektrode, die einen hohen Durchsatz einer großen Anzahl von Proben ermöglicht

11. Appendix: Mathematical Models

11.1. Oxygen Ingress into MTPs

11.1.1. Without convection

11.1.1.1. Closed or open system

METHOD auto
STARTTIME = 0
STOPTIME=120
DT = 5

{Flows j at adjacent layers of different phases}

{water-sensor}
jLSl=Dw/s^2*(cw[m]-csensor/Ssensor*Sw)
jLSs=Dsensor/q^2*(cw[m]/Sw*Ssensor-csensor)
jLS=(jLSl+jLSs)/2

{sensor-PS}
jSPSs=Dsensor/q^2*(csensor-cps[1]/Sps*Ssensor)
jSPSps=Dps/l^2*(csensor/Ssensor*Sps-cps[1])
jSPS=(jSPSs+jSPSps)/2

{Differential equations for changes in oxygen concentration in different media}

{water layers: 1=top (contact with ambient air at open systems: TopDiff =1; closed systems: TopDiff = 0); m = bottom (contact with sensor)}
d/dt(cw[1])=Dw/s^2*(cw[i+1]-cw[i])+Dw/s^2*(c0-cw[i])*TopDiff
d/dt(cw[2..m-1])=Dw/s^2*(cw[i-1]+cw[i+1]-2*cw[i])
d/dt(cw[m])= -jLS + Dw/s^2*(cw[i-1]-cw[i])

{sensor layer: contact with water and PS}
d/dt(csensor)=jLS-jSPS

{PS layers: 1 = top (contact with sensor; n = bottom (contact with ambient air)}
d/dt(cps[1])= jSPS + Dps/l^2*(cps[i+1]-cps[i])
d/dt(cps[2..n-1])=Dps/l^2*(cps[i-1]+cps[i+1]-2*cps[i])
d/dt(cps[n])=Dps/l^2*(c1-cps[i])+Dps/l^2*(cps[i-1]-cps[i])

{initial values}

TopDiff=0	{factor for open systems = 1, or closes systems =0}
init cps[1..n]=saturation*c1	{initial oxygen concentration in PS}
saturation=0	{factor if PS is not completely deaerated}
init cw[1..m]=0	{initial oxygen concentration in water}
init csensor=0	{initial oxygen concentration in sensor}

{saturation concentration }

c0=p0*Sw*1e+6/22.4	{saturation concentration of oxygen in water [µmol/L]}
c1=p0*Sps*1e+6/22.4	{saturation concentration of oxygen in PS [µmol/l]}
c2=p0*Ssensor*1e+6/22.4	{saturation concentration of oxygen in Sensor [µmol/l]}
p0=101325*0.2095	{oxygen partial pressure in air [Pa]}

{layers}

m=30	{number of water layers}
s=dwater/m	{thickness of one water layer [cm]}
dwater=1	{thickness of whole water sample[cm]}
n=30	{number of PS layers}
l=dPS/n	{thickness of one PS layer [cm]}
dPS=0.08	{thickness of PS [cm]}
q= 0.001	{sensor thickness [cm]}

{diffusion constants and solubilities}

Dw=1.26e-3	{diffusion constant of oxygen in water [cm^2/min]}
Sw=2.67e-7	{solubility of oxygen in water [cm^3/cm^3/Pa]}
Dps=6.6e-6	{diffusion constant of oxygen in PS [cm^2/min]}
Sps=4.29e-7	{solubility of oxygen in PS [cm^3/cm^3/Pa]}
Dsensor=1.26e-3	{diffusion constant of oxygen in sensor [cm^2/min]}
Ssensor=2.67e-7	{solubility of oxygen in sensor [cm^3/cm^3/Pa]}

11.1.1.2. Oil sealing

METHOD auto
STARTTIME = 0
STOPTIME=120
DT = 5

{Flows j at adjacent layers of different phases}

{oil - water}
jOLo=Doil/dzoil^2*(coil[o]-cw[1]/Sw*Soil)
jOLl=Dw/s^2*(coil[o]/Soil*Sw-cw[1])
jOL=(jOLo+jOLl)/2

{water - sensor}
jLSl=Dw/s^2*(cw[m]-csensor/Ssensor*Sw)
jLSs=Dsensor/q^2*(cw[m]/Sw*Ssensor-csensor)
jLS=(jLSl+jLSs)/2

{sensor - PS}
jSPSs=Dsensor/q^2*(csensor-cps[1]/Sps*Ssensor)
jSPSps=Dps/l^2*(csensor/Ssensor*Sps-cps[1])
jSPS=(jSPSs+jSPSps)/2

{Differential equations for changes in oxygen concentration in different media}

{oil layers: 1=top (contact with ambient air); o=bottom (contact with water)}
d/dt(coil[1])=Doil/dzoil^2*(c3+coil[i+1]-2*coil[i])
d/dt(coil[2..o-1])=Doil/dzoil^2*(coil[i-1]+coil[i+1]-2*coil[i])
d/dt(coil[o])=Doil/dzoil^2*(coil[i-1]-coil[i]) - jOL

{water layers: 1=top (contact with oil; m = bottom (contact with sensor)}
d/dt(cw[1])=Dw/s^2*(cw[i+1]-cw[i])+jOL
d/dt(cw[2..m-1])=Dw/s^2*(cw[i-1]+cw[i+1]-2*cw[i])
d/dt(cw[m])= -jLS + Dw/s^2*(cw[i-1]-cw[i])

{sensor layer: contact with water and PS}
d/dt(csensor)=jLS-jSPS

{PS layers: 1 = top (contact with sensor; n = bottom (contact with ambient air)}
d/dt(cps[1])= jSPS + Dps/l^2*(cps[i+1]-cps[i])
d/dt(cps[2..n-1])=Dps/l^2*(cps[i-1]+cps[i+1]-2*cps[i])
d/dt(cps[n])=Dps/l^2*(c1-cps[i])+Dps/l^2*(cps[i-1]-cps[i])

{initial values}

init cps[1..n]=saturationps*c1	{initial oxygen concentration in PS}
saturationps=1	{factor if PS is not completely deaerated}
init cw[1..m]=0	{initial oxygen concentration in water}
init csensor=0	{initial oxygen concentration in sensor}
init coil[1..o]=saturationoil*c3	{initial oxygen concentration in oil}
saturationoil=1	{factor if oil is not completely deaerated}

{saturation concentrations}

c0=p0*Sw*1e+6/22.4	{saturation concentration of oxygen in water [µmol/l]}
c1=p0*Sps*1e+6/22.4	{saturation concentration of oxygen in PS [µmol/l]}
c2=p0*Ssensor*1e+6/22.4	{saturation concentration of oxygen in sensor [µmol/l]}
c3=p0*Soil*1e+6/22.4	{saturation concentration of oxygen in oil [µmol/l]}
p0=101325*0.2095	{oxygen partial pressure in air [Pa]}

{layers}

m=30	{number of water layers}
s=dwater/m	{thickness of one water layer [cm]}
dwater=0.5	{thickness of whole water sample[cm]}
n=30	{number of PS layers}
l=dPS/n	{thickness of one PS layer [cm]}
dPS=0.08	{thickness of PS [cm]}
q= 0.001	{sensor thickness [cm]}
dzoil=oil/o	{thickness of one oil layer [cm]}
oil=0.5	{oil thickness [cm]}
o=30	{number of oil layers}

{diffusion constants and solubilities}

Dw=1.26e-3	{diffusion constant of oxygen in water [cm^2/min]}
Sw=2.67e-7	{solubility of oxygen in water [cm^3/cm^3/Pa]}
Dps=6.6e-6	{diffusion constant of oxygen in PS [cm^2/min]}
Sps=4.29e-7	{solubility of oxygen in PS [cm^3/cm^3/Pa]}
Dsensor=1.26e-3	{diffusion constant of oxygen in sensor [cm^2/min]}
Ssensor=2.67e-7	{solubility of oxygen in sensor [cm^3/cm^3/Pa]}
Doil=1.566e-3	{diffusion constant of oxygen in oil [cm^2/min]}
Soil=1.44e-6	{solubility of oxygen in oil [cm^3/cm^3/Pa]}

11.1.2. With convection

11.1.2.1. Without sealing

```
METHOD auto
STARTTIME = -2
STOPTIME=120
DT = 5

{Flows j at adjacent layers of different phases}

{water – sensor}
jLSl=shake*F_water*Dw/s^2*(cw[m]-csensor/Ssensor*Sw)
jLSs=Dsensor/q^2*(cw[m]/Sw*Ssensor-csensor)
jLS=(jLSl+jLSs)/2

{sensor – PS}
jSPSs=Dsensor/q^2*(csensor-cps[1]/Sps*Ssensor)
jSPSps=Dps/l^2*(csensor/Ssensor*Sps-cps[1])
jSPS=(jSPSs+jSPSps)/2

{Differential equations for changes in oxygen concentration in different media}

{top water layer}
d/dt(cwtop)=Fconv*shake*F_water*Dw/stop^2*(c0+cw[1]-2*cwtop)

{other water layers: 1 = top (contact with top water layer; m = bottom (contact with sensor)}
d/dt(cw[1])=shake*F_water*Dw/s^2*(cw[i+1]+cwtop-2*cw[i])
d/dt(cw[2..m-1])=shake*F_water*Dw/s^2*(cw[i-1]+cw[i+1]-2*cw[i])
d/dt(cw[m])= -jLS + shake*F_water*Dw/s^2*(cw[i-1]-cw[i])

{sensor layer: contact with water and PS}
d/dt(csensor)=jLS-jSPS
```

{PS layers: 1 = top (contact with sensor; n = bottom (contact with ambient air)}
d/dt(cps[1])= jSPS + Dps/l^2*(cps[i+1]-cps[i])
d/dt(cps[2..n-1])=Dps/l^2*(cps[i-1]+cps[i+1]-2*cps[i])
d/dt(cps[n])=Dps/l^2*(c1-cps[i])+Dps/l^2*(cps[i-1]-cps[i])

{initial values}

init cps[1..n]=saturationps*c1	{initial oxygen concentration in PS}
saturationps=0.8	{factor if PS is not completely deaerated}
init cw[1..m]=0	{initial oxygen concentration in water}
init csensor=0	{initial oxygen concentration in sensor}
init cwtop=0	

{saturation concentrations}

c0=p0*Sw*1e+6/22.4*rest	{saturation concentration of oxygen in water [µmol/l]}
rest=1.2	{factor to compensate inaccuracy of the sensor at air saturation (end value > 100 % a.s.)}
c1=p0*Sps*1e+6/22.4	{saturation concentration of oxygen in PS [µmol/l]}
c2=p0*Ssensor*1e+6/22.4	{saturation concentration of oxygen in sensor [µmol/l]}
p0=101325*0.2095	{oxygen partial pressure in air [Pa]}

{layers}

m=30	{number of water layers}
s=(dwater-stop)/m	{thickness of one water layer [cm]}
dwater=0.33	{thickness of whole water sample[cm]}
n=30	{number of PS layers}
l=dPS/n	{thickness of one PS layer [cm]}
dPS=0.08	{thickness of PS [cm]}
q= 0.001	{sensor thickness [cm]}
stop=0.1	{[cm]; thickness of top water layer (0-0.33)}

{diffusion constants and solubilities}

Dw=1.26e-3	{diffusion constant of oxygen in water [cm^2/min]}
Sw=2.67e-7	{solubility of oxygen in water [cm^3/cm^3/Pa]}
Dps=6.6e-6	{diffusion constant of oxygen in PS [cm^2/min]}
Sps=4.29e-7	{solubility of oxygen in PS [cm^3/cm^3/Pa]}
Dsensor=1.26e-3	{diffusion constant of oxygen in sensor [cm^2/min]}

Ssensor=2.67e-7 {solubility of oxygen in sensor [$cm^3/cm^3/Pa$]}

Doil=1.566e-3 {diffusion constant of oxygen in oil [cm^2/min]}

Soil=1.44e-6 {solubility of oxygen in oil [$cm^3/cm^3/Pa$]}

{factors due to convection}

Fconv=10

F_water=5

shake=1

11.1.2.2. Oil sealing with slight or without additional shaking

```
METHOD auto
STARTTIME = 0
STOPTIME=120
DT = 5

{Flows j at adjacent layers of different phases}

{oil - water}
jOLo=shake*F_oil*Doil/dzoil^2*(coil[o]-cw[1]/Sw*Soil)
jOLl=shake*F_water*Dw/s^2*(coil[o]/Soil*Sw-cw[1])
jOL=(jOLo+jOLl)/2

{water - sensor}
jLSl=shake*F_water*Dw/s^2*(cw[m]-csensor/Ssensor*Sw)
jLSs=Dsensor/q^2*(cw[m]/Sw*Ssensor-csensor)
jLS=(jLSl+jLSs)/2

{sensor - PS}
jSPSs=Dsensor/q^2*(csensor-cps[1]/Sps*Ssensor)
jSPSps=Dps/l^2*(csensor/Ssensor*Sps-cps[1])
jSPS=(jSPSs+jSPSps)/2

{Differential equations for changes in oxygen concentration in different media}

{top oil layer}
d/dt(coiltop)=Doil*shake*Fconv/oiltop^2*(c3+coil[1]-2*coiltop)

{other oil layers: 1 = top layer(contact with top oil layer; o = bottom layer (contact with water)}
d/dt(coil[1])=shake*F_oil*Doil/dzoil^2*(coiltop+coil[i+1]-2*coil[i])
d/dt(coil[2..o-1])=shake*F_oil*Doil/dzoil^2*(coil[i-1]+coil[i+1]-2*coil[i])
d/dt(coil[o])=shake*F_oil*Doil/dzoil^2*(coil[i-1]-coil[i]) - jOL
```

{water layers: 1=top (contact with oil; m = bottom (contact with sensor)}
d/dt(cw[1])=shake*F_water*Dw/s^2*(cw[i+1]-cw[i])+jOL
d/dt(cw[2..m-1])=shake*F_water*Dw/s^2*(cw[i-1]+cw[i+1]-2*cw[i])
d/dt(cw[m])= -jLS + shake*F_water*Dw/s^2*(cw[i-1]-cw[i])

{sensor layer: contact with water and PS}
d/dt(csensor)=jLS-jSPS

{PS layers: 1 = top (contact with sensor; n = bottom (contact with ambient air)}
d/dt(cps[1])= jSPS + Dps/l^2*(cps[i+1]-cps[i])
d/dt(cps[2..n-1])=Dps/l^2*(cps[i-1]+cps[i+1]-2*cps[i])
d/dt(cps[n])=Dps/l^2*(c1-cps[i])+Dps/l^2*(cps[i-1]-cps[i])

{initial values}

init cps[1..n]=saturationps*c1	{initial oxygen concentration in PS}
saturationps=1	{factor if PS is not completely deaerated}
init cw[1..m]=0	{initial oxygen concentration in water}
init csensor=0	{initial oxygen concentration in sensor}
init coil[1..o]=c3	{initial oxygen concentration in oil layers}
init coiltop=c3	{initial oxygen concentration in top oil layer}

{saturation concentrations}

c0=p0*Sw*1e+6/22.4	{saturation concentration of oxygen in water [µmol/l]}
c1=p0*Sps*1e+6/22.4	{saturation concentration of oxygen in PS [µmol/l]}
c2=p0*Ssensor*1e+6/22.4	{saturation concentration of oxygen in sensor [µmol/l]}
c3=p0*Soil*1e+6/22.4	{saturation concentration of oxygen in oil [µmol/l]}
p0=101325*0.2095	{oxygen partial pressure in air [Pa]}

{layers}

m=30	{number of water layers}
s=dwater/m	{thickness of one water layer [cm]}
dwater=0.33	{thickness of whole water sample[cm]}
n=30	{number of PS layers}
l=dPS/n	{thickness of one PS layer [cm]}
dPS=0.08	{thickness of PS [cm]}
q= 0.001	{sensor thickness [cm]}
dzoil=(oil/oiltop)/o	{thickness of one oil layer [cm]}

oil=0.5*Voil/150 {oil thickness [cm], 0.5 = 150 µL}
Voil=100 {[µL]; volume of oil sealing: 50, 100 or 150 µL}
o=30 {number of oil layers}

oiltop=Vtop*0.5/150 {[cm]; thickness of top oil layer}
Vtop=25 {[µL] Oil der obersten Schicht}

{diffusion constants and solubilities}

Dw=1.26e-3 {diffusion constant of oxygen in water [cm^2/min]}
Sw=2.67e-7 {solubility of oxygen in water [cm^3/cm^3/Pa]}
Dps=6.6e-6 {diffusion constant of oxygen in PS [cm^2/min]}
Sps=4.29e-7 {solubility of oxygen in PS [cm^3/cm^3/Pa]}
Dsensor=1.26e-3 {diffusion constant of oxygen in sensor [cm^2/min]}
Ssensor=2.67e-7 {solubility of oxygen in sensor [cm^3/cm^3/Pa]}
Doil=1.566e-3 {diffusion constant of oxygen in oil [cm^2/min]}
Soil=1.44e-6 {solubility of oxygen in oil [cm^3/cm^3/Pa]}

{factors due to convection}

Fconv=10
F_oil=1.5
F_water=2.9
shake=1

11.1.2.3. Oil sealing, with rapid shaking

```
METHOD auto
STARTTIME = -2
STOPTIME=120
DT = 5

{Flows j at adjacent layers of different phases}

{oil - water}
jOLo=shake*F_oil*Doil/dzoil^2*(coil-cwtop/Sw*Soil)
jOLl=shake*F_water*Dw/s^2*(coil/Soil*Sw-cwtop)
jOL=(jOLo+jOLl)/2

{water - sensor}
jLSl=shake*F_water*Dw/s^2*(cw[m]-csensor/Ssensor*Sw)
jLSs=Dsensor/q^2*(cw[m]/Sw*Ssensor-csensor)
jLS=(jLSl+jLSs)/2

{sensor - PS}
jSPSs=Dsensor/q^2*(csensor-cps[1]/Sps*Ssensor)
jSPSps=Dps/l^2*(csensor/Ssensor*Sps-cps[1])
jSPS=(jSPSs+jSPSps)/2

{Differential equations for changes in oxygen concentration in different media}

{top oil layer: contact with ambient air and top water layer}
d/dt(coil)=Doil*shake*Fconv/dzoil^2*(c3-coil)-jOL

{top water layer: contact with top oil layer and other water layers}
d/dt(cwtop)=shake*F_water*Dw/watertop^2*(cw[1]-cwtop)+jOL

{water layers: 1=top (contact with top water layer); m = bottom (contact with sensor)}
d/dt(cw[1])=shake*F_water*Dw/s^2*(cw[i+1]+cwtop-2*cw[i])
d/dt(cw[2..m-1])=shake*F_water*Dw/s^2*(cw[i-1]+cw[i+1]-2*cw[i])
```

```
d/dt(cw[m])= -jLS + shake*F_water*Dw/s^2*(cw[i-1]-cw[i])
{sensor layer: contact with water and PS}
d/dt(csensor)=jLS-jSPS

{PS layers: 1 = top (contact with sensor; n = bottom  (contact with ambient air)}
d/dt(cps[1])= jSPS + Dps/l^2*(cps[i+1]-cps[i])
d/dt(cps[2..n-1])=Dps/l^2*(cps[i-1]+cps[i+1]-2*cps[i])
d/dt(cps[n])=Dps/l^2*(c1-cps[i])+Dps/l^2*(cps[i-1]-cps[i])
```

{initial values}

```
init cps[1..n]=saturationps*c1      {initial oxygen concentration in PS}
saturationps=0.8                    {factor if PS is not completely deaerated}
init cw[1..m]=0                     {initial oxygen concentration in water}
init csensor=0                      {initial oxygen concentration in sensor}
init cwtop=0
init coil=c3
init coil=c3
```

{saturation concentrations}

```
c0=p0*Sw*1e+6/22.4                  {saturation concentration of oxygen in water [µmol/l]}
c1=p0*Sps*1e+6/22.4                 {saturation concentration of oxygen in PS [µmol/l]}
c2=p0*Ssensor*1e+6/22.4             {saturation concentration of oxygen in sensor [µmol/l]}
c3=p0*Soil*1e+6/22.4*rest           {saturation concentration of oxygen in oil [µmol/l]}
rest=1.2                            {factor to compensate inaccuracy of the sensor at air
                                    saturation (end value > 100 % a.s.)}
p0=101325*0.2095                    {oxygen partial pressure in air [Pa]}
```

{layers}

```
m=30                                {number of water layers}
s=(dwater-stop)/m                   {thickness of one water layer [cm]}
dwater=0.33                         {thickness of whole water sample[cm]}
n=30                                {number of PS layers}
l=dPS/n                             {thickness of one PS layer [cm]}
dPS=0.08                            {thickness of PS [cm]}
q= 0.001                            {sensor thickness [cm]}
watertop=0.1                        {[cm]; thickness of top water layer (0-0.33)}
dzoil=0.5*Voil/150                  {thickness of oil sealing [cm], 0.5 = 150µl}
```

Voil=100 {[µl] volume of oil sealing}

{diffusion constants and solubilities}

Dw=1.26e-3 {diffusion constant of oxygen in water [cm^2/min]}

Sw=2.67e-7 {solubility of oxygen in water [cm^3/cm^3/Pa]}

Dps=6.6e-6 {diffusion constant of oxygen in PS [cm^2/min]}

Sps=4.29e-7 {solubility of oxygen in PS [cm^3/cm^3/Pa]}

Dsensor=1.26e-3 {diffusion constant of oxygen in sensor [cm^2/min]}

Ssensor=2.67e-7 {solubility of oxygen in sensor [cm^3/cm^3/Pa]}

Doil=1.566e-3 {diffusion constant of oxygen in oil [cm^2/min]}

Soil=1.44e-6 {solubility of oxygen in oil [cm^3/cm^3/Pa]}

{factors due to convection}

Fconv=10

F_water=5

F_oil=2

shake=1

11.2. Oxygen Uptake Rate (OUR) of Enzyme Kinetics

{Michaelis-Menten kinetics}

OUR[1..m]=V[i]-0.5*V3[i]	{µM/min}
V[1..m]=(VM*CG[i]*cw[i])/(KO*cw[i]+KG*CG[i]+CG[i]*cw[i])	{ GOx}
V3[1..m]= (VM2*CH2O2[i])/(KKat+CH2O2[i])	{catalase}

d/dt(CG[1..m])=-V[i]	{decrease of glucose}
d/dt(CH2O2[1..m])= V[i]-V3[i]	{hydrogen peroxide concentration}

{initial concentrations}

init CG[1..m]=1000*1000	{[µM]; initial glucose concentration (1000 mM)}
init CH2O2[1..m]=0	{[µM]; initial concentration of H2O2}

{enzyme kinetic parameters and activities}

VM=act_GOx*CE/Vw	{[µM/min] = [U/L] ; v_{max} for GOx activity in sample (= 133 with CE=0.4)}
VM2=act_cat*Ccat/Vw	{[µM/min]; v_{max} of catalase}
act_GOx=50/1000*x	{[U] = [µmol/min/µg], GOx activity per µg = 50 U/mg}
x=100	{empirical factor for an initial velocity VM of 50U/mg}
act_cat=2200/1000	{[U] = [µmol/min/µg], catalase activity per µg = 2200 U/mg}
CE=0.4	{[µg] GOx; 1µg = 0.05U => 1U = 20µg; 0.02U=0.4µg, 0.005U=0.1µg}
Ccat=100	{[µg] catalase; 1µg = 2.2U => 1U = 0.45µg; 0.88U=0.4µg; 100=excess}
KO=0.2*1000	{µM; affinity constant for oxygen }
KG=25*1000	{µM; affinity constant for glucose}
Kcat= 85.1*1000	{µM; affinity constant for H2O2, catalase}

{other parameters}

Vw=150E-6	{[L]; total sample volume (150µl)}

11.3. Proton Production Rate / Henderson-Hasselbalch Equation

```
METHOD RK4

STARTTIME = 0
STOPTIME=45
DT = 1

pH=pKa+log10(cA/cHA)                          {Henderson-Hasselbalch equation}

d/dt(cA)=-PPR                                 {decrease if basic form [µM/min]}
d/dt(cHA)=PPR                                 {increase of acidic form [µM/min]}

cA0=(ctot*10^(pH0-pKa))/(1+10^(pH0-pKa))      {basic form at start of measurement}
cHA0=ctot-cA0                                 {acidic form at start of measurement}

ctot=1375                                     {total phosphate concentration [µM]}

pKa=7.2                                       {dissociation constant hydrogen
                                              phosphate - dihydrogen phosphate}
pH0=7.2                                       {pH at start of measurement}
init cA=cA0                                   {basic form at start of measurement}
init cHA=cHA0                                 {acidic form at start of measurement}
PPR=5                                         {proton production rate [µM/min]}
```